

Volume. VIII, Issue : I, September - 2016

ISSN : 0975-5624



Acharya Brojendra Nath Seal College
Cooch Behar - 736101

Editor-in-Chief

Dr. Prabir Banerjee

Department of Physics, ABN Seal College

Editorial Board

Dr. Asis Kumar Pandit, Department of Physiology, ABN Seal College

Dr. Ramkrishna Pramanik, Department of Chemistry, ABN Seal College

Dr. Srijit Das, Department of Chemistry, ABN Seal College

Shri Hemen Biswas, Department of Zoology, ABN Seal College

Dr. Lakshmi Narayan De, Department of Mathematics, ABN Seal College

Dr. Anirban Roy, Department of Geography, ABN Seal College

Dr. Aninda Mandal, Department of Botany, ABN Seal College

Shri Prem Rajak, Department of Zoology, ABN Seal College

Chief Advisor

Prof. Nimai Chandra Saha

Director of Public Instructions

Government of West Bengal

Advisory Board

Prof. Syamal Roy

Vice-Chancellor, Cooch Behar Panchanan Barma University

Cooch Behar, West Bengal

Dr. Bimal Kumar Saha

Officer-in-Charge, ABN Seal College

Cooch Behar, West Bengal

Prof. Ashim Kumar Chakraborty

Retd. Professor, Department of Zoology, North Bengal University

Dr. Willie Henry

P G Department of Zoology, ABN Seal College

Cooch Behar, West Bengal

All correspondences regarding the publication should be made to the Editor-in-Chief, B. N. Seal journal of Science

From the Editor's Desk.....

It gives great pleasure that the current issue (Vol. VIII) of the B N Seal Journal of Science is published as usual before the Annual Day Celebration of the College. The present volume brings together a number of original and informative research/review articles of very high quality, which address the current global scenario. The topics encompass practically all disciplines of Science and also interdisciplinary subjects, intimately linked together. I hope that the current issue of this journal has not failed to live up to the expectation, reputation and excellent academic standards set up by the preceding volumes. The readers will definitely find it stimulating, inspiring and thought-provoking.

I would like to thank all the contributors for their scholarship and research acumen. Thanks are due to the entire editorial team for their hard work and support, contribution in critically reviewing the articles and preparation of this issue of the B N Seal Journal of Science. It is worthwhile to acknowledge the help and support rendered by The Publication & Published Material Distribution Cell of this College for bringing out this issue of the Journal on time. I would also like to thank everybody who has contributed in any way, however great or small.

It may please be noted that the paper by Bhaskar Das and others was not included in the hard copy of this Journal due to some inadvertent technical mistake. I thoroughly apologise for this. This has been included in this electronic version.

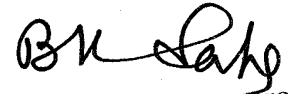
I am immensely grateful to Dr. Bimal Kumar Saha, Officer-in-Charge of this College, for his patronage, support and enthusiasm.

Prabir Banerjee

(Editor-in-Chief)

From the Principal's Desk.....

The undersignatory hopes that this Peer Reviewed National Level Journal will become Peer Reviewed International Level Journal very soon.


Officer-in-Charge
ABN Seal College
Cooch Behar

Sl. No.	Volume VIII	Issue I	September 2016
Contents			
1	Recent Advances in Lab-On-a-Chip [LOC] Impedimetric Biosensors Integrated with Digital Microfluidic System Subhadip Chakraborty, Anupam Karmakar and Sanatan Chattopadhyay		1-11
2	Partially Polarized Fractional Quantum Hall Effect Biplab Kumar Mandal and Dwipesh Majumder		12-16
3	Note on Some Classes of Generalized Continuous Functions Piyali Mallick and Lakshmi Narayan De		17-21
4	Effect of Selective Atomic Substitution on the Magnetic Field Induced Strain and Entropy Change in Ni ₅₁ Mn ₃₅ In ₁₄ Alloys Rahul Das		22-28
5	Monometallic Chromium (II) Complex of 2-[2-(Pyridylamino) Phenylazo] Pyridine with a Singlet Ground State (S=0) and Its Manganese (III) Congener. Synthesis and NMR Studies Srijit Das		29-34
6	Photophysical Property Monitored by Solvent Environment for <i>NNO</i> Coordinating Tridentate Ligand Amar Hens		35-38
7	Solvent-Solvent Interactions in Ethanol-Octanol Binary Solvent Mixtures: A Study of Surface Tension and Fluorescence Anisotropy Ramkrishna Pramanik		39-44
8	Key Players of Innate Immunity in <i>Drosophila melanogaster</i> Prem Rajak, Saurabh Sarkar, Arnab Roy and Sumedha Roy		45-53
9	Genetic Etiology of Biological Ageing Satadal Adhikary		54-60
10	Diversity of Entomofauna amidst an Urban Green Patch: A Study in Cooch Behar Satadal Adhikary, Rachita Saha, Alolika Bose, Poulami Sarkar, Pinki Paul		61-69
11	Vanadium Inhibits Early DNA Damage and Premalignant Lesions in a Rodent Model of Experimental Hepatocarcinogenesis Tridib Chakraborty		70-76
12	Polycystic Ovarian Syndrome: A Brief Mini Review on Current Updates Tuhin Suvro Banerjee and Asis Kumar Pandit		77-88
13	Study on the Trees of Euphorbiaceae <i>s.l.</i> in Cooch Behar District, West Bengal, India Rajendra Prasad De		89-92
14	Naturally Occurring Protein Toxin –“Friends or Foes”-A Multidimensional Analysis Liebig Ranjan Debnath and Debojyoti Dutta		93-106
15	An Approach to Overcome the Total Synthesis of Heliannuol-A Nilay Kumar Maitra and Prabir K. Sen		107-113
16	Ascorbic Acid Promoted Metal Free Borylation of Aromatic Diazonium Salts under Room Temperature Debasish Kundu and Totan Roy		114-117
17	Emergent Universe Models with Bulk Viscosity Partha Sarathi Debnath		118-123
18	Insects in Human Welfares and Benedictions: As Food and Medicine Suppliers Hemen Biswas		124-132
19	Mechanical and Chemical Approaches to fabricate luminescent Silicon Nanoparticles Bhaskar Das, Syed Minhaz Hossain and Mallar Ray		133-138

Recent Advances in Lab-On-a-Chip [LOC] Impedimetric Biosensors Integrated with Digital Microfluidic System

Subhadip Chakraborty, Anupam Karmakar and Sanatan Chattopadhyay*

Department of Electronic Science, University of Calcutta, 92, A.P.C. Road, Kolkata- 700009, India

*Communicating author: scelc@caluniv.ac.in

Abstract

This review represents an overview on the recent progress and developments of biological sensors with an emphasis on impedimetric sensing at micro-scale. The design issue of a bio-impedance based micro-scale biosensor includes a couple of schemes with two and three electrodes. Photolithography is also introduced as a leading technique to fabricate such structures. Quantitative and qualitative estimation of bio-constituents including carbohydrates and proteins can be performed using such micro-scale biosensors. Detection of specific bacterial species and their immobilisation schemes on microelectrodes have been extensively demonstrated. Basic aspects and features of the digital micro-fluidics have been discussed as a superior strategy towards improved bio sensing techniques. Impedance based measurement schemes relevant to several detection techniques have also been discussed in this work.

Key words: Biosensors; lab-on-a-chip; photolithography; specific samples; digital microfluidics; impedance spectroscopy

Publication History: Received: 10th August, 2016; Accepted: 19th August, 2016

Introduction

The development of biological sensors has attracted enormous attention among the global research community since last several decades. It has emerged as the potential domain of research for both the academic and industrial world. Biosensors are the group of analytical devices that enable the analysis of biological components present in a specimen under test. It detects and converts a biological event into a detectable signal by the sequential operation of a receptor, transducer and detector. By incorporating a bio-material in intimate contact with an appropriate transducer, it recognizes the concentration or activity of specific bio- or chemical species in the sample under investigation. The domain is truly multidisciplinary in nature encompassing several fields of electronic engineering, biology, physics, chemistry and materials science. Modern medical diagnosis system has been revolutionized by the routine usage of different types of electronic gadgets dedicated to measure bio-system parameters. A striking progress in terms of accuracy and consequently target oriented treatment has been witnessed in recent time which is undoubtedly attributed to the development and implementation of such modern biomedical tools [Fraden 2004; Wilson 2004]. In biological systems, the species specific activities or reactions under investigation usually generate either a detectable current, potential or charge accumulation or measurably alter the conductive properties of a medium between the electrodes. There are several detection techniques to sense the outcome of a specific electrochemical reaction that is generally used in biosensors including potentiometry, amperometry, voltammetry, impedimetry and optical detection techniques. Potentiometry measures the potential difference between a working electrode and the reference electrode depending upon the concentration-related behavior. In amperometry technique, the output signal of the device is correlated with the concentration of target compounds by applying a voltage between the working electrode and a reference electrode. The transducer employed in the potentiometric technique is usually a gas-sensing electrode or an ion-selective electrode. Voltammetry is the most adapted technique in electrochemical analysis. Both the current and the potential are measured. The position of peak current is correlated with the specific chemical and the peak current density is a function of

concentration of the corresponding species or the compositional gradient of any particular bio-molecule [Arslan et al 2011; Gao et al. 2014; Garjonyte and Malinauskas 1999; Cai and Chen 1999; Wang et al. 2008; Saeedfar et al. 2013; Jha et al. 2008; Li et al. 2012; Krajewska et al. 2008; Islam et al. 2011; Norouzi et al. 2010; Ebrahimi et al. 2011]. Optical detection is usually based on the measurement of absorption, fluorescent, colorimetric, or other optical signals produced by the interaction of microorganisms with the analytes and correlate the observed optical signal with the concentration of target compounds [Mitra et al. 2012; Singh et al 2013; Long et al. 2013].

Amongst several techniques, impedance spectroscopy has flourished as a potential contender in bio-analytical measurements since last decade [Tomčík 2013; Lu et al. 2013; Yeh et al. 2010; Ma et al. 2013]. The technique comprises of a couple of schemes including electrical impedance spectroscopy and electrochemical impedance spectroscopy. In electrical impedance spectroscopy, several electrical parameters like impedance, capacitance and conductance are monitored with a frequency sweep. The change in these parameters is attributed to the variation of effective dielectric constant of the system under investigation caused by density gradient of the species to be detected. Electrochemical impedance spectroscopy (EIS) is a technique that relates the response of an electrochemical cell to small amplitude perturbing sinusoidal voltage signal as a function of frequency. Both of the techniques have marvellous prospective due to salient features like high accuracy, short response time and enhanced sensitivity.

During the last decade, the micro-dimensional bio-microfluidic systems, also known as micro-total-analysis-system (μ TAS), have attracted enormous attention due to the salient features including their portability, high accuracy, short response time and enhanced sensitivity [Lee et al. 2004; Mir et al. 2009]. Being the workhorse of modern electronics, integration of any emerging devices with the matured Si platform will have a magnitude of advantages in terms of integration with mainstream electronics. The sophistication and complexity of biological systems and their parallel nature is agreeably matched to integrated circuits and hence by exploiting the potential of Si based IC technology, bio-analytical instruments are being miniaturized to make lab-on a-chip [LOC] which can perform a variety of experiments such as observation of bio-molecular activities, cellular density and viability monitoring etc [Chen et al. 2011; Choi et al. 2013; Zhang et al. 2009; Kim et al. 2015]. Integration with digital microfluidics makes these devices enable to move, split and sense sample droplets under investigation simultaneously [Kim et al. 2015].

Design and Fabrication

Inter-digitated micro-electrode (IDME) fabrication is the most extensively used scheme to design the 'lab on a chip' biosensors. The IDME system comprises of a couple of design issues depending upon the number of electrodes: either a 3-electrode system, or a 2-electrode system. The 3-electrode system consists of a reference (RE), a counter (CE) and a working electrode (WE). In this type of system, the current flows between the CE and WE and the potential difference is controlled between the WE and CE and measured between RE and WE. In case of a 2-electrode system, the RE and CE are basically shorted and the measurements are performed between the RE and WE. A three electrode and a two electrode system are shown in Fig. 1.

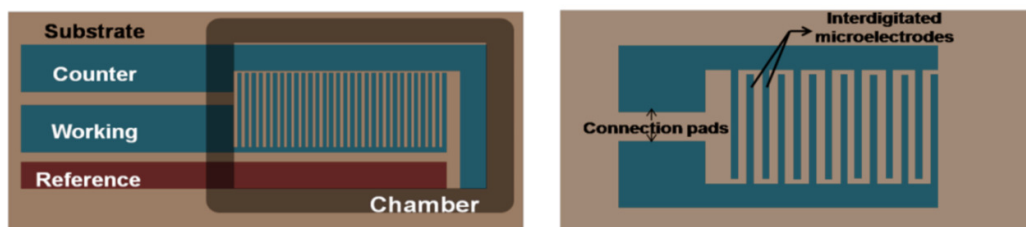


Fig. 1: Schematic diagram of IDME systems: (a) A 3-electrode system; (b) a 2-electrode system.

Photolithography is one of the most widely used fabrication techniques around the globe. This technique is used to transfer a computer-generated pattern onto a substrate [Sun et al. 2008]. Here, a film of photoresist is spin-coated onto the substrate and exposed to UV light through a photolithographic mask; the light exposure transfers the desired pattern to the photoresist. Depending on whether the resist material is “positive” or “negative”, the photoresist is developed by washing off the UV-exposed or unexposed regions. When the substrate is subjected to chemicals, the photoresist would protect the surface below it and thus transfer the pattern to the substrate. Lift-off technique is also used in photolithography to fabricate metal electrodes in such devices [Arya et al. 2010]. This technique comprises of a process flow which includes thermal oxidation over Si wafer, application, exposure and patterning of photoresist, metallization and lift-off of photoresist as depicted in Fig. 2.

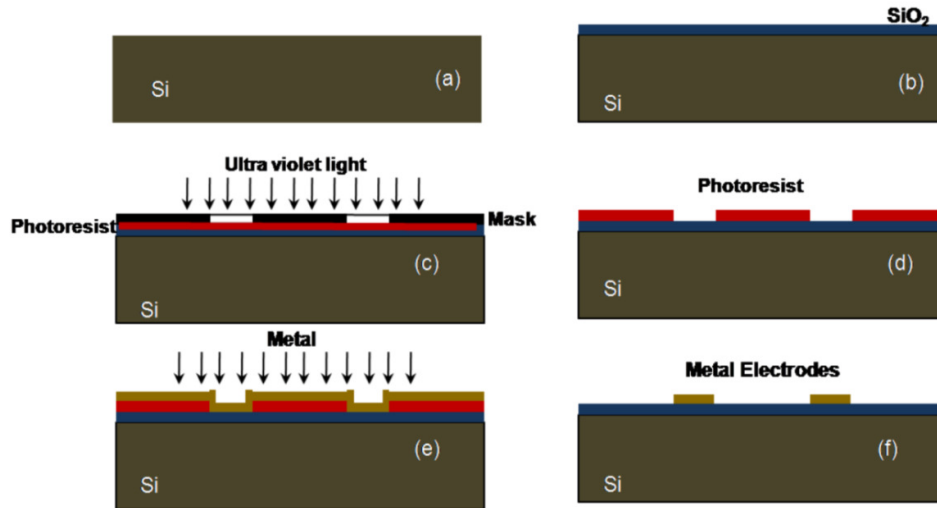


Fig. 2: Device fabrication process flow: (a) RCA clean Si wafer, (b) thermal oxidation to SiO₂ as an insulation layer, (c) apply, expose and pattern photoresist, (d) patterned photoresist, (e) deposit metal using electron beam (e-beam) evaporator or thermal evaporator, (f) lift-off photoresist to get patterned metal electrodes.

Carbohydrate and Protein Sensing

The LOC based impedance studies have been a promising approach for qualitative and quantitative estimation of carbohydrate and protein sensing since last few years [Mok et al. 2014; Choi et al. 2011].

Glucose biosensors are one of the earliest biosensors developed to perform on electrochemical principles and quantify glucose content in different samples. Bio-electrical analysis of carbohydrates has emerged as a potential domain finding magnitude of applications in genomic, bio-medical and food quality assessment based studies due to the huge impact on plant and animal physiology. The impedance spectroscopy by electrical measurement of glucose solutions has been flourished as a very promising technique in recent years due to the novel point-of-care miniaturized glucose monitoring systems [Kim et al. 2015; Wang 2008; Yoon 2011; Olarte et al. 2014; Zhou et al. 2009; Joshi et al. 2005; Greenebaum 2006; Raicu and Popescu 2008]. Glucose in different base solutions exhibits very interesting electrical characteristics for its particular structure and polarization effect. Such electrical properties depend on the polarity of the base solvents and also on the compositional concentration of glucose in the solution [Tura 2008; Tura et al. 2007; Chakraborty et al. 2015]. In recent years, the non-enzymatic sensing of glucose has been proved to be a more comprehensive approach than the general enzyme labelled glucose sensing due to its superior sensitivity, compactness and cost effectiveness.

In case of protein sensing the change in capacitance and impedance as a result of the molecular linkage reactions in an immunoassay of the adsorbed layer on the surface of an electrode or a Metal-Oxide-Semiconductor (MOS) transistor is monitored. Recently, there are few reports available on developing the immunoassay coupled with the existing well matured CMOS technology to enhance detection of signals which originate from the immunoassay process [Ghafar-Zadeh et al. 2009]. Another recent extensive analysis demonstrates direct protein sensing with a critical point of view and promotes the enzyme-linked immunosorbent assay (ELISA) as a more reliable approach in terms of selectivity [Daniels and Pourmand 2007].

For the label-free electronic detections, several impedance based studies have been executed till date with a varying rate of success. A recent comparative analysis describes the label-free protein sensing with a critical outlook and suggests that the classical enzyme-linked immunosorbent assay (ELISA) is preferable on the basis of selectivity [Daniels and Pourmand 2007].

Bacteria Detection

Point of care detection of bacteria has got immense importance in recent times and has become an indispensable domain of research due to the threat on public health from pathogenic bacterial diseases [Gan et al. 2011; Tang et al. 2014; Borghol et al. 2010; Wang et al. 2012]. Conventional processes such as the use of certain agar media for isolating and counting the bacterial cells in the medium, are time consuming and laborious. Hence, the recent decade has witnessed, some dramatic aspects of the impedance based technique attributed to this domain. The recent developments in micro-fabrication technologies mark the comprehensive use of microelectrodes for impedance monitoring and thereby, miniaturizing the impedance microbiology into a chip [Wang et al. 2012]. The biosensors for bacteria sensing are classified into four different categories depending upon the types of bio-receptors: the antibody-based sensors, nucleic acid-based sensors, bacteriophage-based sensors and the lectin-based sensors. In micro-scale impedimetric bacteria sensing devices, antibodies relevant to specific antigens are immobilised on the electrode surface. The general methods for such immobilization, includes the physical adsorption, self-assembled monolayer (SAM) and the formation of biotin-streptavidin system. SAM formation, however, is the most widely used technique for electrode surface modifications and has been exploited to modify electrode surfaces for monitoring cell behavior in bio-analytical measurements [Borghol et al. 2010]. Fig. 3 illustrates the immobilization of antigens on an electrode surface by forming self-assembled monolayer, in presence of mercaptoacetic acid (MACA) and a stable intermediate acyl amino ester generated by EDC and NHS.

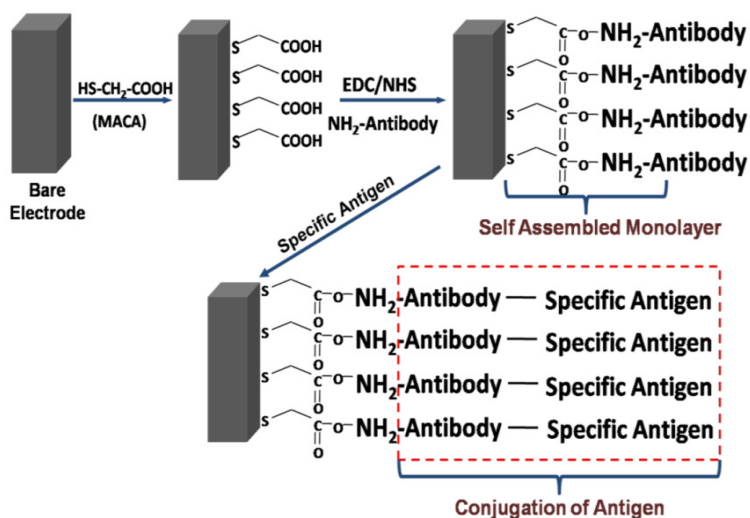


Fig. 3: Schematic diagram of the sample attachment on an electrode surface through SAM formation.

Digital Micro-fluidics in Bio-sensing

Micro-fluidics has many salient advantages including the capability of multiplexing and automated functioning, sample and reagent volume in μ -litre to nano-litre range and precise digital control [Fair 2007; Dutse and Yusof 2011]. Such features are explicitly exploited to design hand-held impedance based biosensors for different types of detections.

Microfluidics is basically the science of designing, manufacturing, and formulating devices and processes to control and manipulate very low volumes of fluid. The prime goal of the bio-microfluidic chips is to integrate several bio-electrical and bio-chemical analyses onto one single platform and establish that platform as a micro-total-analysis-system (μ TAS) to attain enhanced versatility [Su and Chakraborty 2004]. Continuous-flow microfluidics, also referred to as analog microfluidics, is based on the actuation of liquid flow mainly by a pressure gradient. However, it has limitations over complex fluid manipulations and unavoidable shear flow and diffusion in micro-channels creates a considerable probability of inter-sample contamination.

In digital microfluidics, movement of a single droplet is controlled by applying voltage on the micro-electrodes. Electrowetting-on-dielectric (EWOD) and dielectrophoresis (DEP) are the two most general electrical methods for droplet actuation [Zeng and Korsmeyer 2004]. Electrowetting is the phenomenon in which the contact angle between the solid electrode and liquid electrolyte alters on application of an electric field. EWOD is based on low-frequency AC or DC voltages. On the other hand, dielectrophoresis is defined as the exertion of electrical force on a dielectric particle, subjected to a non-uniform electric field and depends upon high frequency AC voltages. In case of DEP actuation, a major problem is attributed to Joule heating, which is virtually eliminated in EWOD actuation due to the presence of dielectric layer covering the electrodes. In EWOD actuation, the interfacial energy, generated due to the electric pressure, is directly controlled by the DC electric fields [Su and Chakraborty 2004; Zeng and Korsmeyer 2004]. A basic unit cell of a EWOD based microfluidic system is depicted in Fig. 4.

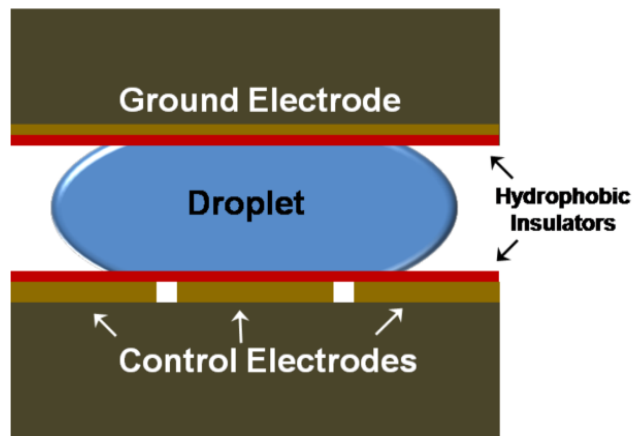


Fig. 4: A basic unit cell of a EWOD based microfluidic system.

A micro-impedance biosensor, thus when integrated with a digital microfluidic system, enables to move, manipulate and sense a specimen droplet under investigation. This class of total analysis systems is suitable for multi-tasking bio-analytical measurements. The working principle of such a system is illustrated schematically in Fig. 5. Specimen droplet under test is transported following microfluidic principles and is placed into the sensing chamber between the micro-electrodes dedicated for sensing the sample.

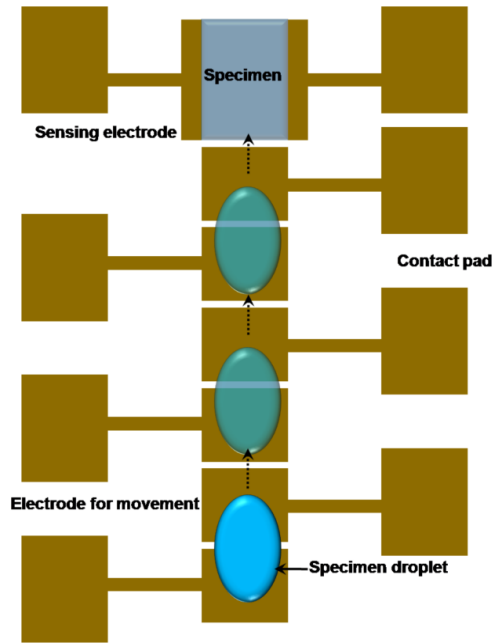


Fig. 5: Schematic representation of a biosensing system integrated with a digital microfluidic system.

Measurement Techniques

Impedance spectroscopy comprising of a couple of schemes including the electrical and the electrochemical impedance spectroscopy, is gaining significant importance for measuring biological samples.

Electrical impedance spectroscopy

The equivalent circuit of the electrical setup, relevant to this measurement scheme, is shown in Fig. 6(a). A couple of capacitors (C_{dl}) and a resistor (R_{sol}) are in series and the third capacitor (C_{sol}) is in parallel with the series combination. C_{dl} arises due to the formation of a double-layer or stern-layer on the electrode surface [Barbieri et al. 2005; Zou et al. 2007]. C_{sol} and R_{sol} represent the capacitance and resistance, respectively, contributed from the medium due to its dielectric nature. In this technique impedance, capacitance and conductance are measured for a frequency range and the change in these parameters is attributed to the change of dielectric constant and conductivity of the specimen under test.

The equivalent impedance of such a circuit is given by

$$|Z| = \frac{|z_1| \cdot |z_2|}{|z_1 + z_2|}$$

where

$$z_1 = R_{sol} - \frac{j}{\pi f C_{dl}}$$

and

$$z_2 = -\frac{j}{2\pi f C_{sol}}$$

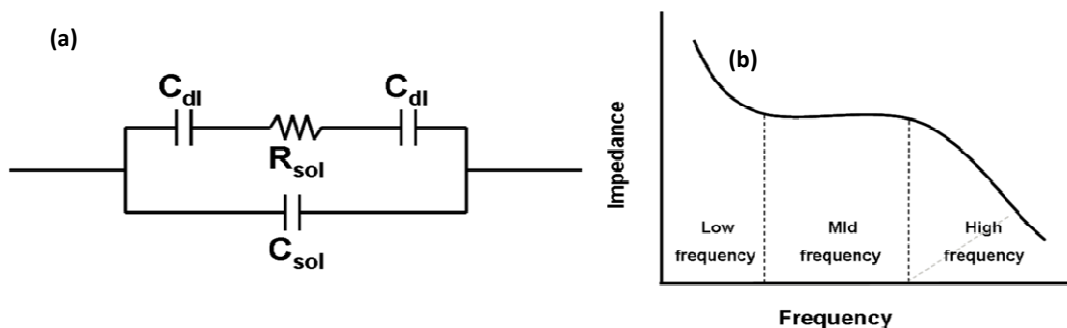


Fig. 6: (a) Equivalent circuit representation of measurement scheme of the electrical impedance spectroscopy technique; (b) typical response of impedance with frequency for such a circuit.

In such a system, as illustrated in figure 6(b), double layer capacitors dominate the total impedance of the circuit at very low frequencies, resistive part dominates in the mid-frequency range, and the dielectric nature of the solution becomes significant at higher frequency range [Ibrahim et al. 2013].

Electrochemical impedance spectroscopy

The electrochemical impedance spectroscopy (EIS) has been effectively used all around the globe to monitor biochemical interactions. It relates the response of an electrochemical cell to small amplitude perturbing sinusoidal voltage signal as a function of frequency [Lisdar and Schäfer 2008; Chattopadhyay et al. 2016; Prodromidis 2010].

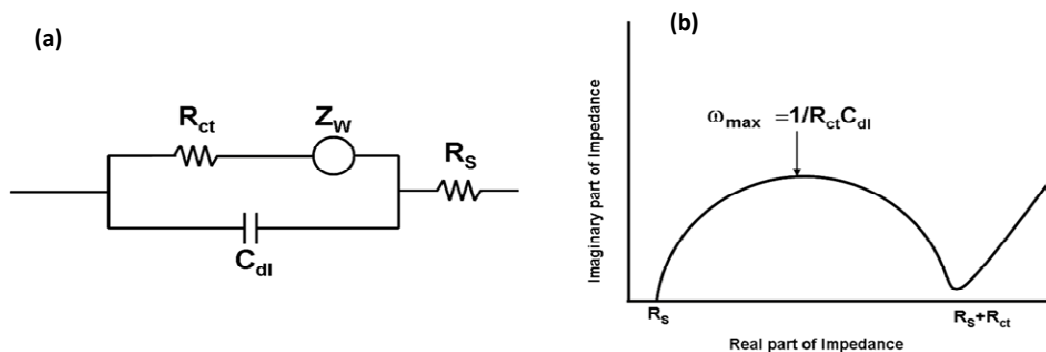


Fig. 7: (a) Equivalent circuit representation of the measurement scheme for electrochemical impedance spectroscopy (EIS) technique; (b) Nyquist plot of such a circuit.

The electrical equivalent circuit relevant to this measuring technique can be represented by Randles circuit consisting of a charge transfer resistance (R_{ct}), the double layer capacitance (C_{dl}), the Warburg impedance (Z_w) and the solution resistance (R_s). To evaluate data, imaginary part of impedance (z'') is plotted against the real part of it (z'), which is also referred to as Nyquist plot as depicted in Fig. 7(b).

The equivalent impedance of the circuit shown in Fig. 7(a) is given by,

$$Z = R_s + [(R_{ct} + Z_w) \parallel (\frac{1}{j\omega C_{dl}})]$$

In most of the cases the Warburg impedance is considered to be negligible for the sake of simplification.

Conclusion

The amperometric glucose enzyme electrode was introduced by L. Clark Jr. in 1962 and widely recognised to be the very first biological sensor. With the multitude of applications of these systems

in bio-medical sciences, a dramatic progress has been witnessed in this domain over the past few decades. The sustained evolution of biosensors has led the development of low cost novel point-of-care diagnosis systems. Development of bio-microfluidic chips dedicated for bio-impedance based sensing has emerged as an indispensable area of bio-medical engineering and stimulated substantial interest from academic, industrial and environmental point of view. In spite of such potential advances, commercialization of these total analysis systems throughout the society is still an issue regarding their social utility. Moreover, level of selectivity and data acquisition for multi-sample detections has not been up to the mark yet. Scientists' community around the globe, however, are trying extensively to address those issues and advance towards more developed bio-microfluidic chips for more accurate, fast and low cost diagnosis which can encompass a larger socio-economic peripheral.

Acknowledgement

Mr. S. Chakraborty likes to acknowledge the Department of Science and Technology (DST), Government of India for providing the Inspire Fellowship to pursue his research. The authors would also like to acknowledge the funding support from DST PURSE, Government of India for developing the Electrical Characterisation Laboratory.

References

- Arslan F, Ustabaş S, & Arslan H (2011). An amperometric biosensor for glucose determination prepared from glucose oxidase immobilized in polyaniline-polyvinylsulfonate film. *Sensors*, 11(8): 8152-8163.
- Arya S K, Chornokur G, Venugopal M, Bhansali S (2010). Dithiobis (succinimidyl propionate) modified gold microarray electrode based electrochemical immunosensor for ultrasensitive detection of cortisol. *Biosens. Bioelectron.*, 25(10): 2296-2301.
- Borghol N, Mora L, Jouenne T, Jaffézic-Renault N, Sakly N, Duncan AC, Chevalier Y, Lejeune P, Othmane A (2010). Monitoring of *E. coli* immobilization on modified gold electrode: A new bacteria-based glucose sensor. *Biotechnol. Bioprocess Eng.* 15(2): 220-228.
- Barbieri O, Hahn M, Herzog A, & Kötz R (2005). Capacitance limits of high surface area activated carbons for double layer capacitors. *Carbon*, 43(6): 1303-1310.
- Cai LT, Chen HY (1999). Electrocatalytic reduction of hydrogen peroxide at platinum microparticles dispersed in a poly (o-phenylenediamine) film. *Sens. Actuators, B*, 55(1): 14-18.
- Chakraborty S, Das C, Saha R, Das A, Bera NK, Chattopadhyay D, Karmakar A, Chattopadhyay D, Chattopadhyay S (2015). Investigating the quasi-oscillatory behaviour of electrical parameters with the concentration of D-glucose in its aqueous solution at room temperature by employing impedance spectroscopy technique. *J Electr Bioimp.*, 6(1): 10-17.
- Chattopadhyay S, Chakraborty S, Das C, Saha R (2016). Recent Progresses on Micro-and Nano-Scale Electronic Biosensors: A Review, In *Nanospectrum: A Current Scenario*; Chakraborty, S.; Mukherjee, P.; Khan, G.G.; Adhikary, A.; Patra, P.; Bal, J. K. (Eds.); Allied Publishers Pvt. Ltd: India, pp. 19-40.
- Chen KI, Li BR, Chen YT (2011). Silicon nanowire field-effect transistor-based biosensors for biomedical diagnosis and cellular recording investigation. *Nano Today*, 6(2): 131-154.
- Choi JH, Kim H, Choi JH, Choi JW, Oh BK (2013). Signal Enhancement of Silicon Nanowire-Based Biosensor for Detection of Matrix Metalloproteinase-2 Using DNA-Au Nanoparticle Complexes. *ACS Appl. Mater. Interfaces*, 5(22): 12023-12028.
- Choi S, Goryll M, Sin LYM, Wong PK, Chae J (2011). Microfluidic-based biosensors toward point-of-care detection of nucleic acids and proteins. *Microfluid. Nanofluid.*, 10(2): 231-247.

- Daniels JS, Pourmand N (2007). Label-free impedance biosensors: Opportunities and challenges. *Electroanalysis*, 19(12): 1239-1257.
- Dutse SW, Yusof NA (2011). Microfluidics-based lab-on-chip systems in DNA-based biosensing: An overview. *Sensors*, 11(6): 5754-5768.
- Ebrahimi B, Shojaosadati SA, Daneshgar P, Norouzi P, Mousavi SM (2011). Performance evaluation of fast Fourier-transform continuous cyclic-voltammetry pesticide biosensor. *Anal. Chim. Acta*, 687(2): 168-176.
- Fair RB (2007). Digital microfluidics: is a true lab-on-a-chip possible?. *Microfluid. Nanofluid.* 3(3): 245-281.
- Fraden J (2004). *Handbook of modern sensors: physics, designs, and applications*. Springer Science & Business Media.
- Gan M, Su J, Wang J, Wu H, Chen L (2011). A scalable microfluidic chip for bacterial suspension culture. *Lab Chip*, 11(23): 4087-4092.
- Gao ZD, Qu Y, Li T, Shrestha NK, Song YY (2014). Development of Amperometric Glucose Biosensor Based on Prussian Blue Functionized TiO₂ Nanotube Arrays, *Sci. Rep.* 4.
- Garjonyte R, Malinauskas A (1999). Amperometric glucose biosensor based on glucose oxidase immobilized in poly (o-phenylenediamine) layer. *Sens. Actuators, B*, 56(1): 85-92.
- Ghafari-Zadeh E, Sawan M, Therriault D (2009). CMOS based capacitive sensor laboratory-on-chip: a multidisciplinary approach. *Analog Integr. Circuits Signal Process.* 59(1): 1-12.
- Greenebaum B, Barnes FS. (Eds.). (2006). *Bioengineering and Biophysical Aspects of Electromagnetic Fields*. CRC press.
- Ibrahim M, Claudel J, Kourtiche D, Nadi M (2013). Geometric parameters optimization of planar interdigitated electrodes for bioimpedance spectroscopy. *J Electr Bioimp.* 4(1): 13-22.
- Islam K, Jang, YC, Chand R, Jha SK, Lee HH, Kim YS (2011). Microfluidic Biosensor for β -Amyloid (1-42) Detection Using Cyclic Voltammetry. *J. Nanosci. Nanotechnol.* 11(7): 5657-5662.
- Jha SK, Topkar A, D'Souza SF (2008). Development of potentiometric urea biosensor based on urease immobilized in PVA-PAA composite matrix for estimation of blood urea nitrogen (BUN). *J. Biochem. Biophys. Methods*, 70(6): 1145-1150.
- Joshi PP, Merchant SA, Wang Y, Schmidtke DW (2005). Amperometric biosensors based on redox polymer-carbon nanotube-enzyme composites. *Anal. Chem.* 77(10): 3183-3188.
- Kim G, Moon JH, Moh CY, Lim JG (2015). A microfluidic nano-biosensor for the detection of pathogenic Salmonella. *Biosens. Bioelectron.* 67: 243-247.
- Kim NY, Adhikari KK, Dhakal R, Chuluunbaatar Z, Wang C, Kim ES (2015). Rapid, Sensitive, and Reusable Detection of Glucose by a Robust Radiofrequency Integrated Passive Device Biosensor Chip. *Sci. Rep.* 5.
- Krajewska A, Radecki J, Radecka H (2008). A voltammetric biosensor based on glassy carbon electrodes modified with single-walled carbon nanotubes/hemoglobin for detection of acrylamide in water extracts from potato crisps. *Sensors*, 8(9): 5832-5844.
- Lee SJ, Lee SY (2004). Micro total analysis system (μ -TAS) in biotechnology. *Appl. Microbiol. Biotechnol.* 64(3): 289-299.
- Li J, Li S, Yang CF (2012). Electrochemical biosensors for cancer biomarker detection. *Electroanalysis*, 24(12): 2213-2229.
- Lisdat F, Schäfer D (2008). The use of electrochemical impedance spectroscopy for biosensing. *Anal. Bioanal. Chem.* 391(5): 1555-1567.

- Long F, Zhu A, Shi H (2013). Recent advances in optical biosensors for environmental monitoring and early warning. *Sensors*, 13(10): 13928-13948.
- Lu YY, Huang JJ, Huang YJ, Cheng KS (2013). Cell growth characterization using multi-electrode bioimpedance spectroscopy. *Meas. Sci. Technol.* 24(3): 035701.
- Ma H, Wallbank RW, Chaji R, Li J, Suzuki Y, Jiggins C, Nathan A (2013). An impedance-based integrated biosensor for suspended DNA characterization. *Sci. Rep.* 3.
- Mir M, Homs A, Samitier J (2009). Integrated electrochemical DNA biosensors for lab-on-a-chip devices. *Electrophoresis*, 30(19): 3386-3397.
- Mitra A, Ignatovich F, Novotny L (2012). Real-time optical detection of single human and bacterial viruses based on dark-field interferometry. *Biosens. Bioelectron.* 31(1): 499-504.
- Mok J, Mindrinos MN, Davis RW, Javanmard M (2014). Digital microfluidic assay for protein detection. *Proc. Natl. Acad. Sci.* 111(6), 2110-2115.
- Norouzi P, Faridbod F, Nasli-Esfahani E, Larijani B, Ganjali MR (2010). Cholesterol biosensor based on MWCNTs-MnO₂ nanoparticles using FFT continuous cyclic voltammetry. *Int. J. Electrochem. Sci.* 5(7): 1008-1017.
- Prodromidis MI (2010). Impedimetric immunosensors—A review. *Electrochim. Acta.* 55(14): 4227-4233.
- Olarte O, Barbe K, Van Moer W, Van Ingelgem Y (2014). Glucose characterization based on electrochemical impedance spectroscopy. In *Instrumentation and Measurement Technology Conference (I2MTC) Proceedings, 2014 IEEE International* (pp. 833-837). IEEE.
- Raicu V, Popescu A (2008). *Integrated molecular and cellular biophysics*. London, UK: Springer.
- Saeedfar K, Heng LY, Ling TL, Rezayi M (2013). Potentiometric urea biosensor based on an immobilised fullerene-urease bio-conjugate. *Sensors*, 13(12): 16851-16866.
- Singh A, Poshtiban S, Evoy S (2013). Recent advances in bacteriophage based biosensors for food-borne pathogen detection. *Sensors*, 13(2): 1763-1786.
- Su F, Chakrabarty K (2004). Module placement for fault-tolerant microfluidics-based biochips. In *ACM Transactions on Design Automation of Electronic Systems (TODAES)* (Vol. 11, No. 3, pp. 682-710). ACM.
- Sun K, Ramgir N, Bhansali S (2008). An immunoelectrochemical sensor for salivary cortisol measurement. *Sens. Actuators, B*, 133(2): 533-537.
- Tang Y, Gan M, Xie Y, Li X, Chen L (2014). Fast screening of bacterial suspension culture conditions on chips. *Lab Chip*, 14(6): 1162-1167.
- Tomčik P (2013). Microelectrode arrays with overlapped diffusion layers as electroanalytical detectors: theory and basic applications. *Sensors*, 13(10): 13659-13684.
- Tura A (2008). Reply to comment on experimental methods and conclusions of impedance spectroscopy of solutions at physiological glucose concentrations by A. Caduff, MS Talary, Y. Feldman. *Biophys. Chem.* 132(2): 167-168.
- Tura A, Sbrignadello S, Barison S, Conti S, Pacini G (2007). Impedance spectroscopy of solutions at physiological glucose concentrations. *Biophys. Chem.* 129(2): 235-241.
- Wang J (2008). Electrochemical glucose biosensors. *Chem. Rev.* 108(2): 814-825.
- Wang Y, Xu H, Zhang J, Li G (2008). Electrochemical sensors for clinic analysis. *Sensors*, 8(4): 2043-2081.

- Wang Y, Ye Z, Ying Y (2012). New trends in impedimetric biosensors for the detection of foodborne pathogenic bacteria. *Sensors*, 12(3): 3449-3471.
- Wilson JS (2004). *Sensor technology handbook*. Elsevier.
- Yeh CH, Chang YH, Chang TC, Lin HP, Lin YC (2010). Electro-microchip DNA-biosensor for bacteria detection. *Analyst*, 135(10): 2717-2722.
- Yoon G (2011). Dielectric properties of glucose in bulk aqueous solutions: Influence of electrode polarization and modeling. *Biosens. Bioelectron*, 26(5): 2347-2353.
- Zeng J, Korsmeyer T (2004). Principles of droplet electrohydrodynamics for lab-on-a-chip. *Lab Chip*, 4(4): 265-277.
- Zhang JY, Wang L, Li B (2009). Design of low-offset low-power CMOS amplifier for biosensor application. *J. Biomed. Sci. Eng.* 2(7): 538.
- Zhou YG, Yang S, Qian QY, Xia XH (2009). Gold nanoparticles integrated in a nanotube array for electrochemical detection of glucose. *Electrochem. Commun.* 11(1): 216-219.
- Zou Z, Kai J, Rust MJ, Han J, Ahn CH (2007). Functionalized nano interdigitated electrodes arrays on polymer with integrated microfluidics for direct bio-affinity sensing using impedimetric measurement. *Sens. Actuators, A*, 136(2): 518-526.

Partially Polarized Fractional Quantum Hall Effect

Biplab Kumar Mandal¹ & Dwipesh Majumder²

¹Department of Physics, A B N Seal College, Cooch Behar

²Department of Physics, IEST, Shibpur, Howrah

Abstract

In this article we have addressed the partially polarized state at $\nu = 2/5$ filling fraction using the recent developed method Chern-Simons Composite Fermion theory. We have seen that the partially polarized state occurs due to the asymmetric interaction between the up-spin and down spin.

Publication History: Received: 10th August, 2016; Accepted: 19th August, 2016

Introduction

An applied magnetic field, \mathbf{B} , perpendicular to the current of a current carrying conductor leads to a voltage drop along the direction perpendicular to both the current and magnetic field. This phenomenon was discovered by E. Hall in the year 1879, and is known as Hall Effect (1). The Hall resistance defined as the ratio between the Hall voltage and the current is observed to be proportional to the applied magnetic field. Drude formula (2) based on the classical electrodynamics for Hall resistance is given by $R_H = B / (\rho e c)$, where ρ is the carrier density, e is the charge of carrier, and c is the velocity of light. The measurement of Hall resistance is thus a standard technique to determine carrier density and the sign of the charge of the carrier.

Industrial development of the semiconductor device made it possible to realize quasi two dimensional (2D) electron systems in semiconductor heterostructures. The Hall measurement in such a device by Von Klitzing, Dorda, and Pepper (3) in 1980 at low temperatures provided a remarkable macroscopic quantum phenomenon-quantization of Hall resistance. The hall resistance quantizes at universal values given by $R_H = \frac{h}{e^2 \nu}$, where ν is an integer, and at the same time, the diagonal resistance exhibit sharp minimum which goes to zero as temperature is lowered. This universality is because of the topological (8) nature of this remarkable quantum liquid. The quantization occurs at integer filling factor ($\nu = \nu$) which are the number of fully filled Landau levels (LLs) formed by the application of magnetic field perpendicular to the plane of the 2D system. This phenomenon is known as integer quantum Hall effect (IQHE). The electron fluid is incompressible which is characterized by the single particle excitation gap due to completely filled LLs.

The effect of Coulomb interaction between electrons in IQHE is perturbative for certain properties and does not have any effect on the quantization. On the other hand, the role Coulomb interaction is crucial for the quantization at the fillings ($\nu < 1$). This was realized by the discovery of fractional quantum Hall effect (FQHE) by Tsui, Stormer, and Gossard (4) in higher mobility sample where the plateau occurs at the filling factor $1/3$ with the quantized value of Hall resistance $3h/e^2$. The FQHE is further observed at several other filling factors (more than 100 in number) with the quantized Hall resistance $\frac{h}{\nu e^2}$ at some rational fraction ν (5,6). Despite the apparent similarity of experimental results, the physical mechanism responsible for the production of excitation gap to obtain IQHE and FQHE are quite different. While the excitation gap in IQHE is due to the single

particle energy spectra, the strong correlation between electrons is responsible for excitation gap in FQHE. Laughlin explain the state as a one component plasma and proposed a wave function for some particular filling fractions (7). However a unified understanding of all the observed fractions in the lowest Landau level given by the sequence of states $\nu = n/(2np \pm 1)$ was achieved by the composite fermions picture (9), in which each electron captures an even number of quantized magnetic vortices to form a composite fermions (CF)

Polarization in FQHE

In sufficiently high magnetic fields, the low-energy states are of course fully spin polarized, that is, the spin is effectively frozen. However, the Zeeman energy (E_z) is rather small in GaAs compared to the cyclotron energy ($\hbar\omega_c$), both because of small g factor and low band mass (The Zeeman energy is defined as the energy required to flip the spin of an electron). Therefore, it may sometimes be energetically favorable for a finite fraction of particles to reverse their spins, provided they can gain more in interaction energy and un-polarized FQHE states are possible in general. Now we consider the state $\nu = n/(2np \pm 1)$, which maps to CFs at filling n-number of Λ -levels out of that $n \uparrow$ number of occupied spin-up CF Landau bands and $n \downarrow$ the number of occupied spin-down CF Landau bands, ie $n = n \uparrow + n \downarrow$. So the polarization is $\frac{n \uparrow - n \downarrow}{n \uparrow + n \downarrow}$, Kukulshkin and other (10) measured the polarization of different filling fraction, and got different polarized states at filling fractions except $\nu = \frac{1}{q}$ where q is odd integer.

CF picture explains all most all the polarized states. $\nu = \frac{1}{q}$ maps into one occupied Λ -level of CF, so there is no option for different filled Λ -level. In figure-1, we have shown explicitly the polarized states of $\nu = 2/5$ fraction.

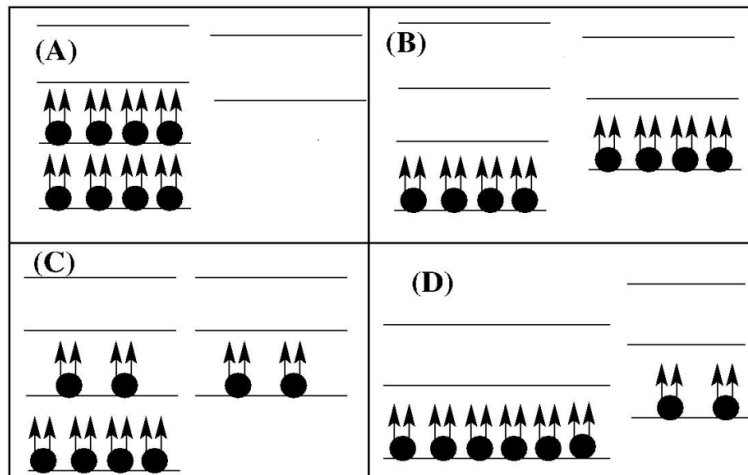


Fig. 1: In each block left panel represent up-spin Λ -level, and right panel represent the down-spin Λ -level. The FQHE filling fraction of a electron $\nu = 2/5(2/3)$ maps into n=2 filled Λ -level (CF Landau level) (A). Fully polarized state, two spin-up Λ -level are filled (B) un-polarized state, one spin-up Λ -level filled and one spin-down Λ -level filled (C) partially polarized Muthé’s density wave state one spin-up Λ -level filled one spin-up Λ -level + one spin-down Λ -level half filled (D) partially polarized state, one spin-up Λ -level filled and one spin down Λ -level filled, but the density of state for the up-spin Λ -level and spin-down Λ -level are different in such a way that $\nu = 1/2$

Block (A) and (B) of the figure explain the polarized and un-polarized states. This picture fail to explain the partially ($\nu = 1/2$) states at $\nu = 2/5$. This puzzle remains unsolved, except one

attempt by Murthy (11), in which he explain the partially polarized state as a partially polarized density wave states by considering the combination of one spin-up Λ -level filled and one spin-up Λ -level + one spin down Λ -level half filled (Block(C) of figure-1). Recent years QHE in grapheme become very popular (12, 13, 14). In this SU (4) symmetric states Regnault (14) proposed a wave function as a extension of the Laughlin state in the multi component plasma state. Also there is a proposed wave function based on the Composite-Fermionic Cherrn-Simson (CF-CS) theory, which is identical with previous wave function if we restrict the CF-CS theory in the lowest Λ -level. This picture also applicable in our present SU(2) system (14). Basic physics in that absorption of flux quanta by the electrons at spin-up Λ -levels and down-spin Λ -levels are different as the interaction between two are different in strength.

Calculation Procedure

Since the spherical geometry does not have any edge, it is beneficial to study the bulk properties of FQHE with small number of electrons. We consider correlated N number of electrons move on the two dimensional surface of a sphere (15) under the influence of a radial magnetic field B. The radial magnetic field, can be thought to emanate from a ‘magnetic monopole’ of strength Q at the centre , which produces a total magnetic flux of $2Q\Phi_0$ through the surface of the sphere. Monopole charge Q must be an integer or half integer, in accordance with Dirac’s quantization condition (16).

Position of an electron on the surface of the sphere is the angular co-ordinates $\Omega (\theta, \phi)$, it is convenient to use complex co-ordinates (u, v) instead of (θ, ϕ)

$$\begin{aligned} u &= \cos(\theta/2) \exp(-i\phi/2) \\ v &= \sin(\theta/2) \exp(i\phi/2) \end{aligned} \tag{1}$$

The single particle basis is known as monopole harmonics which is given by (17)

$$Y_{Q,m,m}(\Omega) = N_{Qnm} e^{iq\phi} u^{Q+m} v^{Q-m} \sum_{s=0}^n (-1)^s \binom{n}{s} \binom{2Q+n}{Q+n-m-s} (v^*v)^{n-s} (u^*u)^s.$$

According to the CF theory, the ground state wave function for filling factor $\nu = \frac{n}{(2pn+1)}$ is given by

$$\Psi_\nu(\Psi_1, \Psi_2, \dots, \Psi_N) = P_{LLL} J \Phi_n(\Psi_1, \Psi_2, \dots, \Psi_N)$$

Where Φ_n is a Slater determinant when N CFs completely fill n number of Λ -levels formed due to the effective flux, the Jastrow factor

$$J = \sum_{i < j}^N (u_i v_j - v_i u_j)^{2p}$$

Representing 2p number of flux attached to each CF, and P_{LLL} represents the projection into the lowest LL. We have used the Jain and Kamilla’s (18, 19) beautiful method of projection on the lowest LL to calculate the ground state energy

$$E_g = \frac{\langle \Psi_\nu | H | \Psi_\nu \rangle}{\langle \Psi_\nu | \Psi_\nu \rangle} - \frac{\epsilon^2}{2\epsilon R}$$

where the last term describe the energy for positive background, ϵ is the dielectric constant of the medium, $R = \sqrt{Q}$ is the radius of the sphere in unit of the magnetic length l, the Hamiltonian of the system is given by $H = \frac{\epsilon^2}{\epsilon} \sum_{i < j} \frac{1}{r_{ij}}$, where the distance between the particles r_{ij} is taken to be the chord distance

$$r_{ij} = 2R |u_i v_j - v_i u_j|.$$

Wave function for the Chern-Simons-CFs

Let us consider as CF-CS state in which up-spin Λ -levels formed by capturing $2k_1$ -number of flux quanta and down-spin Λ -levels formed by capturing $2k_2$ -number of flux quanta and the magnetic field seen one type of spin CF to other type is m flux quanta.

The variational wave function for the state is proposed by Mandal and coworker (12) and is given by

$$\Psi_{k_1 k_2 m} = P_L \Phi_{n_1}(\Omega_1^1, \dots, \Omega_{N_1}^1) \Phi_{n_2}(\Omega_1^2, \dots, \Omega_{N_2}^2) \times J_{11} J_{22} J_{21}$$

where Φ_{n_i} is the Slater determinant of n_i filled Λ -level CFs, $\Omega_1, \dots, \Omega_N$ are the positions of CFs on the spherical surface, upper index indicate the different species of CFs and Jastrow factor is given by

$$J_{12} = \sum_{i,j}^{N_1, N_2} (u_i^{(1)} v_j^{(2)} - u_j^{(2)} v_i^{(1)})^m$$

$$J_{\alpha\alpha} = \sum_{i < j}^{N_\alpha} (u_i^{(\alpha)} v_j^{(\alpha)} - u_j^{(\alpha)} v_i^{(\alpha)})^{2k_\alpha}$$

Results and Conclusion

In the CS-CF picture partially polarized $2/5$ filling fraction is represented in block (D), Figure-1. The flux attachment in the up-spin Λ -levels is $2k_1 = 2$ and flux attachment in the down-spin Λ -levels is $2k_2 = 6$. So the degeneracy per unit area of the spin-up state is higher than the degeneracy of down-spin Λ -level. The inter Λ -level interaction is different from that of intra Λ -level interaction.

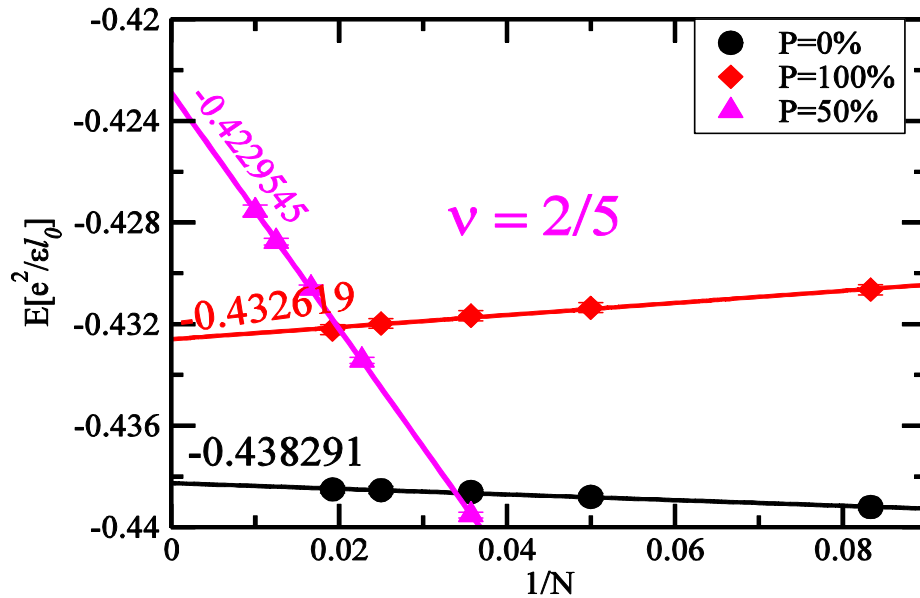


Fig 2: Finite number of particles cannot give the thermodynamic nature, so to get the thermodynamic properties we have linearly extrapolated $1/N \rightarrow 0$, energy expressed in unit $\frac{e^2}{\epsilon l_0}$, where ϵ is the permittivity of the medium and $l_0 = \sqrt{\hbar c / eB}$ is the magnetic length.

We have calculated the ground state energy for the partially polarized $(\gamma = \frac{1}{2}) \nu = 2/5$ state for finite number of particles using CS-CF wave function. To get the thermodynamic limit we have plotted inverse of the particle versus the ground state energy per particle in Figure-2. The lowest

energy state is the fully polarized state, where as the partially polarized state is in the higher energy than the un-polarized state. This is may be due to the asymmetry of inter- particle and intra-particle interaction. There are several similar partially polarized states for different filling fractions remain to study. It will be more clear picture of these states after investigation of further study of such other states, which requires huge computational power. We have these issues for future studies.

Acknowledgments

We would like to thank Department of Physics, IEST for providing us the computational facility.

References

- Edwin Hall. "On a New Action of the Magnet on Electric Currents". American Journal of Mathematics, Vol.2, 287-92 (1879).
- Charles Kittel Introduction to Solid State Physics, 8th Edition, Springer Verlag, New York (1990)
- K.V. Klitzing, G. Dorda, and M. Pepper, Phys. Rev. Lett. 45, 494 (1980).
- D. C. Tsui, H. L. Stormer, and A. C. Gossard, Phys. Rev. Lett. 48, 1559 (1982).
- H. L. Stormer, Rev. Mod. Phys. 71,875 (1999).
- D. C. Tsui, Rev. Mod. Phys. 71, 891 (1999).
- R. B. Laughlin, Phys. Rev. Lett. 50, 1395 (1983).
- S. Girvin, R. E. Prang , S. Girvin, Editor, Quantum Hall Effect, Springer Verlag, New York.
- J. K. Jain, Phys. Rev. Lett. 63, 199(1989).
- I. L . Kukuskin, K.V. Klitzing , and K. Eberl, Phys. Rev. Lett. 82, 3665 (1999).
- Ganpathy Murthy, Phys. Rev. Lett. 84, 350 (2000).
- Sanhita Modak, Sudhansu S. Mandal, and K. Sengupta, Phys. Rev. B 84,165118 (2011).
- C Toke and J. K. Jainj. Phys: Condens. Matter 24 335601 (2012), Phys. Rev. B 76, 081403(R) (2007).
- R. de Gail, N. Regnault, and M. O. Goerbig, Phys. Rev. B 77 165310 (2008).
- F. D. M. Haldane, Phys. Rev. Lett. 51, 605 (1983).
- P. A. M. Dirac, Proc. R. Soc. London, Ser. A 133, 60 (1931).
- T. T. Wu and C. N. Yang, Nucl. Phys. B 107, 365 (1967): T. T. Wu and C. N. Yang Phys. Rev. D 16, 1018 (1977).
- J. K. Jain, and K. K. Kamilla, Phys. Rev. B 55, R4895 (1977): Int. Journal of Mod. Phys. B 11,2621 (1977).
- D. Majumder and S. S. Mandal, Phys. Rev. B 90,155310 (2014)

Note on Some Classes of Generalized Continuous Functions

Piyali Mallick¹ and Lakshmi Narayan De²

¹Department of Mathematics, Bethune College, Kolkata

²Department of Mathematics, A.B.N.Seal College, Cooch Behar

Abstract

In this paper attempt has been made to study some generalized types of continuous functions and to characterize \mathcal{E} -continuity in a topological space having certain properties.

Key words: \mathcal{E} -continuity, quasicontinuity, B -continuity, B^* -continuity, β -continuity, Baire property of a set, categorically closed topological space.

Publication History: Received: 10th August, 2016; Accepted: 19th August, 2016

Introduction and Preliminaries

In recent years a considerable amount of research involving many types of generalized continuity has been studied. The notion of \mathcal{E} -continuity was introduced by M. Matejdes in [3]. As a particular case of \mathcal{E} -continuity we obtain quasicontinuity [2], B -continuity [4], B_r -continuity [4], B^* -continuity [1], β -continuity [7] etc.

Among the papers let us mention the topical survey of T. Neubrunn [5], giving comprehensive information concerning quasicontinuity. In what follows X, Y denote topological spaces. For a subset A of a topological space ClA and $IntA$, the closure and interior of A respectively. Throughout the paper R is the space of real numbers with the usual topology, N stands for the set of natural numbers and \emptyset denotes the empty set. For a Lebesgue measurable set $A(\subseteq R)$, $d(A, x)$ denotes the density of A at $x \in R$.

A subset A of X is said to have the property of Baire[6] if it can be represented in the form $A = (G \setminus P) \cup Q$, where G is open and P, Q are sets of first category in X . Let \mathcal{E} be a non empty family of non empty subsets of X . A function f is said to be \mathcal{E} -continuous at a point $x \in X$ [3] if for each open neighbourhood U of X and each open neighbourhood V of $f(x)$ there is a set $E \in \mathcal{E}$ such that $E \subseteq U$ and $f(E) \subseteq V$. Denote by $\mathcal{E}(f)$, the set of all points at which f is \mathcal{E} -continuous. If $\mathcal{E}(f) = X$, f is said to be \mathcal{E} -continuous on X .

Let

$$\mathcal{O} = \{E \subseteq X : E \neq \emptyset \text{ and open in } X\}$$

$$B = \{E \subseteq X : E \text{ is either non empty open or second category with the Baire property}\}$$

$$B_r = \{E \subseteq X : E \text{ is second category with the Baire property}\}$$

$$B^* = \{E \subseteq X : E \text{ is not nowhere dense with the Baire property}\}$$

$$\beta = \{E \subseteq X : E \text{ is not nowhere dense}\}$$

In the case $\mathcal{E} = \mathcal{O}, (= B, = B_r, = B^*, = \beta)$ we have the \mathcal{E} -continuity as the usual notion of quasicontinuity[2],

($= B$ continuity[4], $= B_r$ continuity[4], $= B^*$ continuity[1], $= \beta$ continuity[7] respectively)

By $Q(f), B(f)$ and $B^*(f)$ we denote the sets of all points at which f is quasicontinuous, B -continuous and B^* -continuous respectively. Then $Q(f) \subseteq B(f) \subseteq B^*(f)$.

Definition 1.1 A topological space is said to be categorically closed if every first category set is closed.

The followings are the examples of a categorically closed topological space.

Example 1.2 Consider R with the topology $T = \{A \subseteq R : 0 \in A\} \cup \{\emptyset\}$

Then (R, T) is a categorically closed topological space.

Example 1.3 Consider R with the density topology

$$T^d = \{A \subseteq R : A \text{ is Lebesgue measurable and } d(A, x) = 1 \text{ for each } x \in A\} \cup \{\emptyset\}.$$

Now for the density topology on R , it is clear that a set is first category if and only if the Lebesgue measure of A is zero. Hence (R, T^d) is a categorically closed topological space.

Example 1.4 Let (X, T) be a Baire space and $T^* = \{G \setminus I : G \in T \text{ and } I \text{ is } T\text{-first category}\}$.

Then it is clear that a set $A (\subseteq X)$ is T^* -nowhere dense if and only if it is T -first category. Hence (X, T^*) is a categorically closed topological space.

Proposition 1.5 In a categorically closed topological space the followings are hold.

- i) If G is open and P is first category then $G \setminus P$ is open.
- ii) If $E \in B_r$, then E contains a non empty open set.
- iii) If $E \in B^*$ then E contains a non empty open set.

Proof i): It follows immediately from the definition of a categorically closed topological space.

Proof ii): Let $E \in B_r$. Then E has the Baire property and so $E = (G \setminus P) \cup Q$, where G is open and P, Q are sets of first category. By i) $G \setminus P$ is open. Suppose $G \setminus P = \emptyset$. Then $E = Q$, a first category set which is not true. So $G \setminus P \neq \emptyset$ hence ii) follows.

Proof iii): Let $E \in B^*$. As in the proof of ii), E contains an open set $G \setminus P$. If $G \setminus P \neq \emptyset$, iii) follows. Suppose $G \setminus P = \emptyset$. Then $E = Q$, a first category set and hence closed. Since E is not nowhere dense and closed, E contains a non empty open set and consequently iii) holds.

Main Results

Let $\mathcal{E}_i (i = 1, 2)$ be two non empty families of non empty subsets of X . We define $\mathcal{E}_1 \leq \mathcal{E}_2$ if for every $E_2 \in \mathcal{E}_2$, there is a set $E_1 \in \mathcal{E}_1$ such that $E_1 \subseteq E_2$.

Theorem 2.1 If $f : X \rightarrow Y$ is \mathcal{E}_2 -continuous at $x \in X$ then it is \mathcal{E}_1 -continuous at x where $\mathcal{E}_1 \leq \mathcal{E}_2$.

Proof: Suppose that f is \mathcal{E}_2 -continuous at x . Then for each open neighbourhood U of x and each open neighbourhood V of $f(x)$ there is a set $E_2 \in \mathcal{E}_2$ such that $E_2 \subseteq U$ and $f(E_2) \subseteq V$. Since $E_2 \in \mathcal{E}_2$ and $\mathcal{E}_1 \leq \mathcal{E}_2$, there is a set $E_1 \in \mathcal{E}_1$ such that $E_1 \subseteq E_2$. Then $E_1 \subseteq U$ and $f(E_1) \subseteq V$. So f is \mathcal{E}_1 -continuous at x .

Corollary 2.2 \mathcal{E}_1 -continuity of $f : X \rightarrow Y$ at a point $x \in X$ implies \mathcal{E}_2 -continuity of f at x where $\mathcal{E}_1 \subseteq \mathcal{E}_2$.

It follows immediately from the theorem 2.1 since $\mathcal{E}_1 \subseteq \mathcal{E}_2$ implies $\mathcal{E}_2 \leq \mathcal{E}_1$.

Remark 2.3 $\mathcal{O} \subseteq B \subseteq B^* \subseteq \beta$ and $B_r \subseteq B$. So by the corollary 2.2 quasicontinuity implies B -continuity ([4]), B -continuity implies B^* -continuity ([1]), B^* -continuity implies β -continuity, B_r -continuity implies β -continuity ([7]).

But the converse of these implications is not true which follows from the following examples.

Example 2.4 Let $Y = \{0,1\}$ and $T = \{Y, \phi, \{0\}\}$. Clearly T is a topology on Y .

Define $f : R \rightarrow Y$ by $f(x) = \begin{cases} 1, & x \text{ is rational} \\ 0, & x \text{ is irrational} \end{cases}$

Then f is B -continuous on R but not quasicontinuous on R . (f fails to be quasicontinuous at any irrational point of R)

Example 2.5 Let $f : R \rightarrow R$ be defined by $f(x) = \begin{cases} 1, & x \text{ is rational} \\ 0, & x \text{ is irrational} \end{cases}$

Then f is B^* -continuous on R but not B -continuous. (f fails to be B -continuous at any rational point of R).

Example 2.6

Let X be a first category topological space. Then any constant function $f : X \rightarrow Y$ is quasicontinuous but not B_r -continuous.

Remark 2.7 By ii) and iii) of the proposition 1.5. if X is a categorically closed topological space $\mathcal{O} \leq B_r$ and $\mathcal{O} \leq B^*$ respectively. So by the theorem 2.1 B_r -continuity of $f : X \rightarrow Y$ implies quasicontinuity and B^* -continuity implies quasicontinuity of f .

Remark 2.8 If $\mathcal{O} \leq B_r$, then $\mathcal{O} \leq B$. So in a categorically topological space X , B -continuity of $f : X \rightarrow Y$ implies quasicontinuity of f .

Corollary 2.9 In a categorically closed topological space X , quasicontinuity, B -continuity, B^* -continuity of $f : X \rightarrow Y$ are all equivalent to each other.

Theorem 2.10 $f : X \rightarrow Y$ is \mathcal{E} -continuous if and only if it is either \mathcal{E}_1 -continuous or \mathcal{E}_2 -continuous where $\mathcal{E} = \mathcal{E}_1 \cup \mathcal{E}_2$.

Proof: If f is \mathcal{E} -continuous then it is obvious that either f is \mathcal{E}_1 -continuous or it is \mathcal{E}_2 -continuous.

Again $\mathcal{E}_1 \subseteq \mathcal{E}_1 \cup \mathcal{E}_2$ and $\mathcal{E}_2 \subseteq \mathcal{E}_1 \cup \mathcal{E}_2$.

So by the corollary 2.2 \mathcal{E}_1 -continuity or \mathcal{E}_2 -continuity implies \mathcal{E} -continuity of f .

Remark 2.11 $B = \mathcal{O} \cup B_r$. So by the theorem 2.10, f is B -continuous if and only if it is either quasicontinuous or B_r -continuous.

Theorem 2.11 Let $\{U_\alpha : \alpha \in \Lambda\}$ be an open cover of X . Then $f : X \rightarrow Y$ is \mathcal{E} -continuous if and only if $f|_{U_\alpha}$ is \mathcal{E} -continuous for each $\alpha \in \Lambda$.

Proof: The 'if part' is straight forward. For the 'only if part' suppose that $f|_{U_\alpha}$ is \mathcal{E} -continuous for each $\alpha \in \Lambda$.

Let $x \in X, U$ be an open neighbourhood of x and V be an open neighbourhood of $f(x)$ in Y . Now there is $\alpha \in \Lambda$. such that $x \in U_\alpha$.

Then $U \cap U_\alpha$ is an open neighbourhood of x in U_α . So there is $E \in \mathcal{E}$ such that $E \subseteq U \cap U_\alpha \subseteq U$ and $f(E) \subseteq V$. So f is \mathcal{E} -continuous on X .

Nets

Theorem 3.1 $f : X \rightarrow Y$ is \mathcal{E} -continuous at $x \in X$ if and only if there is a net $\{x_\alpha\}_{\alpha \in D}$ in $\mathcal{E}(f)$ such that $\{x_\alpha\}_{\alpha \in D}$ converges to x in X and $\{f(x_\alpha)\}_{\alpha \in D}$ converges to $f(x)$ in Y .

Proof: Suppose there is a net $\{x_\alpha\}_{\alpha \in D}$ in $\mathcal{E}(f)$ such that $\{x_\alpha\}_{\alpha \in D}$ converges to x in X and $\{f(x_\alpha)\}_{\alpha \in D}$ converges to $f(x)$ in Y .

Let U, V be open neighbourhoods of x in X and $f(x)$ in Y respectively. Then there is $\alpha \in D$ such that $x_\alpha \in U$ and $f(x_\alpha) \in V$. Now $x_\alpha \in \mathcal{E}(f)$. So there is a set $E \in \mathcal{E}$ such that $E \subseteq U$ and $f(E) \subseteq V$. Consequently f is \mathcal{E} -continuous at x .

Converse part is trivial.

Corollary 3.2 $f : X \rightarrow Y$ is B -continuous (B^* -continuous) at $x \in X$ if there is a sequence $\{x_n\}_n$ in $Q(f)$ (respectively in $B(f)$) such that $\{x_n\}_n$ converges to x in X and $\{f(x_n)\}$ converges to $f(x)$ in Y .

It immediately follows from the theorem 3.1 since $Q(f) \subseteq B(f) \subseteq B^*(f)$.

Remark 3.3 The converse of the corollary 3.2 is not true in general.

Let us consider the function f given in the example 2.5. Here $Q(f) = \phi, B(f)$ is the set of all irrationals and $B^*(f) = R$. Then f is B -continuous at any irrational point $x \in R$. But there is no sequence $\{x_n\}_n$ in $Q(f)$ with $\{x_n\}_n$ converges to x and $\{f(x_n)\}$ converges to $f(x)$.

Now f is B^* -continuous at any rational point x . Let $\{x_n\}_n$ be a sequence in $B(f)$ such that $\{x_n\}_n$ converges to x . Then $f(x_n) = 0 \forall n \in N$. So $\{f(x_n)\}$ converges to $0 \neq f(x)$.

If X is a categorically closed topological space, by the corollary 2.9, $B^*(f) \subseteq B(f) \subseteq Q(f)$.

Then by the theorem 3.1, the converse of the above corollary follows.

So from the above corollary and this remark we can say the following.

Corollary 3.4 Let X be a categorically closed topological space. Then $f : X \rightarrow Y$ is B -continuous (B^* -continuous) at $x \in X$ if and only if there is a sequence $\{x_n\}_n$ in $Q(f)$ (respectively in $B(f)$) such that $\{x_n\}_n$ converges to x in X and $\{f(x_n)\}$ converges to $f(x)$ in Y .

References

- Ganguly D K, Mitra C (2000) B^* -continuity and other generalized continuity. Rev. Acad. Canar. Cienc., (Nums. 1-2): 9-17.
- Kempisty S (1932) Sur les fonctions quasicontinues. Fund. Math., 19: 184-197.
- Matejdes M (1987) Sur les selecteurs des multifonctions. Math. Slovaca., 37: 111-124.
- Matejdes M (1994) Continuity of multifunction. Real Anal. Exch., 19(2): 394-413

Neubrunn T(1988-89) Quasicontinuity . Real Anal. Exch., 14(2):259-306

Oxtoby J C (1971) Measure and category, Springer-Verlag, Berlin, 232-235

Popa V, Noiri T(1996-97) On upper and lower β – continuous multifunctions. Real Anal. Exch., 22(1):362-376.

Effect of Selective Atomic Substitution on the Magnetic Field Induced Strain and Entropy Change in $\text{Ni}_{51}\text{Mn}_{35}\text{In}_{14}$ Alloys

Rahul Das

Department of Physics, A. B .N. Seal College, Cooch Behar-736101, India

Email: rahul04ph4004@gmail.com

Abstract

Effect of applied magnetic field on the martensitic transformation at which large magnetic field induced strain (MFIS) and magneto-caloric effect (MCE) occur in Si and Si/Cu substituted $\text{Ni}_{51}\text{Mn}_{35}\text{In}_{14}$ alloys have been studied. $\text{Ni}_{51}\text{Mn}_{34}\text{In}_{14}\text{Si}_1$ alloy shows a magnetic field induced structural phase transition from ferromagnetic austenitic state to paramagnetic martensitic state accompanied by a magnetic entropy change ($\Delta S_M = 35.4 \text{ Jkg}^{-1}\text{K}^{-1}$ for 2 T field) and a field induced strain [$\varepsilon(H) = 0.006\%$ for 5 T field] at 277 K. This alloy also demonstrated magnetically induced super-elastic behaviour, i.e., $\varepsilon(H)$ could be fully recovered upon removal of the field. On the other hand, the alloy with 0.75 at% Si and 0.25 at% Cu (i.e., $\text{Ni}_{51}\text{Mn}_{34}\text{In}_{14}\text{Si}_{0.75}\text{Cu}_{0.25}$) exhibited a larger irreversible $\varepsilon(H)$ of 0.018% for 5 T field and a smaller ΔS_M of $3.6 \text{ Jkg}^{-1}\text{K}^{-1}$ for 2 T field at 297 K at the paramagnetic austenite to paramagnetic martensite transformation temperature. These studies showcase the multifunctional properties of Ni-Mn-In alloys as well as demonstrate the use of small atomic substitution to tailor these alloys for a desired application at a desired temperature.

Key words: Magnetic shape memory alloys, Martensitic phase transformation, Magnetic field induced strain, Magneto-caloric effect

Publication History: Received: 10th August, 2016; Accepted: 19th August, 2016

Introduction

Ferromagnetic shape memory alloys (FSMAs) exhibit multifunctional thermo-mechanical properties which originate from a first-order solid-state diffusionless martensitic phase transition occurring between the high crystallographic symmetry austenite phase and a low symmetry martensite phase [1-11]. These FSMAs exhibit super-elastic behaviour which is attributed to field-induced reorientation of martensite variants when the magneto-crystalline anisotropy is high. The driving force for this is provided by Zeeman energy ($\mu_0\Delta MH$) of consecutive martensite variants. Giant magnetic field induced strain (MFIS) of up to 9.5% has been realized in off-stoichiometric Ni-Mn-Ga single crystals [12]. However, high room temperature brittleness of Ni-Mn-Ga alloys and the problems associated with obtaining single crystal specimen have hindered development of magnetic field induced actuators from this alloy. Recently, Ni-Mn-In based off-stoichiometric Heusler alloys have been reported to display a variety of field induced physical properties such as MFIS, magneto-caloric effect, magneto-caloric effect (MCE) and magnetic super-elasticity which find applications in sensors and actuators [13-25]. Application of magnetic field generally shifts the martensitic transition of Ni-Mn-In alloys to lower temperatures as indicated by the shift in the characteristic temperature values, viz., austenite start temperature (T_{As}), austenite finish temperature (T_{Af}), martensite start temperature (T_{Ms}), and martensite finish temperature (T_{Mf}) [26-29]. This implies that applied magnetic field induces a change in crystal symmetry, resulting in large MFIS and MCE in this alloy system. In polycrystalline $\text{Ni}_{50}\text{Mn}_{34}\text{In}_{16}$ alloy, strains up to 0.12% have been observed due to magnetic field induced reversible martensitic transition. Normally, the strains in FSMAs are induced by twin boundary motion. However, the large strain observed in $\text{Ni}_{50}\text{Mn}_{34}\text{In}_{16}$ has been attributed to change in lattice parameters during the field induced transition [16]. Large change in magnetic entropy (ΔS_M) of $12 \text{ Jkg}^{-1}\text{K}^{-1}$ has been reported in this alloy at 190 K for an applied field of 5 T. The strong influence of small

variations in composition on the magnetic and structural transition temperatures provides a way to tailor these characteristic temperatures and hence the MFIS and MCE. In this work, we report magnetic super-elasticity as well as MCE in $\text{Ni}_{51}\text{Mn}_{34}\text{In}_{14}\text{Si}_1$ and $\text{Ni}_{51}\text{Mn}_{34}\text{In}_{14}\text{Si}_{0.75}\text{Cu}_{0.25}$ alloys near ambient temperature at which its martensitic transition occur.

Experimental

Polycrystalline $\text{Ni}_{51}\text{Mn}_{34}\text{In}_{14}\text{Si}_1$ and $\text{Ni}_{51}\text{Mn}_{34}\text{In}_{14}\text{Si}_{0.75}\text{Cu}_{0.25}$ alloy ingots were prepared by arc melting high purity (99.99%) elements. After melting several times, the weight loss was $< 1.5\%$ of the initial weight. The ingots were then sealed in fused silica ampoules under a pressure of 10^{-3} Pa and annealed at 1173 K for 20 h and quenched in ice water. The annealed ingots were crushed into a fine powder for structural analysis using a powder X-ray diffractometer (Seifert, 3003T/T) operating with $\text{Cu-K}\alpha$ radiation ($\lambda = 0.15406$ nm). Elemental composition of the alloys was verified using an energy dispersive spectrometer (EDS) attached to a scanning electron microscope (SEM, Leo 1430VP). Magnetization measurements were carried out using a vibrating sample magnetometer (VSM, Lakeshore 7410). MFIS along the applied field direction was measured using a commercial strain-gage mounted inside a variable temperature superconducting (5 T) magnet (Oxford Instruments). This system enables MFIS measurements with a measurement accuracy of ± 0.0001 .

Results and Discussion

Room temperature X-ray diffraction (XRD) patterns (not shown here) show cubic $L2_1$ and orthorhombic (Pmmm) crystal structure for $\text{Ni}_{51}\text{Mn}_{34}\text{In}_{14}\text{Si}_1$ and $\text{Ni}_{51}\text{Mn}_{34}\text{In}_{14}\text{Si}_{0.75}\text{Cu}_{0.25}$ alloys, respectively. SEM-EDS analysis showed the measured compositions of the alloys to be $\text{Ni}_{50.69}\text{Mn}_{33.83}\text{In}_{14.07}\text{Si}_{1.41}$ and $\text{Ni}_{50.88}\text{Mn}_{33.97}\text{In}_{13.75}\text{Si}_{0.89}\text{Cu}_{0.51}$, respectively, which are close to the starting composition.

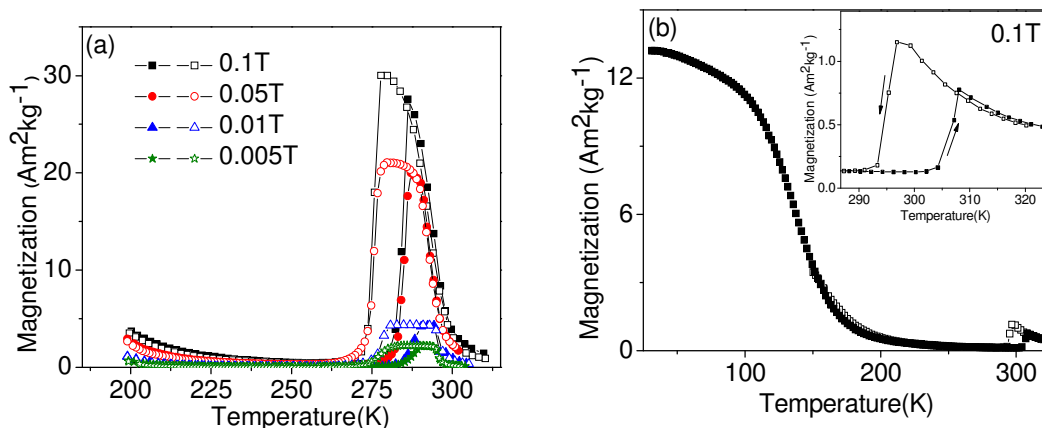


Fig. 1: Thermo-magnetization curves obtained under field-cooled (open symbols) and field-heated (filled symbols) conditions for (a) $\text{Ni}_{51}\text{Mn}_{34}\text{In}_{14}\text{Si}_1$ alloy at different applied fields, and (b) $\text{Ni}_{51}\text{Mn}_{34}\text{In}_{14}\text{Si}_{0.75}\text{Cu}_{0.25}$ alloy at 0.1 T. Inset in (b) provides an enlarged view of the data shown in Fig. 1 (b) near the martensitic transformation.

Fig. 1 shows thermo-magnetization (M-T) curves in the vicinity of the martensitic transformation recorded under field-cooled (FC) and field-heated (FH) conditions. Fig. 1 (a) presents the M-T data for $\text{Ni}_{51}\text{Mn}_{34}\text{In}_{14}\text{Si}_1$ alloy recorded under different applied fields ranging from 0.005 T to 0.1 T. The data shows that upon cooling from room temperature, magnetization (open symbols in fig. 1a) increases sharply due to the symmetry-breaking paramagnetic to high symmetry ferromagnetic phase transition. The Curie temperature ($T_{C,A}$) of the ferromagnetic austenite phase is determined from the inflection point of the $dM/dT(T)$ curve. On further cooling the sample, a sharp decrease in magnetization is observed when the austenite phase undergoes a structural transition to martensite

phase at T_{Ms} . When the sample is heated, it starts transforming to austenite at T_{As} . At T_{Af} it becomes completely austenite and finally the ferromagnetic austenite transforms to paramagnetic austenite at T_C . A thermal hysteresis ΔT ($= T_{Ms} - T_{Af}$) can be observed between the FC and FH curves near the first-order structural transition. When the applied magnetic field is increased, the magnetization change (ΔM) across T_{Ms} increases because the magnetization of ferromagnetic austenitic phase is significantly higher than that of paramagnetic martensitic phase which remains nearly constant. On increasing the magnetic field from 0.005 T to 0.1 T, T_{Ms} (maximum hysteresis temperature ΔT_{max}) shifts from 283 K to 278 K (10.3 K to 9.3 K), while ΔM is significantly enhanced from $2.2 \text{ Am}^2\text{kg}^{-1}$ to $30.1 \text{ Am}^2\text{kg}^{-1}$. M-T FC and FH curves obtained for $\text{Ni}_{51}\text{Mn}_{34}\text{In}_{14}\text{Si}_{0.75}\text{Cu}_{0.25}$ alloy under an external magnetic field of $H = 0.1 \text{ T}$ is shown in Fig. 1 (b). Upon cooling, a martensitic transition is observed at 297 K in the paramagnetic phase and magnetization starts to increase from 200 K. It can be noticed that as the temperature is decreased, the sample undergoes the Curie transition at 138 K in the martensite phase. Similarly, while increasing the temperature, the alloy undergoes both the transitions accompanied by corresponding change in magnetization. The confirmation for the first-order structural transition is the presence of a thermal hysteresis of 11 K between the FC and FH curves near the T_{Ms} (cf. inset of Fig. 1 (b)). In order to verify the effect of magnetic field on the martensitic transformation, M-T curves were recorded for an external magnetic field of $H = 0.005 \text{ T}$ (not shown here) which did not show any perceptible shift in T_{Ms} . But the magnitude of ΔM ($0.05 \text{ Am}^2\text{kg}^{-1}$) at $H = 0.005 \text{ T}$ is lower than that ($1 \text{ Am}^2\text{kg}^{-1}$) observed for $H = 0.1 \text{ T}$. The large change of ΔM across T_{Ms} results in a large Zeeman energy ($\mu_0\Delta M.H$) which drives the structural transformation accompanied by large field-induced meta-magnetic behavior.

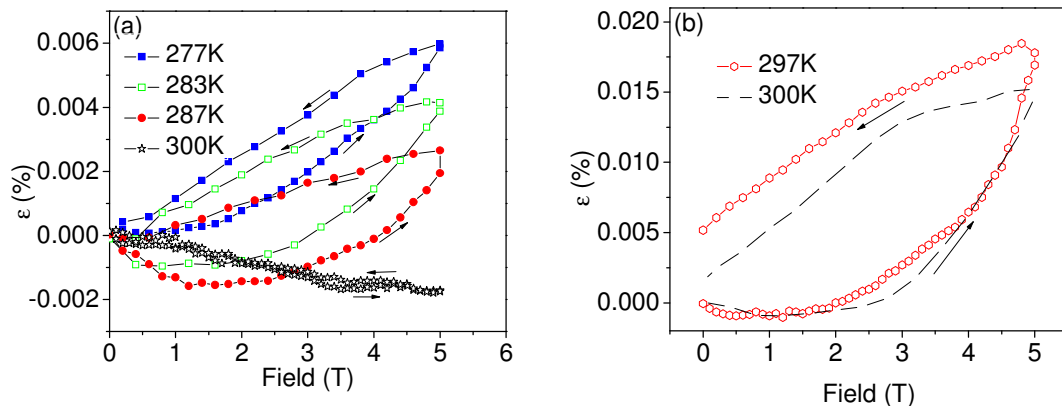


Fig. 2: Isothermal magnetic field dependence of strain at various temperatures for (a) $\text{Ni}_{51}\text{Mn}_{34}\text{In}_{14}\text{Si}_1$ and (b) $\text{Ni}_{51}\text{Mn}_{34}\text{In}_{14}\text{Si}_{0.75}\text{Cu}_{0.25}$ alloys.

The field induced structural transition in $\text{Ni}_{51}\text{Mn}_{34}\text{In}_{14}\text{Si}_1$ alloy has strong influence on the overall reversible strain ϵ ($= \Delta l/l_i$) induced macroscopically by the applied magnetic field as shown in Fig. 2 (a). Fig. 2 shows the MFIS $\epsilon(H) [= (l_H - l_i)/l_i]$, where l_i is the initial length in the absence of the field and l_H is the final length in the presence of field H . At room temperature (300 K), $\text{Ni}_{51}\text{Mn}_{34}\text{In}_{14}\text{Si}_1$ alloy which is in paramagnetic austenite state, exhibits a small negative $\epsilon(H)$ due to intrinsic magnetostriction. Such behaviour has also been reported in $\text{Ni}_{50}\text{Mn}_{34}\text{In}_{16}$ alloy [16, 19]. However, a positive $\epsilon(H)$ is observed in the temperature range $T_{Af} < T < T_{Ms}$. A hysteresis is also observed in $\epsilon(H)$ when the field is cycled. ϵ_{max} of 0.006% was observed at 277 K for an applied field of $H = 5 \text{ T}$, but maximum hysteresis in $\epsilon(H)$ was observed at 283 K. This hysteresis behaviour of $\epsilon(H)$ is also reflected in the field dependence of magnetization $M(H)$ at the respective temperatures depicted in Fig. 3. This observation shows that field induced twin boundary movement is not very

mobile at the beginning of martensitic transition as compared to its movement when well inside the martensitic phase.

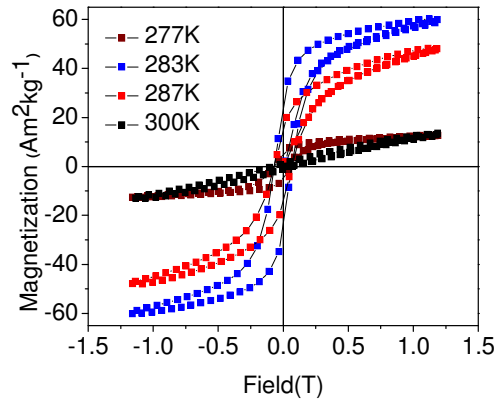


Fig. 3: Isothermal field dependence of magnetization curves for Ni₅₁Mn₃₄In₁₄Si₁ alloy at various temperatures.

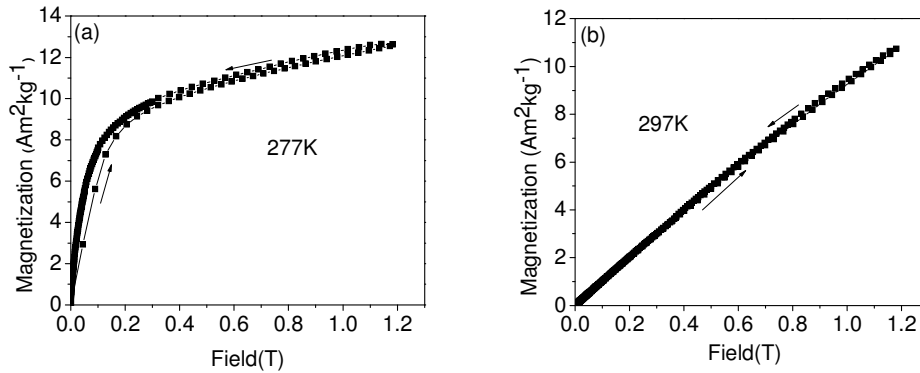


Fig. 4: Isothermal initial magnetization curves at 277K and 297K temperatures for (a) Ni₅₁Mn₃₄In₁₄Si₁ and (b) Ni₅₁Mn₃₄In₁₄Si_{0.75}Cu_{0.25} alloys respectively.

Fig. 2 (a) and Fig. 4(a) show zero remanence values of strain and magnetization, respectively, indicating their full recovery at zero fields for Ni₅₁Mn₃₄In₁₄Si₁ alloy. Fig. 2 (b) shows that MFIS exhibited by Ni₅₁Mn₃₄In₁₄Si_{0.75}Cu_{0.25} alloy at T_{M_s} as well as at 300 K, which are in paramagnetic but structurally intermediate (mixed austenite and martensite) phase, is irreversible. While recording the data displayed in Fig. 2 and Fig. 4, the sample was first cooled from 300 K to the target temperature in a zero magnetic field (ZFC). Subsequently, isothermal ε(H) and M(H) data were recorded by increasing the magnetic field to the maximum value and then decreasing it back to 0 T. Paramagnetic behaviour of Ni₅₁Mn₃₄In₁₄Si_{0.75}Cu_{0.25} alloy at T_{M_s} results in the observed zero remanence in the M(H) data presented in Fig. 4(b). Highest ε of 0.018% was observed at T_{M_s} (297 K) with maximum hysteresis in ε (H) for an applied field of H = 5 T. Significant change in ΔM observed across the magnetic field induced first order structural transition can help in realizing substantial change in ΔS_M [16]. ΔS_M is a measure of MCE in the material. Isothermal ΔS_M and refrigerant capacity (RC) which are the two important MCE parameters can be estimated using the following relations [30, 31]

$$\Delta S_M(T, H) = \int_0^H \left(\frac{\partial M(T)}{\partial T} \right)_H dH \quad \dots\dots (1)$$

$$RC = \int_{T_1}^{T_2} \Delta S_M(T, H) dT \quad \dots\dots (2)$$

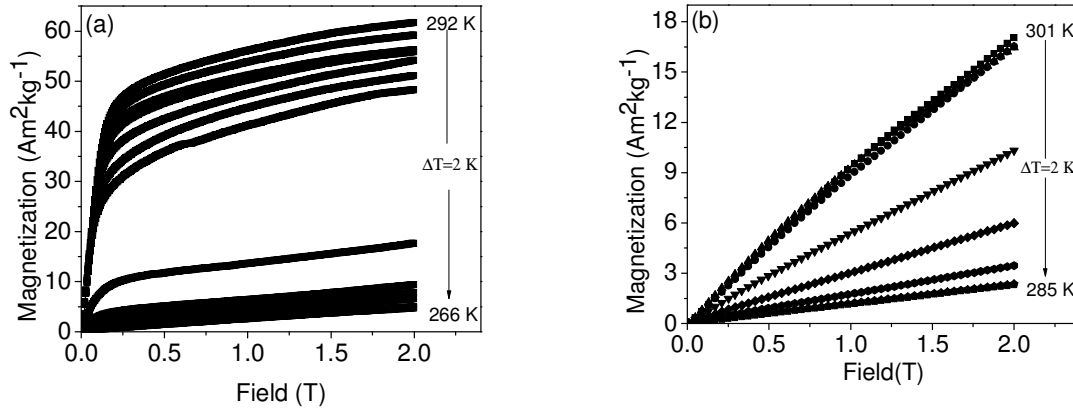


Fig. 5: Isothermal initial magnetization curves for (a) Ni₅₁Mn₃₄In₁₄Si₁ and (b) Ni₅₁Mn₃₄In₁₄Si_{0.75}Cu_{0.25} alloys in the vicinity of the first order structural transition.

In order to evaluate the values of ΔS_M , isothermal initial M(H) curves of the alloys were obtained close to the first order structural transition. M(H) data were recorded as a function of increasing magnetic field from 0 to 2 T at different temperatures with 2 K interval and the same are shown in Fig.5. In the case of Ni₅₁Mn₃₄In₁₄Si_{0.75}Cu_{0.25} alloy, the M(H) data are linear functions of H for both temperature regions, just above and below T_{Ms} . This behaviour is a confirmation of the paramagnetic structural phase transformation (paramagnetic austenite to paramagnetic martensite), which is the main reason for the meta-magnetic-type behavior observed between 297 K and 295 K. Such behavior has also been reported for Ni₅₀Mn_{36.5}In_{13.5} alloy [32]. On the other hand, Ni₅₁Mn₃₄In₁₄Si₁ alloy exhibits distinct meta-magnetic behaviour between 280 K and 278 K, close to the ferromagnetic austenite to paramagnetic martensite transition at T_{Ms} , where large ΔS_M is also observed.

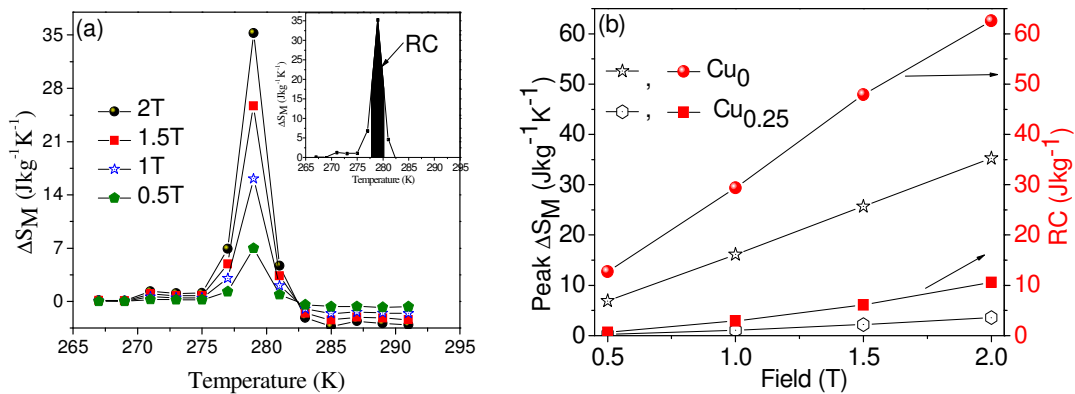


Fig. 6: (a) Temperature dependence of ΔS_M obtained for Ni₅₁Mn₃₄In₁₄Si₁ alloy with for different ΔH . Inset shows the procedure for estimating RC of the same alloy for $\Delta H = 2$ T. (b) Field dependence of ΔS_M and RC of Ni₅₁Mn₃₄In₁₄Si₁ and Ni₅₁Mn₃₄In₁₄Si_{0.75}Cu_{0.25} alloys.

Fig. 6(a) depicts the temperature dependence of ΔS_M for Ni₅₁Mn₃₄In₁₄Si₁ alloy under different ΔH of 0.5, 1, 1.5 and 2 T. The sign of ΔS_M for both the alloys is positive, which means that an inverse

MCE is displayed by these alloys. Similar behaviour has been reported in Ni-Mn-In alloy [16, 32-34]. It can be seen from Fig. 6(b) that with increasing ΔH , the maximum (or peak) value of ΔS_M near T_{Ms} increases and shows a nearly linear variation for an applied field range of 0.5 T to 2 T. This is an important feature, since in practical application of this alloy as a refrigerant; field beyond 2 T would be technically prohibitive. The change in peak ΔS_M per unit field is $19 \text{ Jkg}^{-1}\text{K}^{-1}\text{T}^{-1}$ and $1.6 \text{ Jkg}^{-1}\text{K}^{-1}\text{T}^{-1}$ for $\text{Ni}_{51}\text{Mn}_{34}\text{In}_{14}\text{Si}_1$ and $\text{Ni}_{51}\text{Mn}_{34}\text{In}_{14}\text{Si}_{0.75}\text{Cu}_{0.25}$ alloys, respectively. RC values were obtained by integrating the area under the $\Delta S_M(T)$ curves over their full width at half maximum value as depicted in the Inset of Fig. 6 (a). $\text{Ni}_{51}\text{Mn}_{34}\text{In}_{14}\text{Si}_1$ alloy shows the highest peak ΔS_M (RC) of $35.4 \text{ Jkg}^{-1}\text{K}^{-1}$ (63 Jkg^{-1}) at 279 K for $\Delta H = 2 \text{ T}$. A survey of relevant literature reveals ΔS_M and ϵ values obtained for $\text{Ni}_{50}\text{Mn}_{34}\text{In}_{16}$ ($\sim 9.5 \text{ Jkg}^{-1}\text{K}^{-1}$ at 190 K and $\sim 0.019\%$ at 195 K for $\Delta H = 2 \text{ T}$ and $12 \text{ Jkg}^{-1}\text{K}^{-1}$ at 190K and 0.12% at 195 K for $\Delta H = 5 \text{ T}$) [16], $\text{Ni}_{45}\text{Co}_5\text{Mn}_{36.7}\text{In}_{13.3}$ single crystal ($15.2 \text{ Jkg}^{-1}\text{K}^{-1}$ at 292 K and $\sim 0\%$ at 298K for $\Delta H = 2 \text{ T}$) [35] and $\text{Ni}_{49}\text{Cu}_1\text{Mn}_{34}\text{In}_{16}$ ($25.8 \text{ Jkg}^{-1}\text{K}^{-1}$ at 292 K and $\sim 0.06\%$ at 290 K for $\Delta H = 4.5 \text{ T}$) [23]. Comparing these data with the present results shows how small amounts of selective atomic substitution to Ni-Mn-In alloys can help in tailoring MCE and MFIS suitable for applications near the ambient.

Conclusion

We have investigated the MFIS and MCE in $\text{Ni}_{51}\text{Mn}_{34}\text{In}_{14}\text{Si}_1$ and $\text{Ni}_{51}\text{Mn}_{34}\text{In}_{14}\text{Si}_{0.75}\text{Cu}_{0.25}$ alloys around the martensitic transition. Both these distinct properties originate from the field induced structural transition and exhibit high values close to the martensitic transformation. The maximum value of ΔS_M obtained by $\text{Ni}_{51}\text{Mn}_{34}\text{In}_{14}\text{Si}_1$ alloy was $35.4 \text{ Jkg}^{-1}\text{K}^{-1}$ for a magnetic field change of 2 T at 279 K which is closer to the ambient temperature. This alloy also exhibited large RC value of 63 Jkg^{-1} . Magnetic-field-induced strain up to 0.006 % has been observed under an applied magnetic field of 5 T in this alloy. On the other hand, $\text{Ni}_{51}\text{Mn}_{34}\text{In}_{14}\text{Si}_{0.75}\text{Cu}_{0.25}$ alloy exhibited larger irreversible strain of 0.018% at 297 K. The high MCE and a reversible MFIS in $\text{Ni}_{51}\text{Mn}_{34}\text{In}_{14}\text{Si}_1$ alloy showcases its multifunctional properties.

Acknowledgments

I am very much thankful to Dr. A. Srinivasana, Professor of Indian Institute of Technology Guwahati, am also thankful to Dr. S. B. Roy, Scientist of Raja Ramanna Centre for Advanced Technology, Indore for their support, cooperation and lab facilities.

References

- [1] K. Ullakko, J.K. Huang, C. Kantner, R.C. O'Handley, Appl. Phys. Lett. **69** (1996) 1966.
- [2] K. Otsuka, C. M. Wayman, Eds. Shape Memory Materials (Cambridge Univ. Press, Cambridge, 1998).
- [3] H. D. Chopra, C. Ji, V. V. Kokorin, Phys. Rev. B **61** (2000) 913.
- [4] S.J. Murray, Magneto-mechanical properties and applications of Ni-Mn-Ga ferromagnetic shape memory alloy, Ph.D. Thesis, MIT, February 2000.
- [5] K. Ullakko, Y. Ezer, A. Sozinov, G. Kimmel, P. Yakovenko, V.K. Lindroos, Scripta Mater. **44** (2001) 475.
- [6] C. Biswas, R. Rawat, and S. R. Barman, Appl. Phys. Lett. **86** (2005) 202508.
- [7] M. Pasquale, C. P. Sasso, L. H. Lewis, L. Giudici, T. Lograsso, and D. Schlagel, Phys. Rev. B **72** (2005) 094435.
- [8] O. Söderberg, I. Aaltio, Y. Ge, O. Heczko, and S. -P. Hannula, Mater. Sci. Eng. A **481-482** (2008) 80.
- [9] V. A. Chernenko, and S. Besseghini, Sensors Actuators A: Physical **142** (2008) 542.
- [10] A. Planes, L. Mañosa, and M. Acet, J. Phys.: Condens. Matter **21** (2009) 233201.
- [11] H. Morito, K. Oikawa, A. Fujita, K. Fukamichi, R. Kainuma, and K. Ishida, J. Phys.: Condens. Matter **21** (2009) 256002.
- [12] A. Sozinov, A. A. Likhachev, N. Lanksa and K. Ullakko, Appl. Phys. Lett. **80** (2002) 1746.

- [13] K. Oikawa, W. Ito, Y. Imano, Y. Sutou, R. Kainuma, K. Ishida, S. Okamoto, O. Kitakami, and T. Kanomata, *Appl. Phys. Lett.* **88** (2006) 122507.
- [14] Z. D. Han, D. H. Wang, C. L. Zhang, S. L. Tang, B. X. Gu, and Y. W. Du, *Appl. Phys. Lett.* **89** (2006) 182507.
- [15] A. K. Pathak, M. Khan, I. Dubenko, S. Stadler, and N. Ali., *Appl. Phys. Lett.* **90** (2007) 262504.
- [16] T. Krenke, E. Duman, M. Acet, E. F. Wassermann, X. Moya, L. Mañosa, A. Planes, E. Suard, and B. Ouladdiaf, *Phys. Rev. B* **75** (2007) 104414.
- [17] C. Jing, J. Chen, Z. Li, Y. Qiao, B. Kang, S. Cao, and J. Zhang, *J. Alloys Compd.* **475** (2009) 1.
- [18] S X Xue, S S Feng , P Y Cai, Y Zhou and W P Chen, *Journal of Physics: Conference Series* **152** (2009) 012044.
- [19] V K Sharma, M K Chattopadhyay, A Chouhan and S B Roy, *J. Phys. D: Appl. Phys.* **42** (2009) 185005.
- [20] L. Mañosa, D. González-Alonso, A. Planes, E. Bonnot, M. Barrio, J. L. Tamarit, S. Aksoy and M. Acet, *Nature Mater.* **9** (2010) 478.
- [21] L. S. Sharath Chandra, M. K. Chattopadhyay, V. K. Sharma, S. B. Roy, and S. K. Pandey, *Phys. Rev. B* **81** (2010) 195105.
- [22] N. V. Rama Rao, V. Chandrasekaran, and K. G. Suresh, *J. Appl. Phys.* **108** (2010) 043913.
- [23] V. K. Sharma, M. K. Chattopadhyay, A. Khandelwal, and S. B. Roy, *Phys. Rev. B* **82** (2010) 172411.
- [24] V. D. Buchelnikov, V. V. Sokolovskiy, S. V. Taskaev, and P. Entel, *Mater. Sci. Forum* **635** (2010) 137.
- [25] A. P. Kazakov, V. N. Prudnikov, A. B. Granovsky, A. P. Zhukov, J. Gonzalez, I. Dubenko, A. K. Pathak, S. Stadler, and N. Ali, *Appl. Phys. Lett.* **98** (2011) 131911.
- [26] S. Aksoy, T. Krenke, M. Acet, E. F. Wassermann, X. Moya, L. Mañosa, and A. Planes, *Appl. Phys. Lett.* **91** (2007) 241916.
- [27] B. Gao, F. X. Hu, J. Shen, J. Wang, J. R. Sun, and B. G. Shen, *J. Appl. Phys.* **105** (2009) 083902.
- [28] F. X. Hu, J. Wang, J. Shen, B. Gao, J. R. Sun, and B. G. Shen, *J. Appl. Phys.* **105** (2009) 07A940.
- [29] T. Krenke, S. Aksoy, E. Duman, M. Acet, X. Moya, L. Mañosa, and A. Planes, *J. Appl. Phys.* **108** (2010) 043914.
- [30] V. K. Pecharsky, and K. A. Gschneidner, Jr., *J. Appl. Phys.* **90** (2001) 4614.
- [31] A. M. Tishin, and Y. I. Spichkin, *The Magnetocaloric Effect and its Applications* (IOP, Bristol, 2003).
- [32] A. K. Pathak, I. Dubenko, C. Pueblo, S. Stadler, and N. Ali, *Appl. Phys. Lett.* **96** (2010) 172503.
- [33] P. A. Bhoje, K. R. Priolkar, and A. K. Nigam, *Appl. Phys. Lett.* **91** (2007) 242503.
- [34] Z.D. Han, D.H. Wang, C.L. Zhang, H.C. Xuan, J.R. Zhang, B.X. Gu, Y.W. Du, *Solid State Communications* **146** (2008) 124.
- [35] R. Kainuma, Y. Imano, W. Ito, Y. Sutou, H. Morito, S. Okamoto, O. Kitakami, K. Oikawa, A. Fujita, T. Kanomata, and K. Ishida, *Nature Letter* **439** (2006) 957.

Monometallic Chromium (II) Complex of 2-[2-(Pyridylamino) Phenylazo] Pyridine with a Singlet Ground State (S=0) and Its Manganese (III) Congener. Synthesis and NMR Studies

Srijit Das

Department of Chemistry, A.B.N.Seal College P.O & Dist. Coochbehar Pin: 736101

Email: icsrijit77@gmail.com; Phone: +918900657718

Abstract

The extended nitrogen donor ligand, $\text{NH}_4\text{C}_5\text{N}=\text{NC}_6\text{H}_4\text{N}(\text{H})\text{C}_5\text{H}_4\text{N}$, 2-[2-(pyridylamino)phenylazo]pyridine, HL^1 , upon deprotonation behaves as a potential tridentate N-donor. It reacts with $\text{CrCl}_3 \cdot 6\text{H}_2\text{O}$ and $\text{Mn}(\text{ClO}_4)_2 \cdot 6\text{H}_2\text{O}$ to produce octahedral complexes, viz. $[\text{Cr}(\text{L}^1)_2]$ (**1**) and $[\text{Mn}(\text{L}^1)_2](\text{ClO}_4)$ (**2**), respectively. These complexes are diamagnetic and showed highly resolved ^1H and ^{13}C NMR spectra in the normal range of diamagnetic compounds. The two coordinated ligands in these complexes are magnetically equivalent and resonances for one ligand were observed in their spectra. Diamagnetism in the present two $3d^4$ metal complexes may possibly due to pairing of electrons which are delocalized over metal t_{2g} and ligand π^* orbitals. Electronic spectra of the complexes are reported.

Key Words: 1. Chromium(II) Complex 2. Manganese(III) Complex 3. Singlet ground state

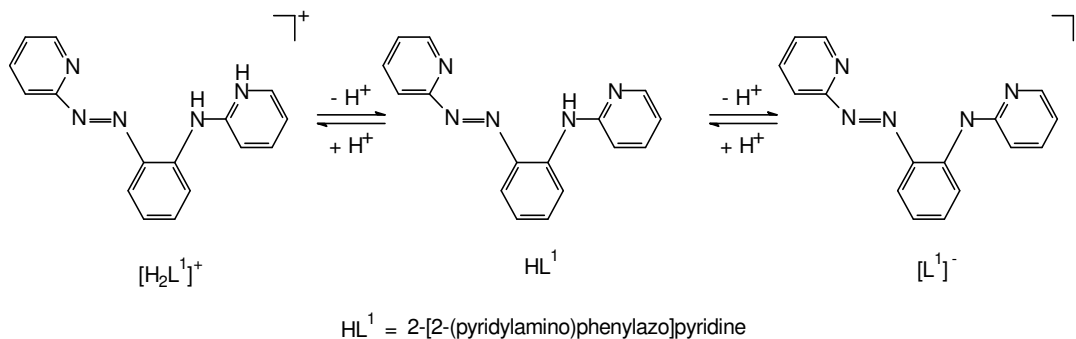
Publication History: Received: 10th August, 2016; Accepted: 19th August, 2016

Introduction

The synthesis and characterization of the tridentate nitrogen donor ligand, HL^1 , ($\text{HL}^1 = 2$ -[2-(pyridylamino)phenylazo]pyridine) was done *via* cobalt promoted $^1\text{C-N}$ bond formation reaction. The ligand HL^1 readily loses its proton and the conjugate base, $[\text{L}^1]^-$ coordinates as a bischelating tridentate nitrogen donor ligand (Scheme 1).

Scheme 1

Pictorial representation of HL^1



In this paper I have described an unprecedented example of a monometallic and diamagnetic (S=0) chromium (II) complex of an anionic tridentate nitrogen donor ligand $[\text{L}^1]^-$. Its manganese (III) congener is also explored. Extensive charge delocalization in the present anionic ligand $[\text{L}^1]^-$ along its ligand backbone is responsible for the singlet (S=0) ground state of these metal ions. We wish to note here that the diamagnetic (S=0) ground state of chromium (II) and manganese (III) are generally an uncommon entity.¹⁻⁷ We are aware of only one precedence of a manganese (III) complex that possess⁸

spectrum are displayed in **Figures 1** and **2** respectively.

Neither of the complexes **1** and **2** showed a N-H resonance. Absence of N-H resonance in their ^1H NMR spectra indicates that the ligand is coordinated to the respective metal ion *via* the deprotonation of the secondary amine proton. Interestingly, each kind of proton of the coordinated ligand, $[\text{L}^1]^-$ in both complexes gave rise to one signal. It implies that the two ligands in the present complexes were magnetically equivalent¹⁵ for which the presence of two-fold symmetry axis is required. In both complexes^{16,17} four phenyl protons resonated in the region (7.0-6.35) δ , while the eight pyridyl resonances were observed in the range (8.4-7.1) δ . Furthermore, temperature dependent ^1H NMR spectra of both complexes were studied up to 375K using $\text{dms}\text{-d}^6$ as solvent. Notably, the spectral features remained unchanged even at high temperature range.

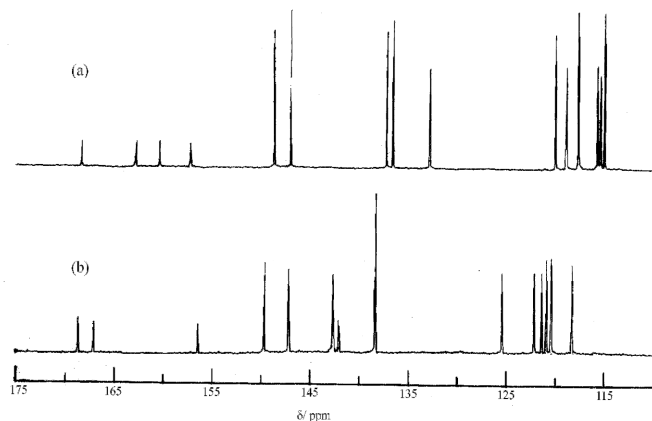


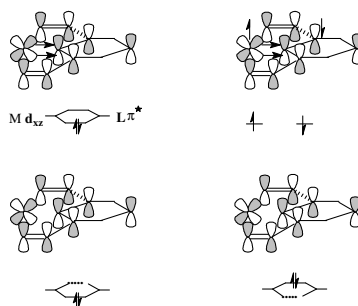
Fig. 2: ^{13}C NMR spectrum of (a) $[\text{Cr}(\text{L}^1)_2]$ (**1**) and (b) $\text{Mn}(\text{L}^1)_2(\text{ClO}_4)$ (**2**) in CDCl_3 .

^{13}C NMR of both complexes consisted of sixteen distinct resonances. Like ^1H NMR, ^{13}C NMR spectra also revealed that the two ligands in the present complexes are magnetically equivalent and each kind of carbon of the coordinated anionic ligand gave rise to one signal, indicating the presence of two-fold symmetry axis. Interestingly there were four non-hydrogen carbons (*viz.* C^2 , C^7 , C^8 and C^{13} in complexes **1** and **2** appeared in the range 168.42, 162.94, 160.55 and 142.13 δ . These signals were absent in the DEPT spectrum as expected.

Some Comments on the diamagnetic nature of the present complexes

Diamagnetism in $3d^4$ -systems is virtually unknown. Since the present complexes displayed their ^1H and ^{13}C NMR signals in the normal range for diamagnetic compounds, such unusual behaviour arises either due to pairing of electrons⁸ which are delocalized over metal t_{2g} and ligand π^* orbitals, or due to the antiferromagnetic coupling^{2,18} between the unpaired spin of metal and ligand radical anions. Schematic representation of backdonation vs. biradical models are given in Scheme 3.

Scheme 3 Delocalized vs. biradical model



In principle, diradical descriptions such as $[\text{Cr}^{\text{IV}}(\text{L}^1)_2]^{2-}$ and $[\text{Mn}^{\text{V}}(\text{L}^1)_2]^{2+}$ of the present complexes are possibilities, however, the closed shell descriptions, $[\text{Cr}^{\text{II}}(\text{L}^1)_2]^-$ and $[\text{Mn}^{\text{III}}(\text{L}^1)_2]^+$ is more valid. In the context of paired vs. biradical description, it appears that the ligand π^* orbital of $[\text{L}^1]$ is energetically close to the Cr(II) and Mn(III) $d\pi$ -orbitals leading to extensive delocalization.¹⁹ The 4d- and 5d- metal orbitals, on the other hand, possess higher energy resulting in somewhat smaller overlap between metal and ligand orbitals, which lead to *pure* biradical description.

b. Electronic Spectra

Both chromium and manganese complexes are freely soluble in common organic solvents. While the chromium complex, **1** is violet; the colour of the manganese complex, **2** is green. The electronic spectra of all the complexes showed multiple low energy structured transitions.

The chromium complex showed two sharp bands near 720 nm (ϵ : 9150 $\text{M}^{-1}\text{cm}^{-1}$) and at 545 nm (ϵ : 13610 $\text{M}^{-1}\text{cm}^{-1}$) along with two shoulders at *ca.* 855 nm and 465 nm. In the UV region, the complex showed one transition at 235 nm (ϵ : 42400 $\text{M}^{-1}\text{cm}^{-1}$). In addition, two shoulders appeared at *ca.* 360 nm and *ca.* 300 nm, respectively. All these transitions in the high energy UV-region are mainly due to $\pi \rightarrow \pi^*$ transitions involving predominantly ligand orbitals.

The cationic mononuclear manganese complex, on the other hand, showed two moderate sharp bands near 775 nm (ϵ : 13975 $\text{M}^{-1}\text{cm}^{-1}$) and 705 nm (ϵ : 13600 $\text{M}^{-1}\text{cm}^{-1}$). In addition to this, three shoulders at 870 nm, 850 nm and 645 nm were observed in the visible region. In the UV region the complex showed two transitions at *ca.* 400 nm (ϵ : 24615 $\text{M}^{-1}\text{cm}^{-1}$) and 245 nm (ϵ : 58540 $\text{M}^{-1}\text{cm}^{-1}$) along with a shoulder appeared at *ca.* 345 nm.

All the major transitions of **1** and **2** are collected in **Table 1** and the spectra of **1** and **2** are displayed in **Figures 3** and **4**, respectively.

Table 1: Electronic Spectral Data.

Compound	Electronic Spectra ^a [$\lambda_{\text{max}}/\text{nm}$ ($\epsilon/\text{M}^{-1}\text{cm}^{-1}$)]
$[\text{Cr}(\text{L}^1)_2]$ (1)	855 ^b (3020), 720(9150), 545(13610), 465 ^b (8490), 360 ^b (16595), 290 ^b (27770), 235(42400)
$[\text{Mn}(\text{L}^1)_2](\text{ClO}_4)$ (2)	870 ^b (8465), 850 ^b (10000), 775(13975), 705(13600), 645 ^b (10525), 400(24615), 345 ^b (20930), 245(58540)

^a Solvent: dichloromethane. ^b Shoulder.

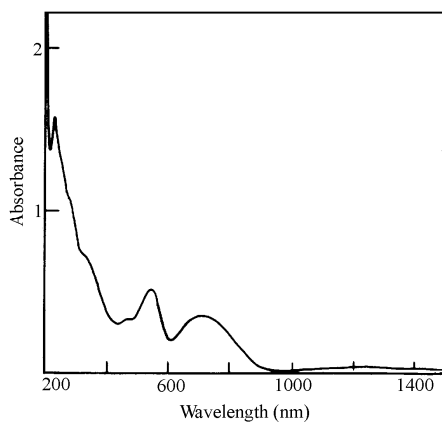


Fig. 3: Electronic spectra of $[\text{Cr}(\text{L}^1)_2]$ (**1**) in dichloromethane.

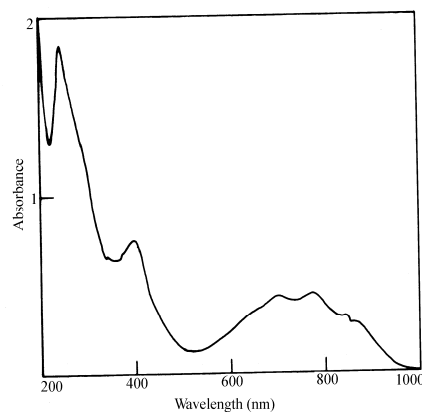


Fig. 4: Electronic spectra of $[\text{Mn}(\text{L}^1)_2](\text{ClO}_4)$ (**2**) in dichloromethane

Conclusion

In this paper I have described the first example of a diamagnetic chromium (II) monometallic complex and its manganese (III) congener. Biradical description of the similar ligand system appears to be more valid in the case of molybdenum and tungsten. Such a dual character of the reference ligand(s) is unique and their metal complexes may find application as redox catalyst.

Acknowledgement

Author is thankful to Professor S. Goswami, Department of Inorganic Chemistry, IACS for helpful discussions and suggestions.

Experimental Section

Physical Measurements

i) ^1H and ^{13}C NMR Spectra

The spectral measurements were performed in CDCl_3 and DMSO-d^6

ii) Electronic Spectra

The electronic spectral measurements had been carried out in dichloromethane solution

Preparation of Compounds

a) Chemicals

All chemicals used for synthesis were of analytical grade. The chemicals and their sources were as follows: hydrated chromium trichloride and $\text{Mn}(\text{ClO}_4)_2 \cdot 6\text{H}_2\text{O}$ was obtained from Arora-Matthey, Kolkata.

b) Solvents

All the solvents used for this work were of analytical grade and were used as received

c) Synthesis of Complexes

i) Synthesis of $[\text{Cr}(\text{L}^1)_2]$ (1)

The ligand HL^1 (100 mg, 0.363 mmol) was dissolved in 25 ml of methanol and 1-2 drops of triethyl amine was added. To this deprotonated ligand solution was added a methanol solution of $\text{CrCl}_3 \cdot 6\text{H}_2\text{O}$ (50mg, 0.18mmol) and the whole mixture was stirred for 2h at room temperature. The colour of the solution gradually changed from orange to violet brown. The crude product was purified by preparative TLC plate. The major violet band was separated with the use of 4:1 CHCl_3 - CH_3CN as the eluent. The violet band was then separated from TLC plate and collected by the complete evaporation of eluates. The compound thus obtained was recrystallized from a dichloromethane-hexane solvent mixture. Yield: 60%.

ii) Synthesis of $[\text{Mn}(\text{L}^1)_2](\text{ClO}_4)$ (2)

The ligand HL^1 (100 mg, 0.363 mmol) was dissolved in 25 ml of methanol and 1-2 drops of triethyl amine was added. To this deprotonated ligand solution was added a methanol solution of $\text{Mn}(\text{ClO}_4)_2 \cdot 6\text{H}_2\text{O}$ (65mg, 0.18mmol) and the whole mixture was stirred for 1h at room temperature. The colour of the solution gradually changed from orange to greenish blue. The resultant mixture was filtered and the solvent was evaporated under vacuum. The green compound thus obtained was recrystallized from a dichloromethane-hexane solvent mixture. Yield: 45%. (**Caution:** Perchlorate salts of metal complexes are generally explosive. Although no detonation tendencies have been observed, care is advised and handling of only a small quantity recommended).

References

1. K. K. Kamar, S. Das, C. -H. Hung, A. Castiñeiras, C. Rillo, M. Kuzmin and S. Goswami; *Inorg. Chem.*, **2003**, *42*, 5367.
2. C. G. Pierpont; *Inorg. Chem.*, **2001**, *40*, 5727.
3. (a) K. P. Bryliakov and E. P. Talsi; *Inorg. Chem.*, **2003**, *42*, 7258. (b) K. P. Bryliakov, D. E. Babushkin and E. P. Talsi; *Meendeleev Commun.*, **2000**, 1.
4. A. B. Blake, B. N. Figgis, P. A. Reynolds, L. M. Engelhardt, B. Moubaraki and K. S. Murray; *J. Chem. Soc., Dalton Trans.*, **1994**, 1121.
5. D. Ghosh and R. K. Mukherjee; *J. Phys. Chem. Solids*, **1979**, *40*, 691.
6. J. A. Bonadies, M. J. Maroney and V. L. Pecoraro; *Inorg. Chem.*, **1989**, *28*, 2044.
7. (a) S. Ganguli, S. Karmakar and A. Chakravorty; *Inorg. Chem.*, **1997**, *36*, 116. (b) P. Basu and A. Chakravorty; *Inorg. Chem.*, **1992**, *24*, 4980. (c) P. Basu and A. Chakravorty; *J. Chem. Soc., Chem. Commun.*, **1992**, 809.
8. (a) P. H. M. Budzelaar, B. Bruin, A. W. Gal, K. Wieghardt and J. H. vanLenthe; *Inorg. Chem.*, **2001**, *40*, 4649. (b) B. De Bruin, E. Bill, E. Bothe, T. Weyhermuller and K. Wieghardt; *Inorg. Chem.*, **2000**, *39*, 2936.
9. J. P. Collman and R. Boulatov; *Angew. Chem. Int. Ed.*, **2002**, *41*, 3948 and references therein.
10. F. A. Cotton, B. E. Hanson, W. H. Ilsley and G. W. Rice; *Inorg. Chem.*, **1979**, *18*, 2713.
11. R. A. Andersen, R. A. Jones and G. Wilkinson; *J. Chem. Soc., Dalton Trans.*, **1978**, 446.
12. B. N. Figgis and R. L. Martin; *J. Chem. Soc.*, **1956**, 3837.
13. S. G. Sreerama and S. Pal; *Inorg. Chem.*, **2002**, *41*, 4843.
14. W. J. Geary; *Coord. Chem. Rev.*, **1971**, *7*, 81.
15. G. Orellana, C. A. Ibarra and J. Santoro; *Inorg. Chem.*, **1988**, *27*, 1025.
16. A. K. Mahapatra, B. K. Ghosh, S. Goswami and A. Chakravorty; *J. Ind. Chem. Soc.*, **1986**, *53*, 101.
17. S. Choudhury, M. Kakoti, A. K. Deb and S. Goswami; *Polyhedron*, **1992**, *11*, 3183.
18. (a) H. Chun, C. N. Verani, P. Chaudhuri, E. Bothe, E. Bill, T. Weyhemuller and K. Weighardt; *Inorg. Chem.*, **2001**, *40*, 4157. (b) C. G. Pierpont and C. W. Lange; *Prog. Inorg. Chem.*, **1994**, *41*, 331.
19. M. H. Kuchma, T. Nicholson, A. Davison, W. M. Davis and A. G. Jones; *J. Chem. Soc., Dalton Trans.*, **1997**, 3185.

Photophysical Property Monitored by Solvent Environment for NNO Coordinating Tridentate Ligand

Amar Hens

Department of Chemistry, A. B. N. Seal College, Cooch Behar, 736101, India

E-mail: Email: amarjuchem@gmail.com; amar_abnsc@rediffmail.com

Abstract

Here NNO coordinating tridentate Schiff base 2,4-Dibromo-6-((quinolin-8-ylimino)methyl)phenol (**HL**) was synthesized and characterized by various methods such as elemental analysis, ¹H NMR, FT-IR, UV-Vis and emission spectroscopy. The ligand show stronger fluorescence intensity with gradually bathochromic shift in different polarity solvent. The solvent polarity function plot shows that excited state of the ligand is more polar than the ground state.

Keywords: Tridentate Ligand / UV-vis study / Emission / Solvent Polarity Function.

Publication History: Received: 10th August, 2016; Accepted: 19th August, 2016

Introduction

The organic fluorescent materials have attracted intensive interest because of their potential applications in organic light emitting diodes (OLED), organic field effect transistors (OFET), fluorescent sensors, etc. Schiff bases play a vital role in modern coordination chemistry,¹⁻³ where tridentate salen-types ligands are one of the most popular classes⁴⁻⁶ of Schiff-base ligands amongst the coordination chemists.

A diversity of fluorescent-sensing approaches have been extensively investigated pertaining to the signaling mechanisms of metal-ligand charge transfer (MLCT),^{7a} internal charge transfer (ICT),^{7b} photo induced electron transfer/energy transfer (PET),^{7c} metal-ligand charge transfer (MLCT),^{7d} excimer/exciple formation as well as the excited state intramolecular/intermolecular proton transfer (ESIPT).^{7d} The fluorescence of the ligand (HL) appears due to ESIPT⁶ mechanism but the emission intensity is very weak in contrast with the complexes, probably due to quenching by the lone pair of electrons of the donor atoms in the ligand through the PET mechanism.^{7c}

Experimental Section

Materials

3,5-dibromo phenol was purchased from sigma Aldrich. All the solvents were spectroscopic grade and used after proper distillation. The purity was also verified by recording the emission spectra in the studied spectral region.

Physical measurements

UV-Vis spectra were recorded on a Perkin-Elmer LAMBDA 25 spectrophotometer. IR spectra were recorded on a Perkin-Elmer L-0100 spectrophotometer. ¹H NMR spectra were measured on Bruker FT 300 MHz spectrometer with TMS as the internal standard. Elemental analyses (C, H, N) were performed on Perkin-Elmer 2400 series II analyzer. The emission data were collected on a Perkin-Elmer LS 55 fluorescence spectrometer.

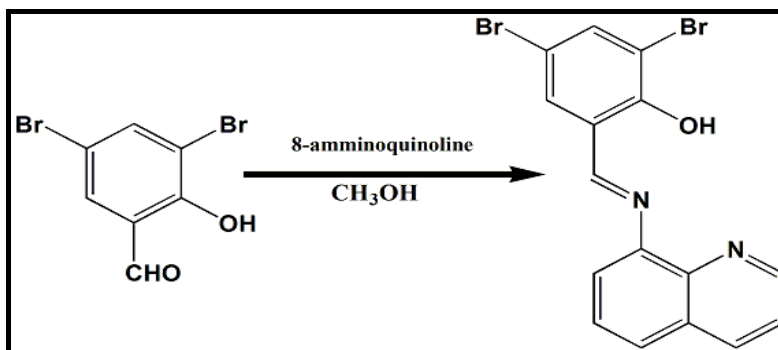
Methodology

Synthesis of ligand

Synthesis of ligand takes place in the following step. The figure 1 shows the schematic diagram of ligand synthesis HL.

Preparation of 2,4-Dibromo-6-((quinolin-8-ylimino)methyl)phenol (HL):

To a methanolic solution (20 mL) of 3,5-dibromo-2-hydroxybenzaldehyde (560 mg, 2 mmol) and 8-aminoquinoline (288 mg, 2 mmol) in presence of 3-4 drops of acetic acid was refluxed in water bath for 2 h. After cooling to room temperature, the solvent was removed under reduced pressure. The crude mass was subjected to column chromatography on a silica gel column (60-120 mesh). A red band was eluted using 5% ethylacetate in hexane solution. A red coloured solid was obtained after removal of solvent under reduced pressure to afford the desired ligand (HL). Yield: 610 mg (76%). Elemental Anal. Calc. for $C_{16}H_{10}Br_2N_2O$: C, 47.32; H, 2.48; N, 6.90. Found: C, 47.89; H, 2.34; N, 6.88. 1H NMR {300 MHz, $CDCl_3$, δ (ppm), J (Hz)}: 8.17 (CH=N, s), 4.98 (OH, bs) 7.70-7.14 (8H, ArH). Selected FT-IR bands (KBr, cm^{-1}): ~3443 (b), 1809 (s), 1516 (m), 1432 (m), 1364 (m), 1230 (s), 1080 (m), 793 (s).



Scheme 1. Schematic representation for the preparation of ligand **HL**.

Result and Discussion

Synthesis of the Ligand (HL)

The preparation of Schiff base 2,4-Dibromo-6-((quinolin-8-ylimino)methyl)phenol (**HL**) was presented in Scheme 1. The ligand (**HL**) is diamagnetic and display well resolved 1H NMR spectra. A sharp singlet azo methine peak appeared at 8.17 ppm and the aromatic protons were observed near 7.70 to 7.14 ppm in **Fig. 1a**. A broad singlet peak that appeared at 4.98 ppm was attributed for phenolic proton. The IR spectrum of the ligand was recorded in a KBr disk. The ligand showed $C-O_{phenoxo}$ stretching at 1230 cm^{-1} whereas $C=N$ stretches at 1516, respectively and the broad band at the region of 3500 cm^{-1} due to aromatic $C-H$ stretching vibrations. The bands in the region of $1600\text{--}1430\text{ cm}^{-1}$ were consistent with the skeletal vibration of the aromatic system (**Fig.1b**).

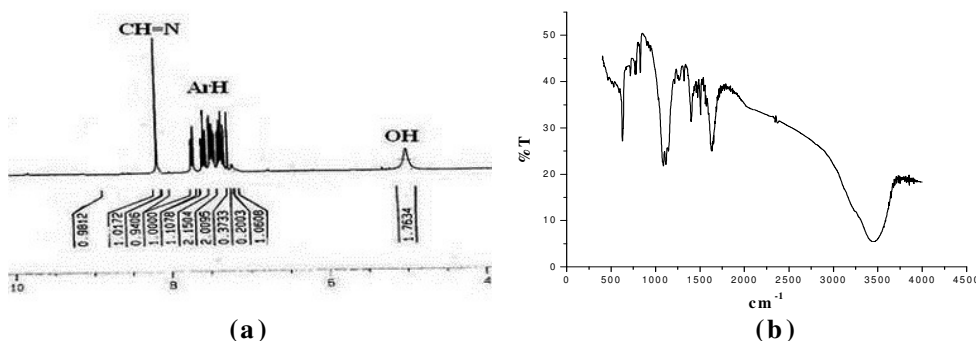


Fig. 1(a): The 1H NMR spectra of **HL** in $CDCl_3$; **(b):** IR Spectra of **HL**

Ligand photophysical study

The UV-Vis absorption spectrum of the ligand shows two well resolved peaks near around 390 and 280 nm in solvent of different polarity at room temperature. As shown in **Fig. 2a**, **HL** shows low energy band at approximately 390 nm which is attributed to the $n-\pi^*$ electronic transition whereas the

prominent high energy band around at 280 is due to the $\pi-\pi^*$ electronic transition.¹ A characteristic hump appears near at 320 nm in presence of low polarity solvent, whereas with enhancement of solvent polarity the hump gradually diminishes. The details photophysical data is given in Table1.

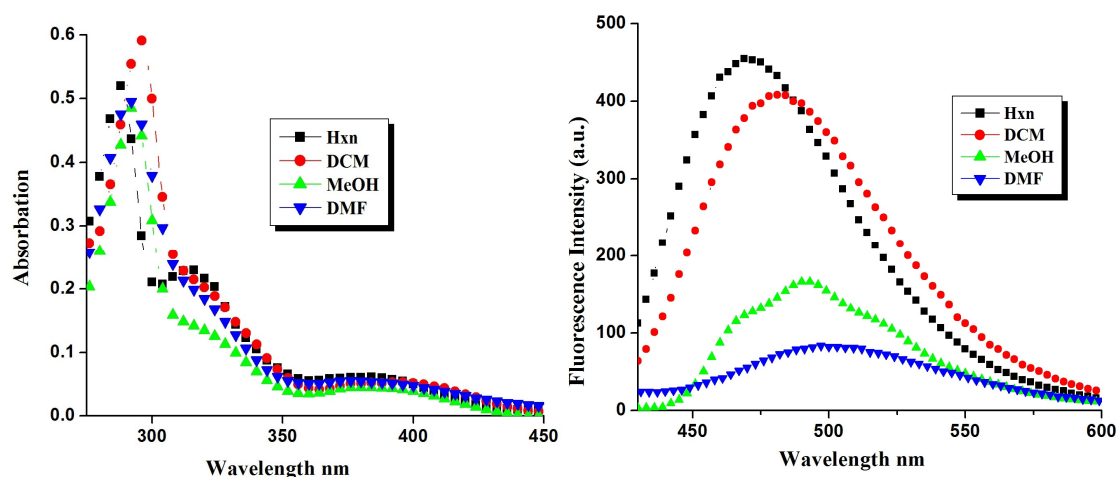


Fig. 2 (a) The absorbance spectra of **HL** ($\sim 1 \times 10^{-5}$ M) in different solvents at room temperature. (b) A representative diagram of emission intensity vs solvent polarity of the ligand.

Table 1: Photophysical parameters of **HL** in different solvent at room temperature

Solvent	Hexane	DCM	MeOH	DMF
λ_{abs} mn	377	381	387	394
λ_{em} mn	468	477	489	500

Emission spectral properties

The ligand emits a weak emission band in the region of 450 to 550 nm when excited at 390 nm in presence of different polarity solvent (**Fig. 2b**). Both the absorption maxima (λ_{abs}) and emission maxima (λ_{em}) of this particular ligand shifted towards longer wavelength as the polarity of the solvent increases (Table 1). This indicates that the excited state S1 of the ligand is more polar than ground S0 state.⁸ The excess vibrational energy is rapidly lost by the polar solvent molecules and stabilized by the S1 state which leads bathochromic shift towards more polar solvent. More structured and intense emission spectra were observed for the ligand in the least polar solvent like hexane (Fig. 2b). As the polarity of the solvent increase the intensity of outcome fluorescence spectra sharply diminishes and broadens. We measured the absorption ($\lambda_{\text{abs max}}$) and fluorescence ($\lambda_{\text{em max}}$) band maxima in different solvents along with the solvent polarity function, Δf (eq. 1)⁹

$$\Delta f = (\epsilon - 1/ 2\epsilon + 1) - (\eta^2 - 1/ 2\eta^2 + 1) \dots\dots\dots 1$$

where ϵ and η are the static dielectric constant and refractive index of the solvent, respectively. A reasonably good linear fits were obtained when the absorption ($\nu_{\text{abs max}}$) or emission ($\nu_{\text{em max}}$) band maxima (in cm^{-1}) for **HL** in different solvents were plotted vs Δf . The higher slope for the $\nu_{\text{em max}}$ vs Δf plot as compared to that for the $\nu_{\text{abs max}}$ vs Δf plot (Fig. 3) suggested that the excited state of the ligand was more polar than the ground state.⁹ To substantiate these results, we also tried to correlate the Stokes' shifts (i.e., $\Delta\nu = \nu_{\text{abs}} - \nu_{\text{em}}$) with the Δf values of the solvents.

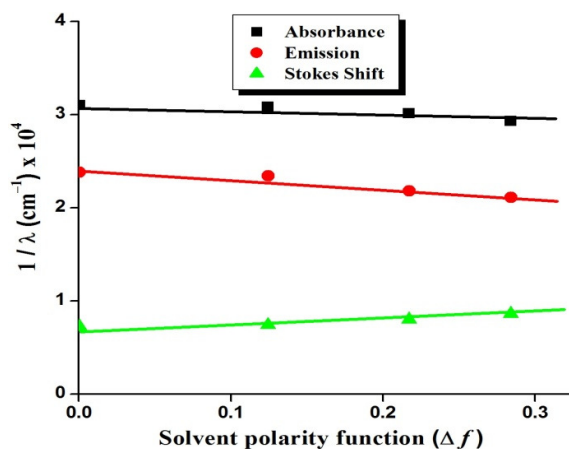


Fig. 3 (a) The black (square), red (circle) and green (triangle) lines are represented **HL**; from top to bottom the lines are represented the absorption maxima, fluorescence maxima and stokes shifts ($\nu_{\text{abs}}^{\text{max}}$, $\nu_{\text{fl}}^{\text{max}}$ and $\Delta\nu_{\text{Stokes shifts}}$ respectively, in cm^{-1}) of **HL** against the solvent polarity function, Δf .

Conclusion

So as a whole we have synthesized a Schiff base and its photo physics has been characterized by absorption, emission techniques. The highest emission intensity was observed less polar solvent. The solvent polarity function plot shows that excited state of the ligand is more polar than the ground state.

Acknowledgements

The valuable discussion and help of Prof. Kajal Krishna Rajak, Dept. of Chemistry, Jadavpur University, Kolkata is kindly acknowledged. The author is also thankful to the Department of Chemistry, A. B. N. Seal College, Cooch Behar.

References

- 1 A. Hens, *RSC Adv.*, 2015, **5**, 54352–54363.
- 2 S. Sen, P. Talukder, S. K. Dey, S. Mitra, G. Rosair, D. L. Hughes, G. P. A. Yap, G. G. Pilet, V. Gramlich and T. Matsushita, *Dalton Trans.*, 2006, 1758–1767.
- 3 P. Bhattacharya, J. Parr and A. T. Ross, *J. Chem. Soc., Dalton Trans.*, 1998, 3149–3150.
- 4 R. T. Ruck and E. N. Jacobsen, *J. Am. Chem. Soc.*, 2002, **124**, 2882–2883.
- 5 D. M. Epstein, S. Choudhary, M. R. Churchill, K. M. Keil, A. V. Eliseev and J. R. Morrow, *Inorg. Chem.*, 2001, **40**, 1591–1596.
- 6 A. Hens, P. Mondal and K. K. Rajak, *Dalton Trans.*, 2013, **42**, 14905–14915.
- 7 (a) S. S. Sun, J. A. Anspach, A. J. Lees and P. Y. Zavalij, *Organometallics*, 2002, **21**, 685–693; (b) F. Y. Wu, Z. Li, L. Guo, X. Wang, M. H. Lin, Y. F. Zhao and Y. B. Jiang, *Org. Biomol. Chem.*, 2006, **4**, 624–630; (c) D. Das, B.G. Chand, K.K. Sarker, J. Dinda and C. Sinha, *Polyhedron*, 2006, **25**, 2333–2340; (d) V. Luxami and S. Kumar, *RSC Advances*, 2012, **2**, 8734–8740.
- 8 S. Nad, M. Kumbhakar and H. Pal, *J. Phys. Chem. A*, 2003, **107**, 4808–4816.
- 9 P. Mahato, S. Saha and A. Das, *J. Phys. Chem. C*, 2012, **116**, 17448–17457.

Solvent-Solvent Interactions in Ethanol-Octanol Binary Solvent Mixtures: A Study of Surface Tension and Fluorescence Anisotropy

Ramkrishna Pramanik

Department of Chemistry, A B N Seal College

E-mail: pramanik72@rediffmail.com

Abstract

Surface tensions of binary system, ethanol+octanol have been measured at three different temperatures over the entire mole fraction range at atmospheric pressure. The excess surface tensions, γ^E , have been calculated and fitted to Redlich-Kister polynomial equation. Surface entropy, S_γ and surface enthalpy H_γ , have been determined. The excess surface tension values are explained in terms of solvent-solvent interactions. A suitable parameter of fluorescence anisotropy of ketocyanine dyes in this solvent mixture is used to get information regarding solvent-solvent interactions. The results are compared and explained.

Key words: Surface tension, excess surface tension, Redlich-Kister polynomial equation, surface entropy, surface enthalpy, fluorescence anisotropy, ketocyanine dye

Publication History: Received: 10th August, 2016; Accepted: 19th August, 2016

Introduction

Complete knowledge of physical properties of binary liquid systems is of great importance for industrial applications and fundamental research. They are often used to modify molecular environments in order to modulate processes such as chromatographic separation, organic synthesis, reaction kinetics and protein folding¹. It is well established that the properties of liquids contain information about intermolecular interactions². In a pure liquid (1) one has to consider only (1-1) interactions. But the use of binary mixture (1+2) adds an extra dimension to the problem. Besides (1-1) and (2-2) interactions present in the pure components, (1-2) interactions are also present in a liquid mixture. Surface tension study of binary liquid mixture provides information about these 1-2 interactions. The literature dealing with surface tension of binary mixtures is extensive, but the systems involving alcohols are interesting³⁻⁷, because of their inherent nature of forming associations in the form of hydrogen bonds within themselves or with other components in a solvent mixture.

Solvation of a solute in mixed binary solvents is another phenomenon, which depends on the mutual interaction of solvents. It is thus instructive to compare the nature of these interactions as obtained from studies involving two different procedures.

Fluorescence anisotropy, representing the rotational characteristics of a fluorophore in a solvent cage acts as a reporter of solvation interaction reflecting solute-solvent as well as solvent-solvent interactions in the microscopic level⁸.

Surface tensions in ethanol-octanol binary mixtures at different temperatures have been measured in order to get solvent-solvent interactions and the results have been compared with previously reported fluorescence anisotropy studies of ketocyanine dyes⁹.

Experimental

The solvents used were of spectroscopic grade and used as received. All the mixtures were prepared by mass in glass stoppered flasks. The balance precision was $\pm 1 \times 10^{-4}$ g. The accuracy of the mole fractions was estimated to be within ± 0.0001 . The surface tensions of pure components and mixtures at the liquid-vapor interface were measured using the ring detachment method by a tensiometer. The temperature of the measurement cell was controlled within ± 0.1 K by a thermostatic water bath via

an external circulating loop. Each value reported was an average of three measurements with an uncertainty of $\pm 0.01 \text{ mNm}^{-1}$.

Results & discussion

Study of surface tension:

The measured values of surface tension, γ in mNm^{-1} , for ethanol(1) + octanol(2) binary mixtures at different compositions and temperatures are listed in table 1. As the mole fraction of ethanol is increased the surface tension decreases. The variation of surface tension with mole fraction is shown in fig.1.

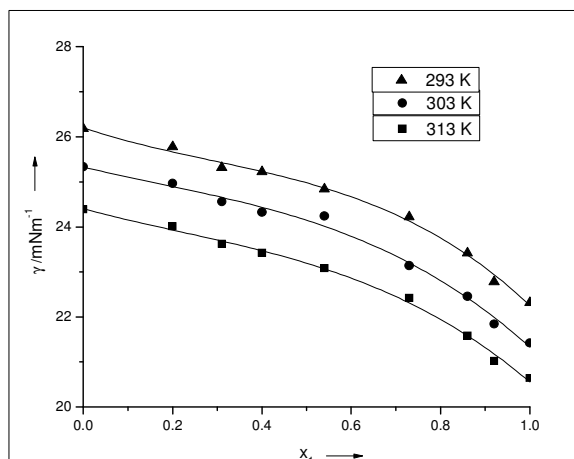


Fig.1: Plot of surface tension vs mole fraction for ethanol(1) + octanol(2) binary mixture at different temperatures. The lines represent polynomial fit.

The variation is non linear indicating deviation from ideal values, i.e., mole fraction average of pure values. The excess surface tensions, γ^E , from ideal values are calculated from the following equation.

$$\gamma^E = \gamma - (x_1\gamma_1 + x_2\gamma_2) \dots\dots\dots (1)$$

Where, γ is the surface tension of mixture; x_1 and x_2 are mole fractions of the component 1 & 2 and γ_1 , γ_2 are the surface tensions of the pure components. Experimental values of γ^E are also shown in table 1.

Table 1: Experimental values of surface tension (γ) and excess surface tension (γ^E) for ethanol(1) + octanol(2) binary mixture at different temperatures (T).

x_1	γ/mNm^{-1}	γ^E	γ/mNm^{-1}	γ^E	γ/mNm^{-1}	γ^E
	T = 293 K		T = 303 K		T = 313 K	
0.0000	26.18	0.00	25.33	0.00	24.39	0.00
0.2001	25.78	0.37	24.96	0.41	24.01	0.37
0.3101	25.32	0.34	24.56	0.44	23.62	0.39
0.4002	25.22	0.58	24.32	0.55	23.42	0.53
0.5401	24.84	0.74	24.24	1.02	23.08	0.72
0.7300	24.22	0.86	23.14	0.66	22.42	0.77
0.8602	23.42	0.56	22.46	0.49	21.58	0.42
0.9203	22.78	0.15	21.84	0.11	21.02	0.08
1.0000	22.32	0.00	21.42	0.00	20.64	0.00

The excess surface tensions, at all compositions, are found to be positive from 293.0 K to 313.0 K. The higher values of surface tension in mixed solvents than the ideal values indicate that the composition in the bulk and surface are different. The added ethanol accumulates more in the surface, and thus decrease the surface tension of the mixture but the accumulation is less than ideal. In this case the 1-2 interactions are preferable than 1-1 or 2-2 interactions. The intermolecular H-bonding plays an important role in this case. The representative graphical variation of excess surface tension with solvent composition is shown in fig. 2.

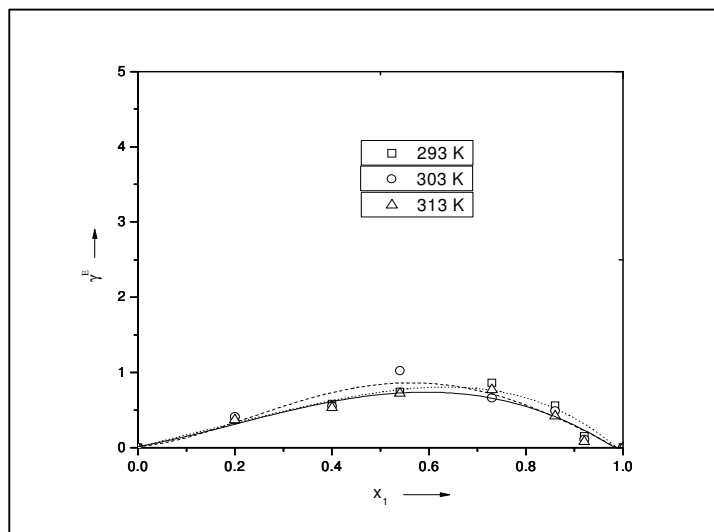


Fig. 2: Plot of excess surface tension γ^E vs. mole fraction of ethanol at different temperatures. The lines represent polynomial fit.

It is clear from the figure that excess surface tension passes through a maximum corresponding to a mole fraction of ethanol > 0.6 . Previous study with excess viscosity and excess energy of activation for viscous flow are also similar in this regard¹⁰. The excess surface tension is also fitted with the Redlich-Kister polynomial equation¹¹,

$$\gamma^E = x_1 x_2 \sum_{i=1}^k A_i (2x_1 - 1)^{i-1} \dots\dots (2)$$

Here, the values of A_i are parameters of the equation. The results are listed in table 2. In all the cases the standard deviations are less than 0.03.

Table 2: Parameters, A_i , of Redlich-Kister Equation of ethanol + octanol binary mixture at different temperatures studied

T/K	A_0	A_1	A_2	A_3	A_4	A_5
293	2.89689	-1.31614	-3.22720	-17.84073	14.93484	42.25515
303	2.10663	1.47874	1.15858	-22.68737	6.85556	40.69801
313	2.70651	-1.33543	-0.71246	-8.03310	5.99797	24.80292

The experimental surface tension values at different temperatures for a given composition of the solution allow estimation of surface entropy ($S_\gamma/\text{Jm}^{-2}\text{K}^{-1}$) and surface enthalpy (H_γ/Jm^{-2}). At a given composition, the surface tension values can be fitted linearly with temperature (T/K) by the following equation.

$$\gamma = A + B(T/K) \dots\dots (3)$$

The parameters A and B give the values of H_γ and S_γ respectively.

$$\gamma = H_\gamma - S_\gamma(T/K) \dots\dots(4)$$

The definition of these quantities are,

$$H_\gamma = \gamma - T\left(\frac{\partial \gamma}{\partial T}\right)_P \text{ and, } S_\gamma = -\left(\frac{\partial \gamma}{\partial T}\right)_P$$

Where S_γ represents the variation of the entropy per unit surface area due to interface formation and is equal to the negative temperature parameter of the surface tension. Surface enthalpy, H_γ is the sum of the surface free energy required to extend the surface and the latent heat required to maintain isothermal conditions. The calculated values are listed in table 3.

Table 3: Derived surface enthalpy (H_γ) and surface entropy (S_γ) for ethanol(1) + octanol(2) binary mixture

x_1	H_γ/mJm^{-2}	$S_\gamma/\text{mJm}^{-2}\text{K}^{-1}$
0.0000	51.96	-0.09
0.2001	50.94	-0.09
0.3101	50.26	-0.09
0.4002	50.89	-0.09
0.5401	48.91	-0.08
0.7300	48.69	-0.08
0.8602	49.38	-0.09
0.9203	48.18	-0.09
1.0000	46.91	-0.08

Fluorescence anisotropy study

Fluorescence anisotropy (r) measurements of a fluorophore in mixed binary solvents can give information about solute-solvent and solvent-solvent interactions. It is instructive to note at this point whether similar information can be obtained or not. Reported values are taken from literature⁹. A suitable parameter ($1/r$) of fluorescence anisotropy is chosen and is given at different mole fractions of ethanol(1) + octanol binary solvent mixtures for two different indicator solutes in table 4.

Table 4: Literature values of emission anisotropy (r) for ethanol(1) + octanol(2) binary mixture for dye I and dye II at 300K

x_1	r (dye I)	r (dye II)
0.00	0.23	0.21
0.20	0.19	0.20
0.40	0.16	0.17
0.60	0.14	0.13
0.80	0.10	0.10
1.00	0.08	0.08

A plot of $(1/r)$ vs. mole fraction of ethanol (x_1) is also shown in fig. 3. Linear plots are obtained. The linear dependence clearly indicates that the values in mixed binary solvents are mole fraction average of pure values, i.e.,

$$\left(\frac{1}{r_{12}}\right) = x_1 \left(\frac{1}{r_1}\right) + x_2 \left(\frac{1}{r_2}\right) \dots\dots(5)$$

Such behavior is often referred to as ideal solvation^{2,12}. Thus ideal solvation behavior is found with both solutes. Ketocyanine dyes (Fig. 4) in the S₁ state interact specifically with protic polar solvents through H-bond interaction. Thus in a protic-protic solvent mixture ideal solvation behavior is expected in view of similar solvent-solvent and solvent-fluorophore interactions.

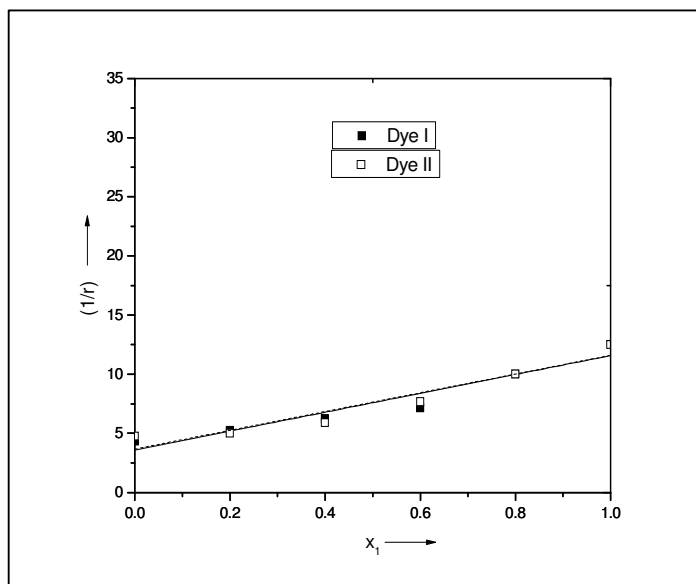


Fig. 3: Plot of a suitable anisotropy parameter ($1/r$) vs. mole fraction(x) in ethanol(1) + octanol binary mixture at 300 K. The lines represent linear fit.

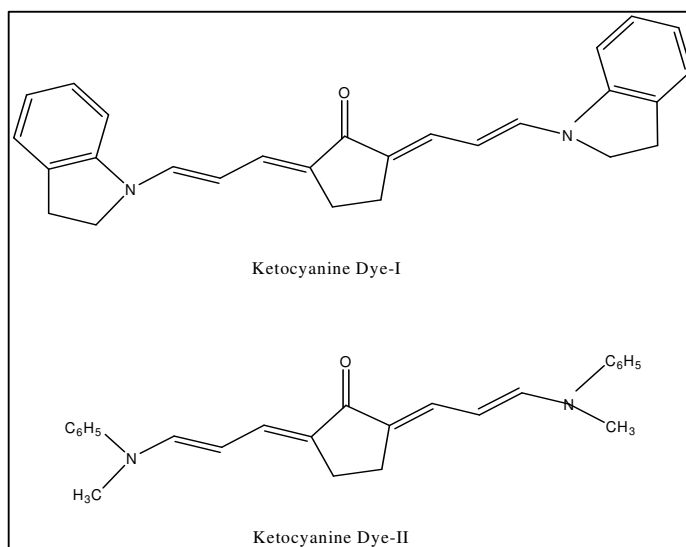


Fig.4: Ketocyanine dyes

Conclusions

The following conclusions can be drawn from the study:

- i) Surface tensions of ethanol+octanol system were measured at different temperatures. In all cases, values of surface tension decrease as the temperature increases. The positive excess surface tension values have been calculated and correlated. Using temperature dependence of surface tensions the entropy change and enthalpy change of surface formation per unit area were also evaluated. The

positive excess surface tension values indicate that 1-2 interactions are preferable than 1-1 & 2-2 interactions.

ii) Fluorescence anisotropy study of ketocyanine dyes in this solvent mixture indicates ideal solvation.

iii) Thus study of surface property (surface tension) gives different information than study of micro-environmental property (fluorescence anisotropy).

Acknowledgement

The author acknowledges the financial support from UGC-India. The Officer-in-Charge, the teaching and non-teaching staff members of the department of Chemistry, A B N Seal College are also gratefully acknowledged for extending their support in carrying out research in the department of Chemistry.

References

1. Catalan J, Diaz C and Garcia-Blanco F (2000), Effects of medium on decarboxylation kinetics: 3-carboxybenzisoxazoles and their potential use as environmental probes in biochemistry, *J. Org. Chem.*, **65**, 9226-9229
2. Marcus Y, *Ion Solvation* (1995), Wiley, Chichester.
3. Vazquez G, Alvarez E, Navaza J M, Rendo R and Romer E (1997), Surface tension of binary mixtures of water + monoethanolamine and water + 2-amino 2-methyl 1-propanol and tertiary mixtures of these amines with water from 25^oC to 50^oC, *J. Chem. Eng. Data*, **42**, 57-59
4. Vazquez G, Alvarez E and Navaza J M (1995), Surface tension of alcohol + water from 20 – 50^oC, *J. Chem. Eng. Data*, **40**, 611-614
5. Hoke Jr. B C and Chen J C (1991), Surface thermodynamics behavior of binary liquid mixtures of benzene + 1,1,2,2 tetrachloroethane: An experimental and theoretical study, *J. Chem. Eng. Data*, **36**, 322-326
6. Azizian S, Hemmati M (2003), Surface tension of binary mixtures of ethanol + ethylene glycol from 20^oC – 50^oC, *J. Chem. Eng. Data*, **48**, 662-663
7. Jimenez E, Cabanas M, Segade L, Garsia-Gakabal S and Casa H (2001), Excess volume, changes of refractive index and surface tension of binary 1,2 ethanediol + 1-propanol or 1-ethanol mixtures at several temperatures, *Fluid Phase Equilib.*, **180**, 151-164
8. Lakowicz J R (1983), *Principles of Fluorescence Spectroscopy*, Plenum Press, New York
9. Pramanik R, Das P K and Bagchi S (2000), Fluorescence anisotropy of ketocyanine dyes in homogeneous and heterogeneous media. Estimation of micellar microviscosity, *Phys. Chem. Chem. Phys.*, **2**, 4307-4311
10. Pramanik R and Bagchi S (2003), study of solvation interaction in ethanol + octan-1-ol mixture, *J. Indian Chem. Soc.*, **80**, 335-339
11. Redlich O and Kister A T (1948), Thermodynamics of nonelectrolytic solutions, algebraic representation of thermodynamic properties and the classification of solutions, *Ind. Eng. Chem.*, **40**, 341-345
12. Banerjee D, Laha A K and Bagchi S (1995), Preferential solvation in mixed binary solvent, *J. Chem. Soc. Faraday Trans.*, **91(4)**, 631-636

Key Players of Innate Immunity in *Drosophila melanogaster*

Prem Rajak¹, Saurabh Sarkar², Arnab Roy² and Sumedha Roy^{2*}

¹Post Graduate Department of Zoology, A.B.N. Seal College, Cooch Behar

²Cytogenetics Laboratory, Department of Zoology, The University of Burdwan, Burdwan

*E. mail: roysumedha@gmail.com

Abstract

Drosophila melanogaster completely relies upon innate immunity to destroy invaded pathogens inside the body. Innate immunity is mediated through cellular and humeral responses. Cellular response is driven through the three variants of hemocytes: Plasmatocytes (perform phagocytosis), Lamellocytes (encapsulate larger pathogens) and Crystal cells (catalyzes melanization around the aggregation of pathogens to destroy them). Humeral response is mainly comprised of Toll (specific for fungal and gram positive infections) and Imd pathways (specific for gram negative infections). These pathways end up with the production of Anti-microbial Peptides (AMPs) that destroy pathogens by disrupting their cell membrane. Immune reactions in *Drosophila* shares many homologies with that of higher vertebrates including human. Therefore, procuring a clear knowledge of innate immune mechanisms in *Drosophila* will definitely help researchers to develop various drugs and vaccines for several deadly pathogens (like HIV) and diseases which are still incurable in the present era.

Key words: AMPs, *Drosophila melanogaster*, Hemocytes, Imd pathway, Innate immunity, Toll pathway

Publication History: Received: 10th August, 2016; Accepted: 19th August, 2016

Introduction

Fruit fly, *Drosophila melanogaster* totally relies upon innate immunity for its defense strategies against pathogens. Innate immunity in fruit flies is predominantly mediated through hemocytes in the circulating hemolymph. In *Drosophila melanogaster*, three major lineages of hemocytes have been recognized till now. These include, Plasmatocytes, Lamellocytes and Crystal cells (Wong *et al.*, 2011).

Signaling pathways such as Toll and Imd pathways support the pillars of humeral innate immunity (Tanji *et al.*, 2007). Toll pathway is turned on during fungal and gram-positive bacterial infections while Imd pathway gets activated during Gram-negative mediated infections. These pathways are directly linked to the synthesis and secretion of several antimicrobial peptides (AMPs), which destroy several pathogens by disrupting their cell membranes.

The *Drosophila* host defense mechanism is a multifaceted process. The epithelial surface of the fly sets the first tire of defense mechanism against invasion of various micro-organisms. The epidermis, the cells of digestive and genital tracts, cells of trachea and malpighian tubules as well as fat bodies produce several AMPs to eradicate pathogenic micro-organisms from the body (Onfelt Tingvall *et al.*, 2001).

Micro-organisms which have succeeded to enter the general body cavity (hemocoel) are encountered by both cellular and humeral defenses. Cellular defenses are comprised of immune cells (hemocytes) such as plasmatocytes, lamellocytes and crystal cells. Plasmatocytes are mainly phagocytic in nature. Lamellocytes are larger of all hemocytes and kill large microbes through the process of encapsulation. Crystal cells provide protection against micro-organisms through melanization (Ferrandon *et al.*, 1998) that helps to restrict the pathogens in a particular area to kill them.

The hallmark of humeral immune reactions is the systemic antimicrobial response (Meister *et al.*, 2000). Syntheses of Antimicrobial peptides are induced following the invasion of microbes inside the body. Majority of AMPs are produced by fat bodies but also secreted by cells of digestive tract, Malpighian tubules, trachea and genital tracts (Tzou *et al.*, 2000). AMPs are secreted into the hemolymph where their combined concentration may reach up to 300 μ M in infected flies (Bulet *et al.*, 1999).

The humeral reactions cover several proteolytic cascades. Among these, one important cascade is melanization cascade which locally leads to generation of quinones and toxic Reactive Oxygen Species (ROS) that culminate into melanin production at the wound sites or around microorganisms (Nappi & Ottaviani, 2000). Quinones, ROS & Melanization inhibit microbial growth and eventually kill them. A complement like cascade has also been noticed in *Drosophila* that may trigger opsonization of micro-organisms to facilitate their phagocytosis by plasmatocytes (Lagueux *et al.*, 2000). Hemolymph Zymogen cascade also play crucial role in activating the synthesis of antimicrobial peptides in the fat bodies (Ashida & Brey, 1995).

Sources of infections in *Drosophila*

Insects colonize in areas harboring almost unquantifiable amount of micro-organisms. Some insects, however, are exposed considerably more to pathogens than the average organisms as they feed, lay their eggs and develop on decomposing media. These infection prone insects include *Drosophila* where a major part of its microbial load is introduced in the gut through the digestive process (Kounatidis & Ligoxygakis, 2012). Subsequently, a part of the digested microbes reach and may colonize the gastrointestinal epithelial wall. These micro-organisms may then become part of the commensal flora or induce pathogenicity and systemic immunity. In addition, systemic activation may occur through septic injury by nematodes or by wasps depositing their eggs on fruit fly larvae.

Gut flora of *Drosophila*

Drosophila gets their gut flora mainly through feeding. Gut microbiota shows their colonization in the gastrointestinal epithelial wall. These gut flora may be beneficial or harmful depending upon their nature of colonization. Several researches have suggested that, *Drosophila* harbors a community of gut bacteria (both beneficial & harmful) which is much simpler than the vertebrate gut flora. It is now possible to extract and cultivate these bacteria, use them in re-colonization experiments and produce mutants to interrogate host-pathogen interactions.

Commensal bacteria

Some bacterial flora like *Lactobacillus plantarum*, *Lactobacillus brevis*, *Acetobacter pomorum*, *Enterococcus faecalis*, etc. seems to be necessary for proper growth, development and proper functioning of metabolic processes in fruit flies (Ren *et al.*, 2007) and therefore, these bacteria are commensal in nature. Brummel *et al.* (2004) showed that, when *Drosophila* adult flies were cultured in axenic condition, their life span was reduced significantly. Brummel *et al.* (2004) also proved that, reintroducing normal bacterial flora during first week of adult life can restore the normal longevity.

Lactobacillus plantarum has been reported sufficient on its own to recapitulate natural microbiota growth promoting effect. *Lactobacillus plantarum* exerts its beneficial effect by acting with a rapamycin (TOR) dependent host nutrient sensing system controlling hormonal growth signaling which regulate growth and development of larvae, pupae and adult forms of fruit flies (Storelli *et al.*, 2011).

These findings about the commensal gut flora clarifies that, an association of host-commensal microbiota is needed for proper growth and development of the host organism.

Pathogenic bacteria

Bacterial strains inducing immune responses in hosts are mainly pathogenic in nature. Several pathogenic bacteria have been reported. Out of them, strains of *Erwinia*, *Pseudomonas* & *Serratia* are going to be frequently used for research purposes to understand immune mechanisms.

In a study by Basset et al., 2000, infection of *Drosophila* by different strains of genus *Erwinia* revealed the activation of host immune responses. Importantly, Non-pathogenic strain *Erwinia carotovora carotovora-15* (Ecc-15) has proved to be a valuable tool in exploring immune responses. By using the strain Ecc-15, Tzou et al. (2000) showed that, expression of several Anti-microbial peptides is tissue specific. As for example, dipterixin expression in larvae upon infection by Ecc-15 was noticed only in proventriculus and upper part of mid gut. Ingestion experiments using Ecc-15 confirmed the participation of JAK-STAT pathway in association with Imd pathway to provide gut immunity (Buchon et al., 2009). JAK-STAT signaling pathway participates in intestinal defense mechanism by regulating stem cell proliferation. Using *Pseudomonas entomophila*, Jiang et al. (2009) showed that, activation of JAK-STAT pathway in intestinal cells was due to production of cytokines (Upd, Upd2 and Upd3) in the cells of mid gut.

An important infectious agent in *Drosophila* is *Wolbachia* which is a member of intracellular proteobacteria. *Wolbachia* are very widely spread in both arthropods and nematodes and are reported to have pathogenic or interesting effects on reproduction (O'Neill et al., 1997). *Wolbachia* infection is found to cause cross-incompatibility in *Drosophila simulans* (Hoffmann et al. 1986). Incompatibility occurs due to delayed condensation of sperm pronucleus at first mitosis when sperm from infected male fertilizes egg from uninfected females (Callaini et al., 1997). This effect results in abortion of embryonic development. Cross-incompatibility has been found curable by antibiotic treatment (Louis and Nigro, 1989).

Fungal infection

Fungal infection causes serious damage to fly population and may cause death of larvae and adult flies. When *Cryptococcus neoformans* fungi were ingested to flies, they caused death of flies. The Toll pathway did not show any role in *Drosophila* adult defense mechanism upon ingestion of *C. neoformans* (Apidianakis et al., 2003). However, Toll pathway showed important roles to both clearance of *C. neoformans* cells and survival of adults flies (Glittenberg et al., 2011).

Candida albicans causes extensive JNK-mediated death of gut cells and induces systemic activation of AMP activity in the larval fat body. Both phenomena were partially mediated through fungal proteases. Nitric Oxide and blood cells also plays important roles by inducing systemic immune responses against fungal infections.

Immune cells of *Drosophila* involved in innate immunity

In insects, immune cells are the free circulating hemocytes that remain suspended in the hemolymph of the body cavity. They show cellular defenses by directly interacting with the pathogenic microbes. In *Drosophila*, three types of hemocytes have been recognized (Figure 1). These include:

I. Plasmatocytes: These are most abundant hemocytes in *Drosophila*. They comprise about 95% of all hemocytes. Plasmatocytes are chiefly engaged in phagocytosis of micro-organisms.

II. Lamellocytes: Lamellocytes are flat, elongated cells and are rarely visible in healthy larval hemolymph. Number of lamellocytes increases only in infected conditions and kill large pathogens by means of encapsulation.

III. Crystal Cells: Crystal cells are smallest, dark colored cells, found in larval stage of fruit flies. They constitute about 5% of circulating hemocytes. Crystal cells destroy invading microbes by means of melanization process.

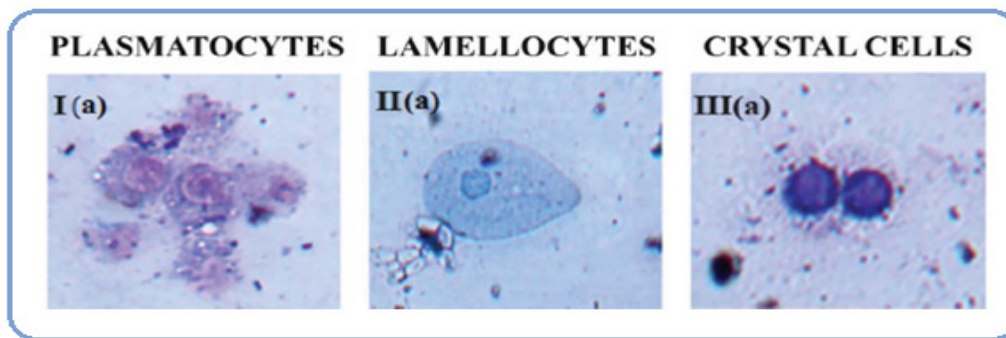


Fig 1: Figure represents Plasmatocytes I(a), Lamellocytes II(a) and Crystal cells III(a) isolated from 3rd instar larvae of *Drosophila melanogaster*. Plasmatocytes are characterized by outer irregular margins and involved in phagocytosis of pathogens, Lamellocytes are large cells involved in encapsulation of larger cells. Crystal cells are small and more or less round cells involved in melanization process. This figure is adopted from Rajak et al., 2014.

Types of immune responses in *Drosophila*

Melanization: It is a preliminary type of immune response that occurs against cuticular or septic invasion of microbial pathogens. This reaction is characterized by darkening of the wound site from where invasion of the pathogen has occurred. Melanization aids in encapsulation of large microbes. Further the intermediate compounds (like phenoloxidase) which are generated during the melanization cascade are also toxic to microbes (Cerenius & Söderhäll, 2004).

Mechanically, melanization starts with the sequential activity of two serine proteases MP1 and MP2 which converts the prophenol-oxidase activating enzyme (PPAE) into its active form. Activated PPAE in turn then cleaves the prophenol-oxidase into active phenol-oxidase state which leads to melanin synthesis resulting in melanization process. The *Drosophila* genome encodes three prophenol-oxidases. Out of them, two (DoxA1 & CG8193) are expressed in crystal cells while one (DoxA3) is expressed in lamellocytes (Pentz et al., 1990).

Phagocytosis: One important, effective and immediate way for fruit flies to eliminate apoptotic bodies, remains of bacterial and fungal infections and fungal spores is their removal by receptor-mediated recognition and phagocytosis. Fruit fly phagocytosis is considered to be a good model for studying the mammalian phagocytosis. This is due to similarity of evolutionary conserved receptors between fruit fly and mammals. These conserved receptors include Croquemort (CRO) which is a paralogue of CD36 receptor (Frank *et al.*, 1996) and Draper which is a paralogue of LPS recognition protein (Awasaki *et al.*, 2006).

Coagulation: An additional immune response that prevents the spread of pathogens from the wound site is the clotting of hemolymph. This process is also called coagulation. In the clot, various characteristic filaments cross-link the bacteria and prevent their spread to other parts of the body. Bidla *et al.* (2005) reported that, crystal cells are important for the hemolymph clot formation and wound healing as their *in vivo* study showed that larvae lacking crystal cells had a reduced ability for clot formation and decreased capacity of wound healing.

Proteomic analysis has identified several proteins involved in clot formation. These comprise Hemolactin (a major component of clot, produced by plasmatocytes), Lipophorin (humoral pro-coagulant), Hexamerin (also called fat body protein 1), Fondue (hemolymph protein, helps in cross-linking of clot fibers) and Transglutaminase (connects bacterial surface with clot matrix).

Secretion of Anti-microbial peptides (AMPs)

Anti-microbial peptides are the effector molecules that are produced in response to invading microbes. Several AMPs have been recognized. Among these, some remarkable AMPs are listed in Table 1:

Table 1: Names of common AMPs, their nature and site of expression

NAME OF AMPs	NATURE	SITE OF EXPRESSION
Diptericin	Anti bacterial (Gram Negative)	Midgut
Attacin	Anti bacterial (Gram Negative)	Midgut
Drosocin	Anti bacterial (Gram Negative)	Calyx, Oviduct, Tracheae
Cecropin	Anti bacterial (Gram Negative)	Calyx, Oviduct, Spermathecae
Defensin	Anti bacterial (Gram Positive)	Seminal receptacle, Spermathecae, labellar gland
Metchnikowin	Anti fungal	Labellar glands
Drosomyacin	Anti fungal	Spermathecae, Tracheae, Salivary glands

Signaling pathways involved in innate immunity of *Drosophila*

Toll and Imd pathways play crucial role in innate immunity. These pathways are selective for particular type of infections. Toll pathway mainly gets activated during the fungal & Gram positive infections whereas Imd pathway gets activated during Gram negative infections (Kappler C *et al.*, 1993). Both pathways ultimately provoke the expression of several genes encoding for AMPs that disrupt the cell membrane of invading micro-organisms to kill them.

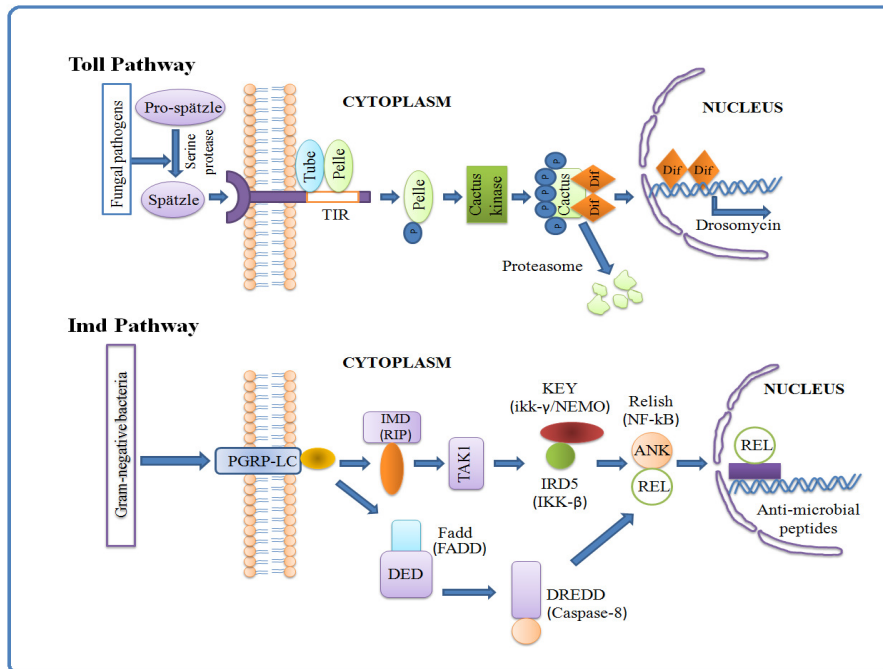


Fig 2: Figure represents a schematic view of Toll and Imd pathways involved in humeral response against fungal and bacterial infections. These pathways ultimately ends with the expression and synthesis of antimicrobial peptide needed for destruction of invasive pathogens. (Above representation is simplified from Hoffmann and Reichhart, 2002).

The Toll pathway

Toll is a trans-membrane receptor having an extracellular domain, a trans-membrane region and an intracellular domain (Hashimoto *et al.*, 1988). Extracellular domain contains leucine-rich repeats and bears ligand binding sites. Intracellular domain shows significant sequence similarity with the intracellular region of the Inter-Leukin 1 Receptor (IL-1R) & hence this region of Toll receptor is referred as the Toll-IL-1R (TIR) domain. TIR domain of toll receptor interacts with those adaptor proteins which have a TIR domain and a death domain (DD). Three adaptor proteins have been recognized in *Drosophila*. These include *Drosophila* homolog of MyD88 (DmMyD88), Tube and Pelle. *Drosophila* genome encodes three Rel proteins (containing Rel homology domain which is responsible for dimerization and DNA binding) such as Dorsal-related Immunity Factor (DIF) , Dorsal and Relish. DIF (a homolog of NF- κ B of mammals) is inactive when it is present in combined form with Cactus. DIF when dissociates from Cactus (a homolog of mammalian I κ B), it activates transcription of a large number of genes. Prominent among these genes are those encoding for the anti-fungal peptides – Drosomycin & Metchnikowin (Figure 2).

When microbes invade the body, circulating pattern recognition proteins identify the microbes to activate a proteolytic cascade which cleaves an important activator protein Spaetzle to its active form. Spaetzle then interacts with extracellular part of Toll receptor for its dimerization and activation. Activated Toll receptor then recruits adaptor proteins such as DmMyD88, Tube and Pelle to constitute a Toll receptor-Adaptor complex which in turn phosphorylates and degrades cactus to release DIF. Free DIF translocates into the nucleus to induce transcription of genes encoding for AMPs.

The Imd pathway

Imd (Immuno-deficient) pathway is activated by Lipo-polysaccharide of Gram-negative bacteria. This pathway resembles TNFR pathway of mammals.

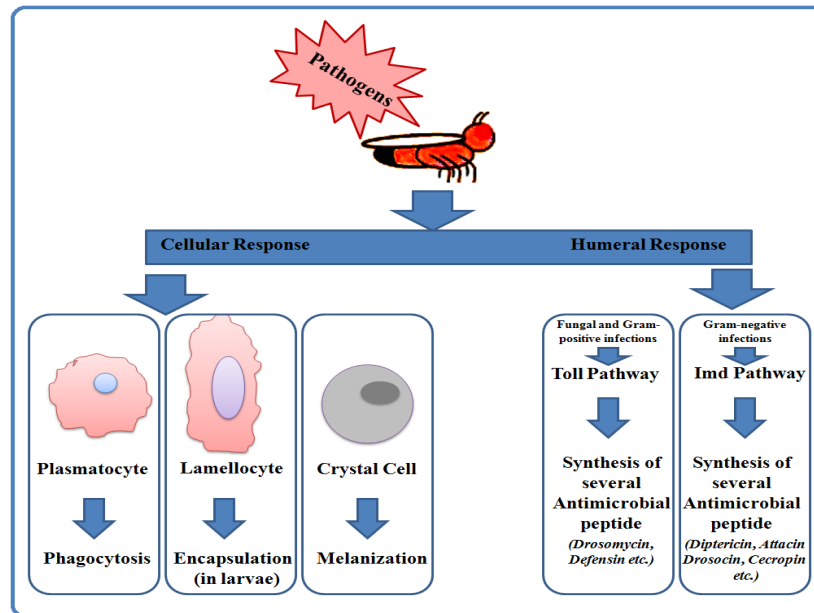


Fig. 3: Schematic representation of cellular and humeral responses in *Drosophila melanogaster* against invasion of the pathogens. Cellular response is mediated by Plasmatocytes (perform phagocytosis), Lamellocytes (encapsulate larger pathogens) and Crystal cells (drives melanization around the aggregation of pathogens to destroy them). Humeral response is mainly comprised of Toll (specific for fungal and gram positive infections) and Imd pathways (specific for gram negative infections). These pathways end up with the production of Antimicrobial Peptides which destroy the plasma membrane of pathogens to kill them.

Activation of Imd Pathway: Imd pathway is induced by diaminopimelic acid (DAP) type peptidoglycan present in cell wall of Gram-negative bacteria. The pathway is triggered from outside the cell by binding of DAP-PGNS to pattern-recognition receptors namely, peptidoglycan recognition protein (PGRP)-LC or intracellularly bind to PGRP-LE receptor. This pathway can also be turned on from the cytoplasm via a splicing variant of PGRP-LE. Binding of DAP-PGNS (found in Gram negative bacteria) to the PGRP receptors lead to dimerization/multimerization of the receptors. This results in recruitment of adaptor proteins IMD and DFADD along with caspase-8 orthologue DREDD. Mean while, TAK1 (*Drosophila* Transforming Growth Factor-activated kinase 1) and its partner TAB-2 are possibly activated through the IAP-2: Bendless (BEN): UEV1a Ubiquitin E3 ligase complex. Activated TAK-1 & TAB-2 in turn phosphorylates the IKK- β ortholog IRD-5. IRD-5 in complex with IKK- γ orthologue Kenny (KEY), phosphorylates the NF- κ B orthologue Relish (Rel). Rel consists of an N-terminal nuclear factor containing domain REL-68 and an inhibitory C-terminal domain (REL-49) rich in ankyrin repeats responsible for anchoring REL in the cytoplasm. Phosphorylated form of Relish is the target of DREDD which cleaves the C-terminal inhibitory ankyrin repeats leading to translocation of Relish inside the nucleus. Relish then activates transcription of genes encoding for antimicrobial peptides specific for Gram-negative bacterial infection (Figure 2).

Conclusion

The first line of defense mechanism used by our body to protect us from pathogens is the innate immunity. Similarly in *Drosophila*, it is the effective and immediate response which is shown by our body against most infections. Several primary modes of responses like phagocytosis, encapsulation, pattern recognition etc have been studied in vast details. But still there are many unexplored areas which have to be explored with the help of modern facilities and techniques. Several peptides involved in encapsulation process have been isolated, yet we don't know about their exact mechanism of action. Phagocytosis process by which plasmatocytes engulf their target materials seems to be an easier mechanism apparently but it is not also parctically. Several interactions between cell surfaces of plasmatocytes and microbes might be going on for phagocytosis process which still remained to be explored with details and clarity. Procedure of Opsonization and the molecules involved in it is still remaining unclear and need proper research. Two major pathways such as Toll and Imd pathways (Figure 3) have been reported to be involved in innate immunity but some steps in these pathways are still unclear and even represented by 'question marks' (?). These fields need to be unraveled in the near future to provide better understanding of immune mechanisms. Procuring a clear knowledge of immune mechanisms would definitely help researchers to develop various drugs and vaccines for the pathogens (like HIV) and diseases which are still incurable in the present era.

References

- Apidianakis Y, Rahme LG, Heitman J, Ausubel FM, Calderwood SB, Mylonakis E (2003), Challenge of *Drosophila melanogaster* with *Cryptococcus neoformans* and role of the innate immune response. Eukaryot Cell 3:413–419.
- Ashida M, Brey PT (1995), Role of the integument in the insect defense: pro-phenol oxidase cascade in the cuticular matrix. Proc Natl Acad Sci USA 92:10698-10702.
- Awasaki T, Tatsumi R, Takahashi K, Arai K, Nakanishi Y, Ueda R, Ito K (2006), Essential role of the apoptotic cell engulfment genes draper and ced-6 in programmed axon pruning during *Drosophila* metamorphosis. Neuron 50:855–867.
- Basset A, Khush RS, Braun A, Gardan L, Boccard F, Hoffmann JA, Lemaitre B (2000). The phytopathogenic bacteria *Erwinia carotovora* infects *Drosophila* and activates an immune response. Proc Natl Acad Sci USA 97:3376-3381.

- Bidla G, Lindgren M, Theopold U, Dushay MS (2005). Hemolymph coagulation and phenoloxidase in *Drosophila* larvae. *Dev Comp Immunol* 29:669–679.
- Brummel T, Ching A, Seroude L, Simon AF, Benzer S (2004). *Drosophila* lifespan enhancement by exogenous bacteria. *Proc Natl Acad Sci USA* 101:12 974–12 979.
- Buchon N, Broderick NA, Chakrabarti S, Lemaitre B (2009). Invasive and indigenous microbiota impact intestinal stem cell activity through multiple pathways in *Drosophila*. *Genes Dev* 23:2333–2344.
- Bulet P, Hetru C, Dimarcq JL, Hoffmann D (1999). Antimicrobial peptides in insects; structure and function. *Dev Comp Immunol* 23:329-344.
- Callaini G, Dallai R, Riparbelli (1997). Wolbachia induced delay of paternal chromatin condensation does not prevent material chromosomes from entering anaphase in incompatible crosses of *Drosophila simulans*. *J Cell Sci* 110:271-280.
- Cerenius L, Söderhäll K (2004). The prophenol oxidase activating system in invertebrates. *Immunol Rev* 198:116–126.
- Ferrandon D. *et al.* (1998). A drosomycin-GFP reporter trans-gene reveals a local immune response in *Drosophila* that is not dependent on the Toll pathway. *EMBO J* 17:1217-1227.
- Frank NC, Dimarcq J-L, Lagueux M, Hoffmann J, Ezekowitz RAB (1996). Croquemort, a novel *Drosophila* hemocyte/macrophage receptor that recognizes apoptotic cells. *Immunity* 4:431–443.
- Glittenberg MT, Kounatidis I, Christensen D, Kostov M, Kimber S, Roberts I, Ligoxygakis P (2011). Pathogen and host factors are needed to provoke a systemic host response to gastrointestinal infection of *Drosophila* larvae by *Candida albicans*. *Dis Model Mech* 4:515-525.
- Hashimoto C, Hudson KL, Anderson KV (1988). Toll gene of *Drosophila*, Required for dorsal-ventral embryonic polarity, appears to encode a transmembrane protein. *Cell* 52:269-279.
- Hoffmann JA, Reichhart JM (2002). *Drosophila* innate immunity: an evolutionary perspective. *Nature immunol* 3:121-126.
- Hoffmann AA, Turelli M, Simmons GM (1986). Unidirectional incompatibility between populations of *Drosophila simulans*. *Evolution* 40: 692-701.
- Jiang H, Patel PH, Kohlmaier A, Grenley MO, McEwen DG, Edgar BA (2009). Cytokine/Jak/Stat signaling mediates regeneration and homeostasis in the *Drosophila* midgut. *Cell* 137: 1343–1355.
- Rajak P, Dutta M, Roy S (2014). Effect of acute exposure of acephate on hemocyte abundance in a non-target victim *Drosophila melanogaster*. *Toxicol Environ Chem* 96:768-776.
- Kappler C *et al.* (1993). Insect immunity. Two 17bp repeats resting a kB-related sequence confer inducibility to the dipterin gene and bind a polypeptide in bacteria challenged *Drosophila*. *EMBO J* 12:1561-1568.
- Kounatidis I, Ligoxygakis P (2012) *Drosophila* as a model system to unravel the layers of innate immunity to infection. *Open Biol* 2:120075.
- Lagueux M, Perrodou E, Levashina EA, Capovilla M, Hoffmann JA (2000). Constitutive expression of a complement-like protein in toll and JAK gain of function mutants of *Drosophila*. *Proc Natl Acad Sci USA* 97, 11427-11432.
- Meister M, Hetru C, Hoffmann JA (2000). The antimicrobial host defense of *Drosophila*. *Curr Top Microbiol Immunol* 248:17-36.
- O’Neil SL, Hoffmann AA, Werren JH (1997). Influential passengers. Inherited microorganisms and arthropod reproduction. Oxford university press, United kingdom.

Onfelt Tingvall T, Roos E, Engstrom Y (2001). The imd gene is required for local cacropin expression in *Drosophila* barrier epithelia. EMBO Rep 2:239-243.

Pentz ES, Black BC, Wright TR (1990). Mutations affecting phenol oxidase activity in *Drosophila*: quicksilver and tyrosinase-1. Biochem Genet 28:doi:10.1007/BF00561334, 151–171.

Ren C. *et al.*, (2007). Increased internal and external bacterial load during *Drosophila* aging without lifespan trade-off. Cell Metab 6:doi:10.1016/j.cmet.2007.06.006, 144–152.

Storelli G, Defaye A, Erkosar B, Hols P, Royet, Leulier F (2011). Lactobacillus plantarum promotes *Drosophila* systemic growth by modulating hormonal signals through TOR-dependent nutrient sensing. Cell Metab 14, 403–414.

Tanji T, HU X, Weber ANR, Tony Y (2007). Toll and IMD pathways synergistically activate an innate immune response in *Drosophila melanogaster*. Mol Cell Biol. 27: 4578-4588.

Tzou P *et al.* (2000). Tissue specific inducible expression of antimicrobial peptide gene in *Drosophila* surface epithelia. Immunity 13:737-748.

Wong CN, Ng P, Douglas AE (2011). Low diversity bacterial community in the gut of the fruitfly *Drosophila melanogaster*. Environ. Microbiol. 13, 1889–1900.

Genetic Etiology of Biological Ageing

Satadal Adhikary

P.G. Department of Zoology, A B N Seal College, Cooch Behar

Email: adhikary.satadal@yahoo.com)

Abstract

Ageing is the deterioration of normal physiological functions in the body which is observed in an organism at the ultimate time of its lifespan. A number of genetic factors have been found to be responsible to bring about the characteristics of ageing. One of the best-known events associated with ageing is the gradual shortening of telomeres. Most of the multicellular eukaryotes have limited amounts of telomerase which results in shortening of telomere during cell division. Apart from that a number of signalling pathways, which involve a wide array of genes play crucial role in ageing. Up regulation and down regulation of certain genes in model organisms and the subsequent observation of their altered lifespan and aging associated bodily features indicate that the insulin-like signalling pathway, TOR pathway, catabolic processes activated by AMP Kinase are involved in this process. Along with that, the role of genes regulating DNA and histone methylation and DNA acetylation processes, genes controlling the morphology and division of mitochondria are also significant.

Key words: Ageing, Gerontogene, Telomere, Signalling pathway, Epigenetics

Publication History: Received: 10th August, 2016; Accepted: 19th August, 2016

Introduction

Ageing is the time-related deterioration of normal physiological functions in the body, which comes with the misbalance in homeostasis. In usual frame, it is discussed under two major facets: in terms of the longevity of an organism, i.e. how long it lives; and secondly, in terms of health, i.e. how healthily an organism lives. Ageing manifests itself in the physiological degradation in course of time, known as senescence- which is the signature of old age. With the onset of ageing, physiological functions such as regenerative ability and reproductive power gradually deteriorate. Organisms become more susceptible to stress and diseases. Losses of essential functions of the body tend to bring up age-associated complications which ultimately lead to death.

From time to time, many theories of ageing have been postulated, proposing the underlying mechanisms of ageing in the living entities.

The discovery of gerontological genes or gerontogenes, and research works on the members of certain conserved biological pathways across species have enlightened the genetic etiology of biological aging. These discoveries opened a new vista in pharmacology and medicinal treatments that can extend healthy lifespan by altering the ageing processes.

Causative Factors of Ageing and Senescence

With the development and progression of gerontology and allied scientific researches, different theories regarding ageing have emerged so far which can be narrowed down to a few titles. It is well proved that several factors are directly associated with ageing. These factors include:

Telomere Shortening

Telomeres are specialized structures present at the ends of eukaryotic chromosomes that prevent the chromosome ends from being recognized as a DNA break. In vertebrates, telomeres are characteristically composed of TTAGGG repeats and is bound by a protein complex known as shelterin (also known as the telosome) (Liu et al, 2004). Telomere repeats are produced by a cellular reverse transcriptase known as telomerase (telomerase reverse transcriptase, or Tert). Telomerase can recognize the 3'-OH at the ends of chromosomes and adds telomere repeats *de novo* with the help of

an associated RNA molecule that works as a template (telomerase RNA component, or Terc) (Chan et al, 2002). Eukaryotes have limited amounts of telomerase which results in shortening of telomere during cell division. Such shortening of telomere happens as DNA polymerases are unable to replicate the ends of chromosomes.

Telomere repeats are bound by shelterin multiprotein complex (De Lange, 2002). Protein factors which are the constituent of this multi-protein complex bind directly to the G-strand overhang and to the double-stranded telomeric regions. Some of the factors are the telomere repeat binding factors TRF1 and TRF2 and their interacting proteins Rap1 (repressor activator protein 1) and Tin2 (TRF1-interacting nuclear protein 2) (Liu et al, 2004). TRF1 is also involved in the recruitment of the TANK1 and TANK2 poly (ADP)-ribosylases which are also known as tankyrases (Smith et al, 1998). TRF1 and the TRF1-interacting proteins have been proposed to regulate telomere length by controlling the access of telomerase to the telomeric regions.

The role of TRF2 in telomere protection is also crucial. It may be associated to their involvement with DNA damage signaling and repair factors (Blasco 2005). TRF2 has been proposed to bind to ATM and to shut down the ATM-triggered damage response, indicating that TRF2 has a role in preventing a DNA damage response at telomeres (Karlseder et al, 2004).

Telomerase is composed of two molecules each of the telomerase reverse transcriptase subunit (Tert), the telomerase-associated RNA molecule (Terc) and one molecule of dyskerin, a protein which is known to stabilize the telomerase complex. The erosion of telomeric DNA that takes place during ageing is probably a result of limited amounts of telomerase activity in the adult organism.

Up until now, one of the best-known events associated with ageing is the gradual shortening of telomeres. Some evidences in support for this correlation are presented in the passages following.

The telomerase-deficient mice

The *Terc*-deficient mouse model is an important tool for studying the impact of decayed telomeres in ageing and is considered to be one of the best models for studying ageing and senescence. *Terc*-deficient mouse was first generated in the laboratory by elimination of the mouse *Terc* gene (Blasco et al, 1995). The longevity of the *Terc*^{-/-} mouse strain is severely hampered, and only a few generations can be derived from them. They also exhibit pathologies associated with loss of telomeric repeats (Lee et al, 1998). These pathologies include male and female infertility, heart failure, immunosenescence etc. (Lee et al, 1998).

In connection to this, the *Terc*-deficient mouse model has also been used to elucidate of the role of telomeres and telomerase in tumorigenesis. *Terc*-deficient mice with short telomeres have been observed to be resistant to both induced and spontaneous tumorigenesis (Gonzalez-Suarez et al, 2000).

Furthermore, mice, simultaneously deficient in telomerase and the tumor suppressor proteins like p16, p21, APC, ATM, etc. also show diminished tumorigenesis. It is a clear indication that short telomeres are potent suppressors of cancer (Wong 2003).

Mice with altered expression of the shelterin proteins

A crucial role for mammalian shelterin components in disease has been suggested by the fact that TRF1, TRF2 and Tin2 are upregulated in some human carcinomas (Bellon et al, 2006).

To be precise, TRF2 has been involved in telomere-length regulation (Smogorzewska et al, 2000). Experimental mice with increased TRF2 expression in stratified epithelial cells show conspicuously short telomeres. Interestingly, they also manifests symptoms like premature deterioration of the skin and increased UV-induced skin carcinogenesis, which are similar to the skin pathologies observed in case of human tumor-prone xeroderma pigmentosum syndrome (Blanco et al, 2005). Overexpression of telomerase is unable to hinder telomere shortening or the ageing pathologies

in these mice (Blanco et al, 2005), which also suggests that short telomeres generated by TRF2 over-expression cannot be rescued by telomerase (Blanco et al, 2005).

A precise and well documented role for the TRF1 shelterin component in human is unknown other than the observation that this protein is up regulated in some human tumors (Bellon et al, 2006). Mice deficient in TRF1 show embryonic lethality in the absence of defective telomere length or loss of telomere protection.

Finally, the specific involvement of Pot1 in human disease remains yet to be demonstrated. Deletion of the genes encoding Pot1 in mice results in chromosomal instability which in turn may influence carcinogenesis (Wu et al., 2006).

Telomere shortening and stem cell dysfunction

According to the emerging concepts of gerontology, cancer and ageing are considered to be as stem cell diseases.

Telomerase is expressed at very high levels during embryonic development, but its expression is down-regulated a few weeks after birth in most of the tissues. The only exception to this rule happens in case of stem cells.

Experimental findings show that Hematopoietic Stem Cells (HSCs) from *Terc*-deficient mice with short telomeres show a reduced ability to repopulate irradiated mice (Allsopp et al, 2003). It has also been reported that mobilization of ESCs out of the hair follicle niche upon mitogen-induced proliferation is inhibited in *Terc*^{-/-} mice with characteristically short telomeres (Flores et al, 2005). This mobilization deficiency results in lower rates of proliferation in the hair follicle stem cell niche leading to defective hair growth. Interestingly, this is also a common symptom seen in aged persons.

Ageing: Involvement of some signalling pathways and gerontogenes

Using different model organisms, a number of genes whose activity was altered in long-lived mutants have been identified. The finding shows the participation of various signalling pathways, which are involved in regulating the ageing process. Some of them are insulin/IGF-1, TOR, MAPK, AMPK etc. Under normal conditions, these signalling cascades control energy balance, cellular plasticity, and the mechanisms supporting homeostasis, growth, and reproduction (Barzilai et al, 2012). However, under harsh conditions the stress-resistance proteins are activated as the discussion follows.

Insulin like Signalling Pathway

The most studied pathway in this field is the insulin-like signalling pathway. Upon insulin-like growth factor (IGF-1) binding to its receptor, IGF-1 receptor (IGF-1R), the phosphoinositol-3-kinase (PI3K) is activated, leading to formation of the downstream intermediate phosphoinositide-3,4,5-triphosphate. The later one then binds to 3-phosphoinositid-dependent kinase 1 (PDK-1), which, in turn, phosphorylates and activates the kinases Akt/PKB and SGK-1 that control regular growth processes in the cell. At the same time, the stress-resistance factors, such as FOXO transcriptional factor, are inactivated.

In fact, effects of this pathway on lifespan of organisms are conserved among species (Kenyon 2005). In *Drosophila*, inhibiting insulin/IGF-1 signalling or increasing the activity of FOXO (the *Drosophila* orthologue of DAF-16) specifically in adipose tissue increases lifespan (Kenyon 2005). In mice, a striking inverse correlation between IGF-1 levels and lifespan has been observed among inbred strains, which is a strong indication that IGF-1 plays a crucial role in regulation of the lifespan. (Yuan et al, 2009).

In *C. elegans*, mutations decreasing the activity of *daf-2*, which encodes a hormone receptor similar to the insulin and IGF-1 receptors, double the lifespan of the animal. Mutations hampering the downstream phosphatidylinositol 3-kinase (PI(3)K)/ AKT/PDK kinase cascade extend lifespan as well (Herndon et al, 2002).

Mutations impairing IGF-1 receptor function are frequently observed in a cohort of Ashkenazi Jewish centenarians (Suh, Y. et al, 2008) and DNA variants in the insulin receptor gene have been shown to be linked to longevity in a Japanese cohort (Kojima et al, 2004). These are strong evidences for the fact that this pathway plays role in aging and senescence of human.

TOR Signalling Pathway

The TOR kinase is a major amino-acid and a potent nutrient sensor which is involved in the stimulation of growth. Inhibition of TOR pathway increases lifespan in many species. As a response to nutrients, TOR upregulates translation by activating the ribosomal subunit S6 kinase and inhibiting 4E BP, a translation inhibitor. When nutrient levels and TOR activity fall, rate of translation falls. This has shown an impact on lifespan, as inhibition of S6 kinase has been observed in extending the lifespan in yeast, worms, flies and mice (Hansen et al, 2007).

AMPK

AMP kinase activates catabolic pathways and represses anabolic pathways when the cell's AMP/ATP ratio rises. Over expression of AMP kinase extends lifespan in *C. elegans* (Apfeld et al., 2004), and the anti-diabetic drug metformin, activating AMP kinase, can extend lifespan in mice (Anisimov et al., 2008). AMP kinase is also required for insulin/IGF-1 mutations to be able to extend worm lifespan (Apfeld et al, 2004).

Sirtuins

Sirtuins are NAD⁺-dependent protein deacetylases. Its overexpression has been reported to extend lifespan in yeast, worms and flies (Kenyon 2005). In *C. elegans*, overexpression of the sirtuin gene, sir-2.1 extends lifespan by activating DAF-16/FOXO19 (Berdichevsky et al., 2006). SIR-2.1 has been proposed to activate DAF-16 by deacetylation process, as mammalian SIRT1 is known to deacetylate FOXO proteins in response to oxidative stress. As sirtuins can deacetylate FOXO proteins, and insulin/IGF-1 pathway mutants do not require the involvement of sir-2.1, it can be concluded that sirtuins influence DAF-16/FOXO and lifespan independently of insulin/IGF-1 signalling pathway.

Epigenetics of Ageing

It has been established that epimutations accumulate with age, which leads to the activation of genes, which are normally downregulated epigenetically (Bennett-Baker et al., 2003). Genetically identical twins exhibit significant differences in genome methylation pattern. This might be an explanation for differential lifespan in twins.

During ageing, the activities of methyltransferases DNMT1 and DNMT3a (Casillas, 2003) and deacetylase SIRT1 (Marton, 2010) are reduced. On the other hand, the activities of histone demethylases Jmjd3 and Jarid1b (Nijwening et al, 2011) are enhanced. These result in alterations of epigenetic landscape, thereby changing gene expression pattern leading to ageing.

Mitochondria and ageing

Mitochondrial theory of ageing proposes that, progressive accumulation of somatic mutations in mtDNA during an individual's lifetime causes a decline in mitochondrial normal bioenergetic function and is a contributory factor of ageing.

Change in mitochondria morphology with age: Role of hFis1 gene

It has been established that the morphology of mitochondria is regulated by proteins controlling fission, such as hFis1 and Drp1, and fusion, such as *mitofusin 1* and 2 (MFN1 and 2) and OPA1. These proteins play an important role in the pathophysiology of neurodegenerative diseases observed in old age (Chen and Chan 2009).

Reducing the expression of hFis1 by RNA interference in mammalian cells, it was found that mitochondria become enlarged and flattened (Lee et al., 2007). Along with that it was also observed

that these morphological changes are correlated with increased β -galactosidase activity, a marker of cell senescence. It was also reported to be correlated with decreased mitochondrial membrane potential, increased ROS generation and DNA damage. This suggests that, hFis1 plays an important role in cell senescence and both the structure and dynamics of structure (Lee et al., 2007).

Role of BubR1: A Spindle Assembly Checkpoint protein

It is well proved that, DNA maintenance and repair pathways play a crucial role in ageing processes. A study demonstrated that, mice expressing only 10% normal mitotic spindle assembly checkpoint protein BubR1 leads to progressive aneuploidy and development of specific early ageing-associated phenotypes, including short life span (Baker et al, 2004). Supporting this view, it was also observed that, natural ageing of wild-type mice is marked by decreased BubR1 expression in multiple tissues, suggesting that this protein may be a regulator of normal ageing (Baker et al, 2004).

Analysis of the morphology of arteries from BubR1H/H mice showed reduced numbers of smooth muscle cells. This observation is coherent with the age-related decline in proliferative capacity of vascular smooth muscle cells of humans and mice. With the decrease of smooth muscle cells in arterial media, major changes occur in extracellular matrix which include increased content of collagen and decreased levels of elastin. This in turn causes fibrosis of vascular wall, a phenomenon observed in aged arteries of human and rat (Hajdu et al, 1990).

Conclusion

The discussion so far summarizes the fact that aging in animals is not controlled by a single factor. A number of factors are responsible for the onset of ageing and age related deterioration of the body. Therefore, elucidation of the genetic etiology of biological aging and senescence has a major prospect in the field of medical science. At the same time, it should be noted that, ageing is not a disease rather it is a natural process of decay of normal physiological functions at old age. Therefore, the future research on gerontology should not be focused to increase the lifespan of human by violating the nature. The potentiality of the researches on gerontology lies on finding out the causation of senescence and thereby treating premature aging syndromes and providing older people a better living standard.

Acknowledgement

The author remains thankful to Dr. Sujoy Ghosh, Assistant Professor of Zoology, University of Calcutta for his guidance during the preparation of this work. The valuable suggestions given by Mr. Prem Rajak, Assistant Professor of Zoology, A. B. N. Seal College, Cooch Behar are highly appreciated.

References

- Allsopp RC, Morin GB, DePinho R, Harley CB, Weissman IL (2003), Telomerase is required to slow telomere shortening and extend replicative lifespan of HSCs during serial transplantation. *Blood* 102(2):517-20
- Anisimov VN, Berstein LM, Egormin PA, Piskunova TS, Popovich IG, Zabezhinski MA, Tyndyk ML, Yurova MV, Kovalenko IG, Poroshina TE, Semenchenko AV (2008), Metformin slows down aging and extends life span of female SHR mice. *Cell Cycle*. 7(17):2769-73
- Apfeld J, O'Connor G, McDonagh T, DiStefano PS, Curtis R (2004), The AMP-activated protein kinase AAK-2 links energy levels and insulin-like signals to lifespan in *C. elegans*. *Genes Dev* 18(24):3004-9
- Baker DJ, Jeganathan KB, Cameron JD, Thompson M, Juneja S, Kopecka A, Kumar R, Jenkins RB, de Groen PC, Roche P, van Deursen JM. BubR1 insufficiency causes early onset of aging-associated phenotypes and infertility in mice (2004). *Nat Genet*. 36:744 –749.
- Barzilai N, Huffman DM, Muzumdar RH, Bartke A (2012), The critical role of metabolic pathways in aging. *Diabetes*. 61(6): 1315-22

- Bellon M, Datta A, Brown M, Pouliquen JF, Couppie P, Kazanji M, Nicot C (2006), Increased expression of telomere length regulating factors TRF1, TRF2 and TIN2 in patients with adult T-cell leukemia. *Int. J. Cancer.* 119:2090–2097
- Bennett-Baker PE, Wilkowski J, Burke DT (2003), Age-associated activation of epigenetically repressed genes in the mouse. *Genetics.* 165(4):2055-62.
- Berdichevsky A, Viswanathan M, Horvitz HR, Guarente L (2006), *C. elegans* SIR-2.1 interacts with 14-3-3 proteins to activate DAF-16 and extend life span. *Cell.* 125(6):1165-77
- Blasco MA (2005), Telomeres and human disease: ageing, cancer and beyond. *Nat Rev Genet.* 6(8):611-22.
- Blasco MA, Funk W, Villeponteau B, Greider CW (1995), Functional characterization and developmental regulation of mouse telomerase RNA. *Science.* 269(5228):1267-70.
- Blasco MA, Lee HW, Hande MP, Samper E, Lansdorp PM, DePinho RA, Greider CW (1997), Telomere shortening and tumor formation by mouse cells lacking telomerase RNA. *Cell* 91(1):25-34
- Casillas MA Jr, Lopatina N, Andrews LG, Tollefsbol TO (2003), Transcriptional control of the DNA methyltransferases is altered in aging and neoplastically-transformed human fibroblast. *Mol Cell Biochem.* 252(1-2):33-43
- Chan, S.W. & Blackburn, E.H. (2002), New ways not to make ends meet: telomerase, DNA damage proteins and heterochromatin. *Oncogene* 21: 553–563
- Chen H and Chan DC (2009), Mitochondrial dynamics—fusion, fission, movement, and mitophagy—in neurodegenerative diseases. *Hum Mol Genet.* 18(R2): R169–R176.
- De Lange, T (2002), Protection of mammalian telomeres. *Oncogene* 21(4): 532–540.
- Flores, I., Cayuela, M.L. & Blasco, M.A (2005), Effects of telomerase and telomere length on epidermal stem cell behavior. *Science* 309: 1253–1256.
- Gonzalez-Suarez, E., Samper, E., Flores, J.M. & Blasco, M.A (2000), Telomerase-deficient mice with short telomeres are resistant to skin tumorigenesis. *Nat. Genet.* 26(1):114-7.
- Hajdu MA, Heistad DD, Siems JE, Baumbach GL. Effects of aging on mechanics and composition of cerebral arterioles in rats (1990), *Circ Res.* 66:1747–1754.
- Hansen M, Taubert S, Crawford D, Libina N, Lee SJ, Kenyon C (2007), Lifespan extension by conditions that inhibit translation in *Caenorhabditis elegans*. *Aging Cell* 6(1):95-110.
- Herndon LA, Schmeissner PJ, Dudaronek JM, Brown PA, Listner KM, Sakano Y, Paupard MC, Hall DH, Driscoll M (2002), Stochastic and genetic factors influence tissue-specific decline in ageing *C. elegans*. *Nature.* 419(6909):808-14
- Karlseder J, Hoke K, Mirzoeva O K, Bakkenist C, Kastan M B, Petrini J, De Lange T (2004), The Telomeric Protein TRF2 Binds the ATM Kinase and Can Inhibit the ATM-Dependent DNA Damage Response. *PLoS Biol.* 2(8): e240. doi:10.1371/journal.pbio.0020240.
- Kenyon C (2005), The plasticity of aging: insights from long-lived mutants. *Cell* 120: 449–460
- Kojima T, Kamei H, Aizu T, Arai Y, Takayama M, Nakazawa S, Ebihara Y, Inagaki H, Masui Y, Gondo Y, Sakaki Y, Hirose N (2004), Association analysis between longevity in the Japanese population and polymorphic variants of genes involved in insulin and insulin-like growth factor 1 signaling pathways. *Exp Gerontol.* 39(11-12):1595-8.
- Lee HW, Blasco MA, Gottlieb GJ, Greider CW, DePinho RA (1998), Essential role of mouse telomerase in highly proliferative organs. *Nature* 392: 569–574
- Lee S, Jeong SY, Lim WC, Kim S, Park YY, Sun X, Youle RJ, Cho H (2007), Mitochondrial fission and fusion mediators, hFis1 and OPA1, modulate cellular senescence. *J Biol Chem.* 282(31):22977-83.

- Liu D, O'Connor MS, Qin J, Songyang Z (2004), Telosome, a mammalian telomere-associated complex formed by multiple telomeric proteins. *J Biol Chem.* 279(49):51338-42.
- Marton O, Koltai E, Nyakas C, Bakonyi T, Zenteno-Savin T, Kumagai S, Goto S, Radak Z (2010), Aging and exercise affect the level of protein acetylation and SIRT1 activity in cerebellum of male rats. *Biogerontology* 11(6):679-86.
- Nijwening JH, Geutjes EJ, Bernards R, Beijersbergen RL (2011), The Histone Demethylase Jarid1b (Kdm5b) Is a Novel Component of the Rb Pathway and Associates with E2f-Target Genes in MEFs during Senescence. *PLoS ONE* 6(9): e25235. doi:10.1371/journal.pone.0025235.
- Smith, S., Giriat, I., Schmitt, A. & de Lange, T (1998), Tankyrase, a poly(ADP-ribose) polymerase at human telomeres. *Science* 282: 1484–1487.
- Smogorzewska A, van Steensel B, Bianchi A, Oelmann S, Schaefer MR, Schnapp G, de Lange T (2000), Control of human telomere length by TRF1 and TRF2. *Mol Cell Biol.* 20(5):1659-68.
- Suh Y, Atzmon G, Cho MO, Hwang D, Liu B, Leahy DJ, Barzilai N, Cohen P (2008), Functionally significant insulin-like growth factor I receptor mutations in centenarians. *Proc Natl Acad Sci U S A.* 105(9):3438-42.
- Wong KK, Maser RS, Bachoo RM, Menon J, Carrasco DR, Gu Y, Alt FW, DePinho RA (2003), Telomere dysfunction and Atm deficiency compromises organ homeostasis and accelerates ageing. *Nature* 421(6923):643-8.
- Wu L, Multani AS, He H, Cosme-Blanco W, Deng Y, Deng JM, Bachilo O, Pathak S, Tahara H, Bailey SM, Deng Y, Behringer RR, Chang S (2006), Pot1 deficiency initiates DNA damage checkpoint activation and aberrant homologous recombination at telomeres, *Cell* 126: 49–62.
- Yuan R, Tsaih SW, Petkova SB, Marin de Evsikova C, Xing S, Marion MA, Bogue MA, Mills KD, Peters LL, Bult CJ, Rosen CJ, Sundberg JP, Harrison DE, Churchill GA, Paigen B (2009), Aging in inbred strains of mice: study design and interim report on median lifespans and circulating IGF1 levels. *Aging Cell.* 8(3):277-87.

Diversity of Entomofauna amidst an Urban Green Patch: A Study in Cooch Behar

Satadal Adhikary*, Rachita Saha, Alolika Bose, Poulami Sarkar, Pinki Paul

Post Graduate Department of Zoology, A. B. N. Seal College, Cooch Behar

*Email: adhikary.satadal@yahoo.com

Abstract:

Studying biodiversity of a particular area involves the study of prevailing species population. This paper deals with some unique observations made in the greenery located in front of Bio-Science Departments, A.B.N. Seal College, Cooch Behar at (26.32°N, 89.45°E). The main interest of the study was to estimate the local diversity of entomofauna in the month of April and May 2016 and the interactions of different entomofauna with the sited vegetation in the greenery. It was found that the community was dominated by the red cotton bugs (*Dysdercus cingulatus*), whereas, the ants (*Dicamma intricatum*) are the second most dominant species. The dominance of the red cotton bug species was observed due to the ample presence of its host plant like - *Parthenium*, Climbing hemp vine, kadam etc.

Key words: Biodiversity, Entomofauna, Vegetation, Red cotton bug, Host plant

Publication History: Received: 10th August, 2016; Accepted: 19th August, 2016

Introduction

The existence of many different kinds of plants and animals in an environment is called biodiversity. Defining biodiversity completely actually requires the inclusion of a multitude of point of views which has led the biologists to define biodiversity as the "totality of genes, species, and ecosystems of a region" (Tor-Björn 2001; Davis et al., 2010).

Studying species diversity of a particular area involves the study of different interactions among organisms. Some of the interactions are plant-plant interactions, plant-animal interactions, animal-animal interactions. Biodiversity can be studied at various levels, viz. large scale regional biodiversity and small scale local bio-diversity. Local biodiversity of an area, often known as alpha diversity, is the mean species diversity at a local scale. The term was first introduced by R. H. Whittaker in 1972 (Whittaker 1960; Whittaker 1972). It depends on the number of species and the proportion in which each species is represented in the community. Therefore, a community will have a high alpha diversity, when there is a high number of species and their abundances are much similar. The aim of our study was to study the local entomological diversity in an urban greenery of Cooch Behar. The lawn in front of the Bio-Science departments of A. B. N. Seal College, Cooch Behar was selected as the study site for this purpose.

Materials and Methods

Study Site

The greenery located in front of the Biological science departments of the A. B. N. Seal College, Cooch Behar at 26.32°N, 89.45° E was opted as the study site. The area is located at the heart of the city Cooch Behar amidst a completely urban settlement. It is spread over an area of 2448 square feet and represents mainly a tropical herb vegetation of naturally growing herbs, a few shrubs, climbers, small grasses and a few large trees. Since this area is less manipulated, it has fuelled the growth of a wild population of vegetation supporting a number of entomofauna. This area is a part of the A. B. N. Seal College campus which is surrounded by high brick made wall all over the sides, making the sampling area completely free from the invading outsiders and therefore under least anthropogenic disturbance. The present survey was aimed to prepare a document of entomological diversity of this site, which was not available till date.

Sampling

Field study:

Field survey was done to find out the profile of entomofauna and their host plant present in the area of interest. The data was collected between 18/4/2016 to 13/5/2016 which covers nearly a month's duration. A fixed path was walked once a day with 5 m on either side at a constant pace between 10 a.m. – 2 p.m. The samplings were done at a random interval of days and the whole experimental garden was covered each day and was also repeated in the next sampling. All the entomofauna which were spotted were recorded with date and number of individuals that were seen. Observed species were identified on spot and photographs were taken when it was possible to do so. No capture of fauna was made.

Later in the study, when the red cotton bugs were found to be the dominant species of the community, the survey was further extended towards the study of red cotton bugs and their host plant.

Statistical Analysis

Simpson's Diversity Indices

Simpson's Diversity Index was used in our study to analyze the observations statistically (Simpson 1949). In community ecology, this is often used to quantify the biodiversity of the habitat of interest. In our present study, we have used this reliable tool, which have several closely related versions.

The term 'Simpson's Diversity Index' is referred to any one of 3 closely related indices, two of which have been used in our present study.

Simpson Index (λ) measures the probability that two individuals, if selected randomly from a sample will belong to the same species. With this index, 0 represents infinite diversity and 1 represents no diversity. Therefore, the higher value of λ represents lower diversity (Begon et al., 1996; Magurran 1988; Rosenzweig 1995).

$$\lambda = \sum_{i=1}^R p_i^2$$

P_i = Proportional abundance, λ = True Diversity

Simpson's Index of Diversity ($1 - \lambda$)

As proposed by some workers, $1 - \lambda$ is a better estimate of biodiversity (Sagar et al. 2012). This value also ranges between 0 and 1, but, unlike the previous one, the greater the value, the greater the sample diversity. In this case, contrarily to the Simpson's Index as discussed earlier, the index represents the probability that two individuals randomly selected from a sample will belong to different species.

Shannon index (H')

Species diversity was calculated using the Shannon Index, which is one of the most widely used indices for studying biodiversity (Shannon et al, 1949). It combines the number of species within a sampling site with the relative abundance of each species (Magurran 1988; Krebs 1989; Odum 1997)

$$H' = -\sum p_i \ln p_i$$

Where, p_i is the proportion of the i^{th} species in the total sample.

Pielou's Evenness Index (Equitability) (J')

This index refers to how close in numbers each species in an environment are. The more the species occurs in uniform number, the greater the evenness is and it is reflected by Pielou's Equitability Index (Pielou 1969).

$J' = H'/H'_{\max}$, where H' = Shannon's index and $H'_{\max} = \ln(S)$ where S is the number of species present. That means, J' equals to observed diversity divided by maximum diversity for that number of species. J' is constrained between 0 and 1. The less variation, i.e. the greater the evenness is in a community between the species, the higher the value of J' is obtained.

Berger-Parker Dominance Index

It is simply a measurement of the prevalence of the most abundant species of the community. Berger-Parker dominance index was calculated by the formula n_{\max}/N where n_{\max} is the number of individual of the most abundant species and N is the total number of individuals of all species of the community (Berger and Parkar 1970).

Results and Discussion

Vegetation

Since the prevalence of most of the entomofauna depends on the types of vegetation that exists in an area, study of the available plant types before our study made better sense. The said garden is enriched with different plants belonging to the families such as asteraceae, asclepediaceae, poaceae, verbenaceae, vernoniaceae etc. Brief information of the plants within the said garden is tabulated as follows:

Table 1: Vegetation profile of the sampling area

COMMON NAME	SCIENTIFIC NAME	FAMILY
Milk weed	<i>Asclepias curassavica</i>	Asclepediaceae
Iron weed	<i>Vernonia cinerera</i>	Vernoniaceae
Durva grass	<i>Cynodon dactylon</i>	Poaceae
Bhringraj	<i>Eclipta prostrate</i>	Asteraceae
Simul tree	<i>Bombax ceiba</i>	Asteraceae
Kakronda	<i>Blumea lacera</i>	Asteraceae
Hairy crabgrass or Hairy finger-grass	<i>Digitaria sanguinalis</i>	Poaceae
Frogfruit	<i>Lippia nodiflora</i>	Verbenaceae
Congress grass	<i>Parthenium hysterophorus</i>	Asteraceae
Climbing hemp vine	<i>Mikania scandens</i>	Asteraceae
Bhang	<i>Cannabis Sativa</i>	Cannabaceae

The garden was observed to be enriched with milkweed plant. This plant bears latex type of sap and its flowers contain nectar. For this reason it is a preferred host for many insects. The garden was also predominated by durva grass. Other types of grasses present were hairy crabgrass, hairy figure grass, large crabgrass, crab figure grass, purple crab grass. Other plants like iron weed, simul tree, frog fruit plant were also seen.



Fig 1: Different plants observed at the study site (**A.** *Parthenium hysterophorus*. **B.** *Asclepias curassavica*. **C.** *Bombax ceiba*. **D.** *Mikania scandens*. **E.** *Spilanthes acmella*)

Entomofauna

Table 2: Profile of observed entomofauna

Common name	Scientific name	Systemic position
Plain tiger	<i>Danaus chrysippus</i>	Class- Insecta Order-Lepidoptera Family-Nymphalidae
Cloudless sulphur	<i>Phoebis sennae</i>	Class- Insecta Order- Lepidoptera Family- Pieridae
European cabbage butterfly	<i>Pieris rapae</i>	Class- Insecta Order- Lepidoptera Family- Pieridae
Swallowtail butterfly	<i>Papilio polyxenes</i>	Class- Insecta Order- Lepidoptera Family- Papilionidae
Gray marble butterfly	<i>Anthocharis lanceolata</i>	Class- Insecta Order- Lepidoptera Family- Pieridae
Ant	<i>Dicamma intricatum</i>	Class- Insecta Order- Hymenoptera Family- Formicidae
Monarch larvae	<i>Danaus chrysippus</i>	Class- Insecta Order-Lepidoptera Family-Nymphalidae

Beetle	<i>Coccinella septempunctata</i>	Class- Insecta Order- Coleoptera Family- Coccinellidae
Red cotton bug	<i>Dysdercus cingulatus</i>	Class- Insecta Order- Hemiptera Family- Pyrrhocoridae
Hopper	<i>Austroaeschna tasmanica</i>	Class- Insecta Order- Odonata Family- Aeshnoidae

The faunal community of the studied area included a wide variety of insect species, notably red cotton bug (*Dysdercus cingulatus*) in huge number. The red cotton bugs usually preferred the *Parthenium* plant as their host. This garden was also observed to be enriched by diverse types of butterflies which include plain tiger, cloudless sulphur butterfly, European cabbage butterfly, swallowtail butterfly, gray marble butterfly. Other insects observed were beetles, ants, and hoppers.



Fig. 2: Different types of entomofauna of the study site (A. Ants. B. Monarch butterfly. C. European cabbage butterfly. D. Beetle. E-H. Different stages of Red cotton Bug)

Table 3: Date* wise observation and the calculated biodiversity indices

Name of insects	Date -18/4	Date -19/4	Date -21/4	Date -26/4	Date -27/4	Date -10/5	Date -11/5	Date -12/5	Date -13/5
Monarch Butterfly	6	7	7	1	5	4	3	6	1
Cloudless sulphur (butterfly)	2	2	5	4	2	0	1	2	1
European cabbage butterfly	7	7	5	5	4	2	2	3	3
Swallowtail butterfly	1	2	2	1	1	2	0	0	1
Gray marble	5	8	9	4	5	5	9	5	4

Butterfly									
Ant	6	5	9	9	7	10	11	10	12
Beetle	6	1	6	0	0	2	0	0	1
Red cotton bug	0	35	54	5	26	44	37	23	11
Hopper	1	1	2	0	0	1	0	0	0
Total number of Species	8	9	9	7	7	8	6	6	8
Total number of organism	34	68	99	25	25	70	27	27	34
Average Population size	4.25	7.556	11	3.571	3.571	8.75	4.5	4.5	4.25
Simpson Index	0.14	0.297	0.32	0.19	0.16	0.42	0.27	0.21	0.23
Simpson's Diversity Index	0.86	0.70	0.68	0.81	0.84	0.58	0.73	0.79	0.77
Shannon Index	1.9	1.59	1.58	1.66	1.75	1.29	1.41	1.57	1.61
Equitability Index	0.91	0.72	0.72	0.85	0.90	0.62	0.79	0.88	0.78
Berger-Parker Dominance Index	0.21	0.51	0.55	0.36	0.28	0.63	0.41	0.37	0.35

* All the trials were performed in the year 2016

The observation clearly indicates that the dynamics of the red cotton bug is most conspicuous in the community. From the initial state of sampling towards the middle, there was a gradual increase in the number of adult red cotton bugs, followed by gradual decline in the number of adults. The two deviations from this trend, which was observed on 26/4/16 and 27/4/16, may result from sampling error or due to some other factors which requires further investigation. Overall, the trend of gradual rise and fall of this entomofauna (red cotton bug) and its eventual effect on the diversity indices clearly depicts its pivotal role in the community structure of the said experimental garden.

The Berger-Parker Index increases with the increasing population size of red cotton bug. This index clearly depicts that red cotton bug is the predominant species in this community. Further, with the observation, that, in the latter half of the study the Berger-Parker Index did not fall to that extent with the decline of red cotton bug population, was clearly due to the rise in ant population, which are second most dominant species in the community.

Table 4: Summarized data spanning the months of April 2016 and May 2016

Name of insects	Average (Month of April)	Average (Month of May)	Average (Month of April & May)
Monarch butterfly	5.2	3.5	4.4
Cloudless sulphur (butterfly)	3	1	4.8
European cabbage butterfly	5.6	2.5	9.5
Swallowtail butterfly	1.4	0.8	1.1
Gray marble Butterfly	6.2	5.8	6
Ant	7.2	10.8	8.8
Beetle	2.6	0.8	1.8
Red cotton bug	24	28.8	26.1
Hopper	0.8	0.25	0.6
Total number of Species	9	9	9

Total number of Organism	317	556	577
Average Population size	35.22	61.78	64.11
Simpson Index	0.16	0.32	0.27
Simpson's Diversity Index	0.84	0.68	0.73
Shannon Index	1.9	1.5	1.6
Equitability Index	0.88	0.67	0.74
Berger-Parker Dominance Index	0.23	0.52	0.45

Shannon Indices of 1.9 in the April, 1.5 in the May and 1.6 as a gross, delineates that the community has moderate biodiversity, not so high. This is because of the urban settlement surrounding the area and the lesser size of the sampling garden that accommodates lesser diversity of host plant and limited geophysical architecture. Further, Simpson's diversity index of 0.84 in the April, 0.68 in the May, and 0.73 as a gross, indicates moderate evenness in the community structure. Equitability index value of 0.74 on average throughout the study time also supports the same.

Table 5: Monthly percentage of entomofauna

Name of Entomofauna	Month of April	Month of May
Monarch butterfly	9.29	6.45
Cloudless sulphur (butterfly)	5.36	1.84
European cabbage butterfly	10	4.61
Swallowtail butterfly	2.5	1.47
Gray marble butterfly	11.07	10.69
Ant	12.86	19.91
Beetle	4.64	1.47
Red cotton bug	42.86	53.09
Hopper	1.43	0.46

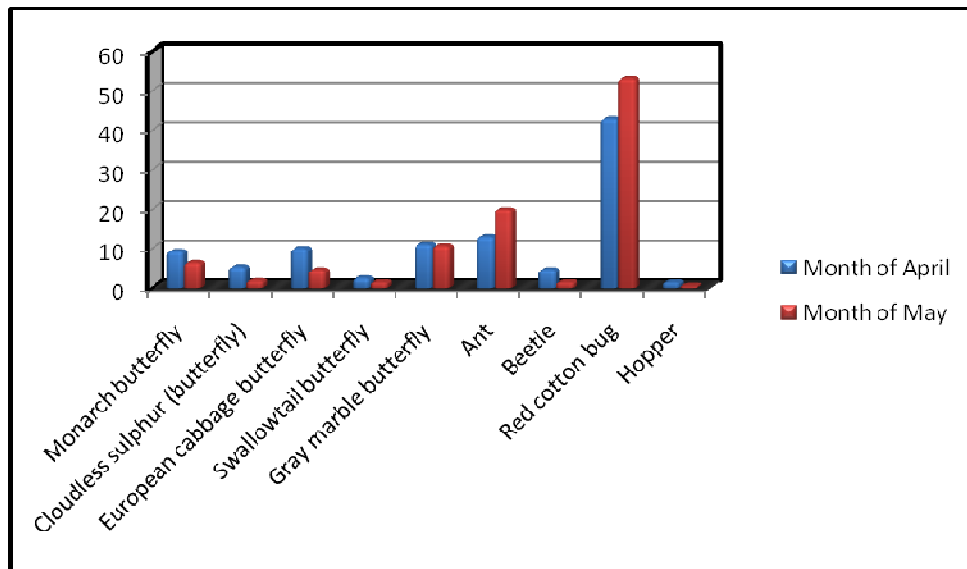


Fig. 3: Bar diagram of percentage of entomofauna on a monthly basis

Interestingly, it was found that the percentage of only the red cotton bug and ant population increased in May 2016 compared to April 2016, while rest others declined. Is there any existing relationship amongst these species is yet to be investigated.

Table 6: Combined percentage of entomofauna in the month of April 2016 & May 2016

Name of Entomofauna	Combined percentage of Entomofauna
Monarch butterfly	6.97
Cloudless sulphur (butterfly)	7.61
European cabbage butterfly	15.06
Swallowtail butterfly	1.74
Gray marble butterfly	9.51
Ant	13.95
Beetle	2.85
Red cotton bug	41.36
Hopper	0.95

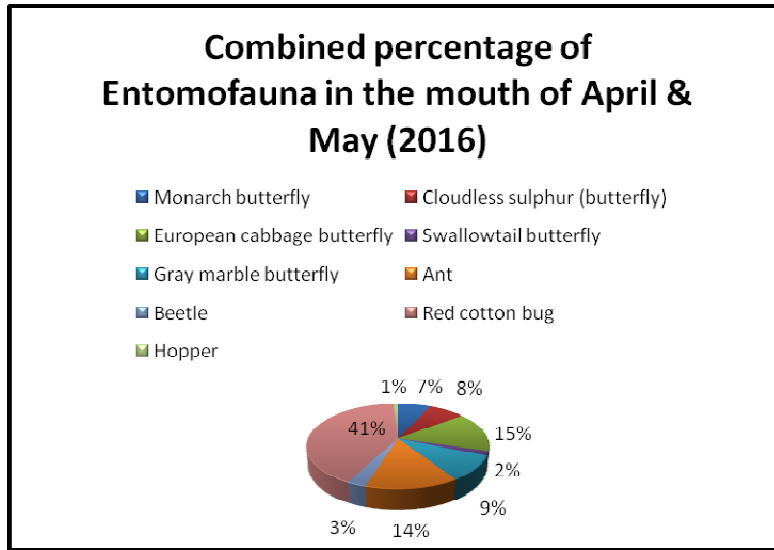


Fig. 4: Pie chart of combined percentage of entomofauna

The pie chart is based on combined average percentage of entomofauna in the experimental garden. Red cotton bug was most abundant (41%), whereas Hopper was found to be the least abundant (1%). Other species like ants (14%), European cabbage butterflies (15%) etc. were also found.

With the general observation that Red cotton bug is the dominant species of the community under investigation, the study was further extended to explore the occurrence of this species with respect to its host plant. The finding has been tabulated as follows:

Table 7: Host plants profile of Red Cotton Bug

Common name	Scientific Name	Observed life history stages of Red Cotton Bug
Climbing hemp vine	<i>Mikania scandens</i>	Red Cotton Bug Nymph Stage
Carrot grass (Congrass grass)	<i>Parthenium hysterophorus</i>	Red Cotton Bug Nymph & Adult Stage
Bhang	<i>Cannabis sativa</i>	Red Cotton Bug Adult Stage
Love Grass	<i>Chrysopogon aciculatus</i> .	Red Cotton Bug Adult Stage

In our study we observed nymph stages of red cotton bug mainly on the plant *Mikania scandens* & *Parthenium hysterophorus*. Adults were seen in *Parthenium* and two other plants viz. *Canabis sativa*, *Chrysopodon aciculatus*.

Conclusion

In the study it was observed that there are a number of insect species in the greenery. The biodiversity indices calculated on the basis of the observation depicts that the overall biodiversity of the community is moderate. This happened because the sampling area was located at the heart of an urban settlement and the size of area was relatively small. For this reason this area accommodated lesser plant diversity and has limited homogeneous geophysical architecture.

It was also observed that the red cotton bug was the dominant species in this community. The red cotton bugs preferred several wild host plants. The nymph stages preferred plant Climbing hemp vine and *Parthenium* whereas the adults preferred plant *Parthenium* and Bhang.

If the community was studied for longer duration spanning other seasons then it would have provided us with the complete knowledge on the entomological community structure of the said area.

Acknowledgement

The authors are thankful to Dr. Rajandra Prasad De, Assistant Professor of Botany for his suggestions and all the faculty members and teaching assistants of the Post Graduate Department of Zoology, A.B.N. Seal College, Cooch Behar for their cooperation during the conduction of this work.

Reference

- Begon M., Harper JL., Townsend CR.,(1996). Ecology: Individuals, populations and communities. Blackwell Science, Oxford, U.K..
- Berger WH.,Parker FL.,(1970). Diversity of planktonic foraminifera in deep-sea sediments . Science. 168:1345-1347
- Davis ML., Cornwell DA., (2010) Introduction to Environmental Engineering. Tata McGraw Hill Education Pvt. New Delhi. India.
- Krebs CJ.(1989) Ecological Methodology. Harper Collins, New York.
- Magurran AE. (1988). Ecological Diversity and its Measurement. Princeton University Press, Princeton, NJ.
- Odum EP.(1997) Ecology: A Bridge between Science and Society. Sinauer Associated Inc. Sunderland, Massachusetts, USA.
- Pielou EC.(1969) An Introduction to Mathematical Ecology. John Wiley, New York.
- Rosenzweig ML. (1995). Species Diversity in Space and Time. Cambridge University Press, UK.
- Sagar R., Sharma GP. (2012), Measurement of alpha diversity using Simpsons Index ($1/\lambda$): the jeopardy. Environmental Skeptics and Critics. 1(1):23-24
- Shannon CE., Weaver W.(1949) The Mathematical Theory of Communication, University of Illinois Press, Urbana.
- Simpson EH (1949), Measurement of diversity. Nature 163: 688.
- Tor-Björn L., (2001). Biodiversity Evaluation Tools for European Forests . Wiley-Blackwell. NJ
- Whittaker RH., (1960) Vegetation of the Siskiyou Mountains, Oregon and California. Ecological Monographs. 30: 279–338.
- Whittaker RH., (1972). Evolution and Measurement of Species Diversity. Taxon, 21:213-251.

Vanadium Inhibits Early DNA Damage and Premalignant Lesions in a Rodent Model of Experimental Hepatocarcinogenesis

Tridib Chakraborty

Department of Physiology, A.B.N. Seal College, Cooch Behar – 736 101, West Bengal, India.

E-mail : chakraborty_t_ju@yahoo.com

Abstract

In recent years, one of the focused areas in cancer chemoprevention research has been directed toward exploring the potentialities of dietary micronutrients, antioxidants and phytochemicals owing to their several important biological properties with minimal toxicity unlike chemotherapeutics. Vanadium, a dietary micronutrient has been shown to elicit profound anticarcinogenicity at a 'low dose' in various chemical carcinogenesis models. Carcinogen-induced DNA damage, viz., formation of oxidative DNA bases 8-hydroxy-2'-deoxyguanosines (8-OHdGs) and DNA-protein crosslinks (DPCs) has been implicated as one of the early events in chemical carcinogenesis. Histomorphometric analysis of precancerous focal lesions following carcinogenic assaults has been used as an end-point biomarker in a chemical carcinogenesis model. Hepatocarcinogenesis was induced in male Sprague-Dawley rats with a single, necrogenic, intraperitoneal (i.p.) injection of diethylnitrosamine (DEN) (200 mg/Kg body weight). Phenobarbital (PB) was administered as a carcinogenic promoter in a long-term regimen (0.05% in basal diet). There was a significant and steady elevation of modified DNA bases 8-OHdGs and DPCs following DEN exposure. Supplementation of vanadium at a dose of 0.5 ppm abated the formations of 8-OHdGs (83.79%; $P < 0.0001$) and DPCs (61.54%; $P < 0.0001$) in preneoplastic rat liver studied at various time points. Continuous vanadium administration also decreased nodular incidence (68.98%) and nodule multiplicity (67.12%; $P < 0.001$) along with substantial improvement in the altered hepatocellular phenotype when compared to DEN+PB -treatment alone. Results of the study indicate that, 0.5 ppm vanadium treatment is effective in limiting early DNA damage and premalignant lesions in rat liver, therefore pointing its potential as a chemopreventive agent in hepatocarcinogenesis.

Key Words: Vanadium; Hepatocarcinogenesis; DEN; DNA damage; 8-OHdGs; DPCs; Preneoplasia; Chemoprevention

Publication History: Received: 10th August, 2016; Accepted: 19th August, 2016

Introduction

Vanadium, a group VB, first transition series, ultra-trace element (molecular weight 50.942) with various oxidation states ranging from -1 to +5, and an endogenous constituent of plants, animals and mammalian tissues is generally present in most of the human diet, including grain, fish, chicken flesh, cereals, fruits and vegetables, spinach, oysters, black pepper, parsley, liver, oils and fats (French and Jones 1993). This dietary micronutrient is believed to have a regulatory role in biological systems and is very probably an essential element, just like other 40 essential micronutrients, requiring small amount for normal cell metabolism as well as for proper growth and development of mammals (Nielsen and Uthus 1980; French and Jones 1993). Vanadium compounds have been found to be potentially effective against murine leukaemia, fluid and solid Ehrlich ascites tumour (Köpf-Maier and Köpf 1988), human lung, breast, and gastrointestinal tract, and nasopharyngeal carcinomas (Köpf-Maier 1994; Sakurai et al. 1995), and human leukemia cells, multiple myeloma cells and a number of solid tumours derived from cancer patients (D'Cruz and Uckun 2002). Furthermore, *in vivo* and *in vitro* antitumor and apoptosis-inducing properties of different vanadium compounds have also been documented by several workers (Jackson et al. 1997; Navara et al. 2001; Scrivens et al. 2003).

Liver is the unique organ for studying chemically-induced carcinogenesis. Liver has got several advantages for studying chemical carcinogenesis *in vivo* during the early stages of initiated cells as altered foci : (i) it proves helpful and simultaneously feasible in that histomorphological analysis of preneoplastic lesions and hepatic nodules can be done on the same tissue sample by examination of the serial sections or counter staining of the histological slides (Farber 1984), and (ii) it further provides a potential experimental model for studying pathological, cellular and subcellular changes all through, from the time of the first administration of an initiating dose of a carcinogenic agent to the development of visible preneoplastic lesions.

Numerous studies have focused on a series of microscopic lesions called "foci" and "nodules" which have been designated "preneoplastic" or "pre-malignant" (Farber and Cameron 1980). These preneoplastic lesions can be easily identified, counted, and their number and size can be determined by quantitative morphometry to measure multistage hepatocarcinogenesis. Among the most abundant and mutagenic oxidative base modifications, 8-hydroxy-2'-deoxyguanosine (8-OHdG), produced by the oxidation of deoxyguanosine (dG) is considered as the most sensitive and potential marker of oxidative DNA damage. It has been shown that 8-OHdG is closely associated with certain diseases, including cancer, and is produced in various experimental models of chemical carcinogenesis (Shen et al. 2003). Besides 8-OHdGs, the extent of the formation of DNA-protein crosslinks (DPCs) is a measure of genotoxicity following carcinogen exposure. The inability of cells to repair such damages adequately is a putative causal event in chemical carcinogenesis. The present study was designed to assess the chemopreventive potential of vanadium in limiting DNA damage and preneoplastic lesions in a rodent model of experimental hepatocarcinogenesis.

Materials and Methods

Materials and Maintenance of Animals

All the reagents and biochemicals, unless otherwise mentioned were obtained from Sigma Chemicals Co. (St. Louis, MO), USA and E. Merck, (Darmstadt) Germany.

Male Sprague-Dawley rats obtained from the Indian Institute of Chemical Biology (CSIR), Kolkata, India weighing 80-100 gm at the beginning of the experiments were used throughout the study. The animals were acclimatized to standard laboratory conditions (temperature $24\pm 1^{\circ}\text{C}$, relative humidity $55\pm 5\%$ and a 12 hour photoperiod) in Tarson Cages (four to five rats per cage) for 1 week before the commencement of the experiment. During the entire period of study, the rats were supplied with a semi-purified basal diet (Lipton India Ltd., Mumbai, India) and water *ad libitum*. The recommendations of Jadavpur University's "Institutional Animal Ethics Committee" ["Committee for the Purpose of Control and Supervision of Experiment on Animals" (CPCSEA Regn. No. 0367/01/C/CPCSEA) INDIA] for the care and use of laboratory animals were strictly followed throughout the study and the particular project was approved by the Chairman of the Committee.

Experimental Regimen

Rats were randomly divided into four experimental groups for carrying out various experiments. In a short-term experimental protocol, groups C and D rats were the DEN-treated groups that received a single, necrogenic, intraperitoneal (i.p.) injection of DEN (200 mg/kg body weight in 0.9% saline) at 9 weeks of age, i.e. at week 4 of experimentation. Group A rats were the normal control; whereas, Group B (vanadium treatment) and D (vanadium+DEN) rats received 0.5 ppm (4.27 $\mu\text{mol/L}$) vanadium (w/v) as ammonium metavanadate (NH_4VO_3 , +V oxidation state) in drinking water, *ad libitum* starting 4 weeks prior to DEN initiation and stopped at week 4. Solutions of vanadium (pH 7.0) were renewed every 2-3 days. Daily food and water intakes were noted and the body weights of the animals from each group were recorded every second day. All the rats were sacrificed by decapitation between 0900 and 1100 hours under proper light ether anesthesia after week 4 to carry

out histo-morphometric studies. All the animals were fasted over night before sacrifice. For the estimation of 8-OHdGs and DPCs, rats were sacrificed after 3, 6, 12, 18, 24 and 48 hours of DEN challenge, livers were promptly excised and hepatic DNA was isolated.

For the assessment of histomorphometry of preneoplastic lesions, rats comprising of 4 groups [group E (normal control); group F (vanadium treatment); group G (DEN + PB treatment); and group H (vanadium + DEN + PB)] were sacrificed after 33 weeks, starting the experiment at week 0 (long-term experimental protocol). All the DEN-initiated rats (groups G and H) at week 4 were administered PB as the carcinogenic promoter in basal diet (0.05%), once daily for 5 days a week after a 3 weeks of recovery from DEN initiation, i.e. after week 7 and continued thereafter till 32 weeks. Vanadium at the same concentration as given in the short-term treatment was supplemented throughout the study, i.e., for 32 consecutive weeks.

Measurement of 8-OHdGs

DNA was extracted from perfused livers of different groups of rats with chloroform only (because phenol exposure would artificially increase oxidative base concentration in DNA samples) following the protocol of Dahlaus and Appel (1993) with minor modifications. The content of 8-OHdGs in the digested DNA was measured by an electrochemical detector (ECD) coupled with high performance liquid chromatography (HPLC-ECD system, available at Jadavpur University, Kolkata, India) which consisted of a Waters 600E pump, a Whatman Partisphere-5 C₁₈ column and a UV detector (Hewlett-Packard 1050, 254 nm) connected to an ECD (Hewlett-Packard 1049A) in series for monitoring dGs and 8-OHdGs respectively. The mobile phase consisted of 10 mM NH₄H₂PO₄, 10 mM KCl, 1 mM EDTA and 10% aqueous methanol (pH 4.7) and the flow rate was set at 1.0 ml/min. The content of 8-OHdGs in each DNA sample was expressed as the molar ratio of 8-OHdG X 10⁵ to total dG based on the peak height of authentic 8-OHdGs with EC detector and the UV absorbance at A₂₅₄ of dGs (Shen et al. 1995). On prolonged incubation of the DNA sample with *E. coli* alkaline phosphatase under the conditions described above, the content of 8-OHdG increased at the rate of 0.4 ± 0.1 residue/10⁵ dG/hour. Therefore this blank value for 8-OHdGs was subtracted from the observed data.

Isolation and Quantitation of DPCs

DPCs were measured as described by Zitkovitch and Costa (1992). Liver tissue was homogenized in 2% SDS and 1mM PMSF in 20 mM Tris-HCl (pH7.5) followed by incubation at 37°C with ribonuclease A (RNase A, 200 µg/ml) for 1 hour. To initiate isolation of DPC, DNA was sheared by passage of the lysate (20-25 times) through a 24-gauge needle using a hypodermic syringe. After a further addition of 0.5 ml of 100 mM KCl containing 20 mM Tris HCl, pH 7.5 (Solution A), the mixture was vigorously vortexed and heated at 65⁰C for 10 min, inverted and then placed on ice for 5 min to form the KCl-SDS-Protein-DNA precipitates which was collected by centrifugation at 5,000 g for 6min at 4°C. The pellet was resuspended in Solution A and the washed precipitate was then incubated with 0.2 mg/ml proteinase K at 50°C for 3 hour containing 0.1 M KCl and 10 mM EDTA in 20 mM Tris-HCl (pH 7.5). Released SDS was removed by cooling the sample in presence of Bovine serum albumin. The amount of DNA in the supernatant was determined using a fluorescent dye (Hoechst 33258) in a spectrofluorimeter (Perkin Elmer, USA; available at Jadavpur University, Kolkata, India) with excitation and emission wavelengths of 365 and 460 nm, respectively. Total hepatic DNA was determined by measuring the free DNA in the supernatants following several washings. The DPC coefficient was expressed as a ratio of the percentage of SDS-precipitable DNA in treated sample to the percentage of SDS-precipitable DNA in untreated control sample.

Histo-Morphometry of Liver Tissue

For the rats sacrificed at 33 weeks, livers were promptly excised, blotted, and weighed. The livers were then examined macroscopically on the surface as well as in 3-mm cross sections for gross visible

persistent nodules (PNs), which represent focal proliferating, hepatic lesions with a low tendency for spontaneous regression (Farber 1984). The PNs were easily identified from the reddish-brown non-nodular surrounding parenchyma (NNSP) by their greyish-white color which clearly differentiated them from the adjacent liver tissue. The PNs that approximated spheres were measured in two perpendicular directions to the nearest mm to obtain an average diameter of each nodule. The PNs were divided into three categories, with respect to their diameter and total area of liver parenchyma occupied, namely, ≥ 3 , $< 3 - > 1$ and ≤ 1 mm (Moreno et al. 1991).

After draining the blood, liver slices were taken from each lobe of the liver. The tissue slices were at once immersed in 10% buffered formalin solution for fixation, dehydrated with graded ethanol solutions from 50%-100%, and then embedded in paraffin. Sections of 5 μ m in thickness were cut and stained with haematoxylin and eosin. The histopathological slides were observed under a photomicroscope.

Statistical Analysis

The data were analyzed using the GraphPad Prism software package, Version 4.01. Student's t-test was performed to compare sample means and the results were expressed as Mean \pm S.E. Statistical significance was set at $P < 0.05$ for all the values.

Results

Hepatic Nodulogenesis and Histopathological Profile of Liver

There were no visible hepatocyte nodules in the livers of normal control (group E) and vanadium-treated (group F) rats. There was 100% nodular incidence in DEN+PB -treated rats (group G). Supplementation of vanadium decreased nodular incidence (68.98%), total number of nodules (90.53%) and nodule multiplicity (67.12%; $P < 0.001$) in the group H rats when compared to group G. There was a maximum occurrence of nodules ≥ 3 mm (58.32%) in group G rats, whereas there was no occurrence of this type of nodules in group H.

Phenotypically altered hepatocyte populations including persistent nodules (PNs) were found scattered in the livers of DEN+PB -treated groups (i.e., groups G and H); but no such alterations were noticeable in untreated normal control (group E; Fig. 1A) or in the vanadium treatment group (group F) (figure not shown).

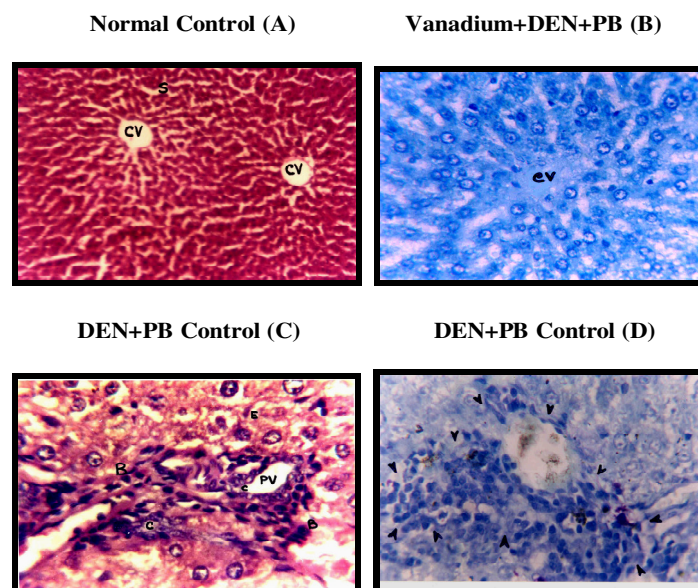


Fig. 1. Hepatic Histopathological Photomicrographs

In group G rats (DEN+PB control) (Fig. 1C, 1D), a gross alteration in hepatocellular architecture was found and hepatocytes appeared oval or irregular in shape with extensive vacuolation in the cytoplasm. The altered hepatocytes of foci and nodules were found to be consistently enlarged with more than one nucleus, which were moreover largely vesiculated with centrally located nucleoli. Some nuclei in the cells were large and hyperchromatic (basophilic), indicating prominent hyperbasophilic preneoplastic focal lesions around the portal vein that were clearly distinguishable from the surrounding non-nodular normal parenchyma. In contrast, the cellular architecture of hepatic lobules seemed to be almost like that of normal liver in group H rats (vanadium+DEN+PB) (Fig. 1B) that received vanadium supplementation during the entire period of study. Liver sections from this group presented only a few clear cell foci. The cells were generally filled with cytoplasmic material and were less vacuolated. The size of the nuclei was essentially the same as that of normal cells and cells with two nuclei were considerably fewer than in group G rats.

Effect of Vanadium on the Levels of Formation of 8-OHdGs in Rat Liver Induced by DEN at Sequential Time Points

The formation of 8-OHdGs in DNA was significant and rapid and the time dependency of hepatic DNA base lesion to reach a maximal level ranged from 3 to 18 hours following DEN exposure (96.68%; $P < 0.0001$) when compared to group A. After that, there was a steady maintenance of oxidative adducts in the DEN-treated group (group C). On the other hand, there was a significant reduction in 8-OHdG levels in vanadium-supplemented rat liver (group D) at 18 hours (17.37%; $P < 0.05$), 24 hours (46.53%; $P < 0.01$) and 48 hours (83.79%; $P < 0.0001$) when compared to group C. The background 8-OHdG levels (0.8-1.2 residue/ 10^5 dG) in control DNA samples were subtracted.

Effect of Vanadium on the Formation of Hepatic DPCs (DPC Coefficient)

It is evident that, there was a significant induction of DPC in DEN-treated (group C) rats at all the specified time intervals (i.e., after 3, 6, 12, 18, 24 and 48 hours of DEN injection) but the amount of DPC formation was maximum (76.98%; $P < 0.0001$) after 18 hours of DEN exposure when compared to normal control rats (group A). Vanadium supplementation significantly reduced ($P < 0.0001$) the formation of DPC in group D rats. There was a gradual reduction in the DPC coefficients (i.e., 23.19% at 6 hours.....61.54% at 18 hours) in group D rats when compared to group C.

Discussion

The results of this study indicate that, vanadium at the 0.5 ppm concentration, which is considered to be a “low dose” of vanadium, exerts potential anticarcinogenic effect by reducing genotoxic DNA damage, i.e., tissue-specific oxidative DNA bases 8-OHdGs and DPCs in hepatocytes. Vanadium effect was also noticed in decreasing nodulogenesis and in remodeling of preneoplastic liver tissue toward normal phenotype.

Induction of a significant and high steady level of 8-OHdG essentially plays a critical role for the activation of carcinogenic properties of cells (Shen et al. 1995). Using the sensitive HPLC-ECD method, a substantial level of 8-OHdG in hepatic DNA of rats treated with DEN has been detected that supported this concept. Moreover, the longer maintenance of high levels of 8-OHdG in liver DNA could be explained by the exhaustion and/or disturbance of DNA repair mechanisms leading to further DNA damages, such as DNA strand-breaks and DPCs. The enhanced formation of DPCs might also result in chromosomal and chromatid-type aberrations and therefore may be used as another important biomarker in chemical carcinogenesis (Sugiyama et al. 1986). The time-response studies reveal a unique correlation pattern of 8-OHdGs and DPCs formations. They both followed the same trend, i.e., there were significant inductions of DPCs and 8-OHdGs adducts 18-20 hours after DEN challenge which are the indicators of substantial genotoxicity and thereby initiation of the

carcinogenic event. Thus, vanadium-mediated reduction of promutagenic lesions as observed herein may have an important role in modulating the initiation event of hepatocarcinogenesis.

In aqueous solution, vanadium is found predominately as oxo-anions (e.g., VO_4^{3-}) and as such may exhibit nucleophilic character for the electrophilic agents to attack, thereby preventing DNA damage as per the "carcinogen interception mechanism" as proposed by Hamilton and Wilker (2004; 2006). The ability of vanadium to attenuate the formation of specific oxidative DNA adducts in liver may indicate its broad-spectrum potential to modulate the kinetics of adduct formation and removal *in vivo*. There is a correlation between inhibition of carcinogenesis by trace metals and lowering of carcinogen binding to cells and DNA. These might involve molecular interactions between metal and carcinogen at different enzymatic and regulatory sites of target cells undergoing neoplastic transformation, as well as stimulation of the host immune system. It is interesting to note that, one electron reduction of vanadium (+V) to vanadium (+IV) has been implicated in the physiological action of this trace element (Sabbioni et al. 1993). Zhang et al. (2002) have shown that, vanadium is able to induce S and G₂-M phase cell cycle growth arrest in a dose- and time-dependent manner through activation of p53- and p21- dependent pathways, and may thus prolong the repair mechanisms of oxidative DNA lesions.

Supplementation of 0.5 ppm vanadium in drinking water throughout the study prominently decreased the development of visible persistent nodules (PNs) and a smaller number of nodules per nodule-bearing rat liver when compared to DEN+PB -treated rats. It also reduced the size of PNs by more than 3 mm in diameter. Even though, not all the hepatocyte nodules become malignant during the life span of the animals, numerous observations support the concept that the hyperplastic/neoplastic nodules are the precursors of hepatocellular carcinoma [Farber and Cameron 1980]. In view of this, inhibition of nodule incidence and enhancement of their regression by supplementary vanadium may be important for cancer chemoprevention. Histopathological findings also indicate that, long-term vanadium treatment resulted in reduced hepatocyte aggregation and basophilicity with a reversal of heterogeneity towards normal cytology. Vanadium-mediated inhibition of early DNA damage and premalignant lesions therefore reflects the ability of this trace element in combating DEN insults in rat liver.

Conclusion

One area of cancer chemoprevention that has been intensively studied in recent years is the use of biological modifiers of cancer cells, particularly dietary micronutrients, such as vitamins and trace minerals, phytochemicals, herbal formulations, pharmacological agents etc. It is a potential strategy of cancer control in which the progression of precancerous lesions and the occurrence of the disease process are prevented by administration of one or more such agents that may interfere with and target the cancer-inducing mechanisms and pathways, e.g. DNA damage, DNA repair, cell proliferation, cell death etc. In this report, the protective role of vanadium supplementation in limiting early DNA damage was evident. Vanadium is effective in suppressing hepatocellular premalignant transformation *in vivo*. Data from several studies suggest that pharmacologically safe dose of vanadium could become a promising antineoplastic agent in near future.

References

- D'Cruz OJ, Uckun FM (2002), Metvan: a novel oxovanadium(IV) complex with broad spectrum anticancer activity. *Expert Opin Investig Drugs* 11:1829-1836
- Dahlaus M, Appel KE (1993), N-Nitrosodimethylamine, N-nitrosodiethylamine, and N-nitrosomorpholine fail to generate 8-hydroxy-2'-deoxyguanosine in liver DNA of male F344 rats. *Mutat Res* 285:295-302

- Farber E, Cameron R (1980), The sequential analysis of cancer development. *Adv Cancer Res* 31:125-226.
- Farber E (1984), The multistep nature of cancer development. *Cancer Res* 44:4217-4223.
- French RJ, Jones PJ (1993), Role of vanadium in nutrition: metabolism, essentiality and dietary consideration. *Life Sci* 52:339-346.
- Hamilton EE, Fanwick PE, Wilker JJ (2006), Alkylation of inorganic oxo compounds and insights on preventing DNA damage. *J Am Chem Soc.* 128:3388-3395.
- Hamilton EE, Wilker JJ (2004), Inorganic oxo compounds react with alkylating agents: implications for DNA damage. *Angew Chem Int Ed Eng* 43:3290-3292.
- Jackson JK, Min W, Cruz TF, Cindrias S, Arsenault L, Von Hoff DD, Degan D, Hunter WL, Burt H (1997), A polymer-based drug delivery system for the antineoplastic agent bis(maltolato)oxovanadium in mice. *Br J Cancer* 75:1014-1020
- Kopf-Maier P, Kopf H (1988), Transition and main-group metal cyclopentadienyl complexes: preclinical studies on a series of antitumor agents of different structural type. *Struct Bond* 70:103-185.
- Köpf-Maier P (1994), Complexes of metals other than platinum as anti-tumour agents. *Eur J Clin Pharmacol* 47:1-16.
- Moreno FS, Rizzi MBSL, Dagli MLZ, Penteadó MVC (1991), Inhibitory effect of β -carotene on preneoplastic lesions induced in Wistar rats by the resistant hepatocyte model. *Carcinogenesis* 12:1817-1822.
- Navara CS, Benyumov A, Vassilev A, Narla RK, Ghosh P, Uckun FM (2001), Vanadocenes as potent anti-proliferative agents disrupting mitotic spindle formation in cancer cells. *Anticancer Res* 12:369-376.
- Nielsen FH, Uthus EO (1980), The essentiality and metabolism of vanadium. In: Chasteen ND (ed) *Vanadium in Biological Systems*. Kluwer Academic Publishers, The Netherlands, pp 51-62.
- Sabbioni E, Pozzi G, Devos S, Pintat A, Casella L, Fischbach M (1993), The intensity of vanadium (V)-induced cytotoxicity and morphological transformation in BALB/3T3 cells is dependent on glutathione-dependent bioreduction to vanadium (IV). *Carcinogenesis* 14: 2565-2568.
- Sakurai H, Tamura H, Okatani K (1995), Mechanism for a new antitumor vanadium complex: hydroxyl radical dependent DNA cleavage by 1, 10-phenanthroline-vanadyl complex in the presence of hydrogen peroxide. *Biochem Biophys Res Commun* 206:133-137.
- Scrivens PJ, Alaoui-Jamali MA, Giannini G, Wang T, Loinnon M, Batist G, Sandor VA (2003), Cdc25A-inhibitory properties and antineoplastic activity of bisperoxovanadium analogues. *Mol Cancer Ther* 2:1053-1059.
- Shen HM, Ong CN, Lee BL, Shi CY (1995), Aflatoxin B1-induced 8-hydroxydeoxyguanosine formation in rat hepatic DNA. *Carcinogenesis* 16:419-422.
- Shen J, Wanibuchi H, Salim EI, Wei M, Kinoshita A, Yoshida K, Endo G, Fukushima S (2003), Liver tumorigenicity of trimethylarsine oxide in male Fischer 344 rats--association with oxidative DNA damage and enhanced cell proliferation. *Carcinogenesis* 24:1827-1835.
- Sugiyama M, Wang XW, Costa M (1986), Comparison of DNA lesions and cytotoxicity induced by calcium chromate in human, mouse, and hamster cell lines. *Cancer Res* 46:4547-4551.
- Zhang Z, Huang C, Li J, Shi X (2002), Vanadate-induced cell growth arrest is p53-dependent through activation of p21 in C141 cells. *J Inorg Biochem* 89:142-148.
- Zhitkovich A, Costa MA (1992), A simple, sensitive assay to detect DNA-protein crosslinks in intact cells and in vivo. *Carcinogenesis* 13:1485-1489

Polycystic Ovarian Syndrome: A Brief Mini Review on Current Updates

Tuhin Suvro Banerjee*, Asis Kumar Pandit

Department of Physiology, A. B. N. Seal College, Cooch Behar, Pin-736101

Email: tuhin.banerjee1@gmail.com

Abstract

Polycystic ovarian syndrome (PCOS) is an endocrine disorder affecting women of reproductive age group. It is characterized by anovulatory cycles, hirsutism and presence of numerous ovarian cysts. PCOS is often a resultant effect of several environmental, metabolic and endocrine conditions like insulin resistance, hyperinsuliemia and also hyperandrogenism besides various other factors like anti-mullerian hormone, interleukins, leptin, etc. Long term effects of PCOS include cardiovascular diseases, sleep apnoea, infertility and even cancer. Treatment of PCOS comprises of mainly conversion of the anovulatory cycles into mono-ovulatory cycles by various procedures that includes treatment with clomiphene citrate, letrozole, metformin and also the surgical procedure of laparoscopic ovarian drilling (LOD). However further studies are required for the complete insight into the etiopathogenesis of the syndrome which would be helpful in complete amelioration of PCOS in the affected women.

Keywords: polycystic ovarian syndrome, infertility, insulin resistance, hyperandrogenism

Publication History: Received: 10th August, 2016; Accepted: 19th August, 2016

Introduction

Polycystic ovarian syndrome, commonly known as PCOS is a common female endocrinopathy of women in the reproductive age group. Under present scenario, 5-10% of such women are affected by PCOS. Different signs and symptoms of PCOS are shown in the Figure 1.

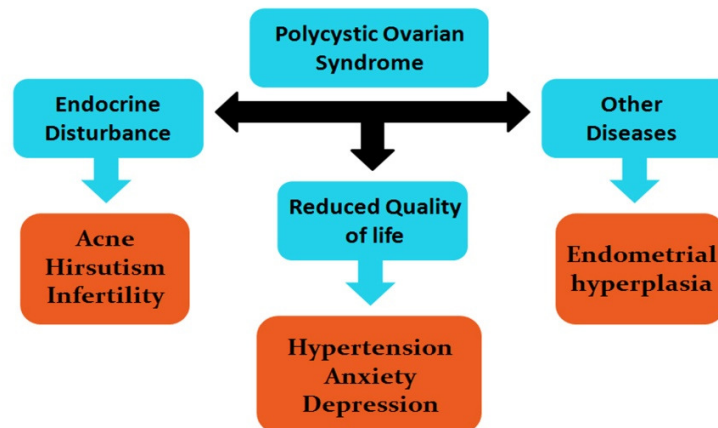


Fig. 1: Flow chart showing possible consequences and outcomes of PCOS

The most common characteristic of PCOS include oligo/anovulatory cycles, multiple cysts in the ovary, hirsutism along with considerable prevalence of insulin resistance (IR). It may be stated here that from the available literature the complete aetiology of PCOS is yet to be clearly understood. But nonetheless PCOS is a multifaceted disorder having its roots of cause embedded deep into

multiple factors: environmental, metabolic, endocrine as well as genetic abnormalities (Franks *et al.*, 2006).

The major features of PCOS in almost 80% of affected women include: obesity, insulin resistance and subsequent hyperinsulinemia (Carmina and Lobo, 2004). Studies have also shown that insulin through IGF1R signalling or through classical insulin receptor signalling enhances androgen secretion and induces development of polycystic ovaries. Furthermore, hyperinsulinemia inhibits hepatic production of sex hormone binding globulin (SHBG) and subsequently increases the level of free testosterone in serum. Additionally, increased androgen levels facilitate the release of free fatty acids from visceral fat tissue, what exacerbates insulin resistance (Holte, 1996). Insulin resistance in PCOS is also associated with abdominal obesity and other components of metabolic syndrome. Again all these abnormalities cause an increased risk of cardiovascular disorders in PCOS patients later in life (Lugue-Ramirez and Escobar-Morreale, 2014).

Diagnostic Criteria

The disease was first recognised in 1935 by Stein and Leventhal. Since then many scientific societies and workshop groups developed different diagnostic criteria, with an aim to provide a more inclusive definition of PCOS. The National Institute Health (NIH) diagnostic criteria were based on the results of a survey among experts who considered a woman with PCOS if she presented with the combination of chronic oligo- or anovulation and clinical or biochemical signs of hyperandrogenism, with the exclusion of other related endocrine disorders (Zawadski and Dunaif, 1992). In 2003, the European Society of Human Reproduction and Embryology (ESHRE)/American Society of Reproductive Medicine (ASRM)-Sponsored PCOS Consensus Workshop Group suggested the addition of a third criteria, i.e., the presence of polycystic ovarian morphology (PCOM) (Rotterdam consensus, 2004). The diagnosis of PCOS is based on at least two of the following features: oligoanovulation, hyperandrogenism and polycystic ovaries (Rotterdam consensus, 2004). In 2006, the Androgen Excess Society (AES) put forward a more simplified diagnosis (Zawadski and Dunaif, 1992) criteria to diagnose PCOS, viz., clinical and/ or biochemical hyperandrogenism simultaneously with oligo/anovulation and ultrasonographic evidence of polycystic ovaries (Aziz *et al.*, 2006). Table 1 represents different phenotypes of PCOS as adapted from Moran and Teede, 2009.

Table 1: Diagnostic phenotypes of PCOS (Moran and Teede, 2009)

Phenotype A	NIH PCOS: hyperandrogenism and oligo/anovulation with PCO
Phenotype B	NIH PCOS: hyperandrogenism and oligo/anovulation without PCO
Phenotype C	Non-NIH PCOS: hyperandrogenism with PCO but with normal ovulation
Phenotype D	Non-NIH PCOS: no hyperandrogenism but with oligo/anovulation and with PCO

Etio-pathogenesis of PCOS

PCOS is a complex disorder. Hence, endocrine, genetic as well as environmental factors play important role in its pathophysiology. The key players in PCOS pathogenesis include metabolic features like IR, hyperinsulinemia and obesity, hyperandrogenism and altered ovarian morphology as well as genetic, epigenetic and several other factors.

Ovarian Dysmorphology

In PCOS, ovarian histology revealed more atretic follicles and less number of corpora lutea (representing less number of ovulations). Stromal hypertrophy and increased ovarian weight were also reported. Prominent hyperthecosis along with thecal cell proliferation and excessive androgen biosynthesis were noted (Dunaif *et al.*, 1985). Studies also showed abnormal ovarian cortex with

growth arrested medium-sized antral follicles (5-10 mm) suggesting developmental failure and subsequent subfertility (Barber *et al.*, 2010).

Insulin resistance (IR) and hyperinsulinemia

Several studies have suggested that IR and associated compensatory hyperinsulinemia are robustly associated with PCOS and hence play a key role in its pathogenesis. Women with both anovulation and hyperandrogenism show increased incidence of IR (Robinson *et al.*, 1993). Conversely, treatment of insulin resistance have shown to improve ovulatory functions, menstrual cyclicity, fertility conditions in such women, independent of weight loss (Yilmaz *et al.*, 2005; Gambineri *et al.*, 2006). Patients with severe genetic forms of IR were often found to have PCOS-like conditions (Semple, 2011).

It might also be noted from available literature that PCOS likely represents a state of “partial” IR. Under such circumstances, the preserved insulin signalling in ovarian theca cells causes excessive androgen synthesis and theca cell proliferation, with subsequent hyperandrogenemia (Willis *et al.*, 1996; Musso *et al.*, 2005). Hyperinsulinemia further leads to reduced hepatic synthesis of sex hormone-binding globulin (SHBG), thereby increasing free testosterone, hypersecretion of pituitary luteinizing hormone (LH), and reduced insulin-like growth factor-binding protein (Kelly *et al.*, 2011). This latter effect potentially modulates the paracrine growth factor-dependent regulation of early follicle development and dominant follicle selection.

Hormonal Dysregulation

Another important factor playing a primary role in PCOS pathogenesis is hyperandrogenism. Besides being a defining feature of PCOS in both ovulatory as well as anovulatory females, hyperandrogenism and other conditions associated with excess androgen exposure are also responsible for producing PCOS (Barnes *et al.*, 1994). Disruption of ovarian follicular development and dominant follicle selection by promoting excessive early follicular growth is often brought about by androgens. Whereas on the systemic front androgens bring about development of IR and other metabolic dysfunctions (Coubould, 2007, 2008; Demissie *et al.*, 2008). In PCOS androgens appear to play a key role during the developmental windows before the onset of IR (Frank and Berga, 2012). Prenatally, androgenized rhesus monkeys and sheep demonstrate ovarian hyperandrogenism and IR in adulthood, with increased follicle numbers, anovulation, and LH hypersecretion (Bruns *et al.*, 2004; Dumesic *et al.*, 2007).

Androgen exposure in utero often causes dysregulation and reprogramming of the hypothalamus– pituitary–ovarian (HPO) axis. This causes development of PCOS after onset of puberty. Reprogramming of HPO axis causes hypersecretion of LH, persistently rapid LH pulse frequency, and below-normal levels of follicle-stimulating hormone (FSH) (Taylor *et al.*, 1997; Haisenleder *et al.*, 1991). These alterations most likely contribute to the disrupted follicle development in PCOS, while high levels of LH also synergize with insulin to promote theca androgen production. However, it is noteworthy that many patients have normal LH levels, suggesting that elevated gonadotrophin levels is unlikely to be the primary defect in PCOS (Adams *et al.*, 2004). However it may here be noted that since the foetus is protected by placental aromatase activity and by high maternal SHBG concentrations, the source of intra-uterine androgens excess is unlikely to be maternal. In newborn daughters of PCOS women, elevated testosterone levels have been observed in the umbilical venous blood in the mid-gestational period (Mehrabian and Kelishadi, 2012; Barry *et al.*, 2010). Interestingly, it is found that this elevated midgestation maternal testosterone levels often predicts high anti-mullerian hormone (AMH) levels in adolescent daughters (Hart *et al.*, 2010). Elevated AMH often represents a characteristic of adolescents and women with PCOS (Sir-Peterman *et al.*, 2009; Crisoto *et al.*, 2012) and daughters of PCOS women. Thus, suggesting a cross-

generational relationship between the degree of maternal hyperandrogenism and the development of PCOS in their daughters.

Obesity

Daughters of PCOS women have exaggerated adrenarche compared to daughters of non-PCOS women of similar pubertal stage and body mass index (BMI) (Lewy *et al.*, 2001). This is consistent with a role of obesity-related insulin-resistance in causing hyperandrogenemia in these girls through an effect of insulin on adrenal and ovarian steroidogenesis (Maliqueo *et al.*, 2009), manifesting as early adrenarche (Rosenfield, 2001) and subsequent PCOS (Jabbar *et al.*, 1991). This kind of hyperandrogenemia appears to modulate gonadotropin levels as also observed in obese peri-pubertal girls. These girls were found to have increased LH frequency but low LH amplitude, and diminished overnight LH pulse amplitude compared with normal-weight girls (Apter *et al.*, 1995) thus pointing at an initial effect of obesity on LH pulses (McCartney *et al.*, 2009). Subsequently, hyperandrogenemia lead to a reduction in the inhibition of GnRH pulse frequency by progesterone, causing rapid LH pulse secretion and further increase in ovarian androgen production (Burt *et al.*, 2010; Blank *et al.*, 2009).

Genetic factors

Though the exact model depicting the inheritance of PCOS is yet to be well defined yet there exist multiple postulates regarding the mechanism of inheritance of PCOS. Proposed theories range from PCOS being an autosomal dominant transmission linked to a single genetic defect to a polygenic pathology. However, the major candidate genes modulated variously include genes encoding factors for synthesis, transport and regulation of androgens, factors involved in insulin metabolism and such related genes. An association has also been reported between “proinflammatory” genotypes and PCOS, linked to polymorphism of genes coding for TNF- α , IL-6 and IL6 receptor (Frank and McCarthy, 2005). Further notable is the fact that recent evidences of altered early gonadotropin-independent folliculogenesis patients with PCOS also suggests the involvement of genes regulating and bringing about folliculogenesis which may also be candidates in the etiopathogenesis of this syndrome (Rotterdam consensus, 2004).

Environmental factors

Although the occurrence of PCOS is similar in almost all countries yet its prevalence in Caucasian women varies regionally, ranging from 4.5% in Alabama to 6.5% in Spain and 6.8% in Greece (Escobar-Morreale *et al.*, 2005). These observations suggest the existence of different environmental factors, such as diet, physical activity and life-style in general that brings a variation regionally.

Other factors

Interleukins (IL)

These are cytokines released by leucocytes that play important roles in regulation of folliculogenesis, ovulation as well as corpus luteum function. In this regard IL-1, IL-2, IL-6, IL-11, IL-12 and IL-13 are of immense importance. Reduced follicular fluid (FF) concentrations of IL-12 and elevated FF concentrations of IL-13 in PCOS patients are found to be correlated with reduced oocyte maturation, fertilization and pregnancy (Oiao and Feng, 2011; Diamanti-Kandarakis *et al.*, 2008).

Heat shock protein (HSPs): HSPs are conserved family of molecules playing key role in protein folding. Many HSPs are known to regulate pro-apoptotic and apoptotic pathways (Fan *et al.*, 2009). A decrease in levels of HSPs 10, 27 and 60 in the granulosa cells and ovarian tissue in PCOS patients probably contributes to the apoptotic changes within ovarian follicles (La Marca *et al.*, 2009).

Leptin: Leptin is a protein hormone that is instrumental in regulating energy supply and demand. High FF and serum concentrations of leptin have been found to be closely associated with a decrease in

oocyte maturity and embryo quality in PCOS patients. Certain studies have shown leptin to play a role in PCOS pathogenesis, by inhibiting E2 production and interfering with follicle development and oocyte maturation. Various other studies have also deterred from considering leptin as a useful marker of PCOS (Oiao and Feng, 2011; Diamanti-Kandarakis *et al.*, 2008).

Oxidative stress: In women with PCOS, elevated levels of reactive oxygen species (ROS) in FF and reduced antioxidant capacity have been closely associated with reduced oocyte maturation and low embryo quality (Oiao and Feng, 2011; Diamanti-Kandarakis *et al.*, 2008). These molecules have also been proposed for the probably reduced oocyte quality by altering the equilibrium of FFFs in the follicular microenvironment.

Clinical indications of PCOS

The most common clinical manifestations of PCOS include anovulatory cycles, hirsutism and ultrasonographic evidences of ovaries containing multiple cysts. Overweight and/or obesity have also been reported in many women with PCOS which have later posed to cause serious metabolic dysfunctions. Clinically patients with PCOS have also been found to report frequent occurrence of miscarriage, hypertension as well as gestational diabetes (Elting *et al.*, 2000; Bekx *et al.*, 2010).

Two other important manifestations also include acne and alopecia. Acne has been reported in 12–14% of PCOS patients and ethnic variations are often observed, the highest being reported in Indo-Asian women and lowest in Pacific islanders (Deplewski and Rosenfield, 2000). Alopecia consists in progressive hair loss or thinning. Hair loss in PCOS usually involves thinning at the vertex with maintenance of the frontal hairline. Hyperandrogenism is often correlated with the incidence of alopecia (Deplewski and Rosenfield, 2000). Some of the main features of PCOS in adolescents are enlisted in Table 2 (adapted from Tsikouras *et al.*, 2015).

Table 2: Main features of PCOS in adolescents (Tsikouras *et al.*, 2015)

Hormones		Metabolic Markers	
Testosterone	High/normal	A1 apolipoprotein	Low
Free androgen index (FAI)	High	Cholesterol	Normal/high
Sex hormone binding globulin (SHBG)	Low	HDL/LDL cholesterol ratio	Low
D4-Androstenedione	Normal/high	Triglycerides	Normal/high
DHEAS	Normal/high	Insulin	High/normal
LH	Normal/high	Hba1c	High/normal
LH/FSH ratio	Normal/high		

Clinical Sequelae of PCOS

The incidence and pathophysiology of PCOS is often accompanied by various other long term consequences like infertility, glucose intolerance as well as cardiovascular risk and even cancer.

Infertility

Subfertility has often been associated with PCOS but over a period of time subsequent epidemiological studies have helped to draw conclusion towards the occurrence of PCOS associated infertility in affected women of reproductive age group (Stein and Leventhal, 1935). In patients with PCOS, primary infertility was reported in 50% of women, while secondary infertility was reported in 25% of women (Balen *et al.*, 1995). Factors in PCOS patients contributing to infertility include IR (Tian *et al.*, 2007) and obesity (Jungheim *et al.*, 2009). These were independently related to an

increased risk of abortion and to reduced pregnancy and live-birth rates. Endometrial abnormalities were also reported in PCOS women (Palomba *et al.*, 2006) affecting potentially the implantation. Finally, ovarian alterations at several levels were described, i.e., ovarian/follicular/corpus luteum vascularity follicular fluid environment (Palomba *et al.*, 2010) and subsequent oocytes competence (Teissier *et al.*, 2000) and quality (Wood *et al.*, 2007). The most recent guidelines of the Endocrine Society-appointed Task Force of Experts (Legro *et al.*, 2013) suggested that PCOS is a risk factor for infertility only in the presence of oligoanovulation; thus they recommended screening ovulatory status using menstrual history in all women with PCOS seeking fertility.

Cardiovascular risk

Various studies and societies have reported the increased prevalence of classical risk factors associated with cardiovascular disease (CVD) in women with PCOS (Fauser *et al.*, 2012; Conway *et al.*, 2014). These classical factors include hypertension, dyslipidemia, diabetes, and obesity and nonclassic risk factors such as C-reactive protein (CRP), homocysteine, and tumor necrosis factor- α (Toulis *et al.*, 2011). It is estimated that the prevalence of each risk factor is approximately double for women with PCOS when compared with normal women, while it is 1.5 times higher in BMI-matched studies beginning in adolescence and it is found in every decade (Fauser *et al.*, 2012). More and more scientific evidences suggest a role of nonclassic CVD risk factors, related to a systemic inflammatory state, in PCOS patients, such as CRP. CRP is commonly considered a vascular inflammatory marker that predicts the development of CVD and Type 2 diabetes mellitus (T2DM) (Ridker, 2003) Studies reported higher CRP levels in women with PCOS (Oh *et al.*, 2009) although the serum CRP levels seem to be more associated with obesity than with the presence of PCOS per se (Möhlig *et al.*, 2004).

Sleep Apnoea

Many studies have shown an elevated incidence of sleep apnoea and several other sleep related disorders like sleep disordered breathing in women with PCOS (Vgontzas *et al.*, 2001; Fogel *et al.*, 2001). Under normal circumstances sleep apnoea and other such disorders are normally uncommon in premenopausal women. However increased incidence of such disorders has been associated with hyperandrogenism and IR (Vgontzas *et al.*, 2001; Fogel *et al.*, 2001).

Cancers

Many studies have reportedly associated the occurrence of several types of cancers like ovarian carcinoma, breast carcinoma and endometrial carcinomas with the incidence of PCOS. But the best association of PCOS is with endometrial carcinomas on account of the presence of a number of risk factors in PCOS patients that can be associated with the patients with endometrial cancers (Hardiman *et al.*, 2003).

Treatment of PCOS

PCOS is associated with infertility caused by anovulation in over 80% of the affected women (ESHRE/ASRM consensus, 2008). The main goal of treatment includes induction of mono-ovulatory cycles in the affected women. A step-wise approach in management of the infertility of PCOS patient leads to the achievement of pregnancy and live birth(s) (Berger and Bates, 2014) as enlisted below:

1. Appropriate living style, such as diet and physical exercises in order to reduce weight.
2. Oral medication agents:
 - The first-line oral agents include clomiphene citrate (CC) (selective estrogen receptor modulators) with 49% of ovulation rate, 30% of pregnancy rate, and 23% of live birth rate at 6 months. Therefore, there is an 8% increase in the rate of multiple gestations.
 - The other first-line oral agent is Letrozole (aromatase inhibitors) with recent evidence recommending the use of letrozole: – the ovulation rate is 61.7% for letrozole versus 48.3% for CC, $p < 0.0001$; – the live birth rate is 27.5% for letrozole versus 19.2% for CC, $p = 0.007$; – there is 44%

higher live birth rate with letrozole in patients with high body mass index (BMI) and long standing infertility.

- Metformin (insulin sensitizers) is an adjunct to induction of ovulation in patients with glucose intolerance and obesity.

For women with WHO Group II ovulation disorders who are known to be resistant to CC, both the Agency for Healthcare Research and Quality (AHRQ) and the National Institute for Health and Clinical Excellence (NICE) consider one of the following second-line treatments, depending on clinical circumstances and the woman's preference:

- Laparoscopic ovarian drilling (LOD),
- Combined treatment with CC and metformin if not already offered as first-line treatment, or
- Gonadotrophins (NGC, AHRQ, 2013; NICE, 2013)

3. Gonadotrophins are the second-line treatment in case of CC resistance or CC failure (no pregnancy after four to six ovulatory cycles) (NGC, AHRQ, 2013; French National college, Clinical practice recommendations, 2010).

4. The LOD may be considered as a second-line treatment in a selected population (ESHRE/ASRM consensus, 2008; Berger and Bates, 2014). LOD may be considered in women with CC-resistant PCOS, particularly when there are other indications for laparoscopy, if there is a high risk of multiple pregnancies or a contra-indication of multiple pregnancies (NGC, AHRQ, 2013; French National College, Clinical practice recommendations, 2010).

5. In vitro fertilization (IVF) is indicated in the treatment of PCOS-associated infertility with high success rates and potentially lower rate of multiple gestations if it is well managed. Indeed, careful monitoring of controlled ovulation aims to avoid multiple pregnancies when using gonadotrophins in IVF (Berger and Bates, 2014).

In conclusion, all meta-analysis confirmed that LOD is a second-line treatment in PCOS patients, especially those with CC resistance (Farquhar and Marjoribanks, 2012). The main benefits are shorter time to pregnancy and less need to ovulation induction drugs. The other advantages of this technique are more comfort, cost-effectiveness, and possibility to be performed ambulatory. However, the results of LOD are not better than those of CC as a first-line treatment in PCOS (Lebbi *et al.*, 2015).

Conclusion

It may thus be concluded that PCOS is an endocrine disorders whose complete etiology is yet to be completely understood. However, recent therapeutic approaches and tools have improved the understanding as well as treatment of the syndrome in itself rather than mere treatment of only the secondary symptoms. Further it may be stated that more knowledge about the syndrome and its causes if imparted among the susceptible age group would prove to be fruitful in preventing the prevalence of PCOS through maintenance of various factors that often lead to the development of the syndrome.

References

1. Adams JM, Taylor AE, Crowley WF, Hall JE (2004), Polycystic ovarian morphology with regular ovulatory cycles: insights into the pathophysiology of polycystic ovarian syndrome. *J Clin Endocrinol Metab* 89:4343-4350.
2. Adashi EY, Hsueh AJ, Yen SS (1981), Insulin enhancement of luteinizing hormone and follicle-stimulating hormone release by cultured pituitary cells. *Endocrinology* 108:1441-1449.
3. Apter D, Butzow T, Laughlin GA, Yen SS (1995), Metabolic features of polycystic ovary syndrome are found in adolescent girls with hyperandrogenism. *J Clin Endocrinol Metab* 80:2966-2973.

4. Aziz R, Carmina E, Dewailly D (2006), Criteria for defining polycystic ovary syndrome as a predominantly hyperandrogenic syndrome: An Androgen Excess guideline. *J Clin Endocrinol Metab* 91:4237-4245.
5. Balen AH, Conway GS, Kaltsas G (1995), Polycystic ovary syndrome: the spectrum of the disorder in 1741 patients. *Hum Reprod* 10:2107-2111.
6. Barber TM, Alvey C, Greenslade T, Gooding M, Barber D, Smith R (2010), Patterns of ovarian morphology in polycystic ovary syndrome: a study utilising magnetic resonance imaging. *Eur Radiol* 20:1207-1213.
7. Barnes RB, Rosenfield RL, Ehrmann DA, Cara JF, Cuttler L, Levitsky LL (1994) Ovarian hyperandrogenism as a result of congenital adrenal virilizing disorders: evidence for perinatal masculinization of neuroendocrine function in women. *J Clin Endocrinol Metab* 79:1328-1333.
8. Barry JA, Kay AR, Navaratnarajah R, Iqbal S, Bamfo JE, David AL (2010), Umbilical vein testosterone in female infants born to mothers with polycystic ovary syndrome is elevated to male levels. *J Obstet Gynaecol* 30:444-446.
9. Bekx MT, Connor EC, Allen DB (2010), Characteristics of adolescents presenting to a multidisciplinary clinic for polycystic ovarian syndrome. *J Pediatr Adolesc Gynecol* 23:7-10.
10. Berger JJ, Bates GW Jr (2014), Optimal management of subfertility in polycystic ovary syndrome. *Int J Womens Health* 6:613-621.
11. Blank SK, McCartney CR, Chhabra S, Helm KD, Eagleson CA, Chang RJ (2009), Modulation of gonadotropin-releasing hormone pulse generator sensitivity to progesterone inhibition in hyperandrogenic adolescent girls-implications for regulation of pubertal maturation. *J Clin Endocrinol Metab* 94:2360-2366.
12. Bruns CM, Baum ST, Colman RJ, Eisner JR, Kemnitz JW, Weindruch R (2004), Insulin resistance and impaired insulin secretion in prenatally androgenized male rhesus monkeys. *J Clin Endocrinol Metab* 89:6218-6223.
13. Burt Solorzano CM, McCartney CR, Blank SK, Knudsen KL, Marshall JC (2010), Hyperandrogenaemia in adolescent girls: origins of abnormal gonadotropin releasing hormone secretion. *BJOG* 117:143-149.
14. Carmina E, Lobo RA (2004), Use of fasting blood to assess the prevalence of insulin resistance in women with polycystic ovary syndrome. *Fertil Steril* 82:661-665.
15. Conway G, Dewailly D, Diamanti-Kandarakis E (2014), The polycystic ovary syndrome: a position statement from the European Society of Endocrinology. *Eur J Endocrinol* 171:1-29.
16. Corbould A (2007), Chronic testosterone treatment induces selective insulin resistance in subcutaneous adipocytes of women. *J Endocrinol* 192:585-594.
17. Corbould A (2008), Effects of androgens on insulin action in women: is androgen excess a component of female metabolic syndrome? *Diabetes Metab Res Rev* 24:520-532.
18. Crisosto N, Echiburua B, Maliqueo M, Perez V, Ladron de Guevara A, Preisler J (2012), Improvement of hyperandrogenism and hyperinsulinemia during pregnancy in women with polycystic ovary syndrome: possible effect in the ovarian follicular mass of their daughters. *Fertil Steril* 97:218-224.
19. Demissie M, Lazic M, Foecking EM, Aird F, Dunaif A, Levine JE (2008), Transient prenatal androgen exposure produces metabolic syndrome in adult female rats. *Am J Physiol Endocrinol Metab* 295:262-268.
20. Deplewski D, Rosenfield RL (2000), Role of hormones in pilosebaceous unit development. *Endocr Rev* 21:363-392.
21. Dumesic DA, Abbott DH, Padmanabhan V (2007), Polycystic ovary syndrome and its developmental origins. *Rev Endocr Metab Disord* 8:127-141.

22. Dunaif A, Hoffman AR, Scully RE, Flier JS, Longcope C, Levy LJ (1985), Clinical, biochemical, and ovarian morphologic features in women with acanthosis nigricans and masculinization. *Obstet Gynecol* 66:545-552.
23. Elting MW, Korsen TJ, Rekers-Mombarg LT, Schoemaker J (2000), Women with polycystic ovary syndrome gain regular menstrual cycles when ageing. *Hum Reprod* 15:24-28.
24. Escobar-Morreale HF, Luque-Ramírez M, San Millán JL (2005), The molecular genetic basis of functional hyperandrogenism and the polycystic ovary syndrome. *Endocr Rev* 26:251-282.
25. ESHRE/ASRM-Sponsored PCOS Consensus Workshop Group (2008), Consensus on infertility treatment related to polycystic ovary syndrome. *Fertil Steril* (2008) 89:50-55.
26. Fan L, Ling J, Ma X, Cui YG, Liu JY (2009), Involvement of HSP10 during the ovarian follicular development of polycystic ovary syndrome: Study in both human ovaries and cultured mouse follicles. *Gynecol Endocrinol* 25:392-397.
27. Farquhar C, Brown J, Marjoribanks J (2012), Laparoscopic drilling by diathermy or laser for ovulation induction in anovulatory polycystic ovary syndrome. *Cochrane Database Syst Rev* 6:11-22.
28. Fauser BC, Tarlatzis BC, Rebar RW (2012), Consensus on women's health aspects of polycystic ovary syndrome (PCOS): the Amsterdam ESHRE/ASRM-Sponsored 3rd PCOS Consensus Workshop Group. *Fertil Steril* 97:28-38.
29. Fedorcsak P, Dale PO, Storeng R, Tanbo T, Abyholm T (2001), The impact of obesity and insulin resistance on the outcome of IVF or ICSI in women with polycystic ovarian syndrome. *Hum Reprod* 16:1086-1091.
30. Fertility: Assessment and treatment for People with Fertility Problems (2013), Rockville MD: National Guideline Clearinghouse (NGC), Agency for Healthcare Research and Quality (AHRQ).
31. Fogel RB, Malhotra A, Pillar G, Pittman SD, Dunaif A (2001), Increased prevalence of obstructive sleep apnea syndrome in obese women with polycystic ovary syndrome. *J Clin Endocrinol Metab* 86:1175-1180.
32. Franks S, McCarthy M (2004), Genetics of ovarian disorders: polycystic ovary syndrome. *Rev Endocr Metab Disord* 5:69-76.
33. Franks S, Mc Carthy M, Hardy K (2006), Development of polycystic ovary syndrome: involvement of genetic and environmental factors. *Int J Androl* 29:278-285.
34. Franks S, Berga SL (2012), Does PCOS have developmental origins? *Fertil Steril* 97:2-6.
35. French National College of Gynecology and Obstetrics, Clinical Practice recommendations (2010), Management of the infertile couple. *J Gynecol Obstet Biol Reprod. Paris*, 39(Suppl2)113-118.
36. Gambineri A, Patton L, Vaccina A, Cacciari M, Morselli-Labate AM, Cavazza C (2006) Treatment with flutamide, metformin, and their combination added to a hypocaloric diet in overweight-obese women with polycystic ovary syndrome: a randomized, 12-month, placebo-controlled study. *J Clin Endocrinol Metab* 91:3970-3980.
37. Haisenleder DJ, Dalkin AC, Ortolano GA, Marshall JC, Shupnik MA (1991), A pulsatile gonadotropin-releasing hormone stimulus is required to increase transcription of the gonadotropin subunit genes: evidence for differential regulation of transcription by pulse frequency in vivo. *Endocrinology* 128:509-517.
38. Hardiman P, Pillay OS, Atiomo W (2003), May 24 Polycystic ovary syndrome and endometrial carcinoma. *Lancet* 361:1810-1812.
39. Hart R, Doherty DA, Norman RJ, Franks S, Dickinson JE, Hickey M, Sloboda DM (2010), Serum anti-mullerian hormone (AMH) levels are elevated in adolescent girls with polycystic ovaries and the polycystic ovarian syndrome (PCOS). *Fertil Steril* 94:1118-1121.
40. Holte J (1996), Disturbances in insulin secretion and sensitivity in women with polycystic ovary syndrome. *Baillieres Clin Endocrinol Metab* 10:221-247.

41. Jabbar M, Pugliese M, Fort P, Recker B, Lifshitz F (1991), Excess weight and precocious pubarche in children: alterations of the adrenocortical hormones. *J Am Coll Nutr* 10:289-296.
42. Jungheim ES, Lanzendorf SE, Odem RR, Moley KH, Chang AS, Ratts VS (2009), Morbid obesity is associated with lower clinical pregnancy rates after in vitro fertilization in women with polycystic ovary syndrome. *Fertil Steril* 92:256-261.
43. Kelly CJ, Stenton SR, Lashen H. Insulin-like growth factor binding protein-1 in PCOS: a systematic review and meta-analysis. *Hum Reprod Update* 17:4-16.
44. La Marca A, Sighinolfi G, Radi D, Argento C, Baraldi E, Artenisio AC, Stabile G, Volpe A (2009), Anti-Mullerian hormone (AMH) as a predictive marker in assisted reproductive technology (ART). *Hum Reprod Update* 16:113-130.
45. Lebbi I, Temime RB, Fadhlou A, Fekis A (2015), Ovarian drilling of PCOS: is it really useful? *Frontiers in surgery*.
46. Legro RS, Arslanian SA, Ehrmann DA (2013), Diagnosis and treatment of polycystic ovary syndrome: an endocrine society clinical practice guideline. *J Clin Endocrinol Metab* 98:4565-4592.
47. Lewy VD, Danadian K, Witchel SF, Arslanian S (2001) Early metabolic abnormalities in adolescent girls with polycystic ovarian syndrome. *J Pediatr* 138:38-44.
48. Luque-Ramírez M, Escobar-Morreale HF (2014) Polycystic ovary syndrome as a paradigm for prehypertension, prediabetes, and preobesity. *Curr Hyper Tens Rep* 16:500.
49. Maliqueo M, Sir-Petermann T, Perez V, Echiburu B, de Guevara AL, Galvez C (2009), Adrenal function during childhood and puberty in daughters of women with polycystic ovary syndrome. *J Clin Endocrinol Metab* 94:3282-3288.
50. McCartney CR, Prendergast KA, Blank SK, Helm KD, Chhabra S, Marshall JC (2009), Maturation of luteinizing hormone (gonadotropin-releasing hormone secretion across puberty: evidence for altered regulation in obese peripubertal girls. *J Clin Endocrinol Metab* 94:56-66.
51. Mehrabian F, Kelishadi R (2012), Comparison of the metabolic parameters and androgen level of umbilical cord blood in newborns of mothers with polycystic ovary syndrome and controls. *J Res Med Sci* 17:207-211.
52. Möhlig M, Spranger J, Osterhoff M (2004), The polycystic ovary syndrome per se is not associated with increased chronic inflammation. *Eur J Endocrinol* 150:525-532.
53. Moran L, Teede H (2009), Metabolic features of the reproductive phenotypes of polycystic ovary syndrome. *Hum Reprod Update* 15:477-488.
54. Musso C, Shawker T, Cochran E, Javor ED, Young J, Gorden P (2005), Clinical evidence that hyperinsulinaemia independent of gonadotropins stimulates ovarian growth. *Clin Endocrinol (Oxf)* 63:73-78.
55. National Collaborating Centre for Women's and Children's Health (2013), *Fertility: Assessment and Treatment for People with Fertility Problems*. National Institute for Health and Clinical Excellence (NICE). London, pp63.
56. Nestler JE, Jakubowicz DJ, de Vargas AF, Brik C, Quintero N, Medina F (1998), Insulin stimulates testosterone biosynthesis by human thecal cells from women with polycystic ovary syndrome by activating its own receptor and using inositol glycan mediators as the signal transduction system. *J Clin Endocrinol Metab* 83:2001-2005.
57. Oh JY, Lee JA, Lee H, Oh JY, Sung YA, Chung H (2009), Serum C-reactive protein levels in normal-weight polycystic ovary syndrome. *Korean J Intern Med* 24:350-355.
58. Palomba S, Orio F Jr, Falbo A, Russo T, Tolino A, Zullo F (2006), Effects of metformin and clomiphene citrate on ovarian vascularity in patients with polycystic ovary syndrome. *Fertil Steril* 86:1694-1701.

59. Palomba S, Falbo A, Russo T, Orio F, Tolino A, Zullo F (2010), Systemic and local effects of metformin administration in patients with polycystic ovary syndrome (PCOS): relationship to the ovulatory response. *Hum Reprod* 25:1005-1013.
60. Ridker PM (2003), Clinical application of C-reactive protein for cardiovascular disease detection and prevention. *Circulation* 107:363-369.
61. Robinson S, Kiddy D, Gelding SV, Willis D, Niththyananthan R, Bush A (1993), The relationship of insulin insensitivity to menstrual pattern in women with hyperandrogenism and polycystic ovaries. *Clin Endocrinol (Oxf)* 39:351-355.
62. Rosenfield RL (2001), Polycystic ovary syndrome and insulin-resistant hyperinsulinemia. *J Am Acad Dermatol* 45:95-104.
63. Rotterdam ESHRE/ASRM–Sponsored PCOS Consensus Workshop Group (2004), Revised 2003 consensus on diagnostic criteria and long-term health risks related to polycystic ovary syndrome (PCOS). *Hum Reprod* 19:41-47.
64. Semple RK, Savage DB, Cochran EK, Gorden P, O’Rahilly S (2011), Genetic syndromes of severe insulin resistance. *Endocr Rev* 32:498-514.
65. Sir-Petermann T, Codner E, Perez V, Echiburu B, Maliqueo M, Ladron de Guevara A (2009), Metabolic and reproductive features before and during puberty in daughters of women with polycystic ovary syndrome. *J Clin Endocrinol Metab* 94:1923-1930.
66. Sir-Petermann T, Ladron de Guevara A, Codner E, Preisler J, Crisosto N, Echiburu B (2012), Relationship between anti-Mullerian hormone (AMH) and insulin levels during different Tanner stages in daughters of women with polycystic ovary syndrome. *Reprod Sci* 19:383-390.
67. Stein IF, Leventhal MI (1935), Amenorrhea associated with bilateral polycystic ovaries. *Am J Obstet Gynecol* 29:181-191.
68. Taylor AE, McCourt B, Martin KA, Anderson EJ, Adams JM, Schoenfeld D (1997), Determinants of abnormal gonadotropin secretion in clinically defined women with polycystic ovary syndrome. *J Clin Endocrinol Metab* 82:2248-2256.
69. Tian L, Shen H, Lu Q, Norman RJ, Wang J (2007), Insulin resistance increases the risk of spontaneous abortion after assisted reproduction technology treatment. *J Clin Endocrinol Metab* 92:1430-1433.
70. Toulis KA, Goulis DG, Mintziori G (2011), Meta-analysis of cardiovascular disease risk markers in women with polycystic ovary syndrome. *Hum Reprod Update* 17:741-760.
71. Vgontzas AN, Legro RS, Bixler EO, Grayev A, Kales A (2001), Polycystic ovary is associated with obstructive sleep apnoea and daytime sleepiness: role of insulin resistance. *J Clin Endocrinol Metab* 86:517-520.
72. Willis D, Mason H, Gilling-Smith C, Franks S (1996), Modulation by insulin of follicle-stimulating hormone and luteinizing hormone actions in human granulosa cells of normal and polycystic ovaries. *J Clin Endocrinol Metab* 81:302-309.
73. Wood JR, Dumesic DA, Abbott DH, Strauss JF 3rd (2007), Molecular abnormalities in oocytes from women with polycystic ovary syndrome revealed by microarray analysis. *J Clin Endocrinol Metab* 92:705-713.
74. Wu XK, Zhou SY, Liu JX, Pöllänen P, Sallinen K, Mäkinen M, Erkkola R (2003), Selective ovary resistance to insulin signalling in women with polycystic ovary syndrome. *Fertil Steril* 80:954-965.
75. Yilmaz M, Biri A, Karakoç A, Törüner F, Bingöl B, Cakir N (2005), The effects of rosiglitazone and metformin on insulin resistance and serum androgen levels in obese and lean patients with polycystic ovary syndrome. *J Endocrinol Invest* 28:1003-1008.

76. Zawadski JK, Dunaif A (1992) Diagnostic criteria for polycystic ovary syndrome; toward a rational approach. In: Dunaif A, Givens JR, Haseltine FP, editors. Polycystic Ovary Syndrome. Blackwell Scientific, Boston MA; 377-384.

Study on the Trees of Euphorbiaceae *s.l.* in Cooch Behar District, West Bengal, India

Rajendra Prasad De

Department of Botany, A. B. N. Seal College, Cooch Behar, Paschimbanga, India

Email: rajendrade.bot@gmail.com

Abstract

Cooch Behar is a small District of West Bengal, India and situated on its extreme north-eastern part. It is located in between 25°57'47" N to 26°36'2" N latitudes and 89°54'35" E to 88°47'44" E longitudes. The District is a deforested area with similar floristic composition of Duars but not so rich in plant diversity. Most plant species of this region are cultivated, wild plant species found in this region are remnant of the past and under threat of increasing human population. Nine tree species under six genera of Euphorbiaceae *s.l.* are found in wild, semi-wild condition or planted in this region. In this present work these plants are enumerated by their botanical names; vernacular name(s) along with their short description and ecological status. An artificial key for the identification of the species with easily recognized morphological characters are also provided.

Key words: Cooch Behar, Euphorbiaceae, Phyllanthaceae, Putranjivaceae

Publication History: Received: 10th August, 2016; Accepted: 19th August, 2016

Introduction

Cooch Behar is a small District of West Bengal, India and situated on its extreme north-eastern part. It is located in between 25°57'47" N to 26°36'2" N latitudes and 89°54'35" E to 88°47'44" E longitudes. It covers an area of 3387 square kilometers (http://coochbehar.gov.in/HTMfiles/CoB_inWB.html).

The District is bounded in east with Kokrajhar and Dhubri Districts of Assam, on the west with Jalpaiguri District, on the north with Alipurduar and Jalpaiguri Districts of West Bengal and on the south with Rangpur District of Bangladesh.

The District is a deforested area with similar floristic composition of Duars but not so rich in plant diversity. Most plant species of this region are cultivated, wild plant species found in this region are remnant of the past and under threat of increasing human population.

Materials and Methods

The investigation on the trees of Euphorbiaceae of Cooch Behar is conducted from 2012, on the seasonal basis following floristic, phenological and community studies through sampling method. Along with this work Herbarium, Museum materials and literatures studies were also done in the same time period. Plant specimens were identified following available literatures (i. e. Haines, 1921-1925; Hooker, 1890; Mooney, 1948; Prain, 1903).

Nine plant species under six genera of Euphorbiaceae family are found in this field study. These plants are arranged alphabetically by their botanical name; vernacular name(s), along with their short description and ecological status. An artificial key for the identification of the species with easily recognized morphological characters are also provided.

List of abbreviations: B – Bangla; E – English; Fl. – Flowering season; Fr. – Fruiting season; R – Rajbansi; *s.l.* – *sensu lato*.

Key to the species

A. Leaves compound, trifoliolate	<i>Bischofia javanica</i>
B. Leaves simple	
B1. Leafy shoot look like pinnately compound leaves	
B1.1. Leaves very small, under 1 cm long	<i>Phyllanthus emblica</i>
B1.2. Leaves larger, more than 1 cm long	<i>Phyllanthus acidus</i>
B2. Leafy shoot not look like pinnately compound leaves	
B2.1. Leaves peltate, entire or lobed	<i>Mallotus roxburghianus</i>
B2.2. Leaves not peltate	
B2.2.1. Leaves ovate	
B2.2.1.1. Fruits green, large (more than 2 cm diameter), indehiscent	<i>Mallotus nudiflorus</i>
B2.2.1.2. Fruits red, small (less than 1 cm diameter), dehiscent	<i>Mallotus philippinensis</i>
B2.2.2. Leaves lanceolate	
B2.2.2.1. Leafy branches pendulous	<i>Glochidion sphaerogynum</i>
B2.2.2.2. Leafy branches not pendulous	
B2.2.2.2.1. Leaf margin wavy; fruits small (less than 1 cm), green	<i>Putranjiva roxburghii</i>
B2.2.2.2.1. Leaf margin not wavy; fruits large (more than 1 cm), brown	<i>Baccaurea ramiflora</i>

Result and Discussion

During the survey 9 trees of Euphorbiaceae *s.l.* have been observed and recorded in the Cooch Behar District. Now the family Euphorbiaceae *s.l.* are divided into a number of families, these trees are placed under 3 separate families, Euphorbiaceae, Phyllanthaceae and Putranjivaceae. The detailed description of the same is enumerated below:

Euphorbiaceae

(1). *Mallotus nudiflorus* (L.) Kulju & Welzen Syn. *Trewia nudiflora* L.

Local name: Ban Gāmāri, Pītuli (B); False white teak (E); Bheliyā, Petkurhā (R).

A large deciduous tree, dioecious. Leaves opposite, ovate. Inflorescens pendulous racems, appear in leaf-less condition. Fruits globose, woody, grayish-green. Frequent.

Fl. March-April. Fr. July-August.

(2). *Mallotus philippinensis* (Lam.) Mull. Arg.

Local name: Kamalāgunrhi (B); Kamala tree (E).

A small evergreen tree, with rusty tomentum on young parts. Leaves alternate, ovate, acuminate. Inflorescens terminal panicle. Fruits capsule, covered with red powder. Less frequent.

Fl. Novenber-December. Fr. January-March.

(3). *Mallotus roxburghianus* Mull. Arg.

Local name: Thoskā (B).

A small dioecious evergreen tree or shrub. Leaves large, peltate, orbiculare, ovate or trilobed. Inflorescence long raceme. Fruits globose capsule, 3-lobed, prickly, grayish-green. Frequent.

Fl. March-May. Fr. May-July.

Phyllanthaceae

(4). *Baccaurea ramiflora* Lour Syn. *B. sapida* (Roxb.) Mull. Arg.

Local names: Latkā, Natko, Natkol, Notkol (B); Burmese grape (E).

A small evergreen tree, dioecious. Leaves alternate, oblanceolate. Raceme long, pendulous. Fruits globose, brown, edible.

Fl. March-April. Fr. June-August.

(5). *Bischofia javanica* Blume.

Local name: Kainjal (B); Bishop wood (E).

A dioecious, medium sized evergreen tree. Leaves alternate, compound, trifoliolate, leaflets serrulate. Inflorescence panicle. Not frequent.

Fl. March-April. Fr. Not found.

(6). *Glochidion sphaerogynum* (Mull.Arg.) Kurz.

A small evergreen tree. Leafy branches pendulous. Leaves alternate, ovate-lanceolate. Flowers small in axillary clusters. Fruits capsule, sessile, globose, lobed. Rare.

Fl. February-April. Fr. March-April.

(7). *Phyllanthus acidus* (L.) Skeels Syn. *Cicca disticha* L., *C. acida* (L.) Merr.

Local name: Harhbarai (B); Star Gooseberry (E).

A deciduous medium sized tree, monoecious. Leaves alternate, ovate, oblique, acute. Fruits globose, lobed, bright green, edible. Rare.

Fl. February-March. Fr. April-May.

(8). *Phyllanthus emblica* L. Syn. *Emblica officinalis* Gaertn.

Local name: Āmlaki (B); Emblic myrobalan (E).

A deciduous medium sized tree, monoecious. Leafy branches look like pinnately compound leaves. Leaves small, sessile, oblong, obtuse. Flowers appear with new leaves. Fruits globose, smooth, green, edible. Frequent, mostly planted.

Fl. February-March. Fr. November-January.

Putranjivaceae

(9). *Putranjiva roxburghii* Wall. Syn. *Drypetes roxburghii* (Wall.) Hurus

Local name: Putranjib (B); Lucky bean tree (E).

A small dioecious, evergreen tree. Leaves alternate, ovate-lanceolate, oblique, repand. Inflorescence axillary, males are clustered, females sub-solitary. Fruits ovoid, 1-seeded drupes. Planted as road-side tree.

Fl. April-May. Fr. September-October.

Conclusion

Nine plant species under 6 genera are found to grow wild or semi-wild condition in this region. 6 plant species such as *Bischofia javanica*, *Glochidion sphaerogynum*, *Mallotus nudiflorus*, *Mallotus philippinensis*, *Mallotus roxburghianus*, *Phyllanthus acidus*, are grown wild; while, *Phyllanthus emblica* and *Putranjiva roxburghii* are planted for fruits and as an avenue tree respectively. *Baccaurea ramiflora* is rarely found to be grown wild; it is mostly cultivated for its fruits and as a sacred plant.

Acknowledgement

The author is very much grateful to Dr. Binod Chandra Sharma, Sri Manabendra Sharmadhikay, Ajoy Das, Aninda Mandal, Alokemoy Basu of A. B. N. Seal College, Cooch Behar for their kind co-operation.

References

Haines HH 1921-1925. *Botany of Bihar and Orissa*. Vol. I-VI. Bishen Singh Mahendra Pal Singh, Dehradun, India

Hooker JD 1890. *The Flora of British India*. Vol. V. Bishen Singh Mahendra Pal Singh, Dehradun, India

Mooney H 1948. *Supplement of the Botany of Bihar and Orissa*. International Book Distributors, Dehradun.

Prain D 1903. *Bengal Plants* Vol. I & II. Bishen Singh Mahendra Pal Singh, Dehradun

Available online: http://coochbehar.gov.in/HTMfiles/CoB_inWB.html

Naturally Occurring Protein Toxin –“Friends or Foes”-A Multidimensional Analysis

Liebig Ranjan Debnath, Debojyoti Dutta*

PG Department of Zoology, A B N Seal College, CoochBehar

*Email-debojyotidutta2001@yahoo.com

Abstract

Naturally occurring protein describes as toxicant or remedy it depends on appropriate measurable level or dose that differ a poison from remedy. An old adage emphasis that even nector or amrita is also a poison, if consumes in excess. Toxicants may be a small molecule, chemically peptide or protein in nature capable of producing harmful diseases or damage on human body through contact or absorption by body tissues interacting with biological macromolecules such as enzymes or cellular receptors when entering in sufficient amount, derived endogenously or exogenously within or out the body or may be produced artificially. Net result is different types of diseases for e.g. Aflatoxin B1 is a potent environmental mutagen & carcinogen for human, α - aminitin derived from *Aminita phalloides* causes inhibition of RNA Polymerase II in human, Benzo[a]pyrene represent as human made toxicant known as potent mutagen for human. Many snake venoms are strong antagonist of neurotransmitter as well as block different channels, which have essential role in nerve impulse transmission. Discovery of mechanism, elimination, detoxification for use the toxic proteins as potential drug for multiple disorder or for drug design. So the area of research now a day is treated as a subject of interdisciplinary relevance.

Key word: Toxicant, Aflatoxin, Cytochrome P450, Detoxification

Publication History: Received: 10th August, 2016; Accepted: 19th August, 2016

Introduction

Toxin are substances endogenously within the cells of living organisms & few exogenously derived from plants, fungi and marine organism, snails or any other animals. Toxic elements are designated as toxicants. Toxicants may be a small molecule, chemically peptide or protein in nature capable of occurring harmful diseases or damage on human body through contact or absorption by body tissues interacting with biological macromolecules such as enzymes or cellular receptors when entering in sufficient amount. It also occurs malfunctioning of vital activities & may lead to impaired health. Although many natural occurring protein toxins used for drug development used as remedy.

Naturally occurring protein describes as toxicant or remedy it depends on appropriate measurable level or dose that differ a poison from remedy. An old adage emphasis that even nector or amrita is also a poison, if consumes in excess. (Pandey *et al*, 2012). Aflatoxin B1 one of the fungal toxin most potent environmental mutagen and also a carcinogen. Botulinum toxin produced by an anaerobic bacterium *Clostridium botulinum* is one of the dead list nerve poisons throughout history & also treated as bioweapon. An enzyme Batroxobin derived from the venoms of *Bothrops atrox* has thrombin like properties. It is hemostatic in lower doses & serves as a blood anticoagulant at higher doses.

Natural v/s artificial toxin

Natural toxin are toxins or chemical substances made up by plants, animals exogenously, endogenously and also by humans itself. Artificial toxin is made through different man-made sources such as industries, atomic, nuclear generator, radioactive full out resulting from nuclear weapon testing and also through between primary pollutant & other pollutants (such as primary pollutant, hydrocarbon and nitrogen oxides, in the presence of sunlight reacts and forms a group of nitrous

compound, PAN or Peroxy Acetyl Nitrate). Although human produced many toxins *in vitro* used as drug in the treatment of different diseases.

Table 1. Some representation of naturally occurring toxin

Type of toxin	Example
Fungal toxin	Aflatoxin B, griseofulvin, amanitin, phalloidin, Cyclosporine-A etc.
Algal toxin	Anatoxin-a, saxitoxin, Cyanatoxin, Ciguatera, Dead zones etc.
Bacterial toxin	Botulinum toxin, tetanus toxin, pertussis toxin, shigatoxin, Diphtheria toxin, Anthrax toxin, Alpha toxin etc.
Marine toxin	Palytoxin, Didemnin-B etc.
Animal toxin	Snake venom, spider venom, scorpion venom, Hymenoptera venom, sea-snail: cone shells, Box jelly fish, Portuguese man of war, Sea-anemone, puffer fish(japan), blue ring octopus etc.

Role of some representative toxin in metabolism

A) Fungal toxin: -

Among the toxins derived from different fungi aflatoxin are the most documented of all mycotoxin produced by *Aspergillus flavus* and *Aspergillus parasiticus*. Chemically aflatoxin are fluorescent compounds characterized by a dihydrofuran or tetra hydrofuran moieties fused to a substituted coumarin heterocycle. Aflatoxins B₁, one type of naturally occurring most potent environmental mutagen as well as carcinogen.

Griseofulvin, a toxicant from *Penicillium griseofulvum* is used as antifungal drug.

Amanitin and Phalloidin, the cyclopeptide toxin produced by poisonous mushroom *Amanita phalloides* composed of α , β , γ amanitin and aminin ten to twenty times more potent than phalloidin (Kapoor, 2010). α -

amanitin disrupts mRNA formation by blocking RNA pol II in animal cells. Cyclosporin -A acts as immunosuppressive drug derived from *Amanita* mushroom. (Kapoor, 2010)

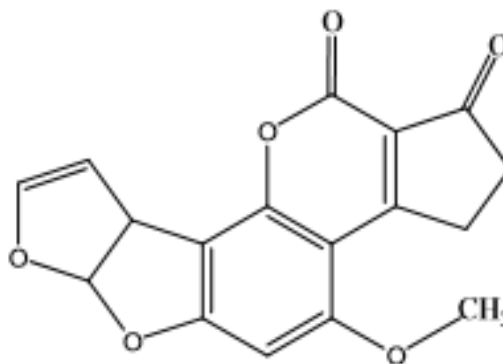


Fig. 1: Chemical structure of aflatoxin B₁ (Kapoor, 2010)

B) Algal toxin:-

Algal toxin Anatoxin-a, is the strongest agonist of nicotinic Ach receptor, produced by fresh water blue green algae *Anabaena flossaquae*. Marine Dinoflagellate *Gonyalux* produces saxitoxin which causes red tides and inhibits transmission of nerve impulse.

C) Bacterial toxin: -

Botulinum toxin (BTX) is a neurotoxic produced by the bacterium *Clostridium botulinum* and related species. BTX is used for number of problems when injected in small amount. But in higher amount BTX have been developed into biological weapons agents for its extreme potency & lethality.

Pathogenic bacteria *Vibrio cholerae* and *Bordetella pertussis* that causes cholera and pertussis toxins that target G-proteins, interfering with normal signaling in host cells.

D) Marine toxin: -

Didemnin B isolated from the extract of *Trididemnum solidum* is a strong antiviral agent active against both DNA and RNA viruses like herpes simple viruses type1 and a strong immunosuppressant that shows some potential in skin graft. It shows strong activity against murine leukemia cells. It has undergone phase II human clinical trials against adenocarcinoma of kidney, advanced epithelial ovarian cancer & metastatic breast cancer. (Kapoor,2010)

E) Animal toxin: -

Venomous animals possess a wide range of toxins for predation & defense. It is difficult to describe the exact number of venomous species or the number of toxins they produce. A number of venomous animals and their toxins have been investigated to explore their biological activities and therapeutic potential is as follows: -

a) Snake venom: -

Snake venom is a mixture of both proteinaceous or non-proteinaceous compound. These toxins are reported to exhibited a variety of pharmacological activities such as myotoxic, neurotoxic, hypotension, hemolytic, platelet aggregation inhibition, anticoagulant, inflammatory, analgesic and bactericidal. (Kapoor,2010)

Table 2. Snake venom-their sources, contents & mode of action

Name of Toxin	Toxin emerge from snake	Contents	Action
α bungurotoxin	<i>Bungurus multicinctus</i>	It has a single polypeptide chain of M.W of about 8000 kDa containing 74 a.a residue with 5 disulfide bridge.	It is a post- synaptic neurotoxin bind selectively and irreversibly to Achr site resulting in skeleton muscle paralysis.
β bungurotoxin	<i>Bungurus multicinctus</i>	Consist of to polypeptide chains cross linked by an interchain disulfide bond. A chain contains 120 a.a and B chain contain 60 a.a residue	It acts as presynaptic A2 neurotoxin. Recently it has been indicated that β -bungurotoxin possess the capability to induce vesicle leakage.
Crotamine	<i>Crotalus durissus terrificus</i>	Composed of single polypeptide chain of 42 a.a with 3 di sulfide bridge	Induced myonecrosis and reported to produce analgesic affect at lower doses. Also used as a tool to study Na ⁺ channel distribution in the muscle fibre membrane.
Batroxobin	Pit viper	Has thrombin like properties	Haemostatic at lower doses and acts as a blood anticoagulant at higher doses.
Myotoxin	<i>Bothrops jararacussu</i>	Small basic peptide (42 to 45 residue)	Causes increase in myoglobin urea and acute renal failure. Myotoxin I & II of <i>Bothrops jararacussu</i> have antibacterial effect against <i>Xanthomonas axonopodis</i> . <i>PV.passiflorae</i> , a gram negative bacteria.
Cobrotoxin	<i>Naja naja atra</i> , Taiwan	Single polypeptide chain	Act as neurotoxin.

Cobra

of 62 a.a crosslinked by 4
disulfide bridge

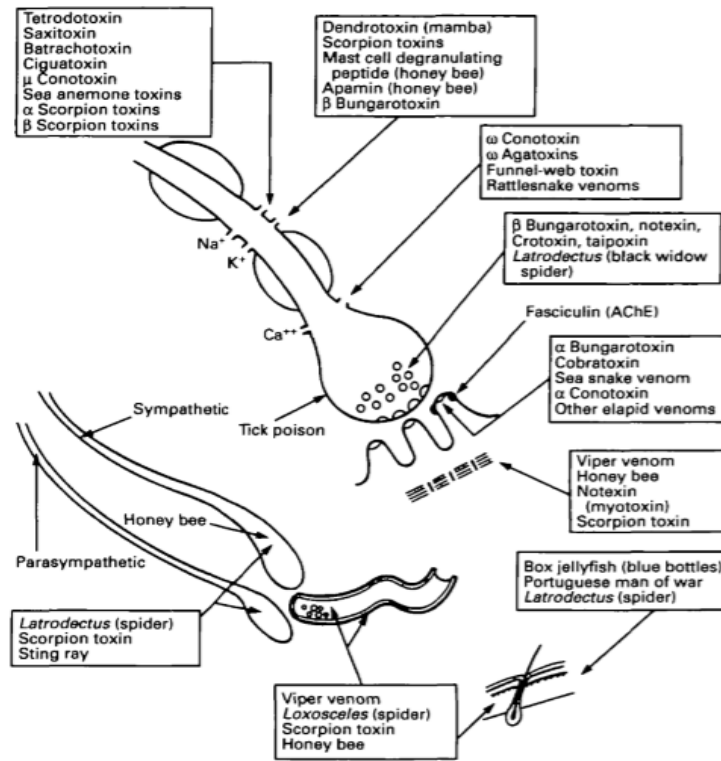


Fig. 2: Diagrammatic representation showing sites of action of animal toxin (adopted from Karalliedde, 1995)

b) Scorpion venoms: -

Scorpion venom are known to enhance the excitability of nerve and muscle cells. Some venom appears to act preferentially on muscle cells while others have effects on neurons and neurotransmitter release. Scorpion venoms have been shown to release acetylcholine, noradrenaline and serotonin. (Karalliedde, 1995)

Mexican scorpion secretes a venom that blocks the voltage gated K⁺ channel which is important receptor for neurotransmitter such as GABA and Gly. Scorpions found in India, north Africa and the middle east cause release of catecholamine produce hypertension, myocarditis, arrhythmias, heart failure and pulmonary oedema. Scorpion venom contains a large number of biologically active substances such as peptide toxins with different in channel specificities, enzymes nucleotides, lipids, mucoproteins, biogenic amines, glycosaminoglycan and histamine. Injection of scorpion venom can induce the secretion of inflammatory mediators such as bradykinin, platelet activating factor, prostaglandins, leukotrienes, cytokines & 5-hydroxytryptamine that contributes top pain response. (Kapoor, 2010)

c) Snail toxin: -

Cone snails are marine predators that use venoms to immobilize their prey. The venoms of these molluscs contain a mixture of peptides that mainly target different voltage- and ligand-gated ion channels. Typically, conopeptides consist of ten to 30 amino acids but conopeptides with more than 60 amino acids. (Becker, Terlau, 2008)

The δ - conotoxins is known to inhibit the fast activation of voltage gated Na⁺ currents, the κ -conotoxin which interact with voltage gated K⁺ channel, the μ -conotoxin interact with voltage gated Na⁺ channel & the ω -conotoxin known to voltage gated Ca²⁺ channel. The ω -conotoxin MVIIA

specifically targets N-type Ca²⁺ channels with little affinity to other Ca²⁺ channel subtypes. Since N-type Ca²⁺ channels are primarily located in presynaptic space, the action of ω-conotoxin MVIIA results in blocking synaptic transmission and therefore during envenomation of prey. (Becker, Terlau, 2008).

Pharmacological specificity of conopeptides resulted in use of different applications. ω-conotoxin used to study the function of Ca²⁺ channel. Especially for transmembrane proteins where no or little structural information is available, the interaction of peptide toxin can be used to determine the structural information of the target proteins by using the interaction surface of peptide as a fingerprint of the interaction surface of the target. (Becker, Terlau, 2008).

d) Lizard toxin: -

Extendin-4 obtains from the venom of lizard *Heloderma suspectum*, a Glucagon like peptides identical to a human hormone GLP-1 or Glucagon like peptides-1 that increases the production of insulin when blood sugar levels are high. Extendin-4 effect much longer than human hormone. (Kapoor, 2010).

Gecko is a traditional Chinese medicine to restrain inflammation and allergic response, detumescence and alimentionation. (Liu *et. al*, 2008). Liu *et. al* found that the high, medium & low dose of the gecko eviscerated processed products powder fed S180 sarcoma mice could inhibit the tumor growth. (Jiang *et. al*, 2014). The methanol extract of fecal droppings of common house lizard/gecko exhibited antimicrobial activity against some of the testisolates. (Ngwoke *et. al*, 2015).

Table 3: Mode of action of lizard venom

Toxin type	Toxic biodiversity
Helokinstatin-1,-2,-3,-4	Bradykinin-inhibition.
Exendin-1,-2,-3,-4	Induction of hypotension, mediated by relaxation of cardiac smooth muscle.
Kallikrein	Release of bradykinin from kininogen.
Lethal toxin 1	Lethal inhibition of direct electrical stimulation.
Natriuretic peptides	Potent induction of hypotension leading to loss of consciousness; mediated through the binding of GC-A resulting in the relaxation of cardiac smooth muscle.
PLA2	Platelet inhibition by epinephrine induced pathway.
Three finger toxin like peptides(3LP-1)	Unknown

(Adopted from Kwok *et.al*, 2010)

e) Frog toxin:

Number of potent bioactive compounds isolated from frog toxin Batrachotoxin and Histrionicotoxin.

Batrachotoxin are potent cardiotoxic and neurotoxic steroidal alkoids obtained from south American poison dart frog of genus *Phyllobates*. It has marked effects on cardiac muscles which are similar to cardiotoxic effects of digitalis. Acting on peripheral nervous system, it causes activation of Na⁺ channel. It also used as biochemical tool for the study of Na⁺ channel. Histrionicotoxin is a piperidine alkoid isolated from the skin of poisonous arrow frog *Dendrobates histrionicus*. It causes non-competitive inhibition of nicotine receptor. Histrionicotoxin used as a biochemical probe for neuromuscular transmission. (Kapoor, 2010)

f) Hymenoptera venoms(Honey bees, wasps, hornets):-

Most death from hymenoptera stings are caused by dysfunction of the body's immune system. Bee venom contains histamine but both phospholipase A2 & mellitin separately or in combination cause histamine release from skin mast cells as a result of cytolytic effects. (Karalliedde, 1995).

Phospholipase A2 is the most allergen in the honey bee. Mellitin the major component of venom, causes lysis of red cells. Apamin was the first neurotoxin found to block K⁺ channels that are activated by increased levels of internal Ca²⁺ ions. It can gain access to the C.N.S to produce hyperactivity and convulsions before birth. (Karalliedde, 1995).

Mechanism of action:

A. Mechanism of action of Aflatoxin B1:-

Aflatoxins are highly lipid soluble compounds and are readily absorbed from the site of exposure usually through the GI tract & respiratory tract into the blood stream. Humans and animals get exposed to Aflatoxin by 2 major routes:

- a. Direct ingestion of aflatoxin contaminated food or ingestion of aflatoxins carried over from feed into milk and milk products like cheese and powdered milk as well as other animal tissue.
- b. By inhalation of dust particles of aflatoxins especially AFB1 in contaminated food in industries and factories (<http://dx.doi.org/10.5772/51201>).

After entering the body, the aflatoxins (AFTs) are absorbed across the cell membrane where they reach the blood circulation. They are distributed in blood to different tissues and to the liver, the main organ of metabolism of xenobiotics (<http://dx.doi.org/10.5772/51201>).

The epoxidation of AFB1 to exo-8, 9 epoxide is a critical genotypic pathway of this carcinogen. The binding of AFB1 to DNA and DNA adduction by AFB1 exo-8,9 epoxide has been reported to cause functional changes of DNA confirmation. The epoxide is highly unstable and binds with high affinity to guanine bases in DNA to form Aflatoxin-N7-Guanine (<http://dx.doi.org/10.5772/51201>). Essigman *et. al* reported that in hepatic DNA from the liver of the rats injected with AFB1, nearly 80% of the adducts present are AFB1-N7-Guanine while AFB1-Formamidopyrimidine (AFB1-FAPyr) constitutes approximately 7%. The alkylation of DNA with AFB1 may lead to loss of a DNA base "apurinic sites". In addition to alkylating DNA, AFB1 can reactive oxygen species (ROS) formation. Guinodon *et. al* suggested that DNA damage might be caused by the AFB1 mediated stimulation of ROS formation, which leads to the oxidation of DNA bases. (Do, Choi, 2007). The Aflatoxin-N7-Guanosine has been shown to be capable of forming guanine to thymine transversion mutations in DNA and hence affecting the P53 suppressor gene in the cell. P53 plays an important role to prevent cell cycle when there are DNA mutations or signaling apoptosis. AFB1 induces transversion of base G to T in the third position of codon 249 and similar mutations have been observed in hepatocellular carcinoma (HCC) in high AFB1 contaminated food in regions of East Asia & Africa (<http://dx.doi.org/10.5772/51201>).

B. Mechanism of action of α -Aminitin:-

α -Aminitin is a molecule made from the "death cap" mushroom and is known as a potent inhibitor of RNA Polymerase. One single mushroom could very easily lead to a fast death in 10 days.

The mechanism of action is that α -aminitin inhibits RNA Pol at both the initiation and elongation states of transcription. The binding site for the inhibitor is the cleft between Rpb1 and Rpb2 in RNA Polymerase. The cleft formed between these two subunits is connected to a helix bridge restricting the movement of the bridge by interaction between aminitin & residues 726, 767, 768, 769 and 822 of Rpb1 and by hydrogen bonding to residue 763 and 765 of Rpb2. (Bushnell *et. al*, 2002)

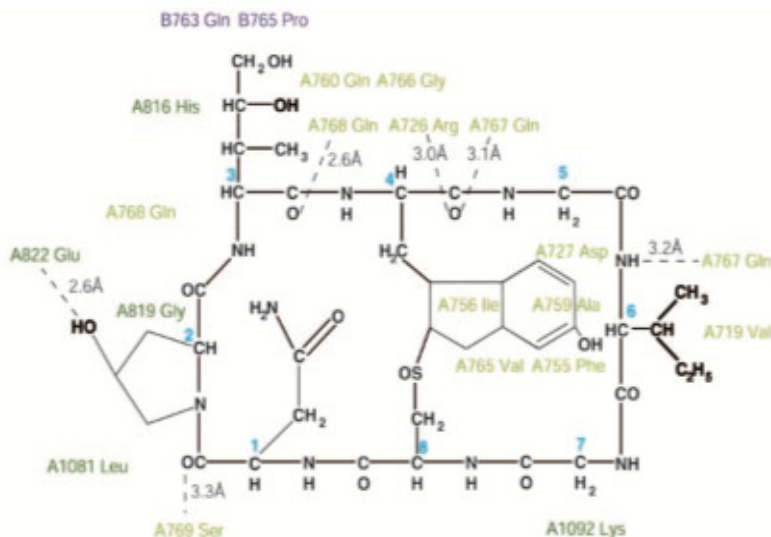


Fig. 3: The chemical structure of α -aminitin showing where the toxin binds to RNA Polymerase II. (Adopted from Bushnell *et. al.*, 2002)

The binding of α -aminitin toxin restricts the movement of the helix bridge and has no effect on the flow of nucleotides to the active site. The restriction of movement of the helix bridge causes the rate of translocation to slow down tremendously, which results in strain placed on the bridge helix. In order for RNA Polymerase to move along the DNA strand, the bridge must move, but when α -aminitin is bound to the helix bridge, it is unable to cause translocation. (Bushnell *et. al.*, 2002).

C. Mechanism of action of Anatoxin-a: -

Anatoxin-a is a neurotoxin that is an irreversible acetylcholinesterase (AChE) inhibitor that binds to the enzyme & renders it unable to hydrolyze acetylcholine (ACh). Since ACh is not hydrolyzed, the ion channel is left open, once again destroying muscle function through exhaustion. (Patocka *et. al.*, 2011)

Anatoxin-a is an only known organophosphate (OP), similar in its action to OP nerve agents such as sarin or soman which inhibits ChEs by phosphorylation of the AChE active site. (Patocka *et. al.*, 2011).

The effects of anatoxin(s) on mean arterial blood pressure, heart rate, respiratory rate, tidal volume, minute volume and phrenic nerve activity were evaluated in rats by Cook *et. al.* The initial effect of anatoxin(s) was to slow the heart rate & reduce blood pressure. In vivo, anatoxin(s) has an important muscarinic effect on the cardiovascular system. It has a remarkable inhibitory action on the central mediation of respiration. (Patocka *et. al.*, 2011).

D. Mechanism of action of saxitoxin (STX): -

Saxitoxin is an inhibitory neurotoxin that induces flaccid paralysis by actively suppressing excitation of neuronal impulses. With a high affinity for binding on site 1 of the voltage-gated sodium ion channel, STX inhibits the temporary permeability of sodium ions by binding tightly to a cell surface receptor site, which is very close to the external orifice of the sodium channel. Widespread blockage of the channel in humans prevents depolarization of the membrane and inhibits subsequent impulse-generation in the peripheral nerves and skeletal muscles, leading to a prolonged relaxed state. (Faber, 2012).

In a study by Kao and Nishiyama on the cellular actions of saxitoxin, STX is observed to completely block the propagation of compound action potentials in de-sheathed frog sciatic nerves(1965). (Faber,2012)

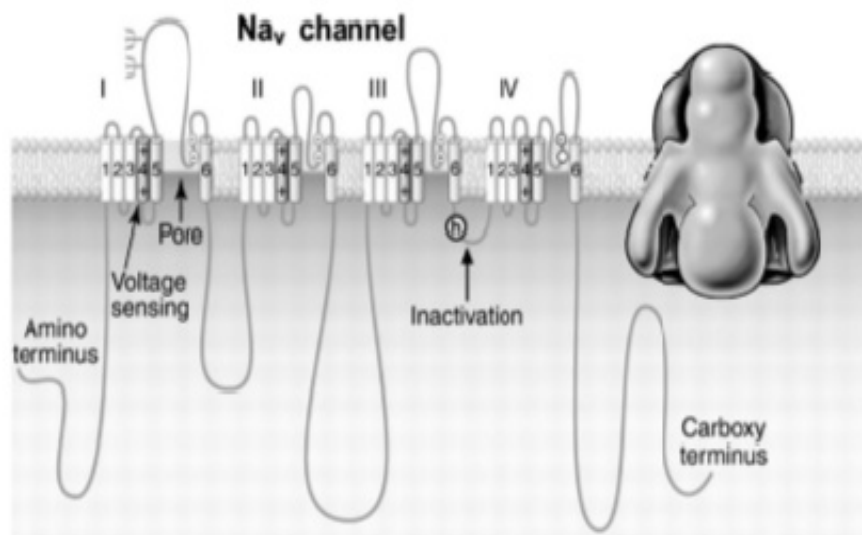


Fig. 4: Voltage gated Na⁺-channel with inactivation at site IV (Adopted from Faber,2012)

E. Mechanism of action of Botulinum toxin (BTX): -

BTX or Botulinum toxin acts by inhibiting the release of Ach from the presynaptic terminal. Physiologically the Ach is released from presynaptic nerve by the assembly of a presynaptic fusion complex that allows the membrane of the synaptic vesicles containing Ach to fuse with neuronal cell membrane. The synaptic fusion complex is a set of SNARE (Soluble N – ethylmaleimide sensitive fusion attachment protein receptor). BTX binds to the neuronal cell membrane at the nerve terminals with the help of heavy chain and enters the neuron by endocytosis. The light chain of botulinum cleaves specific sites on the SNARE proteins preventing complete assembly of the synaptic fusion complex & there by blocking Ach release (Pathak, Gupta 2009)

F. Mechanism of action of Pertussis toxin: -

Pertussis toxin is a secreted protein exotoxin and an important virulence factor produced exclusively by *B. pertussis* (Carbonetti, 2010).

Pertussis toxin (PTX) consists of 5 dissimilar subunits name S1 through S5, according to their decreasing molecular weights & are arranged in 1S1:1S2: 1S3:2S4:2S5 stoichiometry. The S2 to S5 subunits forms B moiety of the toxin, responsible for the interaction of the toxin with the target cell receptors. The S1 subunit also called the A promoter, has enzymatic activity that is responsible for the most,if not all,of the biological activities (Locht, 1999).

S1 has ADP - ribosylation activity using NAD as ADP – ribosyl donar and signal transduction, G-proteins as ADP- ribosyl acceptors. The molecular action of the toxin can be divided into 3 major steps: -

- a. Binding of the toxin to target cell receptors via the 8 oligomer.
- b. Membrane translocation of the S1 subunit into the cytosol. And
- c. ADP-ribosyltransferase activity by the translocated S1 subunit. The ADP-ribosylation of the Gi- protein results in their activation and signals that normally regulate intracellular processes such as

the formation of cAMP. PTX poisoning results in dysregulation of major metabolic pathways although it does not usually kill the target cell (Locht,1999).

G. Mechanism of action of Bungurotoxin:-

After the toxin is injected by the snake, its partially occluded active site and reduced hydrophobicity enable it to avoid binding to non-target membranes and thus diffuse away from the site of injection. Upon reaching the presynaptic membrane, the Kunitz domain binds to its K⁺ channel receptor through the binding region. The initial K⁺ channel is an integral membrane protein and K⁺ channel binding would presumably orient the phospholipase subunit towards the membrane. The tight K⁺ channel interaction would thus compensate for the decreased membrane affinity of the phospholipase. Once hydrolysis occurs, two events further enhance phospholipase affinity .First substrate binding displaces Trp19, flipping it into the membrane where it provides hydrophobic anchor. Second, fatty acids released upon phospholipid hydrolysis, increase the anionic composition of the membrane, thereby enhancing β-bungurotoxin non-specific electrostatic affinity, eventually extensive phospholipid hydrolysis cumulatively interferes with neurotransmitters release ultimately resulting in blockage of neural transmission, the hallmark of β-bungurotoxin neurotoxin action. (Kwong *et. al*, 1995)

Biotransformation:

Biocatalytical conversion of xenobiotic or lipophilic compound known as Biotransformation. Compound that are not found in nature but synthesized industrially- known as Xenobiotics, transformed into hydrophilic compound by a family of enzyme CYP450 or Cyt P-450. Xenobiotic compound are the substrate of those family of CYP450 which are found in ER of hepatocytes. Hydroxylation of these toxicants makes them more soluble in water which is cleaved by kidneys & excreted in urine. Metabolism by CYP450 enzyme limits the drugs lifetime in the blood stream & their therapeutic effects. (Cox & Nelson, 2011).

Mode of action of CYP450:-

Cytochrome P-450 catalyzes hydroxylation reactions in which an organic substrate, RH is hydroxylated R-OH, incorporating one enzyme atom of O₂; the other oxygen atom is reduced to H₂O by reducing equivalents that are furnished by NADH OR NADPH but are usually passed to Cyt P-450 by an iron-sulfur protein. Though the intermediate steps of action of CYP-450 not yet fully understood (Cox & Nelson, 2011).

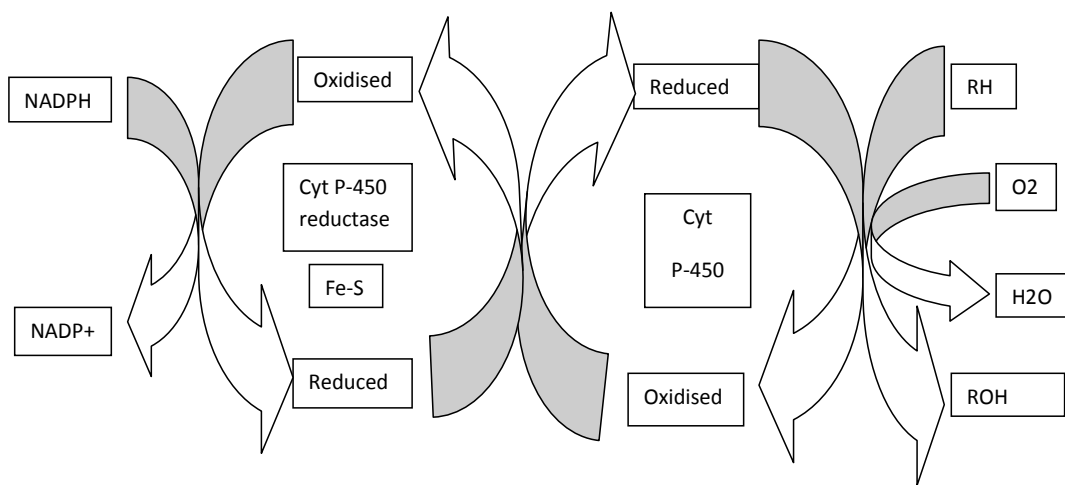


Fig. 5: Action of CYP450 (Adopted from Cox & Nelson, 2011 with modification)

Mechanism of elimination of biotransformable xenobiotic molecule/toxicants:

Actually elimination of the xenobiotic element from the body is a bi-phasic process. First, the xenobiotic element reach blood from routes of entry, then they are distributed by blood to different organs of the body, from where the toxic elements reenter to the blood for re-distribution to the organs of the deposition. (Pandey *et al*, 2012).

A. organs involved in elimination of xenobiotic element:-

- a. Liver:** Excrete anions, cations & non ionized molecules in bile.
- b. Kidneys:** kidneys are the organ that seems to be especially designated for the excretion of xenobiotics and their metabolites. All ionized and polar forms of xenobiotics – organophosphates, alcohol, weak acids, weak bases are completely excreted by glomerular filtration.
- c. GIT:** Heavy metal ions in the form of metallo-protein excreted in gut & then eliminated through feces.
- d. Lungs:** Lungs excrete fluorebenzene, CO, Benzene, Nitrous oxide etc.
- e. Sweat Gland:** Drug used for leprosy such as diethyl dithioliosphthalate excrete through sweat.
- f. Mammary Gland:** Certain xenobiotic compound excreted into milk such as DDT, tetracycline, morphin etc.
- g. Vagina:** Vagina also excrete xenobiotic element reported in cow (Pandey *et al*, 2012).

B. Table 4: Enzymes involved in elimination of xenobiotic element

Enzyme	Reaction
<i>Phase I “Oxygenases”</i>	
Cyt P450	C and O oxidation, dealkylation & others.
Flavin containing monooxygenases(FMO)	N, S & P oxidation
Epoxide hydrolases (mEH,sEH)	Hydrolysis of epoxides
<i>Phase II “Transferases”</i>	
Sulfotransferases(SULT)	Addition of sulfate
UDP-gluconosyltransferases(UGT)	Addition of glucuronic acid
Glutathione S- transferases(GST)	Addition of acetyl group
Methyl transferases(MT)	Addition of methyl group
<i>Other enzymes</i>	
Alcohol dehydrogenase	Reduction of alcohol
Aldehyde dehydrogenase	Reduction of aldehydes
NADPH quinone oxidoreductase(NQO)	Reduction of Quinones

(Adopted from Gonzalez *et al*, 2011)

C. Mechanism of action:-

The process of elimination of chemical substances from the body involves two main phases is as follows:

Phase I: Metabolism of chemical substances that involves the addition of a small polar group containing both positive and negative charges that are added to the xenobiotics element by the process of oxidation, reduction, acetylation and hydrolysis and render it harmless. The process allows the product of Phase I product to “fit” into Phase II enzyme system where they become conjugated (joined together) with another substance to produce a polar or water soluble substance that can easily be excreted by the kidney (Bbosa *et al*, 2013).

Phase II: Phase II metabolism involves sulfate, glucuronide, glutathione and amino acid conjugation reactions to produce the polar and less toxic metabolites that are easily excreted in urine & bile (Bbosa *et al*, 2013).

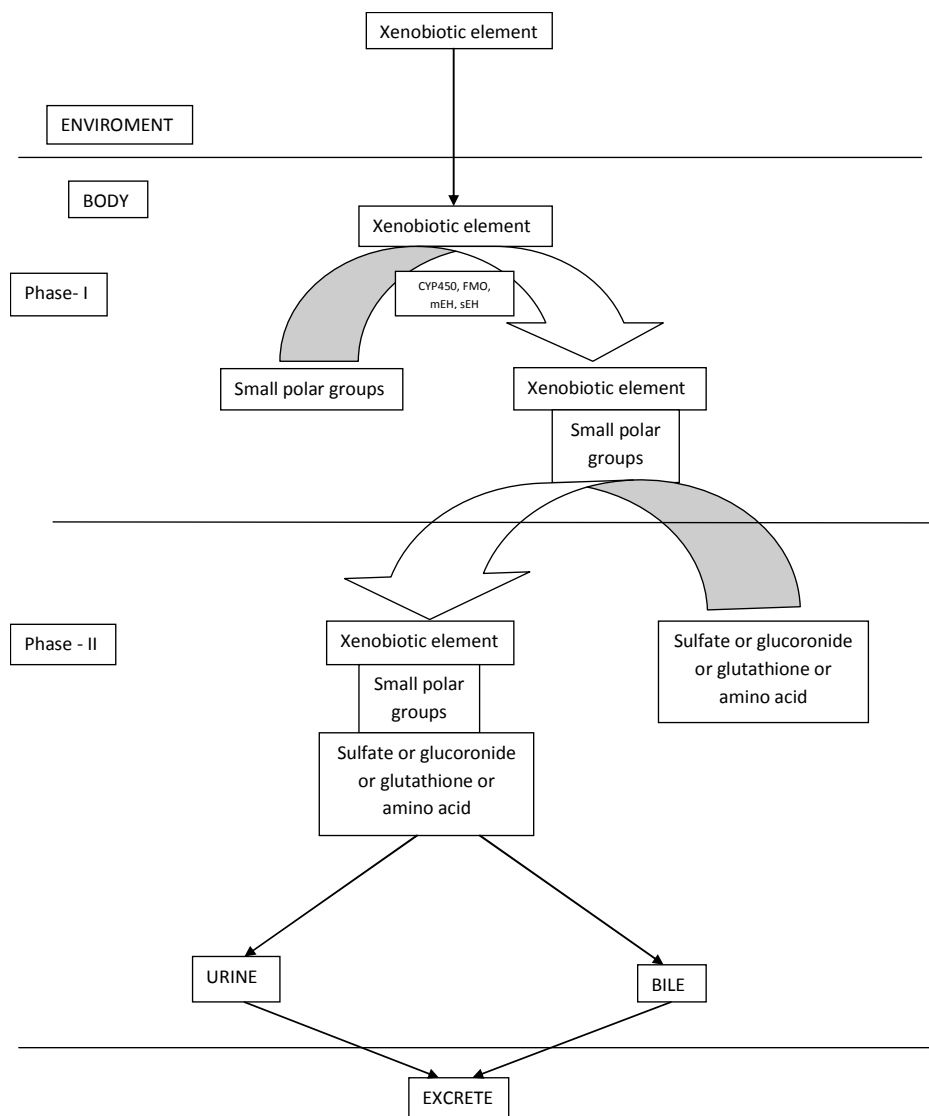


Fig. 6: Diagrammatic representation of mechanism of elimination.

D. E.g. of elimination of Aflatoxin B1 from human body:-

Epoxide hydrolase and glutathione -S- transferase(GST) are both in detoxification of activated AFB1, but GST catalyzed conjugation of glutathione to AFB1-8,9- exo and endo epoxides are conjugated to form AFB mercapturate and the reaction is catalyzed by GST. The glutathione-aflatoxin conjugate is transported from the cells with an ATP-dependent multidrug resistance protein through an accelerate process. The exo & endo epoxide can also be converted non enzymatically to AFB1,8,9, dihydrodiol which in turn can slowly a base catalysed ring opening reaction to a dialdehyde phenolation. Also the aflatoxin dialdehyde are reduced to a dialcohol catalysed by aflatoxin aldehyde reductase (AFAR) (<http://dx.doi.org/10.5772/51201>).

The aflatoxins are metabolized in the liver, mainly by CYP1A2 and CYP3A4 isoenzymes by the initial two electron transfer oxidation reactions. The CYP3A4 metabolizes AFB1 to its reactive intermediates AFB1-exo-8,9-epoxide and then to aflatoxin Q1 (AFQ1), a less toxic metabolite. Other oxidized metabolites include hydroxylated forms, aflatoxin M1 (AFM1), the O-demethylated form and aflatoxin P1 (AFP).

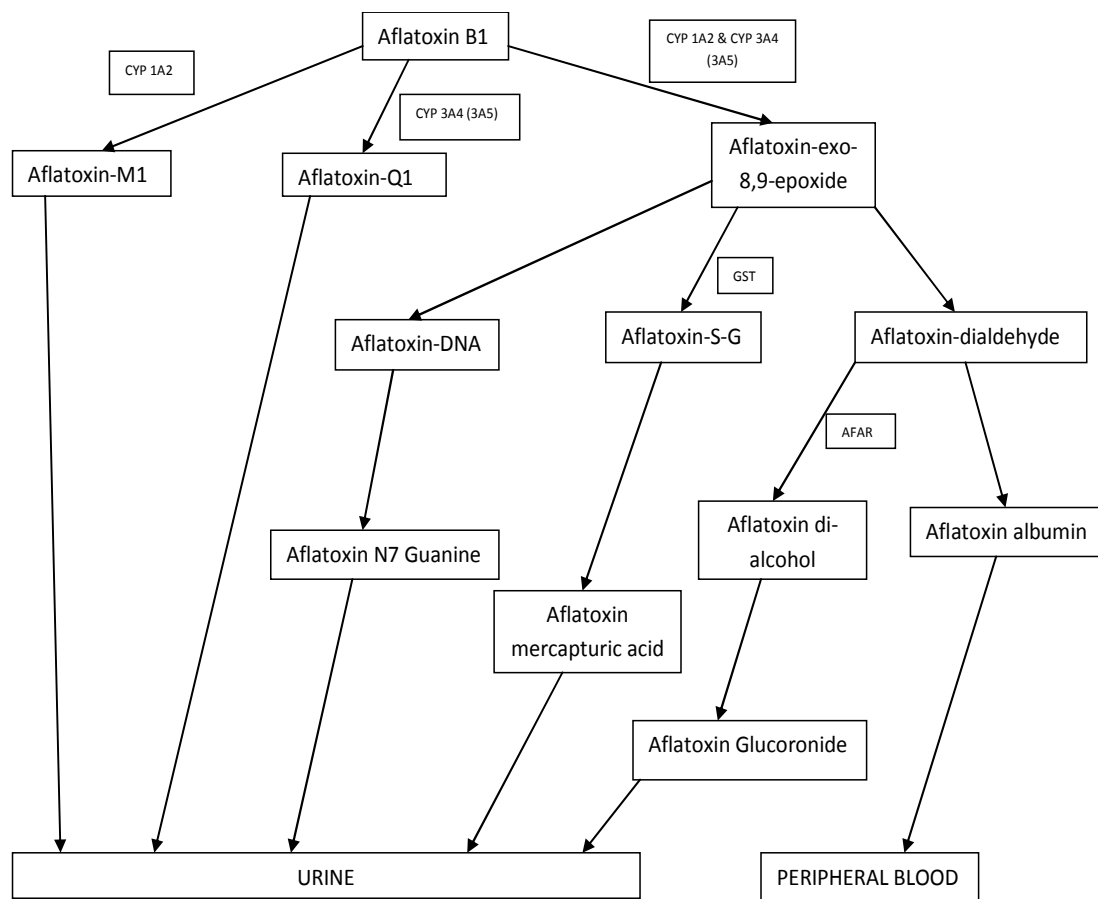


Fig. 7: Elimination of different intermediate forms of Aflatoxin B1 from human body (Bbosa *et. al*, 2013)

Application of venoms:-

- α -aminitin, derived from *Aminita phalloides* causes prevention of RNA Pol II from protein synthesis in human body.
- Anatoxin-a is a neurotoxin that is an irreversible acetylcholine esterase inhibitor that binds to the enzyme & renders it unstable to hydrolyze the acetylcholine. (Patocka *et. al*, 2011)
- Saxitoxin is a neurotoxin derived from marine dinoflagellate causes red tides & inhibits the voltage gated Na⁺ channel.
- Pertussis toxin effects the G-protein signal transduction.
- BTX inhibiting the release of Ach from pre-synaptic nerve & also used as bioweapon.
- PLA2 toxin from lizard causes platelet inhibition by epinephrine induced pathway.
- Extendin-4 from *Heloderma suspectum*, a glucagon like peptide identical to GLP-1 increases the production of insulin where blood sugar levels are high. (Kapoor, 2010).
- Histrionicotoxin derived from the skin of poisonous arrow frog *Dendrobates histrionicus* causes noncompetitive inhibition of nicotine receptor and also used as biochemical probe for neuromuscular transmission
- Aflatoxin B1 a fungal toxin has a potency to make cancer in human body
- Hymenopterans such as honey bees' venom have phospholipase A2 composed of mellitin, causes lysis of RBC and also contain apamin act as K⁺ channel inhibitor in human body

K. Table 5: Drug derived from snake venom

Name of drug	Snake	Target and function of treatment
Captopril	<i>Bothrops jaracusa</i>	Angiotensin converted enzyme inhibitor, high blood pressure.
Eptifibatide	<i>Sistrurus miliarius barbouri</i>	Platelet aggregation inhibitor, acute coronary syndrome.
Tirofiban	<i>Echis carinatus</i>	GP1Ib-IIIa inhibitor, myocardial infarct, refractory ischemia.
Exanta	Cobra	Thrombin inhibitor, arterial fibrillation and blood.
Alfimeprase	<i>Agkistroden contortrix contortrix</i>	Thrombolytic, acute ischemic stroke
Viprinex	<i>Agkistroden rhodostoma</i>	Fibrinogen inhibitor, stroke
Hemocoagulase	<i>Bothrops atrox</i>	Thrombin like effect and thromboplastin activity, preventing and treatment of haemorrhage.

(adopted from Omar, 2013)

L. Table 6: Pharmacology of venom peptides

Source	Name of venom peptides	Action of class
Cone snail	α – GI	Muscle nAChR antagonist.
	α – GID	Neuronal nAChR antagonist
	μ - PIIIA	TTX- sensitive VSSC (Voltage sensitive Ca ²⁺ channel inhibitor
	ω – MVIIA	Ca _v 2.2 inhibitor
	ω - CVID	
	χ – MrIA	NET inhibitor
	ρ –TIA	α - Adrenoceptor inhibitor
Spider	Conantoxin G	NMDA (N-methyl D-aspartate receptor inhibitor)
	Contulakin G	Neurotension receptor agonist
Scorpion	GsMTx4	Mechanosensitive channel inhibitor
Sea Anemone	Chlorotoxin	Cl ⁻ channel inhibitor
	Margatoxin	Kv 1.1,1.2,1.3 channel blocker
	Shk	Kv 1.1,1.3 channel blocker

(Adopted from Lewis & Garcia, 2013)

Future direction

Elements which are toxic for human derived from plants, animals as well as from Bacteria, fungi, algae etc. These toxins are useful elements for plants, animals, bacteria, fungi etc. helping in defense mechanism & others different metabolic activities. Toxic elements are also made by man which have deleterious effect on human being through affecting different metabolic activities. Net result is different types of diseases for e.g. Aflatoxin B1 is a potent environmental mutagen & carcinogen for human, α - aminitin derived from *Aminita phalloides* causes inhibition of RNA Pol II in human, Benzo[a]pyrene represent as human made toxicant known as potent mutagen for human. Many snake venoms are strong antagonist of neurotransmitter as well as block different channels, which have essential role in nerve impulse transmission. Although some molecules of venom possess high receptor specificity, they are used as therapeutic drugs. Most studies on different toxicant structure and function may provide useful information for synthesis of smaller analogous with lower toxicity. Naturally toxicity of toxic elements is depending on doses that means amount of doses differ a poison from remedy. Although in many toxic elements mechanism of action, detoxification and elimination from body is still unknown. Therefore, interaction between scientist might have made it possible for discovering of mechanism, elimination, detoxification for use the toxic proteins as potential drug for multiple disorder or for drug design. So the area of research now a day is treated as a subject of interdisciplinary relevance.

References

- Bbosa S.G, Kitya D, Oddo J, Okang O J(2013),Aflatoxins metabolism, effects on epigenetic mechanisms and their role in carcinogenesis,Health,Vol:5,PP:14-34
- Becker S, Terlau H (2008),Toxins from cone snails: properties, applications and biotechnological production, Applied Microbiology Technology,Vol:79,PP:1-9
- Bushnell A D, Cramer P,Kornberg D R(2002),Structural basis of transcription: α - Aminitin-RNA polymerase II cocrystal at 2.8Å resolution,Proceedings of the National Academy of Sciences,Vol:99,No:3,PP:1218-1222
- Carbonetti H N (2010), Pertussis toxin and adenylate cyclase toxin: key virulence factors of Bordetella pertussis and cell biology tools,Future Microbiology,Vol:5,PP:455-469
- Cox M.M, Nelson L D (2011), Principles of biochemistry, 5th edition,PP:816-817
- Do H J, Choi K D (2007), Aflatoxins: Detection,Toxicity and Biosynthesis, Biotechnology and Bioprocess Engineering, Vol:12,PP:585-593
- Faber S(2012), Saxitoxin and the induction of paralytic shellfish poisoning, Journal of young Investigation,Vol:23,Issue:1
- Gonzalez J P, Coughtrie M, Tukey H R (2011),Goodman & Gilman's The Pharmacological Basis of Therapeutics,Eds: Laurence L. Brunton,12th edition,PP:123-144
- Jiang G,Wang C,Geng Di(2014),Advances on the Anti-Tumor Material Finding from Gecko and the Mechanism Research,Curr Opin Complement Alternative Medical,Vol:1,PP:45-48
- Kapoor V K(2010),Natural and their therapeutic potential,Indian journal of Experimental Biology,Vol:48, PP:228-237
- Karalliedde.L(1995),Animals toxins,British Journal of Anaesthesia,Vol:74,PP:319-327
- Kwok F H, Ivanyi C, Morris A, Shaw C(2010),Proteomic and Genomic studies on Lizard venoms in Last Decade,Proteomics Insights,Vol:3,PP:25-81
- Kwong D P,McDonald Q Neil,Sigler B P,Hendrickson A W(1995),Structure of β_2 – bungurotoxin: potassium channel binding by kunitz modules and targeted phospholipase action,Structure,Vol:3,No:10,PP:1109-1119
- Lewis J R, Garcia L M(2013),Therapeutic potential of venom peptides,Nature,Vol:2,PP:791-802
- Liu F,Wang G J, Wang Y S,Li Y,Wa P Y,Xi M S (2008),Antitumor effect and mechanism of Gecko on human eosophageal carcinoma cell lines in vitro and xenografted sarcoma 180 in Kunming mice,World Journal of Gastroenterology,Vol:14(25),PP:3990-3996
- Locht C(1999),Molecular aspects of Bordetella pertussis pathogenesis, International Microbiology,Vol:2,PP:137-144
- Ngwoke G K, Eze M P, Esimone O C(2015),Antimicrobial Activity of Crude Methanol Extract of Fecal Droppings of Common House lizard/Gecko(*Hemidactylus frenatus*),Journal of Applied Life Sciences International,Vol:2(2),PP:65-70
- Omar M D E H(2013),The biological and medical significance of poisonous animals, Journal of Biology and Earth sciences,Vol:3,Issue:1,PP:M25-M41
- Pandey K, Shukla P J, Trivedi P S(2012),Fundamental of toxicology,1st edition,PP:217-219
- Pathak S S, Gupta R K(2009),botulinum toxin:from a deadly toxin to a useful drug,Journal of Mahatma Gandhi institute of Medical Sciences,Vol:14,No:i,PP:10-17
- Patocka J, Gupta C R,Kuca K(2011),anatoxin-a(s):natural organophosphorus anticholinesterase agent, Military Medical Science Letters,Vol:80,PP:129-139
- Available online: <http://dx.doi.org/10.5772/51201>

An Approach to Overcome the Total Synthesis of Heliannuol-A

Nilay Kumar Maitra^a and Prabir K. Sen^{b*}

^aDepartment of Botany, ABN Seal College, Cooch Behar, 736101

^bDepartment of Chemistry, Barasat Govt. College, 10, K. N. C Road, Barasat, Kolkata- 700 124

*Email: wbespks@gmail.com

Abstract: This is a review that describes the total synthesis of the sesquiterpene Heliannuol-A utilising different methodologies to generate the ring system.

Key words: Heliannuols, sesquiterpene, RCM, Bergallini Condensation

Publication History: Received: 10th August, 2016; Accepted: 22th August, 2016

Heliannuol-A, represents a new class of compounds among the heliannuol family of allelopathic sesquiterpenes isolated from cultivar sunflower *Helianthus annuus* (Macias et al.1994). The other primary constituents are heliannuols B, C and D (Macias et. al.1993; Macias et. al.1999; Macias et. al.1999; Macias et. al. 2002; Morimoto et. al. 2006). These have been implicated in the powerful allelopathic activity displayed by sunflowers. Subsequently, other oxidized variants of some of these primary compounds have also been isolated from this flower (Macias et. al.1994).

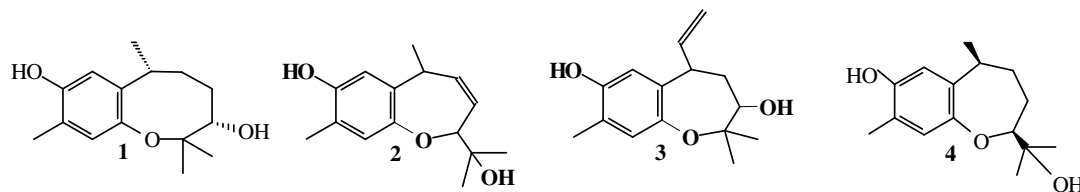


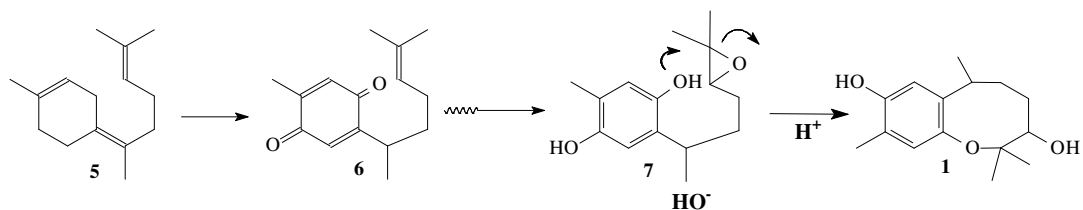
Fig. 1. Heliannuol A (1), Heliannuol B (2), Heliannuol C (3), Heliannuol D (4)

Allelopathy, involving plant–plant and plant–microorganism interactions, has been proposed as an alternative weed management policy [Einhellig et. al. 1998; Molisch 1937; Rice 1983; Rice1984; Worsham et. al 1989]. The growing concern on the natural ecological balance and the arguments against indiscriminate use of synthetic pesticides have provided an impetus for exploration of allelochemicals for effective weed control devoid of any hazardous side effects. In this context, the heliannuols, due to their novel structural features and associated bio-activity, have served as attractive targets for synthesis in many laboratories (Grimm et. al. 1994; Vyvyan et. al. 2000; Takabatake et. al 2000; Sato et. al. 2001; Kishuku et.al. 2003; Kishuku et. al. 2003; Doi et.al 2003; Macias et al. 2003; Kamei et al. 2003; Doi et.al. 2003; Kamei et. al. 2003; Kishuku et. al. 2004; Vyvyan et. al 2005; Morimoto et. al. 2006).

Isolation and structural elucidation Heliannuol A: Heliannuol A (Fig. 1) was isolated from the polar bioactive fraction of the aqueous extract of the fresh leaves of cultivated sun flowers and along with heliannuol B, C and D constitutes the major component. Heliannuol A was obtained as a crystalline solid and the structure was arrived at from extensive spectral studies.

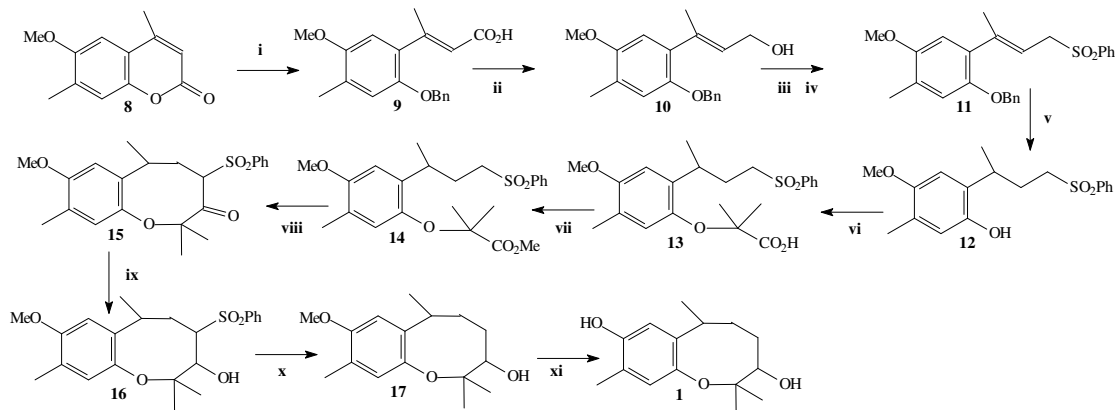
It has been proposed that biogenesis of this new class of sesquiterpenes may proceed through a bisabolene type precursor. This proposal received additional support from the isolation of other bisabolene type sesquiterpenes (5) particularly curcuquinone (6) from the same species, which present a similar oxidation pattern in the aromatic ring of the heliannuols with a quinone structure and a double bond in the side chain. The proposed process is represented in (Scheme 1). Oxidation of the double bond in (6) and aromatization leads to the putative intermediate (7). An acid catalysed cyclisation of this through a more preferred tertiary cation should lead to heliannuol A, whereas a base

catalysed phenolate ion induced cyclisation involving attack at the less hindered end of the epoxide leads to heliannuol **D** (**4**).



Scheme-1

Synthesis: The unique structural diversity combined with their agricultural importance, heliannuols have attracted the synthetic organic chemist as a potential target since their isolation. The pronounced allelopathic activity of Heliannouol-A attracts a number of synthetic chemists for its synthesis. The first total synthesis of Heliannouol-A was reported by Grimm *et. al* [1994]. Their methodology involved an intramolecular sulfone-ester cyclisation to develop the key eight membered ring. Controlled hydrolysis of coumarin (**8**) followed by *in situ* protection of the liberated phenol furnished the acid (**9**) which was reduced to the alcohol (**10**). Conversion to the sulfone (**11**) and subsequent hydrogenation led to the phenol (**12**). A Bargellini reaction involving interaction of the phenol with a mixture of chloroform and powdered sodium hydroxide in acetone resulted in the incorporation of *gem*-dimethyl side chain to afford the acid (**13**) which was converted to the methyl ester (**14**). Treatment of the sulfone ester (**14**) with lithium bis-(trimethyl silyl) amide resulted in a facile intramolecular cyclisation to lead to the keto-sulfone (**15**). Hydride reduction of the ketone proceeded with full stereocontrol to furnish the alcohol (**16**). Desulfonation of (**16**) followed by demethylation finally afforded heliannuol A (**1**). This synthesis exemplified another instance of the author's application of intramolecular sulfone cyclisation for generation of medium ring system. (**Scheme 2**).

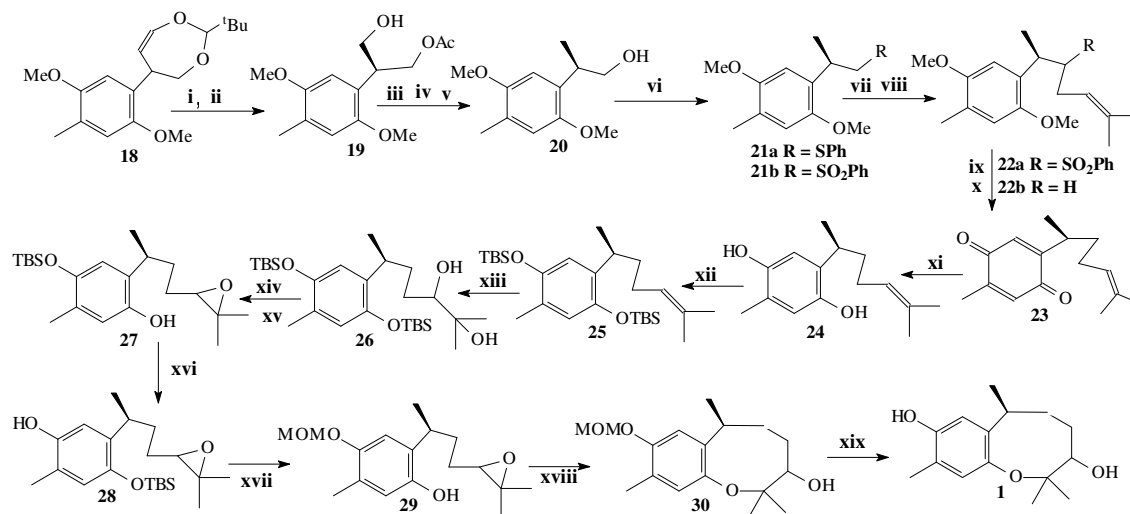


Scheme 2

Reagents and condition: i. NaOH, BnBr; ii. LiAlH₄; iii. PBr₃; iv. PhSO₂Na; v. H₂ / Pd-C; vi. CHCl₃, NaOH, CH₃COCH₃; vii. CH₂N₂; viii. LiDMS; ix. NaBH₄; x. Na-Hg; xi. EtSNa.

The first enantiocontrolled total synthesis of heliannuol A was reported by Shishido *et. al*. [2000]. Their synthesis hinged on the preparation of the configurationally defined enantiopure epoxide (**29**), which on an intramolecular cyclisation will lead to heliannuol -A via 8-*endo* mode of cyclisation. The prochiral diol (**18**) on a *Candida antartica* Lipase (CAL) catalysed transesterification using vinyl acetate as an acetyl donor furnished the monoacetate (**19**) in excellent yield and very high enantioselectivity. Deoxygenation of the hydroxy group followed by reductive cleavage of the acetate produced the alcohol (**20**). A Hata reaction on this alcohol and a subsequent oxidation of the resulting sulfide (**21a**) gave rise to the sulfone (**21b**). Alkylation of this with prenyl bromide and reductive

removal of the sulfone moiety lead to curcuhydroquinone dimethyl ether (**31**). For generation of curcuhydroquinone, this was subjected to a sequential oxidation with CAN and a reduction with dithionite and furnished the curcuhydroquinone (**23**) displaying a negative rotation, an *ent*- isomer of the natural compound. Based on this observation, the absolute configuration for the benzylic carbon center in (**23**) was assigned as *S*. The corresponding *di-tert*butyldimethyl silyl ether (**25**) on an asymmetric dihydroxylation yielded the diol (**26**), assigned the *S* configuration for the newly generated asymmetric center, which was duly transformed to a mixture of epoxides (**27**). Protection of the free phenolic hydroxy group as the methoxymethyl ether (**28**) followed by desilylation and base treatment afforded MOM protected heliannuol - A (**30**). These could be easily separated and a mild acidic hydrolysis furnished heliannuol - A, as *ent*-isomers of the natural compounds (**Scheme 3**).

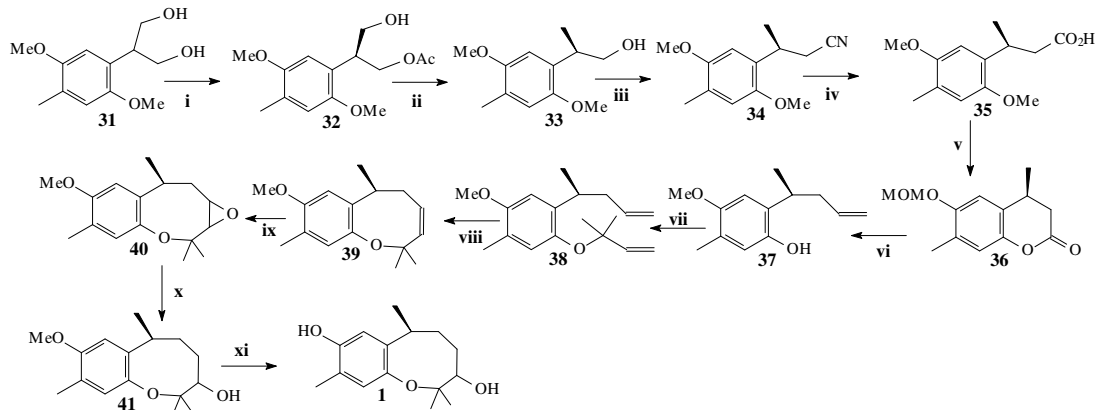


Scheme 3

Reagents and conditions: i. O_3 , MeOH, $NaBH_4$; ii. CAL, Et_2O ; iii. TsCl, Et_3N , 4-DMAP, CH_2Cl_2 ; iv. $NaBH_4$, DMSO; v. $LiAlH_4$, THF; vi. $PhSSPh$, nBuLi , Py; vii. *m*-CPBA, $KHCO_3$, CH_2Cl_2 ; viii. nBuLi , HMPA, THF, $Me_2C=CHCH_2Br$; ix. 5% Na-Hg, $NaHPO_4$, MeOH; x. $(NH_4)_2Ce(NO_3)_6$, MeCN, MeOH, H_2O ; xi. $Na_2S_2O_4$, THF, H_2O ; xii. $^tBu(Me)_2SiCl$, imidazole, 4-DMAP, CH_2Cl_2 ; xiii. AD-mix- α - $MeSO_2NH_2$, tBuOH , H_2O ; xiv. MsCl, Py, CH_2Cl_2 ; xv. K_2CO_3 , MeOH; xvi. MOMCl, iPr_2N Et, 4-DMAP, CH_2Cl_2 ; xvii. CsF, DMF; xviii. aq. 5%NaOH; xix. 6 M HCl, THF.

Another enantioselective synthesis of the unnatural enantiomer (+) heliannuol - A was also reported by Shishido *et.al* [2003]. The synthesis also established the absolute configurations at C-7 and C-10 as *R* and *S* respectively. Recently this group has also completed an enantioselective synthesis of natural isomer (–) heliannuol - A. This synthesis relied on the currently very popular ring closing metathesis to generate the medium ring. The prochiral di-ol (**31**) on porcine pancreatic lipase mediated *trans*-esterification afforded the *R*- monoacetate (**32**). Deoxygenation of the free hydroxy group through tosylation and subsequent reduction with sodium borohydride resulted in the degeneration of the C-7- *R*-methyl group (**33**). A one carbon homologation through mesylation, displacement with cyanide and its (**34**) hydrolysis resulted in the acid (**35**). De-methylation produced the lactone (**36**) where the phenolic moiety was protected as the methoxy methyl ether. DIBAL reduction and Wittig methylenation afforded the phenolic olefin (**37**). Pd-catalysed interaction of this phenol with *isobutyl*-2-methyl, 3-but-en 2-yl carbonate furnished the *gem*-dimethyl incorporated key diene (**38**), set up for the crucial ring closing metathesis reaction. In the event, this diene underwent facile intramolecular ring closure to afford the eight membered alkene (**39**). Epoxidation of the alkene proceeded in a stereocontrolled fashion from the bottom side to afford exclusively the α -epoxide (**40**).

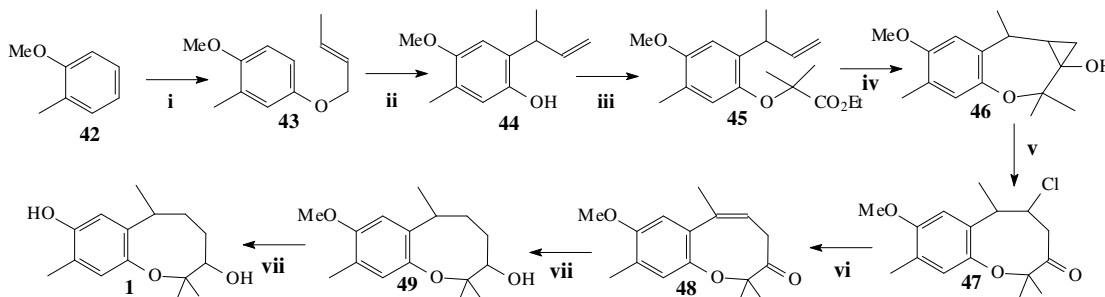
Hydride reduction of this epoxide occurred from the sterically less congested carbon resulting in the alcohol (**41**) which was deprotected to finally afford (–) heliannuol A (**1**) (Scheme 4).



Scheme 4

Reagents and Conditions: i. PPL, vinyl acetate, Et₂O, rt; ii. TsCl, Et₃N, 4-DMAP, CH₂Cl₂, rt; b. NaBH₄, DMSO, 60°C; c. K₂CO₃, aq. MeOH, rt; iii. MsCl, Et₃N, CH₂Cl₂, rt; b. KCN, 18-crown-6, DMSO, 60°C; iv. NaOH, aq. MeOH, reflux; b. PBr₃, CH₂Cl₂, rt; c. MOMCl, ⁱPr₂NEt, CH₂Cl₂, reflux; v. ⁱBu₂AlH, CH₂Cl₂, 78°C; b. Ph₃PMeI, ^tBuOK, toluene, rt; vii. ⁱBuOCOOCMe₂CH=CH₂, Pd(Ph₃P)₆, THF, rt; viii. Grubbs' catalyst, CH₂Cl₂, rt; ix. CF₃COCH₃, oxone, Na₂EDTA.2H₂O, NaHCO₃, CH₃CN, 0°C; x. LiAlH₄, THF, rt; xi. 6 N HCl, THF, rt.

Very recently Lecornue and Ollivier (2004) have disclosed a synthesis of heliannuol A (**1**), demonstrating the application of the methodology they have previously developed for synthesis of benzo fused cyclic ether employing an intramolecular Kulinkovich reaction [9]. A Claisen rearrangement of the crotyl ether (**42**) furnished the styrenol (**43**) which was converted to the ω-alkenoic ester (**45**) through alkylation with ethyl 2-bromo 2-methyl propionate. Intramolecular Kulinkovich reaction on this alkenoic ester furnished the cyclopropanol (**46**) which was oxidatively cleaved to provide the benzoxocanone (**47**). Dehydrohalogenation followed by saturation of the styrenoid bond and subsequent reduction of the ketone (**48**) afforded heliannuol A methyl ether (**49**). Alternatively, the chloroketone (**47**) could be converted to heliannuol A methyl ether by radical dehalogenation and subsequent reduction of the carbonyl group (Scheme 5).

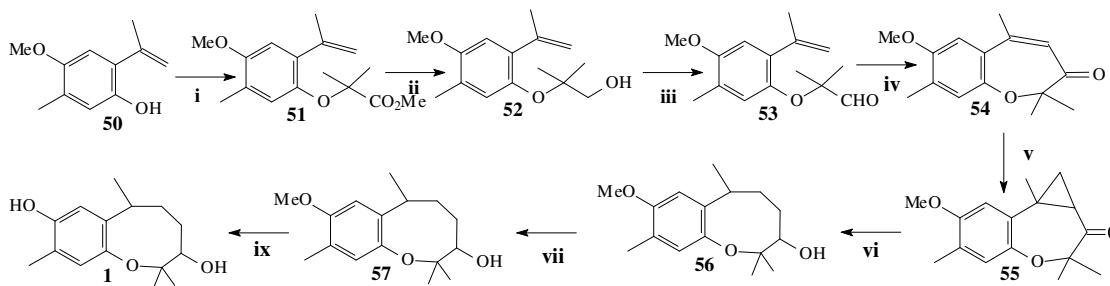


Scheme 5

Reagents and conditions: ia. TiCl₄, MeOCHCl₂, CH₂Cl₂; b. *m*-CPBA, CH₂Cl₂; c. NH₄OH, MeOH; d. MeCH=CHCH₂Cl, K₂CO₃, acetone; ii. PhNMe₂, 180°C, 72h; iii. NaH, DMPU, Me₂CBrCO₂Et, toluene; iv. C₆H₁₁MgCl (4 eqv.), Ti(OⁱPr)₄ (1eqv.), Et₂O-THF; v. FeCl₃, DMF, Py; vi. DBU, Et₂O; viia. Raney Ni, H₂O, THF, Na₂CO₃, H₂. B. NaBH₄, MeOH, viii. NaSEt, DMF.

Tuhina *et al.* [2002, 2007] disclosed a very short and rapid synthesis of heliannuol A (**1**) using regioselective cleavage of a cyclopropyl ketone (**55**) under hydrogenation condition was

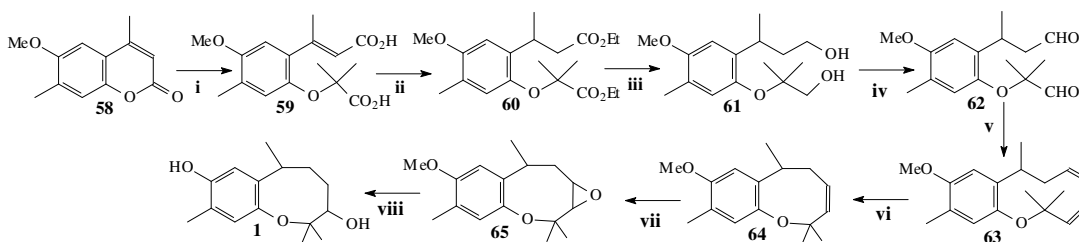
employed to generate the benzoxocane ring system of heliannuol A (**1**) as the key step. The synthesis started with appropriate styrenol (**50**) which on a Bargellini reaction involving condensation with acetone in presence of chloroform and sodium hydroxide followed by diazomethane treatment furnished the *gem*-dimethyl incorporated ester (**51**) which was reduced to the corresponding alcohol (**52**). Swern oxidation to the corresponding aldehyde (**53**) followed by the treatment with PCC resulted in an intramolecular aldo-ene reaction and re-oxidation to furnish the benzoxepinenone (**54**). Palladium catalyzed addition of diazomethane to (**54**) produced the cyclopropyl ketone (**55**). Catalytic hydrogenation of (**55**) proved to be completely regioselective delivering the benzoxocanone (**56**) which on a hydride reduction afforded heliannuol A methyl ether (**56**). Demethylation of this to heliannuol A (**1**) has been reported⁵ concluding a synthesis of this compound (**Scheme 6**).



Scheme 6

Reagents and conditions : ia. CHCl_3 , NaOH, acetone, reflux, 5h; b. CH_2N_2 , ether; ii. LAH, ether, reflux, 4h; iii. $(\text{COCl})_2$, DMSO, CH_2Cl_2 , Et_3N , -78°C , iv. PCC, CH_2Cl_2 , v. CH_2N_2 , $\text{Pd}(\text{OAc})_2$ (cat.), ether, 4h; vi. H_2 , Pd-C (10%), EtOH; vii. NaBH_4 , MeOH, rt, 4h. ix) NaSEt.

Another total synthesis of heliannuol-A (**1**) was reported by Biswas *et.al.* [2007]. The synthesis started with the condensation of coumarin (**58**) with chloroform and acetone in presence of powdered sodium hydroxide under standard Bargellini reaction condition furnished the diacid (**59**) which was converted to the diester (**60**) on catalytic hydrogenation in presence of dry ethanol. Then reduction of (**60**) with LiAlH_4 in THF under refluxing condition furnished the diol (**61**) in excellent yield which was oxidised to the dialdehyde (**62**) employing Swern condition. Wittig reaction employing a slight excess of more than two moles of methylenetriphenylphosphorane on this dialdehyde (**62**) furnished the diene (**63**) which under the well established ring closing metathesis conditions using Grubbs' catalyst (2nd generation) realised the benzoxepene (**64**). Treatment of this benzoxepene (**64**) with *m*-chlorobenzoic acid in NaHCO_3 in dry dichloromethane afforded the epoxides (**65**) as an inseparable mixture of diastereomers. The reduction of this epoxides (**65**) with LiAlH_4 under refluxing THF furnished *O*-methyl heliannuol A which on demethylation produced heliannuol-A (**1**) (**Scheme 7**).



Scheme-7

Reagents and conditions: (i) CHCl_3 , NaOH, acetone, reflux, 5h; (ii) H_2 , Pd-C, EtOH, (iv). LiAlH_4 , Et_2O , reflux, 2 h, 98%; (v). $(\text{COCl})_2$, DMSO, CH_2Cl_2 , Et_3N , -78°C , 5 h, (vi). PhPMeI , $n\text{-BuLi}$, THF,

0^oC, (vii). Grubbs' catalyst (2nd generation), CH₂Cl₂, 6 h, 94%; (viii). m-CPBA, CH₂Cl₂, NaHCO₃, 12 h, (ix) LAH, THF, reflux. (x) NaSEt.

From the above studies it is very clear that total synthesis of sesquiterpene heliannuol-A (1) have achieved a revolution through these years specially stereospecific synthesis as well as cost effectiveness.

Conclusion

In conclusion, this review article describes different approaches towards the racemic as well as stereoselective total synthesis of sesquiterpene heliannuol-A which exhibits allelochemicals activity and can serve as potential agrochemicals as herbicides.

References

1. Biswas B, Sen PK, Venkateswaran RV. (2007) Bargellini condensation of coumarins. Expeditious route to o-carboxyvinylphenoxyisobutyric acids and application to the synthesis of sesquiterpenes helianane, heliannuol A and heliannuol C. *Tetrahedron*, 63: 12026-12036
2. Doi F, Ogamino T, Sugai T and Nishiyama S (2003) Synthesis of bioactive sesquiterpene heliannuol E involving a ring-expansion reaction of spirodienones *Synlett* 411-413
3. Doi F, Ogamino T, Sugai T and Nishiyama S (2003) Enantioselective synthesis of heliannuol E; structural consideration of natural molecule *Tetrahedron Lett.* 44: 4877-4880
4. Einhellig F A and G R Leather (1998) Potentials for exploiting allelopathy to enhance crop production. *J. Chem. Ecol.* 14(10):1829-1844
5. Ghosh S, Tuhina K, Bhowmik D R, Venkateswaran R V (2007) Synthesis of heliannuols A and K, allelochemicals from cultivar sunflowers and the marine metabolite helianane, unusual sesquiterpenes containing a benzoxocane ring system *Tetrahedron* 63(3): 644-651.
6. Grimm E L, Levac S, and Trimble L. A. (1994) Total synthesis of (±)-Heliannuol A. *Tetrahedron Lett.* 35:6847-6850
7. Kamei T, Shindo M and Shishido K (2003) An Alternative Total Synthesis of (-)-Heliannuol E *Synlett.* 2395-2397
8. Kamei T, Shindo M and Shishido K. (2003) First Enantioselective Total Synthesis of (-)-Heliannuol C *Tetrahedron Lett.* 44: 8505-8507
9. Kishuku, H. Yoshimura, T., Kakehashi, T., Shindo, M. and Shishido, K. (2003) Enantiocontrolled Total Synthesis of (+)-Heliannuol D via Palladium Mediated Heterocyclization. *Heterocycles* 61: 125-131
10. Kishuku H, Shindo M and Shishido K. (2003) Enantioselective total synthesis of (-)-heliannuol A *Chem. Commun.*, 350-351
11. Macías F A, Varela R M, Torres A, Molinillo J M G. (1993) *Tetrahedron Lett.*, 34, 1999-2002
12. Macías F A, Molinillo J M G, Varela R M, Torres A, Fronczek F R (1994), Structural elucidation and chemistry of a novel family of bioactive sesquiterpene, Heliannuols. *J. Org. Chem.* 59: 8261-8266
13. Macías FA, Varela RM, Torres A, Molinillo JMG (1999) Heliannuol E, A novel bioactive sesquiterpene of the heliannane family. *Tetrahedron Lett*, 40: 4725-4728
14. Macías FA, Varela RM, Torres A, Molinillo JMG (1999) New bioactive plant heliannuols from cultivar sunflower leaves. *J Nat Prod*, 62: 1636-1639.
15. Macías, F. A., Torres, A., Varela, R. M., Galindo, J. L. G., Álvarez, J. A., and Molinillo, J. M. G. (2002). Bioactive terpenoids from sunflower leaves cv. Peredovick. *Phytochemistry* ,61: 687-692

16. Macías F A, Chinchilla D, Molinillo J M G, Marín D, Varela R M, and Torres A (2003) Synthesis of heliannane skeletons. Facile preparation of (\pm)- heliannuol D. *Tetrahedron* 59:1679-1683
17. Molisch H, (1937) *Der Einfluss einer Pflanze auf die andere Allelopathie*. Verlag G. Fisher, Jena. (English version by S.S. Narwal, 2001, Scientific Publishers, Jodhpur, India)
18. Morimoto S, Shindo M, Yoshida M, Shishido K, (2006) Syntheses of heliannuols G and H; structure revision of the natural products *Tetrahedron Lett.* 47:7353–7356.
19. Rice EL (1983) *Pest Control with Nature's Chemicals*; University of Okalahoma Press: Norman, OK, pp224
20. Rice EL (1984) *Allelopathy*. 2nd ed. New York: Academic 1-7
21. Sato K, Yoshimura T, Shindo, Y., and Shishido, K.(2001). Total synthesis Allelopathy: Chemistry and Mode of Action of Allelochemicals of (-)-heliannuol E. *J. Org. Chem.* 66: 309-314
22. Takabatake, K., Nishi, I., Shindo, M., and Shishido, K. (2000) .Enantioselective total synthesis of heliannuols D and A. *J. Chem. Soc.,Perkin Trans. 1*:1807-1808
23. Tuhina K, Bhowmik D R, and Venkateswaran, R. V. (2002). Formalsyntheses of heliannuols A and D, allelochemicals from *Helianthus annuus*. *Chem. Commun.*, 634-635
24. Vyvyan J R and Looper R. E (2000). Total synthesis of (\pm)-heliannuol D,an allelochemical from *Helianthus annuu*.*Tetrahedron Lett.* 41:1151-1154
25. Vyvyan J R Oaksmith J M, Parks B W and Peterson E M (2005) Total Synthesis of (\pm)-Heliannuol C and E via Aromatic Claisen Rearrangement *Tetrahedron Lett.* 46:2457–2460
26. Worsham A D (1989) In *Phytochemical Ecology: Allelochemical, Micotoxins and Insect Pheromones and Allomones*; G. H. Chou, G. R. Waller, Eds.; Monograph Series No. 9; Institute of Academica Sinica: Taipei, Taiwan, ROC.; pp 275–291

Ascorbic Acid Promoted Metal Free Borylation of Aromatic Diazonium Salts under Room Temperature

Debasish Kundu* and Totan Roy

Department of Chemistry, A. B. N. seal College, Cooch Behar-736101

*Email: debiitkgp123@gmail.com

Abstract

A sustainable and efficient protocol for the synthesis of aryl boronate esters has been reported by the reaction of aryl diazonium tetrafluoroborate and B_2Pin_2 under metal free conditions in room temperature where ascorbic acid plays a key role of single electron transfer agent. The reaction follows a radical mechanistic pathway where generation of aryl radical has achieved by SET process from ascorbic acid. A library of aryl boronate esters bearing different functionalities in the aromatic ring have been synthesized by this procedure in good to excellent yields. This procedure was further extended for the synthesis of bi-aryls and di-aryl chalcogenides through boronate esters.

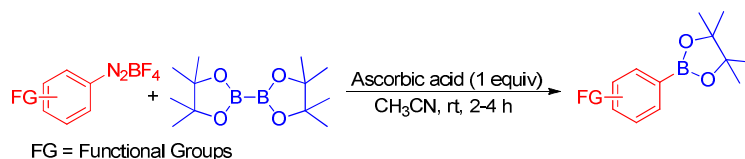
Key words: Diazonium salts, Boronate esters, Ascorbic acid, Green Chemistry

Publication History: Received: 10th August, 2016; Accepted: 22th August, 2016

Introduction

Boronic acids and boronate esters are found to have important applications in organic synthesis as they are widely used as synthons for performing C-C and C-heteroatom cross-coupling reactions for the synthesis of important organic molecules in the field of biological, material and pharmaceutical research.¹ Thus the synthesis of functionalized aryl boron compounds is an important requirement in organic chemistry in recent years. In general, Aryl Grignard and aryl lithium are commonly used reagents for the synthesis of aryl boronates by the reaction with trialkyl boronates.² However, low substrate scope and tedious reaction procedure are the main limitations of these processes. In last decade, several transition metal catalyzed protocols are being reported for the synthesis of aryl boronates. Palladium³ and Copper⁴ catalysts are successfully applied for the synthesis of these compounds in previous years. Most recently Ir⁵- complexes are found to catalyze the borylation through aromatic C-H bond activation. Recently Wang and co-workers (2010) have reported a cost-effective strategy for the synthesis of aryl boronates from aryl amines and B_2Pin_2 by using *tert*-butyl nitrite.⁶

Recently aryl diazonium salts are found as a potential synthon for the several important organic transformations through the generation of aryl radical by a SET process under visible light.⁷ In general organic dyes like eosin Y and metal complexes e.g. $[Ru(bpy)_3]Cl_2$ have been applied as SET catalysts in these reactions. Recently Yan and Co-workers have applied this concept for the synthesis of boronate esters from aryl diazonium fluoroborates. However, high cost of such organocatalysts and problem of their separation from reaction mixture limited their application. Thus an alternative SET reagent for the sustainable development of synthesis of boronate esters is necessary. Recently ascorbic acids are found to be effective SET to form aryl radicals from the diazonium salts.⁸ Here in we are reporting a sustainable protocol of synthesis of aryl boronate esters from aryl diazonium salts by using ascorbic acid as a SET reagent under room temperature (Scheme 1). This protocol excludes the use of any metal catalyst, ligand, base, expensive photocatalysts or heating conditions.



Scheme 1: Ascorbic acid mediated sustainable synthesis of aryl boronate esters from aryl diazonium fluoroborate

Result and Discussions

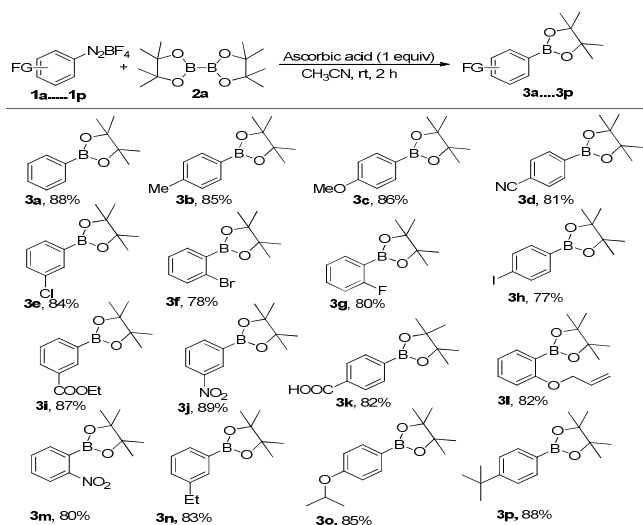
To optimize the reaction conditions a series of experiments have been performed by varying the reaction parameters such as solvent, time, amount of ascorbic acid etc for a representative reaction of 4-methoxy phenyl tetrafluoroborate and B₂Pin₂. The results are summarized in Table 1.

Table 1. Standardization of reaction conditions

Entry	Catalyst	Solvent	Time(h)	Yield(%) ^a
1	Ascorbic acid	DCM	10	trace
2	Ascorbic acid	DMF	10	20
3	Ascorbic acid	DMSO	10	35
4	Ascorbic acid	NMP	10	22
5	Ascorbic acid	CH ₃ CN	4	84
6	—	CH ₃ CN	4	0
7	Ascorbic acid	toluene	10	0

^aReaction conditions: aryl diazonium tetrafluoroborate (0.5 mmol), B₂Pin₂ (0.5 mmol), ascorbic acid (.5 mmol), RT

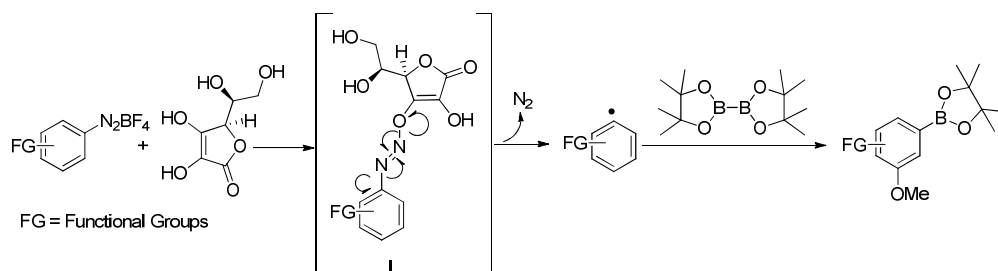
The reaction yielded trace amount of product in DCM. However polar solvents like DMF, DMSO and NMP yielded 20-35% of yield of desired product (table 1, entries 2, 3 and 4). However, when the reaction was performed in CH₃CN, the reaction resulted 84% of yield in just 4 hours under room temperature (table 1, entry 5). No trace of product was observed when the reaction was performed without ascorbic acid (table 1, entry 6). The reaction did not proceed at all in nonpolar solvents like toluene (table 1, entry 7).



^aReaction Conditions: aryl diazonium fluoroborate (1.0 mmol), B₂Pin₂ (1.0 mmol), Ascorbic Acid (1.0 mmol), CH₃CN (3 mL), rt, 2 h

Scheme 2: Synthesis of aryl boronate esters from aryl diazonium fluoroborates^a

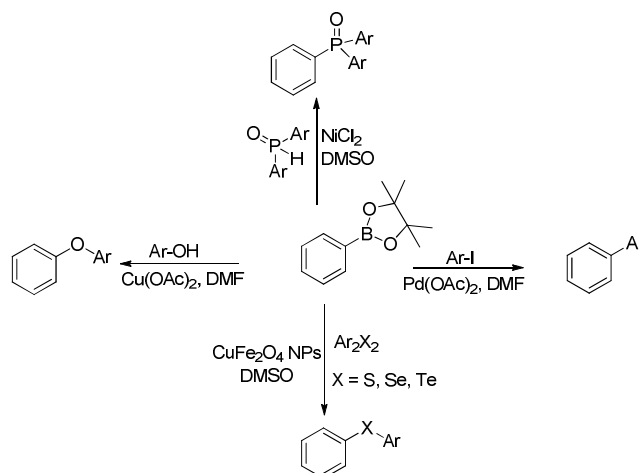
Thus in a typical reaction procedure, 1 equivalent of ascorbic acid was added in a stirred solution of aryl diazonium fluoroborate, B_2Pin_2 and CH_3CN and the reaction was stirred for 2-4 hrs (TLC). The reaction proceeds efficiently with *ortho*-, *para*- and *meta*- substituted aryl diazonium fluoroborates (Scheme 2). Different kinds of electron donating substituent e.g. $-OMe$, $-Me$, $-O$ -allyl, *t*-butyl etc and withdrawing groups e.g. $-NO_2$, $-CN$, $-COOEt$, $-COMe$, $-COOH$ in the aryl ring are compatible with the reaction conditions. The halogen substituents (Cl, Br, I, F) on aromatic ring of diazonium salts are also compatible under the reaction conditions. Thus a library of aryl boronate esters bearing diverse functionalities in the aromatic ring is being prepared by this protocol in absence of any metal catalyst under room temperature.



Scheme 3: Possible mechanistic pathway

In a typical mechanistic pathway, diazonium electrophilic nitrogen was first attacked by the hydroxyl moiety of ascorbic acid leading to the formation of intermediate I which upon dissociation from aryl radical. The aryl radical then readily attacked B_2Pin_2 leading to the formation of product (Scheme 3).

The prepared boronate ester was then successfully applied for the formation of different aryl carbon-heteroatom bonds by transition metal catalysed cross coupling reactions (scheme 4) by previously reported protocols.



Scheme 4: Application of Boronate Esters for the synthesis of different important organic moieties by C-heteroatom bond formations.

Conclusion

Thus we have developed a green protocol for the synthesis of boronate esters starting from aryl diazonium fluoroborate by using ascorbic acid as a radical initiator under room temperature. The methodology is quite successful for the preparation of diverse kind of aryl boronate esters under short reaction time. The boronate ester was further applied for the synthesis of different kinds of important organic molecules via carbon-heteroatom bond formations.

Experimental procedure

Representative procedure for the synthesis of 2-(4-methoxyphenyl)-4,4,5,5-tetramethyl-1,3,2-dioxaborolane: A mixture of B_2Pin_2 (1 mmol, 254 mg), 4-methoxy aryl diazonium fluoroborate (1 mmol, 222 mg) and ascorbic acid (176 mg, 1mmol) in 3 mL CH_3CN was allowed to stir for 2 h (TLC) in a round bottom flask under room temperature. This mixture after being diluted with ethyl acetate was filtered through celite and the filtrate was extracted by ethyl acetate. The extract was washed with brine and dried over anhydrous Na_2SO_4 . The extract was evaporated to leave the crude product which was purified by column chromatography over silica gel with hexane ethyl acetate (98: 2) to furnish the final product 2-(4-methoxyphenyl)-4,4,5,5-tetramethyl-1,3,2-dioxaborolane as a light viscous liquid (3C, 200 mg, 86%); IR (neat) : 2978, 2933, 2526, 1950 cm^{-1} ; 1H NMR (500 MHz, $CDCl_3$) δ 1.33 (s, 12 H), 3.81 (s, 3H), 6.88 (d, $J = 8.0$ Hz, 2H), 7.74 (d, $J = 8.0$ Hz, 2H); ^{13}C NMR (125 MHz, $CDCl_3$) δ 24.9 (4C), 55.2, 83.6 (2C), 113.4 (2C), 136.6 (2C), 162.3. This procedure was followed for all the reactions in table 2. The compounds are known and their spectroscopic data is in good agreement with those previously reported.

Acknowledgement

We gratefully acknowledge financial support from Indian association for the Cultivation of Science and Prof B. C. Ranu for providing the NMR facilities and helpful discussions during the project.

References

1. Li D, Chen Y, Liu Z (2015), Boronate affinity materials for separation and molecular recognition: structure properties and applications, *Chem Soc Rev* 44: 8097-8123.
2. Brown HC, Snebnik M, Cole TE (1986), *Organoboranes*. 48. Improved procedures for the preparation of boronic and boronic esters, *Organometallics* 5: 2300-2303.
3. Ishiyama T, Murata M, Miyaura N (1995), Palladium (0)-catalyzed cross coupling reaction of alkoxydiboron with haloarenes: A direct procedure for aryl boronic esters, *J Org Chem*. 60: 7508-7510.
4. Zhu W, Ma D (2006), Formation of aryl boronates by a CuI catalyzed coupling reaction of pinacolborane with aryl iodides at room temperature, *Org Lett* 8: 261-263
5. Murphy JM, Tzschucke CC, Hartwig JF (2007), One-pot synthesis of aryl boronic acids and aryl trifluoroborates by Ir-catalyzed borylation of arenes, *Org Lett* 9: 757-760.
6. Mo F, Jiang Y, Qiu D, Zhang Y, Wang J (2010), Direct conversion of aryl amines to pinacol boronates: A metal free borylation process, *Angew Chem Int Ed* 49: 1846-1849.
7. Ahammed S, Nandi S, Kundu D, Ranu BC (2016), One-pot Suzuki Coupling of aromatic amines via visible Light photocatalyzed metal free borylation using t-BuONO at room temperature, *Tetrahedron Lett* 57: 1551-1554.
8. Majhi B, Kundu D, Ranu BC (2015), Ascorbic acid promoted oxidative arylation of vinyl arenes to 2-aryl acetophenones without irradiation at room temperature under aerobic conditions, *J Org Chem* 80: 7739-7745.

Emergent Universe Models with Bulk Viscosity

Partha Sarathi Debnath

Department of Physics, A B N Seal College, Dist.: Coochbehar, PIN: 736 101, India.

Abstract

In this work we have investigate the emergent scenario of the universe in the presence of bulk viscosity. The model of emergent universe in the presence of bulk viscosity is possible for both perfect and exotic cosmological fluid. We study cosmological solutions in Einstein theories of gravity in the presence of an exotic equation of state of cosmological fluid which has bulk viscosity type dissipative term. The corresponding cosmological dynamics with the bulk viscosity is obtained for a flat, closed and open homogeneous isotropic Friedmann-Robertson walker spacetime.

Key words: Emergent Universe; Viscosity; Exotic Fluid

Publication History: Received: 10th August, 2016; Accepted: 24th August, 2016

Introduction

In the standard cosmological model, the existence of a big bang singularity in the early universe is still a serious problem. To overcome this problem, in the context of general relativity, Ellis et al. proposed a scenario called an emergent universe [1]. The possibility of the Emergent universe scenario has been studied in the number of literature [2]. In Emergent model, universe ever exists and large enough i.e., classical description of the space time is sufficient. In this model the universe at past in an Einstein static state and then evolves to a subsequent inflationary phase. Once inflation has started most of the volume of the universe will remain in an inflating state. This may be possible mechanism responsible for the present cosmic acceleration [3]. So the universe evolves from an Einstein static state, rather than from a big bang singularity. The emergent universe has a finite initial size, with a finite amount of inflation occurring over an infinite time in the past and with inflation then coming to an end via reheating in the standard way. The leading features of emergent universe is summarized in Ref [4] as follows :

1. The universe is almost static at finite past ($t \rightarrow -\infty$) and isotropic and homogeneous at large scales.
2. It is ever existing and there is no time like singularity;
3. The universe is always large enough so that the classical description of space time is adequate.
4. The universe may contain exotic matter so that the energy conditions may be violated.
5. The universe is accelerating as suggested by Supernova observations.

Ellis et al. [1] provided a realization of a singularity-free inflationary universe by considering a minimally coupled scalar field with a self interacting physically based potential. Mukherjee et al. [4] presented an emergent universe scenario for different combinations of radiation and matter. Mukherji and Chakraborty [5] developed an Emergent universe scenario in Einstein Gauss-Bonnet (EGB) theory for all values of the spatial curvature. Paul et al. [6] predicted the range of the permissible values for the parameters associated with the constraints on exotic matter for an emergent universe. Mukherji and Chakraborty [7] studied Emergent universe scenario in Horava gravity. Rudra [8] studied Emergent universe scenario in loop quantum gravity and Kaluza Klein cosmology.

Recent observational data from Ia supernovae [9] Cosmic microwave background (CMB) radiation, X-rays from the cluster of galaxies [10] and Weak gravitational lensing [11] strongly suggest that the most part of the present universe filled with dark matter (~26.8 %) and dark energy (~68.3 %) and the rest (~ 4.9 %) are usual baryonic matter. Dark matter which is supposed to consist of weakly interacting massive particles (WIMPS) with zero effective pressure particle axions(a particle present in the multiplet of grand unified theories) and neutrinos (light particles present in broken supersymmetric models), but none of these particles could not detected until now. Dark energy, a mysterious entity which is responsible for negative pressure. The cosmological constant (Λ) (which arises as the result of the combination of quantum field theory and general relativity) and its generalizations are the simplest way to describe dark energy. In standard cosmological model one considers perfect fluid (linear equation of state) as a standard cosmological fluid. Here we examine a class of models called barotropic fluids, in which the dark energy pressure (p) is given as explicit function of the density (ρ) (i.e., $p = f(\rho)$). One of the key properties of barotropic fluids is that the sound speed $c_s^2 = \frac{dp/d\rho}{d\rho/d\rho}$, does not have to equal the speed of light. For the stability and causality there is a limit $0 \leq c_s^2 \leq 1$ on the sound speed [12].

In the early universe a number of processes might have occurred leading to a deviation from perfect fluid assumption e.g. viscosity which is to be taken into account seriously. Although real fluids behave irreversibly, however, some processes in cosmology and astrophysics cannot be understood except dissipative processes. Some of the dissipative processes in the early universe may be responsible for viscosity. Viscosity may be arises due to the decoupling of neutrinos from the radiation era, the decoupling of matter from radiation during the recombination era, creation of superstrings in the quantum era, particle collisions involving gravitons, cosmological quantum particle creation processes and formation of galaxies [13]. It has been predicted from observations that a non negligible dissipative bulk stress on cosmological scales at the late universe phase might be important.

It is the purpose of this paper is to build an Emergent universe model in the presence of the bulk viscosity. The plan of this paper is as follows: in sec. 1, we give the gravitational action and set up the relevant field equations. In sec. 2, cosmological solutions are presented. Finally, in sec. 3, we summarize the results obtained.

1. Gravitational Action and Relevant Field Equation:

We consider the homogeneous and isotropic space-time given Friedmann Robertson-Walker (FRW) metric

$$ds^2 = -dt^2 + a^2(t) \left[\frac{dr^2}{1-kr^2} + r^2(d\theta^2 + \sin^2 \theta d\phi^2) \right] \quad (1)$$

where $a(t)$ is the scale factor of the universe. The constant k defined curvature of space time, $k= 0, 1, -1$ represents flat, closed and open spaces respectively. The Einstein equation in FRW metric (i.e., for a homogeneous and isotropic universe) are given by

$$H^2 = \frac{\rho}{3} + \frac{k}{a^2}, \quad 2\dot{H} + 3H^2 = -p + \Pi, \quad (2)$$

$$\dot{\rho} + 3(\rho + p)H = -3\Pi H. \quad (3)$$

where $H = \frac{\dot{a}}{a}$ is the Hubble parameter and an over dot represents derivative with respect to cosmic time (t). Where we consider $8\pi G = 1, c = 1$. Where p is the isotropic pressure of the universe, ρ is the energy density of the universe and $\Pi (\leq 0)$ is the bulk viscous pressure. In this article we consider Exotic kind equation of state (EoS) of the cosmological fluid, i.e.,

$$p = A\rho + B\rho^\alpha. \quad (4)$$

Where $A (\geq 0)$, B and α are constants. The eq. (4) becomes to linear EoS for ($B = 0$ or $\alpha = 1$). The scale factor of Emergent universe yields

$$a(t) = a_i(a_1 + e^{\alpha_2 t})^\omega \quad (5)$$

Where $\alpha_i, \alpha_1, \alpha_2, \omega$ are positive constants to describe Emergent universe to be determined. Eq. (5) shows Hubble parameter and its derivate for Emergent universe of the following form

$$H = \frac{\alpha_2 \omega e^{\alpha_2 t}}{\alpha_1 + e^{\alpha_2 t}}, \quad \dot{H} = \frac{\alpha_1 \alpha_2^2 \omega e^{\alpha_2 t}}{(\alpha_1 + e^{\alpha_2 t})^2}, \quad \ddot{H} = \frac{\alpha_1 \alpha_2^3 \omega e^{\alpha_2 t} (\alpha_1 - e^{\alpha_2 t})}{(\alpha_1 + e^{\alpha_2 t})^3} \quad (6)$$

Here H and \dot{H} are both positive, but \ddot{H} changes sign at $t = \frac{1}{\alpha_2} \ln(\alpha_1)$. Using eq. (5) and (6) to described an Emergent Universe following relation between Hubble parameter and its derivative are obtained

$$\dot{H} = \alpha_2 H - \frac{1}{\omega} H^2, \quad (7)$$

So the scale factor of an Emergent universe should obey eq. (7). In the following section we shall study the possibility of an Emergent universe model in the presence of bulk viscosity.

2. Cosmological Solutions:

The set of equations (2)-(5) are employed to obtain cosmological solutions. The systems of equations are not closed as the numbers of equations are less than the number of unknowns. The bulk viscous stress satisfies following transport equation [14]

$$\Pi = -3\zeta H, \quad (8)$$

where $\zeta (\geq 0)$ is the co-efficient of bulk viscosity. The positive entropy production due to bulk viscosity is confirmed by positive sign of the co-efficient of bulk viscosity (ζ). It is known that the coefficient of bulk viscosity in general function of time (or of the energy density). We, therefore, consider following relation [15]

$$\zeta = \beta \rho^s, \quad (9)$$

where $\beta (\geq 0)$ and $s (\geq 0)$ are constant. The constant β is known as bulk viscous constant. It is worth to note that $\beta = 0$ indicate that there is no dissipative effect in the evolution of the universe. Using eq. (2), (3), (4), (8) and (9) we get

$$2\dot{H} + \frac{3k}{a^2} + (1+A)\left(3H^2 - \frac{3k}{a^2}\right) + B\left(3H^2 - \frac{3k}{a^2}\right)^\alpha = 3\beta H\left(3H^2 - \frac{3k}{a^2}\right)^s \quad (10)$$

The evolution of the universe can be obtained by using eq (10). In the absence of dissipative effect ($\beta = 0$) for flat space time ($k = 0$) eq. (10) shows an Emergent universe model corresponding to an exotic EoS, $p = A\rho - B\rho^{\frac{2}{\alpha}}$. This special case is studied by Mukherjee *et. al.* [4]. To construct an Emergent universe scenario in the presence of dissipative effect we consider following special case as eq. (10) in general is highly nonlinear to obtain an analytic solution.

We note the following:

Case (I) for $\beta \neq 0, k = 0$: In this case eq. (10) reduces to

$$2\dot{H} + (1+A)3H^2 + B(3H^2)^\alpha = 3\beta H(3H^2)^s \quad (11)$$

Eq (11) can be used to build Emergent Universe model in the following special cases.

• If $B = 0, s = 0$: In this special case eq. (11) reduces to the form of eq. (7) i.e., scale factor of the universe exhibits an Emergent universe. So, an Emergent universe model may be build in the presence of bulk viscosity with perfect fluid for flat space time. In this special case $\alpha_2 = \frac{3\beta}{2}, \omega = \frac{2}{3(1+A)}$. So rate of expansion of the Emergent universe is higher for smaller value of EoS parameter (*i.e.*, A) and for the higher value of bulk viscous constant (*i.e.*, β).

• If $B \neq 0, s = 0, \alpha = \frac{1}{2}$: In this special case eq. (11) reduces to the form of eq. (7) i.e., scale factor of the universe exhibits an Emergent universe. So, an Emergent universe model may be build in the presence of bulk viscosity with exotic type fluid for flat space time. In this special case $\alpha_2 = \frac{3\beta - B\sqrt{3}}{2}, \omega = \frac{2}{3(1+A)}$. So rate of expansion of the Emergent universe is higher for smaller value of EoS parameter (*i.e.*, A) and for the higher value of difference between bulk viscous constant (*i.e.*, β) and EoS parameter B . In the special case to obtain an Emergent Universe model bulk viscous constant shows a lower boundary value *i.e.*, $\beta > \frac{B\sqrt{3}}{3}$.

• If $B \neq 0, s = \frac{1}{2}, \alpha = \frac{1}{2}$: In this special case eq. (11) reduces to the form of eq. (7) i.e., scale factor of the universe exhibits an Emergent universe. So, an Emergent universe model may be build in the presence of bulk viscosity with exotic type fluid for flat space time. In this special case $\alpha_2 = \frac{-2\sqrt{3}}{2}, \omega = \frac{2}{3(1+A) - 3\sqrt{3}\beta}$. So rate of expansion of the Emergent universe is higher for smaller value of EoS parameter (*i.e.*, B) and for the higher value of difference between the EoS parameter A bulk viscous constant (*i.e.*, β). In the special case to obtain an Emergent Universe model bulk viscous constant shows a upper boundary value *i.e.*, $\beta < \frac{(1+A)\sqrt{3}}{3}$ and EoS parameter shows a upper boundary value *i.e.*, $B < 0$.

• If $B \neq 0, s = 0, \alpha = 1$: In this special case eq. (11) reduces to the form of eq. (7) i.e., scale factor of the universe exhibits an Emergent universe. So, an Emergent universe model may be build in the presence of bulk viscosity with exotic type fluid for flat space time. In this special case $\alpha_2 = \frac{3\beta}{2}, \omega = \frac{3(1+A+B)}{2}$. So rate of expansion of the Emergent universe is higher for higher value of bulk viscous constant (*i.e.*, β) and for the higher value of difference between the EoS parameters A and B .

Case (II) for $\beta \neq 0, k \neq 0, B = 0$: In this case eq. (10) reduces to

$$2\dot{H} + \frac{3k}{a^2} + (1+A)\left(3H^2 - \frac{3k}{a^2}\right) = 3\beta H \left(3H^2 - \frac{3k}{a^2}\right)^{\alpha} \quad (12)$$

• If $s = 0, A = 0$: In this special case eq. (12) reduces to the form of eq. (7) i.e., scale factor of the universe exhibits an Emergent universe. So, an Emergent universe model may be build in the presence of bulk viscosity with matter dominated universe (MDU) for closed or open space time. In this special case $\alpha_2 = \frac{3\beta}{2}, \omega = \frac{2}{3}$. So rate of expansion of the Emergent universe is higher for higher value of bulk viscous constant (*i.e.*, β).

Case (III) for $\beta \neq 0, k = 1, B \neq 0$: In this case eq. (10) reduces to

$$2\dot{H} + \frac{3}{a^2} + (1+A)\left(3H^2 - \frac{3}{a^2}\right) + B\left(3H^2 - \frac{3}{a^2}\right)^{\alpha} = 3\beta H \left(3H^2 - \frac{3}{a^2}\right)^{\alpha} \quad (13)$$

• If $s = 0, \alpha = 1$: In this special case eq. (13) reduces to the form of eq. (7) i.e., scale factor of the universe exhibits an Emergent universe with the condition, $A + B = 0$. So, an Emergent universe model may be build in the presence of bulk viscosity with exotic type fluid for closed space time. In this special case $\alpha_2 = \frac{3\beta}{2}, \omega = \frac{2}{3}$. So rate of expansion of the Emergent universe is higher for higher value of bulk viscous constant (i. e., β).

3. Discussion:

In this paper we study the possibility of Emergent universe model in the presence of bulk viscosity for homogeneous isotropic space time. We note the following special case to consider Emergent universe: (i) Considering flat ($k = 0$) FRW space time with linear EoS ($B = 0$ or $\alpha = 1$) of cosmic fluid an Emergent universe model is possible in the presence of bulk viscous pressure which is proportional to Hubble parameter (i. e., $\Pi \propto H$). In this special case rate of expansion of the Emergent universe is higher for smaller value of EoS parameter (i. e., A) and for the higher value of bulk viscous constant (i. e., β). (ii) Considering flat ($k = 0$) FRW space time with nonlinear EoS ($B \neq 0$ or $\alpha \neq 1$) of cosmic fluid an Emergent universe model is possible in the presence of bulk viscous pressure which is proportional to Hubble parameter (i. e., $\Pi \propto H$). In this case the EoS of the cosmic fluid becomes $p = A\rho + B\rho^{\frac{2}{3}}$ and lower boundary of the bulk viscous constant becomes $\beta > \frac{B\sqrt{3}}{3}$. (iii) Considering flat ($k = 0$) FRW space time with nonlinear EoS ($B \neq 0$ or $\alpha \neq 1$) of cosmic fluid an Emergent universe model is possible in the presence of bulk viscous pressure which is proportional to Hubble parameter (i. e., $\Pi \propto H^2$). In this case the EoS of the cosmic fluid becomes $p = A\rho + B\rho^{\frac{2}{3}}$ and upper boundary of the bulk viscous constant becomes $\beta < \frac{(1+A)\sqrt{3}}{3}$ and $B < 0$. (iv) In MDU ($A = 0$) one may build an Emergent universe model for flat, open or closed FRW space time in the presence of bulk viscous pressure which is proportional to Hubble parameter (i. e., $\Pi \propto H$). (v) For closed ($k = 1$) FRW space time with linear EoS ($B = 0$ or $\alpha = 1$) of cosmic fluid an Emergent universe model is possible in the presence of bulk viscous pressure which is proportional to Hubble parameter (i. e., $\Pi \propto H$).

Reference

- [1] G. F. R. Ellis, R. Maartens, Class. Quant. Grav. 21, 223 (2004); G. F. R. Ellis, J. Murugan, C. G. Tsaga, Class. Quant. Grav. 21, 233 (2004).
- [2] S. Mukherjee, B. C. Paul, S. D. Maharaj and A. Beesham, gr-qc/0506103; U. Debnath, Class. Quant. Grav. 25 205019 (2008); A. Banerjee, T. Bandyopadhyay and S. Chakraborty, Gen. Rel. Grav. 40, 1603 (2008).
- [3] S. Perlmutter, et. al., ApJ 517, 565 (1999) [astro-ph/9812133]; D. N. Spergel, et. al., Astron. J. Suppl. 148, 175 (2003) [astro-ph/0302209].
- [4] S. Mukherjee, B. C. Paul, S. D. Maharaj and A. Beesham, Class. Quant. Grav. 23, 6927 (2006); U. Debnath, Class. Quant. Grav. 25, 205019 (2008).
- [5] S. Mukerji and S. Chakraborty, Int. J. Theor. Phys 49, 2446 (2010).
- [6] B. C. Paul, et. al., Mon. Not. R. Astron. Soc. 407, 415419 (2010).
- [7] S. Mukerji, S. Chakraborty, Astrophys. Space Sc. DOI: 10.1007/s10509-010-0456-1 (2010).
- [8] P. Rudra, arXiv:gr-qc/1211204v1.

- [9] A. G. Riess et al., *Astron. J.* 116, 1009 (1998); P. Astier et al., *Astron. Astrophys.* 447, 31 (2006).
- [10] D. N. Spergel et al., *ApJS.* J. 170, 377 (2007) [arXiv:astro-ph/0603449v2]; M. Tegmark, et al., *Phys. Rev. D.* 69, 103501 (2004).
- [11] A. Lewis and A. Challinor, *Phys. Rep.* 429, 1(2006).
- [12] W. A. Hiskock and L. Lindblom, *Phys. Rev. D* 31, 725 (1985); W. A. Hiscock, *Phys. Rev. D* 33, 1527 (1986).
- [13] C. W. Misner, *Astrophys. J.* 151, 431 (1968); J. D. Barrow and R. A. Matzner, *Mon. Not. R. Astr. Soc.* 181, 719 (1977); B. L. Hu, in *Advances in Astrophysics*, eds. L. Z. Fang and R. Ruffini (World Scientific, Singapore, 1983).
- [14] C. Eckart, *Phys. Rev. D* 58, 919 (1940).
- [15] V. A. Belinskii and I. M. Khalatnikov, *Sov. Phys. JETP* 42, 205 (1975); W. Zimdahl and J. C. Fabris, *Class. Quantum Grav.* 22, 4311 (2005).

Insects in Human Welfares and Benedictions: As Food and Medicine Suppliers

Hemen Biswas

Post Graduate Department of Zoology, Acharya Brojendra Nath Seal College, Cooch Behar, PIN-736101, West Bengal, India

Email: hemenbiswas8@gmail.com

Abstract

Human society and civilization are remarkably interdependent on various flora and fauna. Entomofauna are one of them. Different insects are having their contributions to meet up society's needs like food and medicines. Insects can serve as constant food sources providing nutrients namely proteins, carbohydrates and fats. They can also be used in traditional, alternative and modern medicines.

Key words: Insects; Entomophagy; Food, Medicine

Publication History: Received: 10th August, 2016; Accepted: 22th August, 2016

Introduction

Insects are everywhere. They are, by far, the most common animals on our planet. Ethnoentomology is the study of the relationship between insects and people. The name is derived from "ethno" - study of people and "entomology" - study of insects. The focus of ethnoentomology is on how insects have been or are being used in human societies around the world. This includes insects used for food medicine, dye, aesthetics, and rituals. In entomology, the term is sometimes used more broadly to encompass arthropods. Entomophagy refers to the eating of insects. Many insects are considered a culinary delicacy in many parts of the world, but the practice is uncommon and even taboo in other societies. Insects used in food include caterpillars, silkworms, Maguay worms, Witchetty grubs and other beetle and moth larvae; crickets, grasshoppers and locusts; and arachnids, such as spiders and scorpions. They can be eaten on their own or mixed with other ingredients, such is the case with casu marzu. Many insects are also used as medicine. The medicinal uses of insects were often defined by the Doctrine of Signatures, which stated that an organism bearing parts that resemble human body parts, animals, or other objects, was thought to have useful relevance to those parts, animals or objects. This doctrine is common throughout traditional and alternative medicine, but is most prominent where medical traditions are broadly accepted, as in Traditional Chinese Medicine and Ayurveda, and less by community and family based medicine, as is more common in parts of Africa, America and India. Various insects are useful for another type of medical therapy such as apitherapy, maggot therapy, etc. On the other hand some insects produce some by product such as silk, bee wax, honey, lac, etc.

Insect is a resource of food

In some cultures, insects, especially deep-fried cicadas, are considered to be delicacies, while in other places they form part of the normal diet. Insects have high protein content for their mass and some authors suggest their potential as a major source of protein in human nutrition. In most first-world countries, food safety laws in many countries do not prohibit insect parts in food, but rather limit their quantity. According to cultural materialist anthropologist Marvin Harris, the eating of insects is taboo in cultures that have other protein sources such as fish or livestock. Due to the abundance of insects and a worldwide concern of food shortages, the Food and Agriculture Organisation of the United Nations considers that the world may have to, in the future, regard the prospects of eating insects as a food staple. Insects are noted for their nutrients, having a high content of protein, minerals and fats and are eaten by one-third of the global population (Maierbrugger 2013).

Entomophagy is more popular in southern parts of Africa, Mexico, Australia, Asia, Netherlands and South America. Nowadays, many dishes are made with insect such as dry roasted crickets, cricket flour, sautéed crickets, chocolate covered crickets, mealworm French fries, cicada licious, bug burger mix, etc.

Crickets as food

There are 1,462 recorded species of edible insects. Crickets are the most popular. Here's why: 100 grams of cricket contains: 121 calories, 12.9 grams of protein, 5.5 g. of fat, 5.1 g. of carbohydrates, 75.8 mg. calcium, 185.3 mg. of phosphorous, 9.5 mg. of iron, 0.36 mg. of thiamin, 1.09 mg. of riboflavin, and 3.10 mg. of niacin. Compare that with ground beef, which, although it contains more protein, about 23.5 g. to be exact, it has 288.2 calories and an enormous amount of fat, 21.2 grams worth.

Why are crickets eaten?

It is probable that insects (including crickets) have formed a significant part of the diet of human beings throughout our history as a species. Apart from bacteria, insects are the most abundant life forms on the planet and they exist with marginal environmental impact. Crickets are widely available throughout the western world and are extremely efficient in generating protein. They require very little feed, water and space and they mature and reproduce rapidly. They are packed with nutrients, low in saturated fat and they taste great. They are the perfect animal proteins, incredibly nutritious and much more sustainable than traditional livestock. Crickets are the future protein of the 21st century.

Crickets are sustainable

Cows require 10 lb of feed to produce 1 lb of protein, crickets only require 2 lb. They have a food conversion ratio that puts all livestock to shame and is also superior to chicken. Crickets are also extremely water efficient. To produce 1 lb of protein from cattle you need 1000 gallons of water. To produce 1 lb of protein from crickets you only need a single gallon of water. Crickets also produce 80x less methane than cattle. Methane is a greenhouse gas which is 20x more potent than carbon dioxide.

Crickets are healthy

Crickets are rich in high quality protein, containing all 9 essential amino acids. Essential amino acids are those which cannot be synthesized by our bodies. They are also low in saturated fats and contain omega 3 fatty acids ("good fats"). They are also rich in micronutrients such as iron magnesium, zinc, calcium and vitamin B6 and B12.

Bugs as food

Bug is used to produce many popular foods such as bug burger mix. The bug burger mix is an exclusive entomochef product. It was designed so that everyone in the world can enjoy a healthy and nutritious snack at home, without a great deal of hassle in the kitchen. The bug burger mix is a mixture of natural products like cornmeal, wheat flour (gluten), soy, onion, celery, grape sugar, natural flavouring, vegetable oil and the types of insects you have chosen.

The bug burger mix is a dry product and can be stored in its packaging in a cool and dry place for a long period of time. The bug burger mix is delivered in dry, airtight and reusable 200 gm packaging, ensuring one can instantly get cooking without the need for weighing scales or other extra materials. The bug burger mix will make child's play of preparing burgers in all shapes and sizes, including balls, nuggets or croquettes.

Mealworms as food

Mealworms can be purchased live, canned or freeze dried from any number of suppliers. Mealworms are relatively easy to keep till you use them in a recipe. Nutritional information: One mealworm contains: 10.63% protein, 3.1% fiber, 420 ppm calcium, and 10.01% fat. Mealworms if alive should be placed in freezer for about an hour to put them to sleep and then boiled for one minute and then

they are ready for inclusion in a recipe. The larvae of the mealworm beetle (*Tenebrio molitor*) are one of the only insects consumed in the Western world. They are raised in the Netherlands for human consumption (as well as for animal feed), partly because they thrive in a temperate climate.

Cicadas as food

Cicadas are a delicacy in the city of Shanghai, China, where this creative recipe originated.

Name of food with cicada is cicada-licious.

Caterpillars as food

Mopane caterpillars — the larval stage of the emperor moth (*Imbrasia belina*) — are common throughout the southern part of Africa. Harvesting of mopane caterpillars is a multi-million dollar industry in the region, where women and children generally do the work of gathering the plump, little insects.

The caterpillars are traditionally boiled in salted water, then sun-dried; the dried form can last for several months without refrigeration, making them an important source of nutrition in lean times. Whereas the iron content of beef is 6 mg per 100 grams of dry weight, mopane caterpillars pack a whopping 31 mg of iron per 100 grams. They are also a good source of potassium, sodium, calcium, phosphorous, magnesium, zinc, manganese and copper, according to the FAO.

Chapulines as food

Chapulines are grasshoppers of the genus *Sphenarium*, and are widely eaten throughout southern Mexico. They are often served roasted (giving them a satisfying *crunch*) and flavoured with garlic, lime juice and salt, or with guacamole or dried chilli powder. The grasshoppers are known as rich sources of protein; some claim that the insects are more than 70 percent protein.

Researchers have noted that the gathering of *Sphenarium* grasshoppers is an attractive alternative to spraying pesticides in fields of alfalfa and other crops. Not only does this eliminate the environmental hazards associated with pesticide sprays, it also gives the local people an extra source of nutrition and income, from the sale of grasshoppers.

Witchetty grubs as food

Among the aboriginal people of Australia, the witchetty grub is a dietary staple. When eaten raw, the grubs taste like almonds; when cooked lightly in hot coals, the skin develops the crisp, flavourful texture of roast chicken. And the witchetty grub is chock full of oleic acid, a healthful omega-9 monounsaturated fat.

Though people often refer to the larvae of several different moths as witchetty grubs, some sources specify the larval stage of the cossid moth (*Endoxyla leucomochla*) as the true witchetty grub. The grubs are harvested from underground, where they feed upon the roots of Australian trees such as eucalyptus and black wattle trees.

Termites as food

Termites generally consist of up to 38 percent protein, and one particular Venezuelan species, *Syntermes aculeosus*, is 64 percent protein. Termites are also rich in iron, calcium, essential fatty acids and amino acids such as tryptophan.

African palm weevils as food

A delicacy among many African tribes, in Ghana, the palm weevil (*Rhychophorus phoenicis*) is collected off the trunks of palm trees. About 4 inches (10 cm) long and two inches (5 cm) wide, the weevils are easily pan-fried because their bodies are full of fats, though they are also eaten raw.

A 2011 report from the *Journal of Insect Science* found that the African palm weevil is an excellent source of several nutrients such as potassium, zinc, iron and phosphorous, as well as several amino acids and healthy monounsaturated and polyunsaturated fatty acids.

Stink bugs as food

Their name certainly does not lend itself to culinary appeal, but stink bugs (Hemiptera order) are consumed throughout Asia, South America and Africa. The insects are a rich source of important

nutrients, including protein, iron, potassium and phosphorus. Because stink bugs release a noxious scent, they are not usually eaten raw unless the head is first removed, which discards their scent-producing secretions. Otherwise, they are roasted, or soaked in water and sun-dried. As an added benefit, the soaking water — which absorbs the noxious secretions — can then be used as a pesticide to keep termites away from houses.

Wasps as food

Wasps are eaten in both adult and larval stage. Boiled, sautéed roasted and fried they taste somewhat butterfly and earthy.

Insects used as resources of medicines

The discipline of medical entomology, or public health entomology, and also *veterinary entomology* is focused upon insects and arthropods that impact human health. Veterinary entomology is included in this category, because many animal diseases can "jump species" and become a human health threat, for example, bovine encephalitis. Medical entomology also includes scientific research on the behaviour, ecology, and epidemiology of arthropod disease vectors, and involves a tremendous outreach to the public, including local and state officials and other stake holders in the interest of public safety. Although some insects are help to cure some diseases they are useful insect. Nowadays, we know there are mainly 3 types of use. Such as, Traditional uses, Alternative uses and Modern Scientific uses.

Traditional and alternative uses of insects in medicines

The medicinal uses of insects were often defined by the Doctrine of Signatures, which stated that an organism bearing parts that resemble human body parts, animals, or other objects, was thought to have useful relevance to those parts, animals or objects. So, for example, the femurs of grasshoppers, which were said to resemble the human liver, were used to treat liver ailments by the indigenous peoples of Mexico (Ramos *et al* 1988). This doctrine is common throughout traditional and alternative medicine, but is most prominent where medical traditions are broadly accepted, as in Traditional Chinese Medicine and Ayurveda, and less by community and family based medicine, as is more common in parts of Africa.

Traditional medicines in China:

Traditional Chinese Medicine (TCM) includes the use of herbal medicine, acupuncture, massage, exercise, and dietary therapy. It is a typical component of modern medical care throughout East Asia and in some parts of Southeast Asia (such as Thailand). Insects are very commonly incorporated as part of the herbal medicine component of TCM, and their medical properties and applications are broadly accepted and agreed upon. Some brief examples follow:

- Centipede is used to treat tetanus, seizures, and convulsions. It is also said to relieve sores and carbuncles on the skin, to alleviate pain, especially that of headaches, and to be a cure for snakebite. Centipede is typically dried, ground into a paste, and applied topically to the afflicted area.
- The Chinese black mountain ant, *Polyrhachis Vicina*, is supposed to act as a cure all and is widely used, especially by the elderly. It is said to prolong life, to have anti-aging properties and to increase virility and fertility. Recent interest in the ants' medicinal qualities by British researchers has led to investigations into the extract's ability to serve as a cancer-fighting agent. Chinese black mountain ant extract is typically consumed mixed with wine.

Traditional medicines in India (Ayurveda):

Ayurveda, is ancient traditional Indian treatment almost universally incorporated alongside Western medicine as a typical component of medical treatment in India. Although Ayurvedic medicine is often effective, it is often plagued by worryingly inconsistent dosages and frequent contamination of natural medicines with toxic heavy metals (Chakravorty *et al* 2011). Some brief examples to follow:

- Termite is said to cure a variety of diseases, both specific and vague. Typically the mound or a portion of the mound is dug up and the termites and the architectural components of the mound are together ground into a paste which is then applied topically to the affected areas or, more rarely, mixed with water and consumed (Srivastava *et al* 2009). This treatment was said to cure ulcers, rheumatic diseases, and anaemia (Chakravorty *et al* 2011). It was also been suggested to be a general pain reliever and health improver (Chakravorty *et al* 2011).
- The *Jatropha* leaf miner, a lepidopteran which feeds preferentially on *Jatropha*, is an example of a major insect agricultural pest which is also a medicinal remedy (Srivastava *et al* 2009). The larvae are harvested, boiled, and mashed into a paste which is administered topically and are said to induce lactation, reduce fever, and sooth gastrointestinal tracts (Srivastava *et al* 2009).

Traditional Medicines in Africa:

Unlike China and India, the traditional insect medicine of Africa is extremely variable. It is largely regional, with few, if any, major agreements on which insects are useful as treatments for which ailments (Srivastava *et al* 2009). Most insect medicinal treatments are passed on through communities and families, rather than being taught in university settings, as Traditional Chinese Medicine and Ayurveda. Some brief examples to follow:

- Grasshopper is both commonly eaten as a delicacy and an excellent source of protein and is consumed for medicinal purposes (Srivastava *et al* 2009). These insects are typically collected, dried in the sun, and then ground into a powder (Srivastava *et al* 2009). The powder can then be turned into a paste when mixed with water and ash and applied to the forehead to alleviate the pain of violent headaches (Srivastava *et al* 2009). Additionally, the headaches themselves can be prevented by a "healer" inserting the paste under the skin at the nape of the afflicted person's neck (Srivastava *et al* 2009).
- Termites are also used in parts of Africa much like they are in India (Chakravorty *et al* 2011). Parts of the mound are dug up, boiled, and turned into a paste, which can then be applied to external wounds to prevent infection or consumed to treat internal haemorrhages (Srivastava *et al* 2009). Interestingly, termites are used not only as a form of medicine, but also as a medical device. If a "healer" wants to insert a medicine subcutaneously, they will often spread that medicine on the skin of the patient, and then agitate a termite and place the insect on the skin of the patient (Srivastava *et al* 2009). When the termite bites, its mandibles effectively serve as an injection device (Srivastava *et al* 2009).

Traditional medicines in Americas:

The Americas were more highly influenced by the Doctrine of Signatures than China, India, or Africa, most likely because of their colonial history with Europe. The majority of insect use in medicine is associated with Central America and parts of South America, rather than North America and most of it is based on the medical techniques of indigenous peoples (Ramos *et al* 1988). Some examples to follow:

- Chapulines, or grasshoppers, are commonly consumed as a toasted regional dish in some parts of Mexico, but they are also used medicinally (Ramos *et al* 1988). They are said to serve as diuretic to treat kidney diseases, to reduce swelling, and to relieve the pain of intestinal disorders when they are consumed (Ramos *et al* 1988). However, there are some risks associated with consuming chapulines, as they are known to harbour nematodes which may be transmitted to humans upon consumption.
- Much like the termites of Africa, ants were sometimes used as medicinal devices by the indigenous peoples of Central America, in some rural, arid areas of Mexico (Ramos *et al* 1988). The soldier cast of the army ant would be collected and is used as living sutures by Mayans (Ramos *et al* 1988). Typically, this would involve agitating an ant and holding its mandibles up to the wound

edges; when it bit down, they would remove the thorax and abdomen, leaving only the head holding the wound together (Ramos *et al* 1988). The salivary gland secretions of the ant were also reputed to have antibiotic properties (Ramos *et al* 1988). The venom of the red harvester ant was used to cure rheumatism, arthritis and polimyelitis via the immunological reaction produced by its sting.

- The silkworm, *Bombyx mori* was also commonly consumed both as a regional food and for medicinal purposes in Central America after it was brought to the New World by the Spanish and Portuguese (Ramos *et al* 1988). Only the immature ones are consumed. Boiled pupae were eaten to treat apoplexy, aphasia, bronchitis, pneumonia, convulsions, haemorrhages, and frequent urination (Ramos *et al* 1988). The excrement produced by the larvae is also eaten to improve circulation and alleviate the symptoms of cholera (intense vomiting and diarrhoea) (Ramos *et al* 1988).

Modern scientific uses of insects in medicines

Though insects were widely used throughout history for medical treatment on nearly every continent, relatively little medical entomological research has been conducted since the revolutionary advantages of antibiotics. Heavy reliance on antibiotics, coupled with discomfort with insects in Western culture limited the field of insect pharmacology until the rise of antibiotic resistant infections sparked pharmaceutical research to explore new resources.

Maggot therapy:

One of the most commonly used insects in medical purposes is the blow fly larvae. The first recorded use of it was during the World War II. Military surgeons noticed that wounds which were left untreated for several days and which became infested with maggots, healed better than wounds not infested with the blow fly larvae. It was later discovered that the larvae secreted a chemical called allantoin, which had a curative effect. Allantoin is now being used to treat the infectious bone disease, osteomyelitis. Maggot debridement therapy is the intentional introduction of live, disinfected fly larvae into non-healing or dead skin and soft tissue wounds of a human or other animal for the purpose of selectively cleaning out only the necrotic tissue within a wound in order to promote wound healing. It is also used to prevent infection and to speed the healing process.

Apitherapy:

Apitherapy is the medical use of honeybee products such as honey, pollen, bee bread, propolis, royal jelly and bee venom. One of the major peptides in bee venom, called melittin, has the potential to treat inflammation in sufferers of rheumatoid arthritis and multiple sclerosis. Melittin blocks the expression of inflammatory genes, thus reducing swelling and pain. It is administered by direct insect sting, or intramuscular injections. Bee products demonstrate a wide array of antimicrobial factors and in laboratory studies and have been shown to kill antibiotic resistant bacteria, pancreatic cancer cells, and many other infectious microbes (Ratcliffe *et al* 2011).

Blister beetle and Spanish fly:

Cantharidin, is obtained from the body of blister beetle, *Mylabris cinchorii* species in India and *Lytra vesicatoria* in Europe are best known species. The blister-causing oil found in several families of beetles, was accepted by the FDA in 2004 as treatment for warts and other skin problems. It also has historical use by the Greeks and Romans and is used as an aphrodisiac in some societies. Recent studies in cell culture and animal models have demonstrated powerful tumour fighting properties of Cantharidin (Ratcliffe *et al* 2011).

Blood-feeding insects:

Many blood-feeding insects like ticks, horseflies, and mosquitoes inject multiple bioactive compounds into their prey. These insects have been used by practitioners of Eastern medicine for hundreds of years to prevent blood clot formation or thrombosis (Yang *et al* 2000). However, modern medical research has only recently begun to investigate the drug development potential of blood-feeding insect saliva. These compounds in the saliva of blood feeding insects are capable of increasing the ease of

blood feeding by preventing coagulation of platelets around the wound and provide protection against the host's immune response. Currently, over 1280 different protein families have been associated with the saliva of blood feeding organisms (Ribeiro *et al* 2009). This diverse range of compounds may include (Francischetti *et al* 2005, Ratcliffe *et al* 2011).

- Inhibitors of platelet aggregation, ADP, arachidonic acid, thrombin and PAF
- Anticoagulants
- Vasodilators
- Vasoconstrictors
- Antihistamines
- Sodium channel blockers
- Complement inhibitors
- Pore formers
- Inhibitors of angiogenesis
- Anaesthetics
- AMPs and microbial pattern recognition molecules
- Parasite enhancers/activators

Currently, some preliminary progress has been made with investigation of the therapeutic properties of tick anticoagulant peptide (TAP) and ixolaris, a novel recombinant tissue factor pathway inhibitor (TFPI) from the salivary gland of the tick, *Ixodes scapularis* (Maritz-Olivier *et al* 2007). Additionally, ixolaris, a tissue factor inhibitor has been shown to block primary tumour growth and angiogenesis in a glioblastoma model (Carneiro-Lobo *et al* 2009). Despite the strong potential of these compounds for use as anticoagulants or immune-modulating drugs no modern medicines, developed from the saliva of blood-sucking insects, are currently on the market (Ratcliffe *et al* 2011).

Honey bee products used as medicine through out the world

Honey bee products are used medicinally across Asia, Europe, Africa, Australia, and the Americas, despite the fact that the honey bee was not introduced to the Americas until the colonization by Spain and Portugal. They are by far the most common medical insect product both historically and currently (Srivastava *et al* 2009).

Honey:

Honey is the most frequently referenced medical bee material. It can be applied to skin to treat excessive scar tissue, rashes, and burns (Feng *et al* 2009) and can be applied as a poultice to eyes to treat infection (Chakravorty *et al* 2011). It is also consumed for digestive problems and as a general health restorative, and can be heated and consumed to treat head colds, cough, throat infections, laryngitis, tuberculosis, and lung diseases (Ramos *et al* 1988)

Apitoxin:

Apitoxin or honey bee venom can be applied via direct stings to relieve arthritis, rheumatism, polyneuritis and asthma (Ramos *et al* 1988).

Propolis:

Propolis, a resinous, waxy mixture collected by honeybees and used as a hive insulator and sealant, is often consumed by menopausal women because of its high hormone content and it is said to have antibiotic, anaesthetic, and anti-inflammatory properties (Ramos *et al* 1988).

Royal jelly:

Royal jelly is used to treat anaemia, gastrointestinal ulcers, arteriosclerosis, hypo- and hypertension and inhibition of sexual libido (Ramos *et al* 1988).

Bee bread:

Bee bread, or bee pollen, is eaten as a generally health restorative, and is said to help treat both internal and external infections (Ramos *et al* 1988). All of these honey bee products are regularly

produced and sold, especially online and in health food stores, though none are yet approved by the FDA.

Conclusion

Though insect is a very small organism but it is very useful for a human being from its day to day life, as here some of the products of the insects have been mentioned such as food, medicine. As the human population continues to inch closer to 8 billion people, feeding all those hungry mouths will become increasingly difficult. A growing number of experts claim that people will soon have no choice but to consume insects. As if to underscore that claim, a group of students from McGill University in Montreal has won the 2013 Hult Prize, for producing a protein-rich flour made from insects. The prize gives the students \$1 million in seed money to begin creating what they call Power Flour.

References

- [1] Athens G A "Dazzling Color in the Land of the Inca: A Centuries-old Dye Still Important in Histology Today." (PDF). *Histologic XLVI* (2)
- [2] "Canary Islands cochineal producers homepage". Retrieved July 14 2005
- [3] Carneiro-Lobo T C, Konig S and Machado D E (2009). Ixolaris, a tissue factor inhibitor, blocks primary tumor growth and angiogenesis in a glioblastoma model. *J. Thromb. Haemost.* 7, 1855e1864
- [4] Chakravorty J, Ghosh S, and Meyer-Rochow V B (2011). Practices of entomophagy and entomotherapy by members of the Nyishi and Galo tribes, two ethnic groups of the state of Arunachal Pradesh (North-East India). *Journal of Ethnobiology and Ethnomedicine* 7(5)
- [5] Dossey A T (2010). Insects and their chemical weaponry: new potential for drug discovery. *Nat. Prod. Rep* 27, 1737e1757
- [6] Feng Y, Zhao M, He Z, Chen Z and Sun L (2009). Research and utilization of medicinal insects in China. *Entomological Research*, 39: 313-316
- [7] Foodnet. "Tropical commodities and their markets". Retrieved July 14 2005
- [8] Foodnet. "Tropical commodities and their markets". Retrieved July 14 2005
- [9] Francischetti I M B, Mather T N and Ribeiro J M C (2005). Tick saliva is a potent inhibitor of endothelial cell proliferation and angiogenesis. *Thromb. Haemost.* 94, 167e174
- [10] Global Steak - *Demain nos enfants mangent des criquets* (2010 French documentary)
- [11] Gullan P J, Cranston P S (2005). *The Insects: An Outline of Entomology* (3ed.). Oxford: Blackwell Publishing. ISBN 1-4051-1113-5
- [12] Maierbrugger A (14 May 2013). "UN: Insects are 'food of the future' (video)". *Inside Investor*. Retrieved 17 May 2013
- [13] Maritz-Olivier C, Stutzer C, Jongejan F, et al (2007). Tick anti-hemostatics: targets for future vaccines and therapeutics. *Trends Parasitol.* 23, 397e407
- [14] Ramos-Elorduy de Concini J and Pino Moreno J M (1988). The utilization of insects in the empirical medicine of ancient Mexicans. *Journal of Ethnobiology*, 8(2), 195-202
- [15] Ratcliffe et al. *Insect Biochemistry and Molecular Biology* 41 (2011) 747e769
- [16] Ribeiro J M C, Arca B (2009). From sialomes to the sialoverse: An insight into salivary potion of blood-feeding insects. *Adv. Insect Physiol.* 37, 59e118
- [17] Srivastava S K, Babu N and Pandey H (2009). Traditional insect bioprospecting--As human food and medicine. *Indian Journal of Traditional Knowledge*, 8(4): 485-494
- [18] Threads in Time, LTD. "Time line of fabrics". Archived from the original on October 28, 2005. Retrieved July 14, 2005
- [19] U. S. Food and Drug Administration (June 09 2015). "Summary of Color Additives for Use in United States in Foods, Drugs, Cosmetics, and Medical Devices". Silver Spring, Maryland: U.S. Department of Health and Human Services. Retrieved July 10 2015
- [20] Wild Flavors Inc. "E120 Cochineal". The wild world of solutions. Retrieved July 19 2005

[21] William Balée (2000). "Antiquity of Traditional Ethnobiological Knowledge in Amazonia: a Tupí-Guaraní Family and Time" *Ethnohistory* 47(2):399-422

[22] Yang X, Hu K, Yan G *et al* (2000). Fibrinogenolytic components in Tabanid, an ingredient in traditional Chinese medicine and their properties. *J. Southwest Agric. Univ.* 22, 173e176 (Chinese)

EXTERNAL LINKS:

[1] Anonymous 5 Examples of Medically Important Insects by Rob Harris

[2] Anonymous Buying the Bug Burger Mix

[3] Anonymous Insects are food, Entomophagy is the Future

[4] Anonymous7 Insects You'll Be Eating in the Future By Marc Lallanilla, Assistant Editor, October 01 2013

[5] <http://en.wikipedia.org/wiki/ethnoentomology>

[6] <http://en.wikipedia.org/wiki/insect>

[7] <http://news.bbc.co.uk/2/hi/health/1809450.stm>

[8] <http://tcm.health-info.org/Herbology.Materia.Medica/wugong-properties.htm>

Mechanical and Chemical Approaches to fabricate luminescent Silicon Nanoparticles

Bhaskar Das^{1,2}, Syed Minhaz Hossain³ and Mallar Ray⁴

¹*Department of Physics, Sister Nibedita Govt. General Degree College for Girls, Hastings House, Kolkata-700027*

^{2,3}*Department of Physics, IEST, Shibpur, Howrah-711103*

⁴*School of Materials Science and Engineering, IEST, Shibpur, Howrah-711103*

Abstract

Blue-violet and green luminescent silicon nanoparticles (NPs) have been prepared by two different methods— (i) mechanical, in which mechanically milled crystalline silicon powder was subjected to repeated etching-oxidation-etching processes, and (ii) chemical, in which (3-aminopropyl)triethoxysilane (APTES) was reduced by sodium ascorbate (SA) in a one-step ‘green’ synthesis method. Colloids of silicon NPs formed by both the routes exhibit intense room temperature photoluminescence (PL) that can be detected with the naked eye. While the former route results in dominant blue-violet PL, the later, exhibits greenish luminescence. PL from the colloidal suspensions of the NPs is found to be stable even after the four months of preparation. Structural investigations reveal that the mechanically prepared samples contain abundant nanocrystals (NCs) along with amorphous oxides. The chemical route however, results in dominant amorphous phase with trace amount of NCs. A comparative analysis of the optical properties of the two samples indicates that violet to green PL from silicon NPs is dominantly due to the contribution of oxide enriched surface states rather than quantum confinement of excitons. Both mechanical milling and one step chemical methods are low cost, simple and easily scalable techniques that may be used to produce a large quantity of NPs.

Key words: silicon, nanoparticles, photoluminescence, oxide.

Publication History: Received: 10th August, 2016; Accepted: 22th August, 2016

Introduction

Silicon is the most important and dominant semiconductor for almost all modern devices. Despite all the success of silicon in the field of electronics, silicon is an indirect semiconductor which requires momentum conserving phonon during transitions as the valence band maximum and conduction band minimum are not at the same position in K- space, which makes the radiative process slow. Hence Si is a poor light emitter. However the observations of absorption and emission shifts of porous Si and Si NPs shows that the size dependent optical properties are present in indirect gap semiconductor as well [1]. However, the size dependent modification of optical characteristics of Si is not yet fully understood. According to one proposition, in Si NCs, the band structure is altered and the electron and hole wave functions overlap allowing recombination without phonon contribution [2,3,4, and 5]. Hence, at the nano regime indirect gap semiconductors have similar optical properties as direct gap semiconductors. In indirect gap semiconductor NPs in addition to quantum confinement (QC), incomplete bonds, surface defects etc., can generate unexpected emission shifts. The mechanism of luminescence from Si NCs therefore is still under active discussion. Broadly, the debate regarding origin of PL in Si NCs may be clubbed under two categories. While one group believes, NCs surface effects play the most important role in the observed PL [6], the other opinion ascribes the origin of PL in Si NCs to quantum confinement effect [7,8]. Ray et al [9, 10] opine the mechanism in favour of quantum confinement as well as interfacial defect related transitions.

A number of fabrication techniques of Si NCs have been reported so far [11-15], yet the rapid, green and low cost preparation of Si NCs has remained a challenge.

In this study, we report a simple and rapid synthesis of blue-violet and green luminescent colloidal Si NPs by two different routes — mechanical and chemical. In chemical synthesis we have used APTES as Si source and modified a method reported by Wang et al. [16] for synthesis of green luminescent Si NPs whereas in the mechanical route we have simply treated mechanically milled Si NCs to obtain blue luminescent NCs.

Experimental

Synthesis of colloidal suspension of Si NPs by mechanical milling:

Commercial Si powder with average particle size of 20 μ m and nominal purity of 99.9% was used as the milling material. The sample was taken at 10:1 balls (of 10mm) to powder weight ratio in a WC vial in Toluene medium. Toluene was used to minimize oxidation and agglomeration. The ball mill was allowed to operate at 300rpm. After a gap of 50hr milled powder was taken out and kept in clean and covered Petri dishes. The sample was allowed to dry for 3 weeks in a glove box in nitrogen environment. To remove trace of organic and metallic contaminants, if any, a standard piranha etch of the dried powder with 2:1 solution of H₂SO₄ (98%) and H₂O₂ (30%) was carried out. The solution (approximately 0.5g Si powder in 5ml H₂SO₄ and H₂O₂ solution) was then heated slowly at 110^oC until the entire liquid evaporated and dry deposits of oxygen rich Si NCs were obtained. The heating was performed in ambient atmosphere inside a fume hood for sufficient oxidation. The piranha etched sample was then transferred in a Teflon bath of aqueous HF solution (10%) to remove oxide layer. The solution was heated at 80^oC to evaporate the liquid (HF) and dry deposit of oxide etched Si NCs were obtained. Subsequently the particles were dissolved in isopropanol and sonicated to get colloidal suspension of particles having crystalline Si core surrounded by an amorphous Si oxide. This sample is referred as S1.

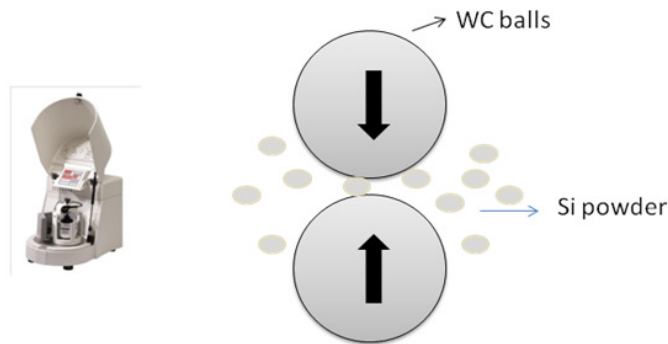


Figure 1: Mechanism of attrition of Si powder in a planetary ball mill

Synthesis of colloidal Si NPs by the reduction of APTES:

APTES (99%) and Sodium Ascorbate (SA) were used as the starting chemicals to prepare Si NPs. APTES was purchased from Sigma Aldrich and SA was synthesised in laboratory with sodium hydroxide and ascorbic acid. 2 mL APTES was taken in a conical flask and 8mL water was added with APTES while stirring with a magnetic stirrer. Then 2.5 mL of SA (0.1M) was mixed with the aqueous solution of APTES. The whole mixture was stirred for 10 minutes. The resulting colloidal Si NPs exhibited intense green luminescence under UV irradiation. It takes 15 minutes to complete the whole process of synthesis. This sample is called S2.

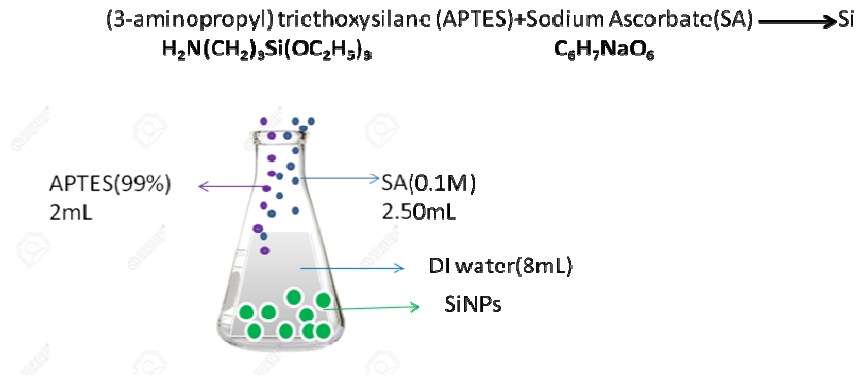


Figure 2: Synthesis of colloidal Si NPs by the reduction of APTES.

Results and Discussions

Figure 3 (a) shows the XRD profile of un-etched samples. Figures 3 (b) and 3(c) show the XRD profiles of piranha and HF etched samples of 50 h ball milled crystalline Si (S1). There is a clear evidence of appreciable broadening of the Bragg diffracted peaks after etching. It is clear that piranha and HF treatment is able form Si NCs of much smaller size. The average crystallite size of the un-etched samples, calculated from the (111), (220) and (311) Bragg reflection line widths using the Scherrer equation is 104 nm and same for the etched samples are ~45 nm. The increase in strain values from 0.1163 to 0.2455 and 0.2438 after HF etching indicates lattice expansion and the increase in FWHM indicates the creation of defects or disorders in the Si NCs after HF etching [17]. From Figures 3 (b) and 3 (c) there is a confirmation of small tungsten carbide contamination in the milled silicon sample. This could be introduced from the tungsten carbide balls and vial which were used as milling media during milling.

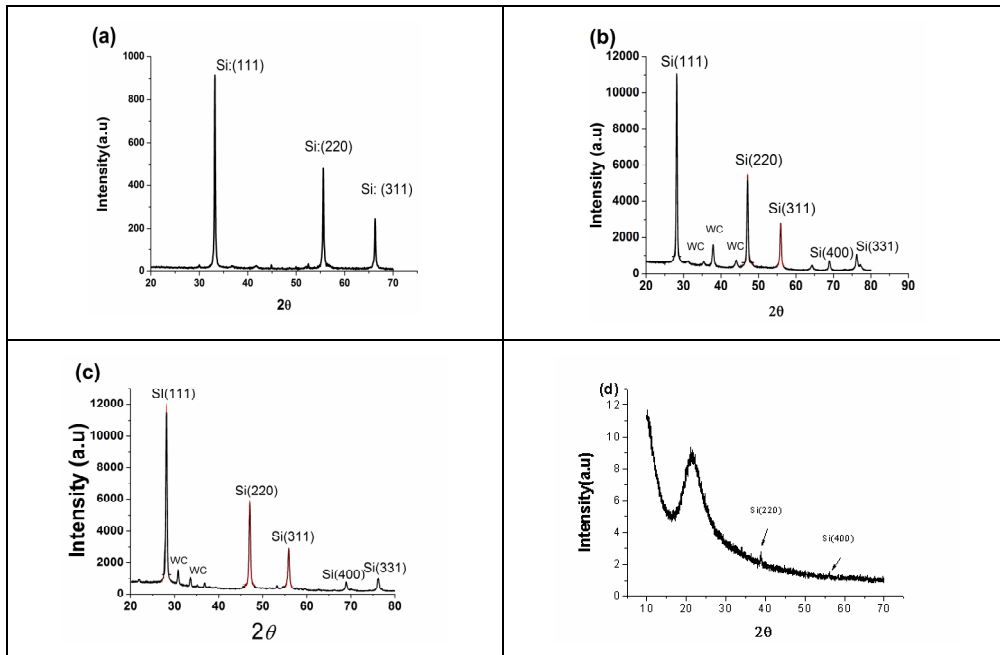
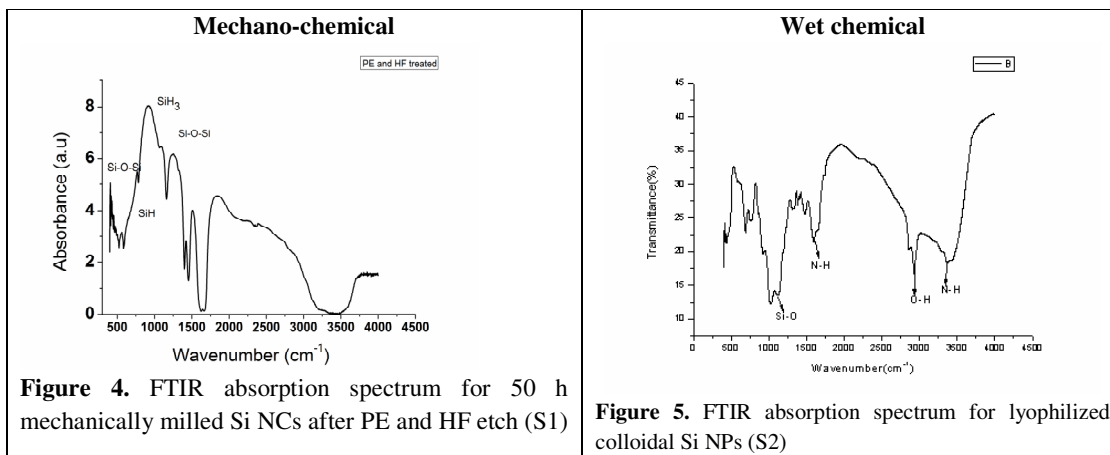


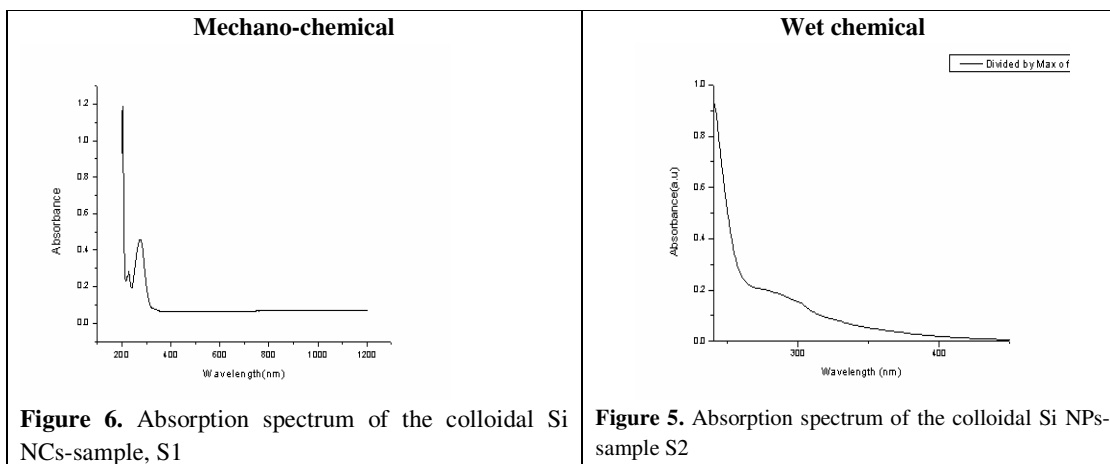
Figure 3. XRD profiles of (a) un-etched 50 h ball milled samples, (b) and (c) piranha and 10% buffered HF etched samples. The different planes of Si are indexed according to JCPDS card: 77-211 and WC contamination indexed according to JCPDS card: 73-0471, (d) XRD profile of lyophilized colloidal Si NPs (S2)The planes of Si are indexed according to JCPDS card: 17-0901.

Crystalline structure of Si with diffraction peaks for (220) and (400) planes can be seen along with amorphous oxides in the X-ray diffraction profile (Fig.3.d) of lyophilized colloidal Si NPs (S2). The most dominant (111) peak is not seen as this peak is masked by the amorphous hump of SiO₂. This result is expected as Si NCs react with water after synthesis and a thick oxide layer is formed on their surfaces.



The FTIR spectra of the sample S1 (Fig.4) indicate the presence of oxygen in the sample. A peak at around 1081 cm⁻¹ of the PE and HF treated Si is indicative of Si-O-Si bond-stretching at 1074 cm⁻¹ with reference to Pai et al [18] and Lucovsky et al [19]. According to them the peak of Si-O-Si stretching band at 1074 cm⁻¹ corresponds to stoichiometric SiO₂. Hence it is concluded that SiO₂ is present in the sample. Pi et al [20] observed that Si NCs are passivated by hydrogen after HF etching yet the growth of Si-O-Si can be explained as the NCs are exposed to atmosphere. The FTIR spectrum of the lyophilized colloidal Si NP (S2) is obtained to examine the chemical bonds of the sample S2 (Fig 5). Here too the Si-O-Si bonds are clearly present along with N-H and O-H bonds. A strong absorption peak at 1140 cm⁻¹ can be assigned to Si-O group of bonding. The absorbance in the range of 2870 – 2960 cm⁻¹ is attributed to the deformation and stretch vibration of the O-H bond. The strong absorbance at 1596 cm⁻¹ corresponds to N–H bending vibration and the same at 3377 cm⁻¹ is attributed to N–H stretching vibration [16, 21].

Hence FTIR results conclude that piranha and HF etch can create isolated Si NCs and hydrogen passivated Si along with defects at the surface which are passivated by oxygen when exposed to ambient atmosphere.



The UV-VIS absorption spectra of the samples S1 and S2 are shown in Fig. 6 and Fig. 7 respectively. There is a sharp peak around 290 nm for the sample S1 and a hump in the same region for sample S2. Hence it could be concluded that there is a signature of crystallinity for the sample S1 and trace presence of nanocrystals in sample S2. In case of sample S2 there is a gradual increase in absorbance with decrease in wavelength from onset wavelength 450 nm (2.75 eV) which is the absorption band edge across the indirect band gap.

Both mechanically milled, chemically and thermally treated colloidal Si NPs (S1) and aqueous solution of Si NPs (S2), prepared chemically, exhibit intense room temperature PL which could be detected with the naked eye (Figs.10 and 11). Fig 8 shows the PL spectra of colloidal Si NPs (S1) within excitation wavelength range 300 to 400 nm and Fig 9. Shows the PL spectra of aqueous solution of Si NPs (S2) within excitation wavelength range 390 to 450 nm. In both the cases there is a clear indication of red-shift of PL emission spectra with the increase in excitation wavelength. At longer excitation wavelengths, the PL peak inconsistently increases or decreases which is inconsistent with the mechanism of PL as explained by quantum confinement effect. There is a clear evidence of blue shift of the sample (S2) with time. Analysis of optical properties of the sample indicates that green to blue PL from Si NPs is dominantly due to the contribution of oxide enriched surface states rather than quantum confinement of excitons.

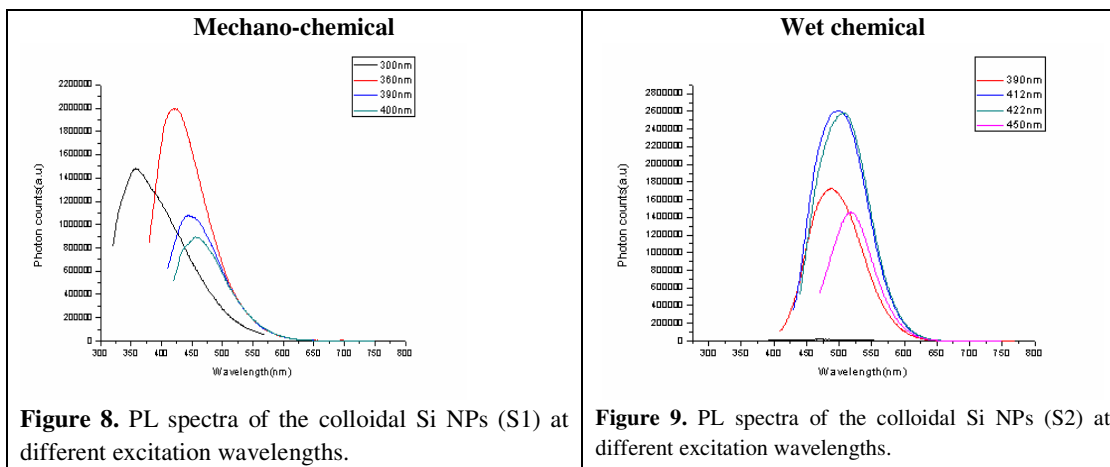


Figure 8. PL spectra of the colloidal Si NPs (S1) at different excitation wavelengths.

Figure 9. PL spectra of the colloidal Si NPs (S2) at different excitation wavelengths.

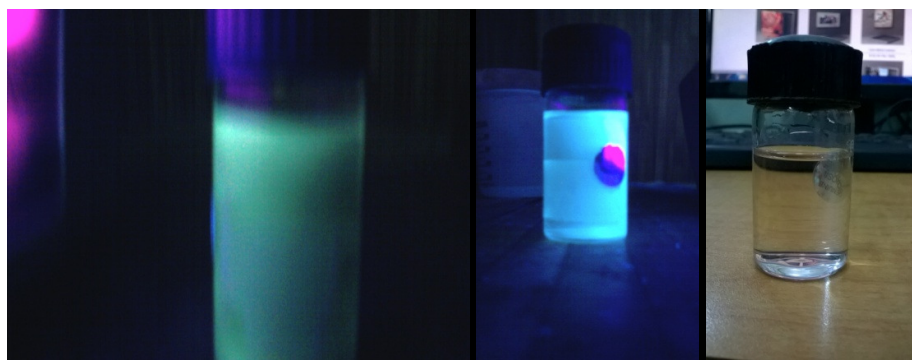


Figure 10. Images of green and blue emission of colloidal SiNPs (S2) under UV- irradiation and as prepared colloidal Si NPs (S2)

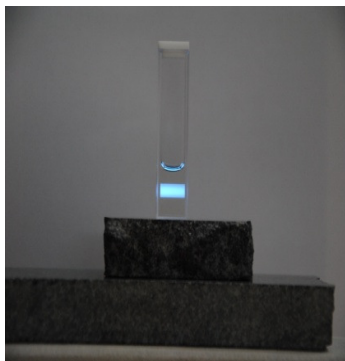


Figure 11. Image of blue emission of colloidal Si NPs (S1) under UV- irradiation

Conclusions

Light emitting Si NPs have been prepared successfully by repeated etching-oxidation-etching of mechanically milled crystalline silicon powder and reduction of APTES by SA in a one-step ‘green’ synthesis method. In case of chemical synthesis method as the Si NCs react with water soon after its formation, huge amount of amorphous oxide is present along with Si NCs in the prepared sample. On studying the optical properties of the samples we propose that PL from silicon NPs is dominantly due to the contribution of oxide enriched surface states rather than quantum confinement of excitons which again needs further investigation.

References

- [1] Kanemitsu .Y, *Phys. Rep.*, 263, 1. (1995)
- [2] Bruhn.B, Doctoral Thesis at Royal Institute of Technology (Stockholm, Sweden 2012)
- [3] Faist.J, Optical Properties of Semiconductors, Eidgenossische Technische Hochschule, Zurich
- [4] Hybertsen M.S, *Phys Rev. Lett.*, 1514-1517(1994)
- [5] Kvalev.D, Heckler.H, Ben-Chorin.M, Polisski.G, Schwartzkopff.M and Koch.F, *Phys Rev. Lett* 81, 2803-2806S(1998)
- [6] Kanemitsu.Y, *Phys. Rev. B* 49, 16845(1994)
- [7] Efremov M.D, Volodin .V.A, Marin .D.V, et al, Pis'ma Zh, Eksp. Teor.Fiz 80, 619(2004) [*JETP Lett.*80, 544 (2004)]
- [8] Vinciguerra.V, Franzo.G, Priolo.F, et al., *J.Appl. Phys.* 87, 8165(2000)
- [9] Ray M, Hossain.S.M, Kile.R.F, Banerjee.K and Ghosh.S, *Nanotechnology* 21 505602 (9pp) (2010)
- [10] Ray M, Basu.T.S, Jana.A, Bandyopadhyay.N.R, Hossain.S.M, Pramanick A.K and Kile R.F., *Journal of Applied Physics* 107, 064311(2010)
- [11] Heinrich .J. L, Curtis.C. L, Credo. G. M., Kavanagh. K .L, and. Sailor, *Science M. J.*, **255**, 66–68, (1992).
- [12] Hua F. J., Erogbogbo F, Swihart. M. T and Ruckenstein.E, *Langmuir*, **22**, 4363–4370,(2006).
- [13] Li.X, He.Y and Swihart .M. T, *Langmuir*, **20**, 4720–4727,(2004).
- [14] Mangolini. L, Thimsen. E and Kortshagen. U, *Nano Lett.*, 5, 655-659 (2005).
- [15] Samara J. P. and G. A, *Appl. Phys. Lett.* 74, 3164-3166 (1999).
- [16] Wang.J, Xin.D.Y, Liang.G.H, Chang.J, Kong J.L, Chen.J.Y, *J.Mater.Chem.B*, 2, 4338-4345 (2014).
- [17] Standaert T E F M., Hedlund.C, Joseph, E.A., Oehrlein.G.S, and.Dalton.T.J, *J. Vac. Sci. Technol. A* **22** 53–60(2004)
- [18] Lucovsky.G, Nemanich.R.J and Knights.J.C, *Phys. Rev. B* **19** 2064–73(1979)
- [19] Hayashi. S, Tanimoto.S and Yamamoto.K, *Appl. Phys.* **68** 5300–8(1990)
- [20] Thompson.P , Cox.D.E and Hastings.J.B, *J. Appl.Crystallogr.* **20** 79–83(1987)
- [21] Coates.J, Interpretation of Infrared Spectra, A Practical Approach (2000)

